INAUGURAL – DISSERTATION

zur Erlangung der Doktorwürde

der

Naturwissenschaftlich – Mathematischen

Gesamtfakultät

der

Ruprecht – Karls – Universität Heidelberg

vorgelegt von

Jonathan J. Bryant

aus USA

Tag der mündlichen Prüfung: 11. Januar 2013

Construction and Investigation of Metallochromic Dyes

Jonathan J. Bryant

Die vorliegende Dissertation wurde im Zeitraum vom Oktober 2010 bis Oktober 2012 am Organisch-Chemischen Institut der Ruprecht-Karls-Universität Heidelberg unter der Anleitung von Professor Dr. Uwe Bunz durchgeführt.

Ich erkläre hiermit, dass ich die vorgelegte Dissertation selbst verfasst und mich keiner anderen als der von mir ausdrücklich bezeichneten Quellen und Hilfen bedient habe.

Ich erkläre hiermit, dass ich an keiner anderen Stelle ein Prüfungsverfahren beantragt bzw. die Dissertation in dieser oder anderer Form bereits anderweitig als Prüfungsarbeit verwendet oder einer anderen Fakultät als Dissertation vorgelegt habe.

Jonathan J. Bryant

27 November 2012

dedicated to

Lien H. Phun

Acknowledgements

First and foremost, I would like to thank Prof. Dr. Uwe Bunz for his support (emotional and financial) and guidance on the long road towards the completion of this work. During my tenure in the Bunz lab, I have grown tremendously as a chemist and as a person. I am grateful for all that I have learned and for the opportunity to work in two different research labs. I am especially grateful for all of the help I received from Kerstin-Antje Windisch – without her I would be lost.

A special thanks goes to my collaborators: Ben Lindner and Yexiang Zhang for their *N*-heteroacene expertise, and Steven Hayden for his cell culturing skills. I have the greatest appreciation also for my students and their hard work in the lab – Eric Sauter for his work on water-soluble substituents and polythiophenes, Vivien Reuscher for her work on pyridine and thiophene cycloadducts, Marcel Schädler for his work on polymers with pendant triazoles, and Jan Freudenberg for his polymer synthesis.

Thanks to Dr. Juan Tolosa, Dr. Ben Coombs, Dr. Jan Fleischhauer, and Dr. Manuel Hamburger for all of their ideas, advice, and moral support, and Kerstin Brödner and Olena Tverskoy for their extremely helpful laboratory skills, and for having all the answers.

Many thanks to my colleagues Thimon Schwaebel, Michael Porz, Malte Jesper, Jens Engelhart, Manuel Schaffroth, Claudia Teusch, Sebastian Menning, Chris Patze, Jan Kumpf, Dominic Mäker, Philipp Biegger, Fabian Paulus, Torben Peters, Martin Petzoldt, Marius Kuhn, and Korwin Schelkle for many things essential to a working lab – donating chemicals, time, or advice, proofreading manuscripts, and overall making the chemistry lab a pleasant place to work (despite all of the carcinogens).

I would also like to acknowledge my parents, for making everything possible, and for spoiling me as a child.

Table of Contents

List of Abbreviations

Acetic acid	AcOH
Aggregation-induced emission	AIE
Adenosine triphosphate	ATP
Boron-dipyrromethene	BODIPY
Cyan fluorescent protein	CFP
Copper-catalyzed azide-alkyne cycloaddition	CuAAC
Dichloromethane	DCM
Diisopropylamine	DIPA
Dimethylformamide	DMF
Dimethylsulfoxide	DMSO
Deoxyribonucleic acid	DNA
Degree of polymerization	DP
Electron impact ionization	EI
Electrospray ionization	ESI
Ethyl acetate	EtOAc
Frontier molecular orbital	FMO
Fluorescence resonance energy transfer	FRET
Gel permeation chromatography	GPC
Highest occupied molecular orbital	HOMO
High-resolution mass spectrometry	HRMS
Infrared	IR
Lithium aluminum hydride	LAH
Limit of detection	LOD
Lowest unoccupied molecular orbital	LUMO

Mass spectrometry	MS
N-bromosuccinimide	NBS
Nuclear magnetic resonance	NMR
Nanoparticle	NP
Poly(aryleneethynylene)	PAE
Polydispersity index	PDI
Photoinduced electron transfer	PET
Poly(phenyleneethynylene)	PPE
Reactive oxygen species	ROS
2,5,8,11,15,18,21,24-octaoxapentacosane (swallowtail)	SW
Tetrabutylammonium bromide	TBAB
Tetrabutylammonium fluoride	TBAF
Triethylamine	TEA
Triethyleneglycol monomethyl ether	TEG
Tetrahydrofuran	THF
Triisopropylsilyl	TIPS
Thin layer chromatography	TLC
Trimethylsilyl	TMS
Para-toluenesulfonate	tosyl or Ts
Yellow fluorescent protein	YFP

List of Figures

List of Tables and Schemes

1 Abstract

Novel fluorophores were synthesized, characterized, and examined with respect to their metal-binding properties. These compounds (Figure 1) consist of a heteroaromatic core substituted with two triazole rings, synthesized via copper-catalyzed azide-alkyne cycloaddition. Binding of a metal ion is achieved through coordination between two nitrogens (one in the triazole ring, and one in the heteroaromatic core). For practical purposes, these sensors must be soluble in water. This is accomplished through the use of a water-soluble side chain; in this case, one with a branched oligoethylene glycol substituent. This bulky side-chain decreases fluorescence quenching from intermolecular aggregation, resulting in metal ion sensors that are brightly fluorescent, even in water.

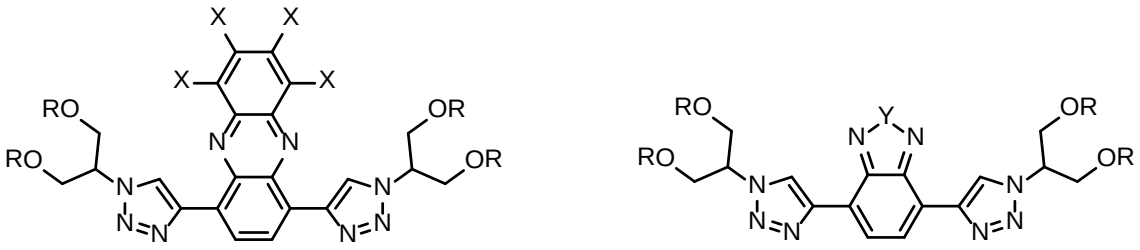

Figure 1 Metal ion sensors. R represents tri(ethylene glycol) monomethyl ether, X represents H, F, or Cl, and Y represents O, S, or Se.

These molecules are designed so that they serve as the binding receptor and the sensing element. We are then able to tune the structure of the core molecule, thereby adjusting the metal-binding activity, as well as the optical properties. In Figure 1, the series of molecules on the left is tunable through halogen substitution of the phenazine core. On the right, variation of the chalcogen heteroatom serves the same purpose. Increasing understanding of this kind of structure-property relationship is vital for the future construction of highly sensitive and selective fluorescent sensors.

The results show that of the phenazine-containing compounds, those that are more electron-poor (halogen-substituted) are not able to efficiently bind metal ions in aqueous solution. A similar effect is seen with the benzochalcogendiazole compounds, with binding affinity increasing moving down the group, parallel to the decreasing electronegativity of the chalcogen atom. The

heteroaromatic core also plays a significant role in the selectivity; the phenazine compound functions as a selective silver sensor, while the benzochalcogendiazole compounds respond to copper, silver, and nickel. The response to each metal is unique, and statistical analysis of the resulting data enables differentiation of these three metals with a single molecule.

2. Kurzzusammenfassung

Im Rahmen dieser Arbeit wurden neuartige Fluorophore synthetisiert und charakterisiert und im Hinblick auf ihre Metall-bindnende Eigenschaften untersucht. Das Bauprinzip dieser Fluorophore bestehen hierbei aus einem heteroaromatischen Kern und zwei Triazoleinheiten, die *via* Kupfer-katalyisierter Cycloaddition an den Kern substituiert wurden (Abbildung 1). Die Bindung eines Metallions entsteht durch die Koordination zwischen einem Triazolring-Stickstoffatom und einem Stickstoffatom des heteroaromatischen Kerns. Aus praktischen Gründen sollen diese Sensoren zudem Wasserlöslichkeit besitzen. Dies wird durch die Verwendung wasserlöslicher oligoethylenglykol Seitenketten erreicht. Diese sperrigen Seitenketten verringern die Aggregation und somit die Fluoreszenzlöschung, wodurch selbst im Wässrigen helle Fluoreszenz entsteht.

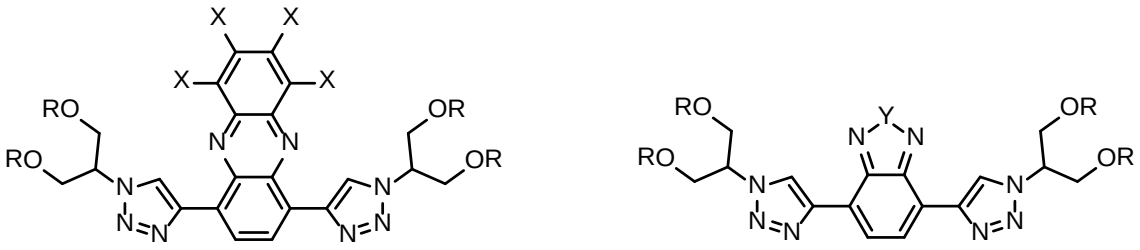

Abbildung 1 Metallionensensoren. R = tri(ethylenglycol)monomethylether; X = H, F oder Cl; Y = O, S oder Se.

Diese Moleküle sind so konstruiert, dass sie sowohl als bindender Rezeptor als auch als „sensing element“ dienen. Somit sind wir in der Lage die Struktur des aromatischen Kerns abzustimmen, um dadurch die Metallbindungs-Eigenschaften, sowie die optischen Eigenschaften zu beeinflussen. Die in Abbildung 2 dargestellten Phenazin-Derivate (links) können durch Halogensubstitution des Kerns beeinflusst werden. Die Chalkogendiazole (rechts) werden hingegen durch Variation des Heteroatoms in ihren optischen Eigenschaften variiert. Das Verständnis dieser Art von Struktur-Eigenschafts-Beziehung ist von entscheidender Bedeutung für die Konstruktion von hochempfindlichen und selektiven Fluoreszenz-Sensoren

Die Ergebnisse zeigen, dass die elektronenarmen, halogensubstituierten Phenazin-Derivate, nicht in der Lage sind, Metallionen in wässriger Lösung effizient zu binden. Ein analoger Trend ist für die Benzochalcogendiazole zu beobachten. Bei dieser Verbindungsklasse nimmt die

Bindungsaffinität, ausgehend vom elektronegativeren Sauerstoff-Derivat hin zum Selen-Derivat, zu. Der heteroaromatische Kern nimmt zudem eine entscheidende Rolle bezüglich der Selektivität ein. So dient die unsubstituierte Phenazin-Verbindung als selektiver Silberatom-Sensor, wohingegen die Benzochalcogendiazole auf Kupfer, Silber und Nickel ansprechen.

Die Reaktion auf jedes dieser Metalle ist einzigartig und die statistische Analyse der Messdaten ermöglicht die Differenzierung dieser drei Metalle nebeneinander durch Detektion mit einer einzigen Verbindung.

3 Introduction

From ores to ions to alloys, metals are ubiquitous in nature and technology. Metal ions play an important role in the body, participating in many biological processes.[1] Iron is an integral part of the hemoglobin protein, which is responsible for oxygen transport in the blood. Copper is a cofactor for cytochrome c oxidase, acting as an electron transfer mediator for the synthesis of adenosine triphosphate (ATP). Many other metals, including zinc, nickel, magnesium, calcium, and potassium, are found in the body and play important roles in metabolism, DNA polymerization, and cell signaling.

These same metals, necessary as they are, can also be cytotoxic at higher concentrations. Other non-essential metals such as mercury, arsenic, and lead are toxic even at very low concentrations. Iron and copper have been shown to generate reactive oxygen species (ROS), which may result in oxidative damage to DNA and tissue (Figure 2).[2]

$$\mathrm{Fe(III)} + \mathrm{O_2^{\cdot -}} \rightarrow \mathrm{Fe(II)} + \mathrm{O_2}$$

$$\mathrm{Fe(II)} + \mathrm{H_2O_2} \rightarrow \mathrm{Fe(III)} + \mathrm{^{\cdot}OH} + \mathrm{^{-}OH}$$

$$\mathrm{Cu(II)} + \mathrm{O_2^{\cdot -}} \rightarrow \mathrm{Cu(I)} + \mathrm{O_2}$$

$$\mathrm{Cu(I)} + \mathrm{H_2O_2} \rightarrow \mathrm{Cu(II)} + \mathrm{^{\cdot}OH} + \mathrm{^{-}OH}$$

Figure 2 Formation of hydroxyl radical catalyzed by iron (Fenton reaction) and copper.

Lead, nickel, cadmium, and chromium are all very popular metals in industry, finding use in paint, metal finishing, and alloys of aluminum and steel. The carcinogenic and toxic properties of these metals are well-known. Their popularity in industry creates a large amount of toxic waste. Even households are capable of generating hazardous waste from batteries, electronic equipment, and chemicals. It is difficult to accurately assess the accumulation of metals in the environment from anthropogenic sources. However, one report from 1988 provides estimates (in thousand tons $\mathrm{year^{-1}}$ of terrestrial plus aquatic addition minus atmospheric emissions) of 120 for As, 30 for Cd, 2150 for Cu, 470 for Ni, 1160 for Pb, and 2340 for Zn.[3] We may be sure that 25 year-old

numbers are inaccurate, but we can be equally sure that the current numbers are large, considering that nearly every industry produces some sort of metal byproduct.

This prevalence of metal ions in the environment and in biological systems has spurred great interest in their detection and quantification.[4] We must have sensitive methods capable of detecting trace quantities of toxic metals. Ideally, these sensors would be robust, easy to use, reliable, and inexpensive. Traditional methods such as atomic absorption spectroscopy and mass spectrometry are elaborate and time consuming; fluorescence spectroscopy has recently emerged as a simple and versatile alternative.[5-9] Its sensitivity and quantitative nature make it a particularly attractive method for both biological systems and wastewater streams.

One of the highlights of using conjugated organic molecules is their versatility. Organic fluorophores can be tailored to exhibit a response to not only metals,[4] but also ionic species[10] and biologically relevant molecules (DNA,[11-13] sugars,[14-16] proteins,[17-19] bacteria[20-22]). For biological applications, the potential for fluorescent *in vivo* imaging is particularly promising.[5] The sensitivity allows imaging on a single-cell level,[23] and fluorescence microscopy can be utilized for deep-tissue and intracellular imaging.[24,25] Application of these techniques may contribute to our further understanding of the action of metal ions in the body.

4 Background

4.1 Fluorescence Spectroscopy as a Sensory Tool

The previous section made some mention of the potential for fluorescence-based sensors. The design and application of these systems requires an understanding of the interactions that may occur between a fluorophore and a target analyte, and how these interactions may be exploited for detection purposes. In the fluorescence process, the first step is the absorption of light. This raises the energy of an electron to an excited electronic state, as shown in Figure 3. The excited electron (exciton) quickly relaxes to the lowest vibrational level of the first excited state (S_1). Emission of light may then be seen upon relaxation of the exciton to the ground state (fluorescence). This relaxation may also occur without emission of light. Alternatively, the exciton may undergo intersystem crossing to the triplet state, from which no fluorescence will be seen. Such a system is quite complex, and there are innumerable ways for a target analyte to interact with and change its properties. As such, imagination is the limit for sensing schemes utilizing fluorescence. In this section, we will only briefly touch on some of the more common methods of detection.

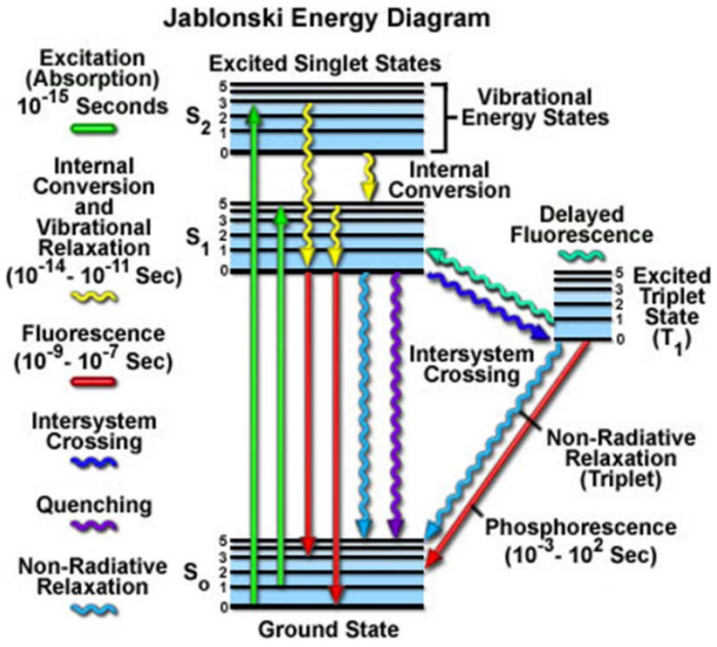

Figure 3 Jablonski diagram showing the excitation of a photon, and its possible relaxation pathways (taken from the Olympus microscopy resource center, www.olympusmicro.com).

4.1.1 Fluorescent Labeling

Fluorescent labeling is a technique used to image a target analyte. The binding site, or receptor, is covalently attached to the fluorophore so that upon binding of the analyte, there is no interaction with the fluorophore. This labeled target can then be visualized using fluorescence techniques. This may be useful for biological imaging purposes. Seeberger *et al.* used a poly(phenyleneethynylene) (PPE) functionalized with mannose groups to fluorescently label *E. coli* through binding of the sugar.[26] Figure 4 shows an example of this technique being used for *in vivo* imaging with a folate-functionalized PPE by Kim and Bunz.[27] Cancer cells overexpress folate receptors on their surface, which bind the fluorescent PPE, allowing for imaging of the cells.

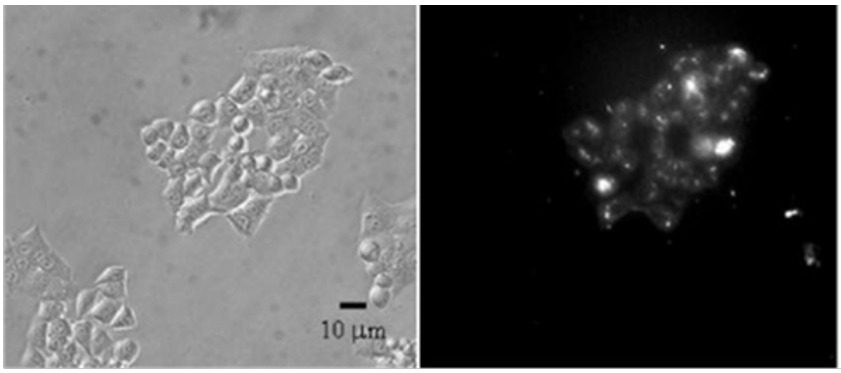

Figure 4 Fluorescence microscopy images of cancer cells after staining with a fluorescent polymer: (*left*) transmittance images and (*right*) fluorescence images (taken from *Bioconjugate Chem.* **2007**, *18*, 815).

4.1.2 Fluorescence Quenching

Fluorescence quenching commonly results from interaction with a target analyte. This may proceed through a number of different mechanisms, a couple of which are shown in Figure 5.[28] These processes are not mutually exclusive, and must be taken into account when considering any fluorescent response. Dynamic quenching occurs via the Dexter mechanism, when an excited fluorophore collides with another species. Because this collisional quenching is random, it is typically not useful for sensing purposes. Fluorescence resonance energy transfer (FRET) is a through-space interaction which involves non-radiative transfer of the exciton to a nearby chromophore. The proximity of the fluorophore and chromophore is important here – FRET is

typically most efficient at distances of 2-6 nm. A third possible quenching mechanism is photoinduced electron transfer (PET), where quenching occurs through a donor-acceptor interaction. In the PET process, the excited fluorophore may play the role of donor or acceptor. Many times, fluorescence quenching occurs as a result of multiple processes, and the few that are mentioned here do not comprise a comprehensive list. This can cause difficulty when interpreting quenching in response to an analyte.

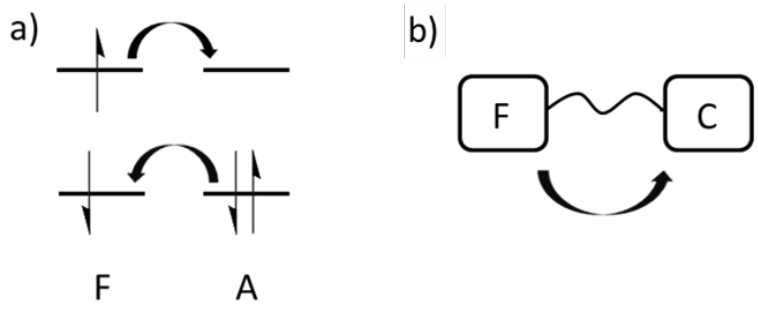

Figure 5 Pictorial representations of some common fluorescence quenching mechanisms. (a) Dexter mechanism, with electron transfer from the LUMO of the fluorophore (F) to the LUMO of the acceptor (A), and also from the HOMO of A to the HOMO of F. (b) FRET quenching, where the fluorophore (F) and the chromophore (C) are bound together. The energy transfer results in the relaxation of F, and the excitation of C.

Figure 6 illustrates an experiment from Bunz and coworkers on the interaction of a fluorescent PPE with the protein concanavalin A (Con A).[29] The polymer is functionalized with mannose groups. The affinity of Con A for mannose leads to binding of the polymer to the protein. This example shows the care that must be exercised when evaluating a quenching response, as the analyte may not be solely responsible. The quenching mechanism in this case is not clearly identifiable, as Con A contains no obvious candidates to induce PET. Further experiments varying the concentration of the PPE show that the quenching response is due to inter-molecular aggregation between polymer chains on the surface of the protein. This aggregation-induced quenching phenomenon is well-known, and quite common among aromatic molecules.[30]

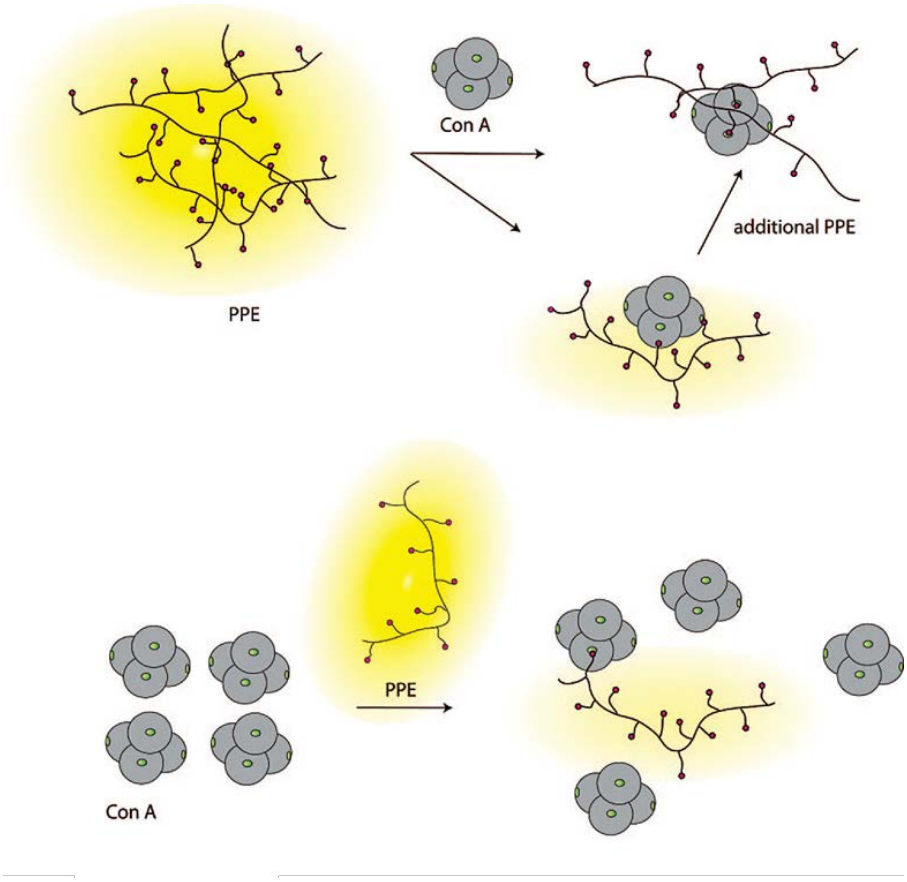

Figure 6 Fluorescent detection of Con A by a mannose-functionalized PPE (taken from *Macromolecules* **2008**, *41*, 7316).

4.1.3 Fluorescence Turn-On

Exactly the opposite of a quenching mechanism, a fluorescence turn-on sensor measures the increase in the fluorescent signal to detect the presence of an analyte. The obvious advantage of this technique over fluorescence quenching is that the latter may be caused by a number of non-specific interactions. An example of a fluorescent turn-on sensor for bacteria from Bunz and Rotello is shown in Figure 7.[22] Initially, fluorescent PPEs are electrostatically bound to positively charged gold nanoparticles (NPs). These complexes are non-emissive due to the superquenching ability of gold NPs.[31] In the presence of bacteria, the nanoparticles preferentially bind to the cell surface, releasing the polymer, and restoring its fluorescence.

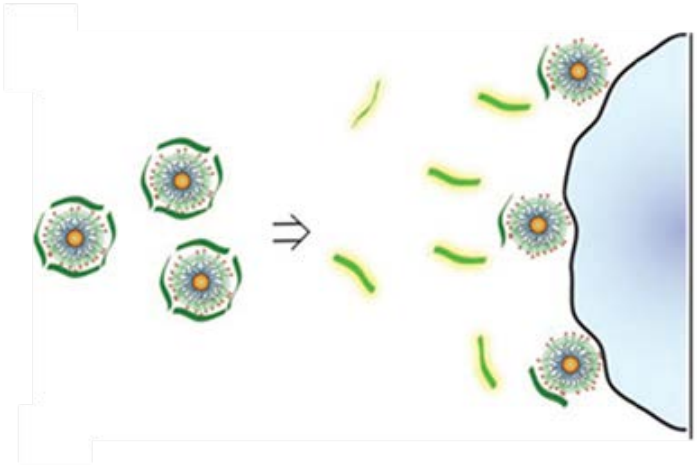

Figure 7 Depiction of NP-PPE complexes and their interaction with bacteria (taken from *Angew. Chem., Int. Ed.* **2008**, *47*, 2590).

Another way that emission may be enhanced is through aggregation. As previously mentioned, aromatic fluorescent molecules, due to their inherently planar nature, are often susceptible to quenching through the formation of pi-stacked aggregates. In 2001, Tang and coworkers demonstrated that aggregation can also induce luminescence, coining the term 'aggregation-induced emission' (AIE).[32] Figure 8 shows a couple of compounds that exhibit this phenomenon. 1-Methyl-1,2,3,4,5-pentaphenylsilole (**1**) is non-emissive in solution, and highly emissive in the solid state. Forced aggregation of this compound in solution also results in a turn-on of the fluorescence. The phenyl rings of **1** in solution are twisted so far out of planarity that there is essentially no conjugation. Upon aggregation, the phenyl rings are forced closer to planarity, so that there is some effective conjugation, yet not enough to allow for efficient pi-stacking.[33] The pi-orbital overlap is a function of the cosine of the torsion angle; sufficient conjugation exists even at twist angles of 23˚, which is typical for polyphenylenes.[34] Tang further demonstrated the biosensory possibilities of AIE with a cationic tetraphenylethene (**2**). This non-emissive molecule aggregates onto bovine serum albumin (BSA) and calf thymus DNA, leading to a fluorescence turn-on.[35]

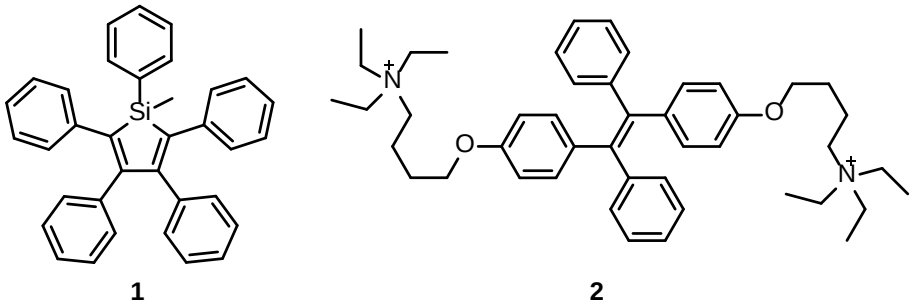

Figure 8 1-Methyl-1,2,3,4,5-pentaphenylsilole (**1**) and a tetraphenylethene derivative (**2**).

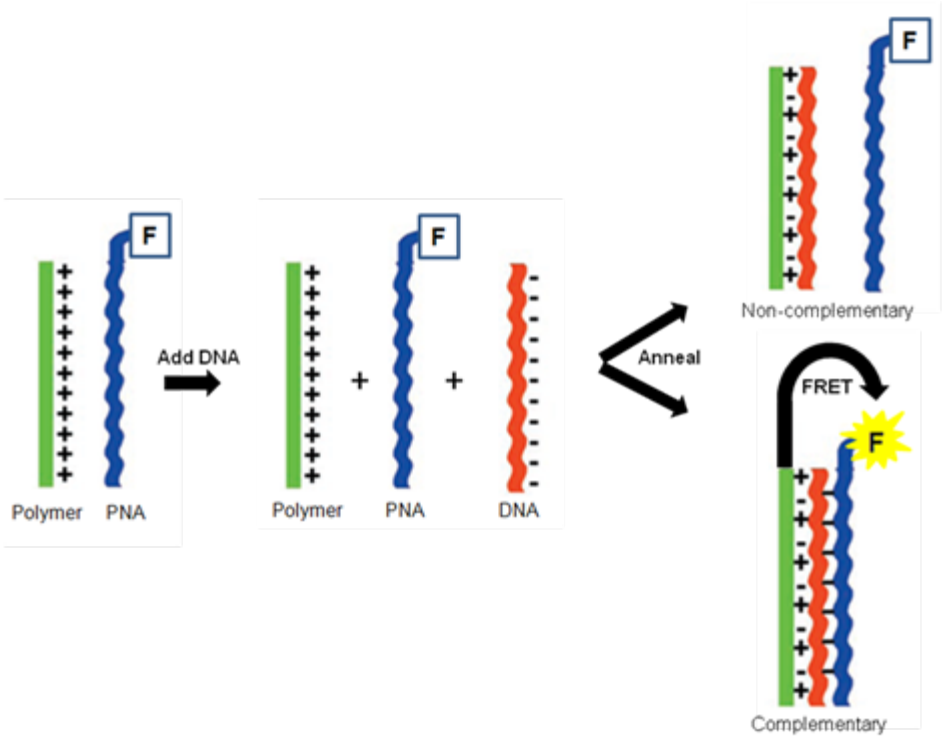

Figure 9 Representation of Bazan's DNA sensor (adapted from *Proc. Nat. Acad. Sci. USA* **2002**, *99*, 10954).

FRET provides yet another method of turn-on sensing. A very popular example of FRET is the cyan fluorescent protein (CFP) in the proximity of the yellow fluorescent protein (YFP). In this case, both species are fluorescent, and upon energy transfer from CFP to YFP, the fluorescent signal from CFP is diminished in favor of the new signal from YFP. Bazan and coworkers

utilized FRET to detect single-stranded DNA (Figure 9).[36] This involves a cationic fluorescent polymer and a peptide nucleic acid (PNA) strand functionalized with fluorescein. The cationic polymer is electrostatically bound to anionic DNA. Only if it is complementary to the PNA strand is the fluorescein brought close enough for FRET to occur. The presence of the specific sequence of DNA is revealed by the increased emission from the fluorescein.

4.1.4 Ratiometric Sensing

A FRET sensor may also be described as ratiometric. This refers to a wavelength shift in the emission maximum upon exposure to an analyte. In the example shown in Figure 9, the response to a complementary sequence of DNA is a turn-on of the emission from fluorescein, accompanied by a quenching of the polymer's emission. The emission becomes dominated by the fluorescein, thus the wavelength of the emission maximum has shifted from that of the polymer, to that of the fluorescein. Figure 10 shows a ratiometric zinc sensor from the Bunz lab in action;[37] the fluorescence changes upon exposure to zinc ion, and again in the presence of an excess amount of zinc.

Figure 10 A picture showing the fluorescence response of cruciform **3** in chloroform (left), after addition of a small amount of zinc (middle), and after addition of an excess of zinc (right) (adapted from *Acc. Chem. Res.* **2010**, *43*, 397).

The explanation for this behavior is found by looking at the mechanism of fluorescence. Relaxation from the first excited singlet state (S_1) to the ground state (S_0) typically involves the relaxation of an electron from the LUMO to the HOMO. When this relaxation process is

accompanied by emission of light, the energy of that light is equal to the energy difference between the two orbitals. Therefore, any changes in the energies of these orbitals will result in a change in the energy (or wavelength) of the emitted photon (provided that emission still occurs). With compound **3**, there are two non-equivalent binding sites for Zn^{2+}, thus two separate binding events. Each of these events affects the energy of the frontier molecular orbitals, thus shifting the optical properties. This process is summarized qualitatively in Figure 11. Binding at the first site stabilizes the HOMO (localized predominantly on the styryl axis) and the second binding event stabilizes the LUMO (localized on the ethynyl axis). Thus, two separate changes are observed in the wavelength of emission maximum, corresponding to the two separate binding events.

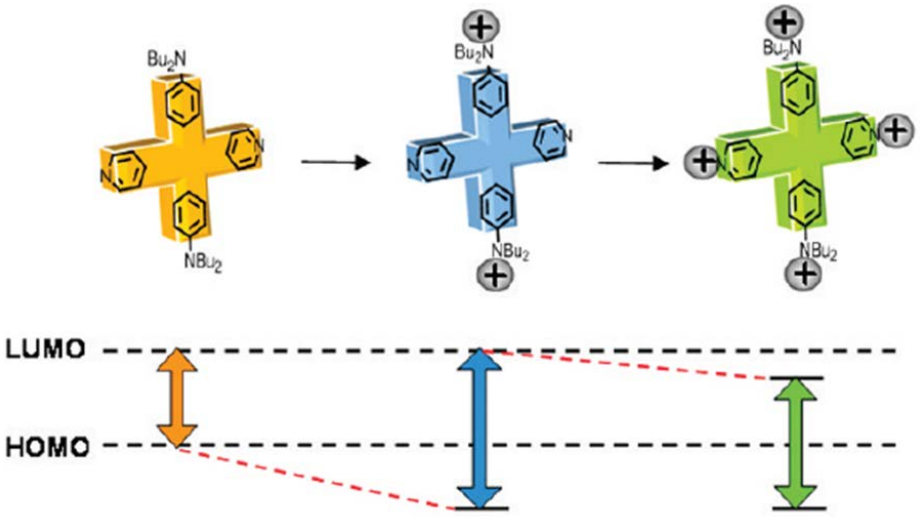

Figure 11 Representation of the effect of Zn^{2+} binding on the frontier molecular orbitals of **3** (taken from *Acc. Chem. Res.* **2010**, *43*, 397).

4.2 Fluorescent Sensors for Metal Ion Detection

When applying the previously discussed detection methods to metal ions, there are some design considerations for the synthesis of the fluorescent materials. In order to avoid the issue of non-specific interactions, the goal is to design molecules capable of forming metal-fluorophore complexes. If the sensors are such that the metal-binding unit and the fluorescent unit are one and the same, then the presence of metal ions may be deduced by measuring and quantifying the complex formation through spectrophotometric means. In this section, the important components of such metal ion sensors are detailed.

4.2.1 Water-Solubility

The first design consideration is water-solubility. For biological or environmental purposes, practical application demands performance in aqueous media. Recent years have seen the development of a large number of fluorescent sensors for metal ions, incorporating small molecules[38-43] and polymeric systems.[44-46] One shortcoming of many of these fluorescent sensors is their limited solubility in water. This results in metal ion detection being undertaken in organic solvent, or a mixture of water and organic solvent (such as THF or DMF). This less than optimal compromise emphasizes how water-solubility remains one of the dominant challenges for fluorescent sensors.

Functionalization of an aromatic molecule with water-soluble substituents is a common method for bringing fluorophores into water. Organic functionalities that bear charges, such as cationic ammonium groups or anionic carboxylate and sulfonate groups, are very popular. To avoid the use of ionic species, which can be sensitive to changes in pH or ionic strength, or may exhibit unwanted interactions, hydrophilic groups such as sugars and ethylene glycol can be employed.

Oligo(ethylene glycol) chains are frequently found in the literature for a number of reasons. They are inexpensive and easy to obtain, water-soluble, unreactive under most conditions (biological conditions, notably), and biocompatible. These traits result in oligo(ethylene glycol) chains of all sizes being used for biological applications – as linkers or spacers, to provide solubility, and to prevent non-specific interactions.[47-50] Some simple chemistry leads us to branched or dendritic ethylene glycol chains, which have been shown to inhibit aggregation in solution, thereby

reducing fluorescence quenching in water.[51,52] The simplest branched ethylene glycol molecule (which we term the 'swallowtail') can be synthesized by the addition of two tri(ethylene glycol) (TEG) chains to epichlorohydrin (Scheme 1). In this work, both of these ethylene glycol chains (**12** and **15**) are used as substituents to provide solubility in water. The structures shown later often abbreviate the tri(ethylene glycol) chain as TEG (**12** = TEGOH) and the swallowtail side chain as SW (**15** = SWOH).

Scheme 1 Synthesis of the Swallowtail Compound

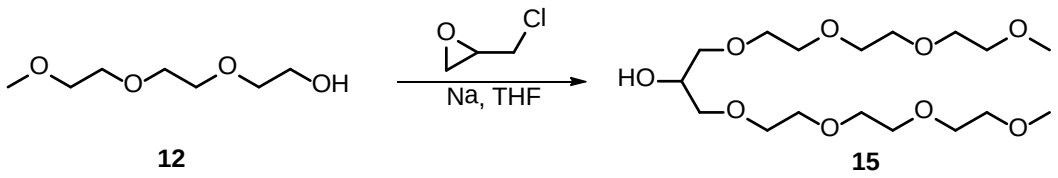

12 **15**

4.2.2 Metal-Binding Fluorophores

The other requirement is that these sensors are able to form complexes with metal ions. Therefore, we must synthesize fluorophores that are capable of coordinating metals. Free electron pairs often prove to be effective. Thus, there are many examples of nitrogen, phosphorus, oxygen, and sulfur atoms participating in metal-binding. Zhu and Qian *et al*. reported a crown ether derivative (**4**) capable of binding mercury and silver ions. A similar strategy was employed by Qian and Jian, *et al*. for their selective silver ion sensor (**5**).

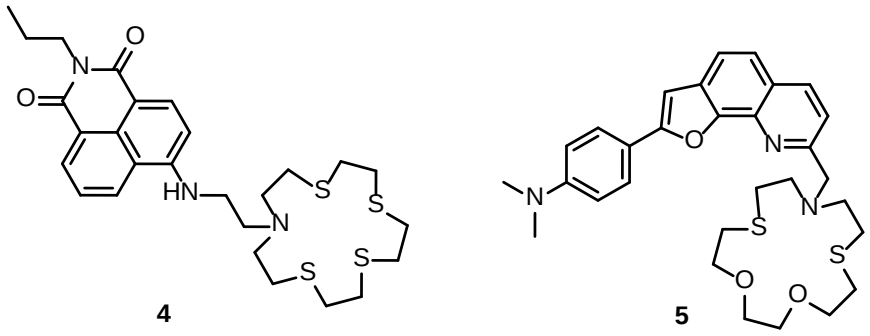

4 **5**

Figure 12 Metal ion binding crown ether derivatives.

Nitrogen is well-known for its metal-coordinating ability. For the purposes of fluorescent sensing, heteroaromatic nitrogen-containing ligands can be particularly useful. There are many

examples of metal ions being coordinated by such heteroaromatic groups.[53-56] Akkaya and coworkers used functionalized BODIPY dye **6** as a zinc sensor,[57] where the metal ion is coordinated in part by the pyridine rings present. Wong and Wong *et al*. reported pyrrole-containing compound **7** as a sensor for silver ions.[58]

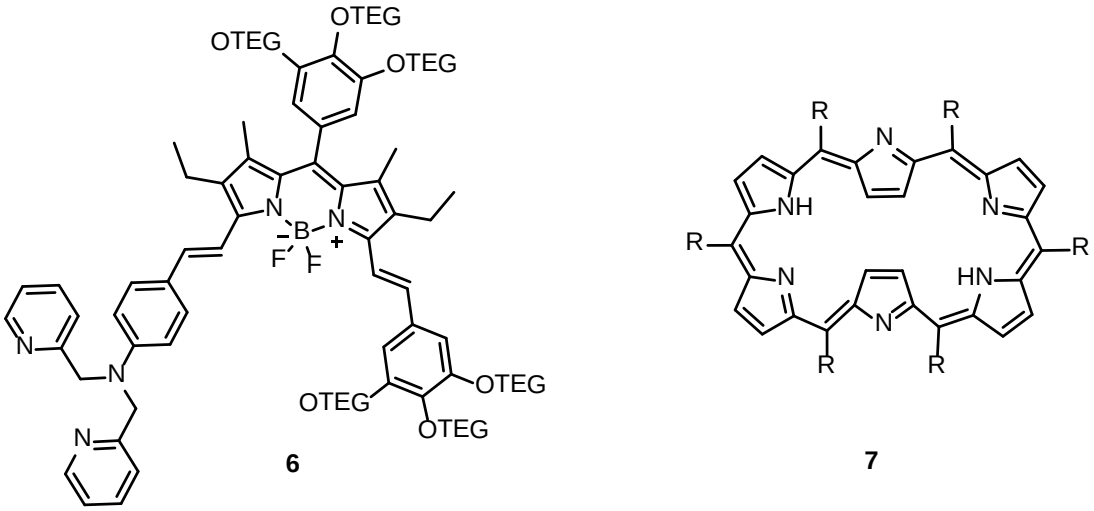

Figure 13 Representative fluorescent sensors with nitrogen-containing ligands. R represents pentafluorophenyl.

A popular theme found in all of these examples is cooperativity. Multiple atoms capable of donating electron density are present in each of these compounds. A couple of prime examples of this type of cooperative binding are porphyrins, which feature four pyrrole rings capable of coordinating metal ions,[59,60] and terpyridine, which has been used in the synthesis of stable metallo-polymers.[61-63] The work presented in this thesis utilizes these same concepts; heteroaromatic compounds with known metal-binding capabilities are functionalized with nitrogen-rich triazole rings to achieve compounds suitable for cooperative binding of metal ions.

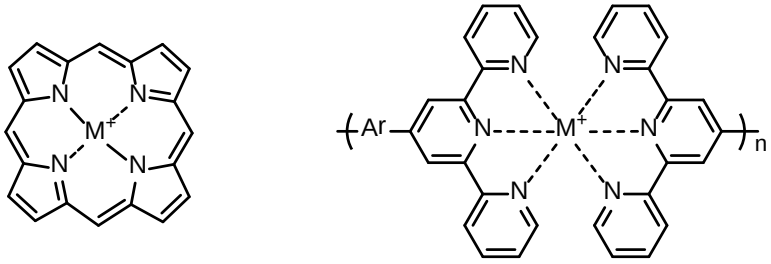

Figure 14 A metal-binding porphyrin (left) and a terpyridine-containing metallo-polymer (right).

4.3 1,2,3-Triazole

Triazole refers to a five-membered heteroaromatic ring containing three nitrogen atoms. There are two possibilities: 1,2,4-triazole, which may serve as a metal ligand[64] or antifungal agent,[65] and 1,2,3-triazole, which is the focus of this work.

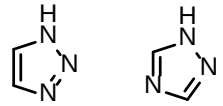

Figure 15 Triazole rings. 1,2,3-triazole (left) and 1,2,4-triazole (right).

4.3.1 Synthesis

Substituted 1,2,3-triazoles are easily reached through the cycloaddition of an azide and an alkyne. This reaction has long been known; the first reported example was published by Michael in 1893.[66] Huisgen and coworkers later studied this reaction in greater detail.[67,68] Huisgen's thermally activated reaction suffers from low rates of reaction and a lack of regioselectivity; the two possible 1,4- and 1,5- triazole products are shown in Figure 16. The independent discovery in 2002 of copper as a catalyst by the groups of Meldal[69] and Sharpless[70] greatly increased the utility of this reaction. Its application has increased tremendously since then,[71] appearing in bioconjugation,[72] polymer and materials chemistry,[73-79] and organic synthesis.[80]

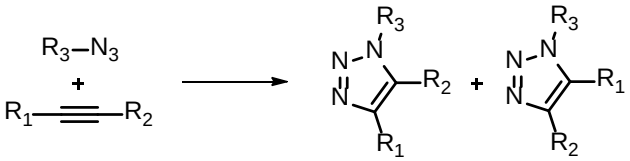

Figure 16 Products of the thermal azide-alkyne cycloaddition.

The copper catalyst increases the reaction rate by a factor of 10^7, and also enables the cycloaddition to be run at room temperature. This copper-catalyzed azide-alkyne cycloaddition (CuAAC) is tolerant of substituents on the triazole or alkyne, though the formation (and necessity) of a copper acetylide intermediate restricts this reaction to terminal alkynes. The reaction is also not solvent-sensitive, running smoothly in protic or aprotic solvents, including water.[81] These characteristics qualify the CuAAC as one example of 'click' chemistry, a term

Sharpless coined in 2001 to describe reactions that are modular, wide in scope, with very high yields.[82] Also, a 'click' reaction should generate only inoffensive, easily removed byproducts, and be stereospecific, involving simple reaction conditions and product isolation.

Copper catalyzes this cycloaddition only in its +1 oxidation state. Even so, many sources of copper have been used, including metal turnings, copper salts such as CuI and $Cu(OAc)_2$, and other ligated copper species.[79] Addition of a Cu^{2+} salt requires the concomitant addition of a reducing agent, such as sodium ascorbate. The aqueous $CuSO_4$/ascorbate catalyst system introduced by Sharpless and coworkers[70] has become standard operating procedure due to its efficiency and ease of use (no deoxygenation required).

Figure 17 shows a proposed mechanism for the CuAAC. The exact mechanism is unknown, and the scheme below is oversimplified. Kinetic investigations into the reaction mechanism indicate a second-order dependence on catalyst. It is clear that the reaction proceeds through copper acetylide intermediates, but the exact nature of these complexes is difficult to elucidate.[81]

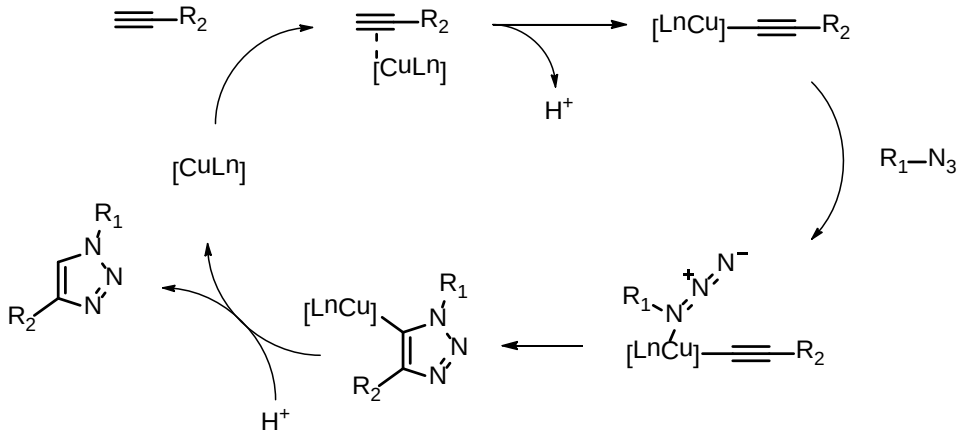

Figure 17 Proposed mechanism of the CuAAC.

4.3.2 Function

There are a number of attractive aspects of the triazole ring. Its chemical stability and ease of synthesis have made it a powerful synthetic tool.[83] The bioorthogonality of this reaction has led to its popularity as a linker for biomolecules.[84] Naturally, the nitrogen-rich triazole is capable of

acting as a hydrogen bond acceptor. In addition, the polarity of the ring allows it to function as a hydrogen bond donor.[85]

For our purposes, we incorporate the triazole so that it will participate in the cooperative binding of metal ions. Triazole has long been known to possess metal-coordinating ability.[64,86] It is only more recently that this function is being put to use in fluorescent sensors.[87] The first reports utilizing the metal-binding function of triazole involve calixarene-based probes **8** and **9**.[88,89] Reinaud's calix[6]arene features the triazole participating in the conjugation of the system, though the probe is non-fluorescent. Bunz and coworkers extended this concept of triazole being an active participant in metal binding, as well as the conjugation.[90] These experiments show that the conjugation of aromatic molecules is extended to the triazole substituents, affecting the electronic properties (auxochromic effect),[91] and also maintaining the fluorescence of the system.

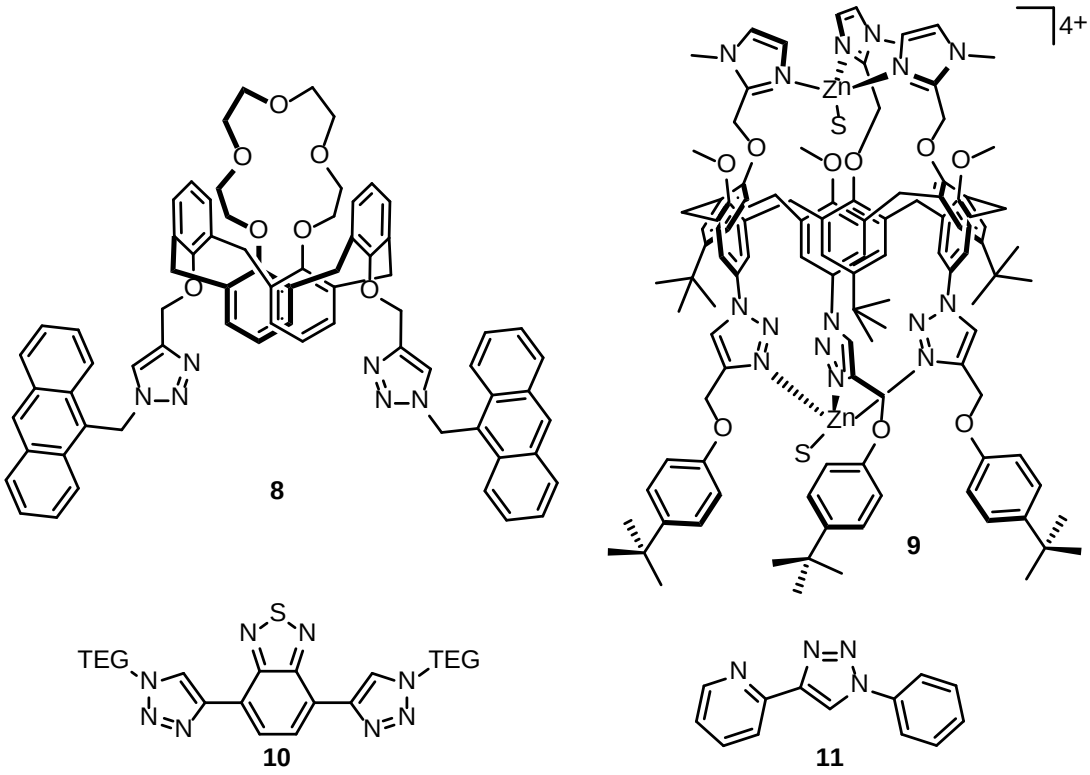

Figure 18 (*top-left*) A calix[4]arene derivative from Chung *et al.* for the fluorescent detection of Pb^{2+}. (*top-right*) A calix[6]arene derivative from Reinaud *et al.* capable of binding Zn^{2+}. (*bottom*) Metal ion sensors from Bunz and coworkers where the triazole exhibits an auxochromic effect.

4.4 Synthesis of Metal-Binding Fluorophores

The triazole ring, as mentioned in the previous section, is very useful as a linker. In the compounds presented here, this function is exploited to link water-soluble oligo(ethylene glycol) side chains to the fluorescent core (Figure 19). In this manner, the triazole ring contributes to the emissive properties of the metal sensor, as well as providing convenient access to water-soluble compounds. The desire for cooperative binding between the triazole and the fluorophore prompts the use of heteroaromatic groups which may show, or have previously shown, metal-binding activity. Here, phenazine and benzochalcogendiazole compounds are used. Not only are these compounds promising for metal-binding, but their synthesis allows for variation of their molecular structure. The interesting question here is how this affects the metal-binding activity. Examples have been given in the previous section with different size binding cavities and different heteroatoms for binding metals. These techniques can be used to adjust the metal-binding properties. The synthesis presented herein allows inquiry into the effect of more subtle variations, such as a change in the electronic properties of the system, or a different neighboring atom.

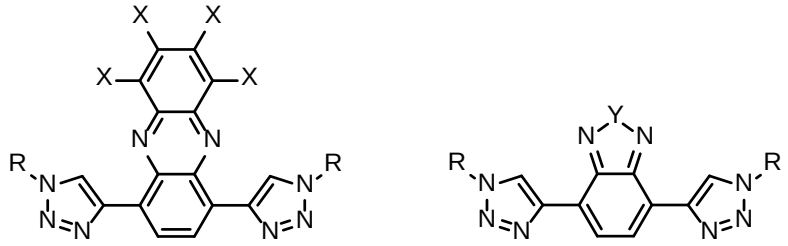

Figure 19 Proposed metal binding fluorophores. R is a solubilizing oligo(ethylene glycol) group. (*left*) Phenazine cycloadducts, where X represents H, F, or Cl. (*right*) Benzochalcogendiazole cycloadducts, where Y represents O, S, or Se.

The target cycloadducts in Figure 19 are shown in what may be termed the ‘anti’ conformation. The bond bridging the triazole to the heteroaromatic core is free to rotate – shown here is the rotamer which maximizes the available hydrogen bonds. For cooperative metal binding to take place, the less stable rotamer, the ‘syn’ conformation, is required. The fact that these rings are free to rotate means that different size binding pockets may be formed. The stability of the different conformers may dictate some selectivity with these fluorescent sensors. Though the

rotamer required to create the binding pocket is less stable, there is no fear that it will not form. Earlier work from Hecht *et al.* on 2,6-bis-triazol-4-yl pyridine compounds shows that the the conformation may be switched through binding of metal ions[92] or even protonation of the triazole ring.[93] This highlights one further benefit of these sensors where the conjugation extends through the triazole ring: we may be able to observe the conformational switching in response to a metal ion with spectrophotometric methods.

4.4.1 Phenazines

Phenazines possess attractive electronic properties and biological activity. The redox properties of phenazine and its derivatives have garnered some interest, finding use in biofuel cells,[94] solar cells,[95] and OLEDs,[96-98] but an even more attractive aspect of phenazines is their role in biochemistry. They are biosynthesized by bacteria and many possess broad-spectrum antifungal and antibiotic activity,[99-101] as well as the capacity for DNA intercalation (leading to cell death).[102,103] Biosensing schemes involving water-soluble phenazine-based dyes include electrochemical detection of biological molecules[104,105] and colorimetric pH sensing.[106] When it comes to metal ions, bare phenazine has demonstrated the ability to bind silver,[107] and peralkynylated phenazine has also displayed an affinity for binding metals.[108]

The planned phenazine cycloadducts are envisioned to be formed in the final step through a CuAAC. The plan is to link phenazine to oligo(ethylene glycol) with this click reaction. The question is, which moiety should bear the alkyne, and which the azide? If we first disregard any synthetic considerations, the end product shown in Scheme 2 places the triazole in such a way that cooperative binding will occur between the phenazine nitrogen and the N3 of the triazole, as opposed to the N2 (the two options are shown in Figure 20). As noted by Schibli in his ‘click to chelate’ report, binding at the N3 is more efficient, probably due to its increased electron density.[109] The electron density at the N3 is evident from the available resonance structure (Figure 21). This connectivity requires the heteroaromatic core to be ethynylated, and the hydrophilic group to bear the azide. Previous reports from the Bunz lab indicate that these starting materials are easily accessible.[108,110]

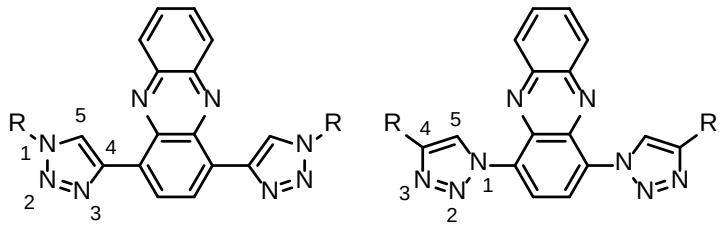

Figure 20 Phenazine cycloadducts with triazol-4-yl (left) and triazol-1-yl (right) substituents.

Scheme 2 Retrosynthesis of Phenazine Cycloadducts

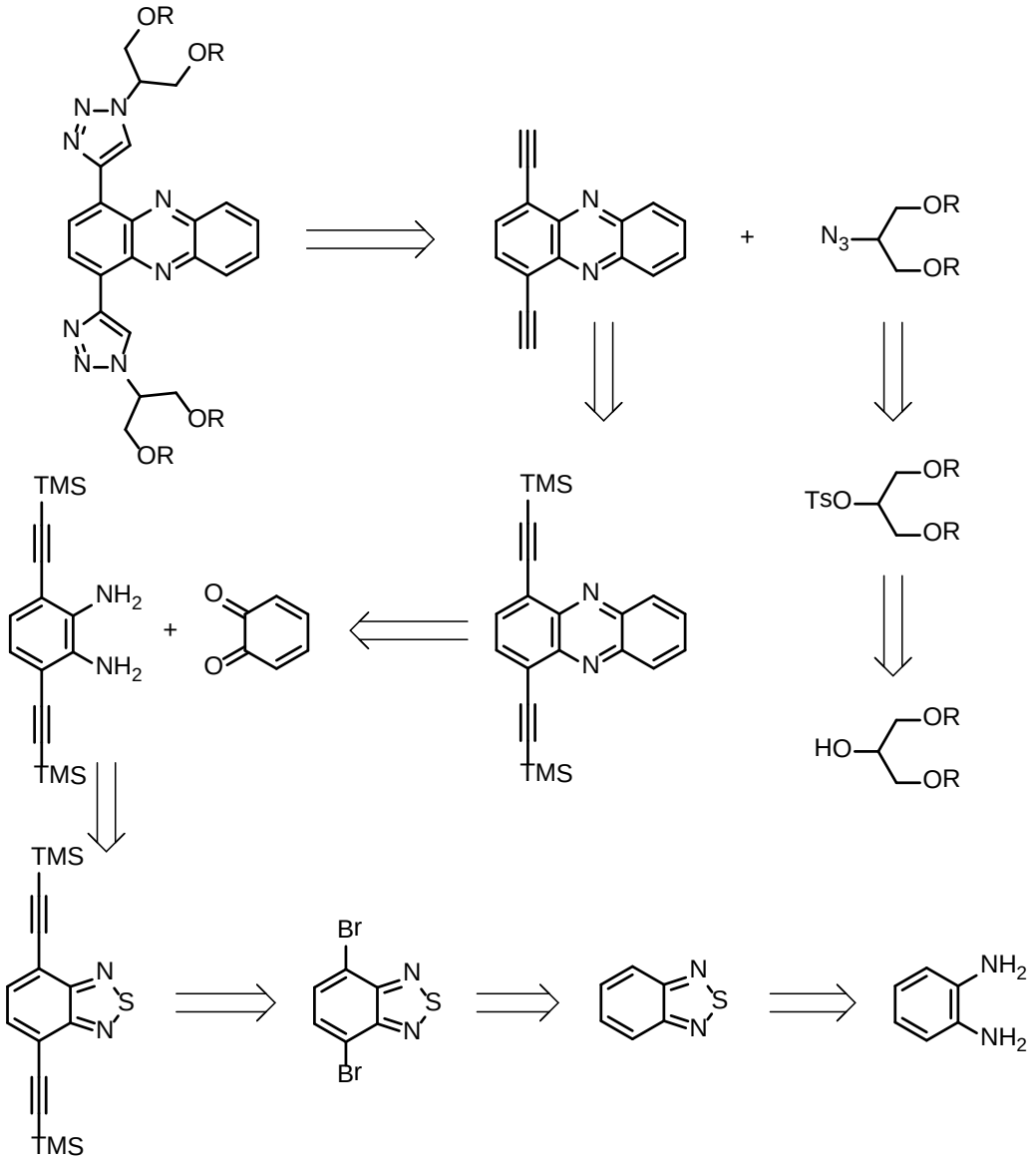

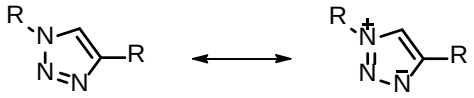

Figure 21 Resonance structures of 1,2,3-triazole.

For the synthesis of the phenazine component, a condensation between benzenediamine and *ortho*-benzoquinone may be utilized. For the question of when and where to introduce the protected ethynyl group, the TIPS-protected 3,6-diethynylbenzenediamine is known from our lab,[111] and only very slight modification is required to give the TMS-protected congener.

It is with the *ortho*-benzoquinone compound that the opportunity arises to craft a series of phenazines with variable electronic properties. Tetrachloro- and tetrabromo-substituted *ortho*-benzoquinones are commercially available. The tetrafluoro-*ortho*-benzoquinone can be synthesized from pentafluorophenol using a known procedure,[112] and the unsubstituted *ortho*-benzoquinone can be made *in situ* via oxidation of catechol.

The azide component may be constructed from alcohol through the tosylated intermediate. This is the same procedure used previously to synthesis TEG azide from TEGOH.[110]

4.4.2 Benzochalcogendiazoles

Of the benzochalcogendiazole compounds, the most commonly encountered is benzothiadiazole. This electron-deficient molecule is a common precursor for the construction of N-heteroacenes,[113] and is popular in donor-acceptor polymers for organic electronic applications.[114] There are also some examples in the literature of benzothiadiazole being used in fluorescent sensing applications.[19,40] The oxygen and selenium congeners are less commonly studied, though selenophene and benzoselenadiazole have attracted some interest as possible components in low-band-gap materials.[115-118]

The synthetic plan is much the same as before, with the final step being the CuAAC (Scheme 3). The only change here is to the ethynylated species. Variability of the electronic properties and molecular architecture is introduced through the use of different chalcogen heteroatoms. Previous work from the Bunz lab has shown the dependence of the optical properties of alkynylated benzochalcogendiazoles on the chalcogen atom present.[111]

Scheme 3 Retrosynthesis of Benzochalcogendiazoles

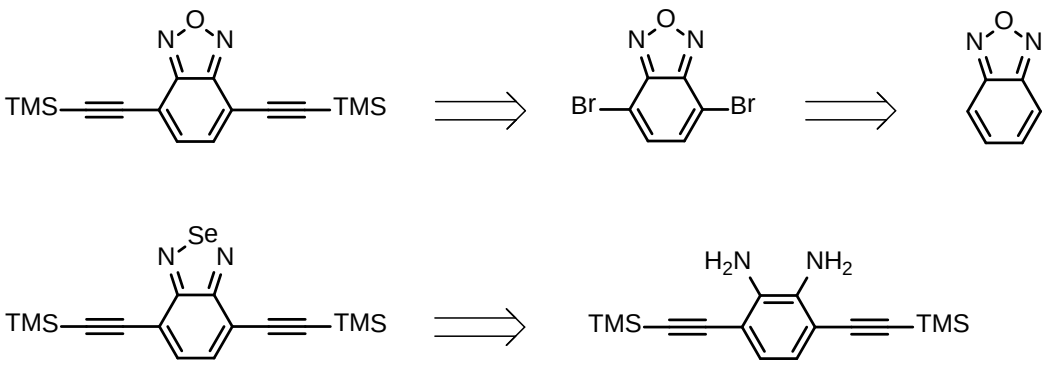

The synthetic route to the alkynylated benzooxadiazole is known;[111] the only change required is that of using TMS as a protecting group. The discovery that benzoselenadiazole is unresponsive towards typical Sonogashira coupling conditions prompted an alternative route, starting from the benzenediamine precursor. The sulfur-containing congener and the benzenediamine precursor appear in the synthesis of the phenazine compounds as well.

The proposed synthetic routes to the azides and alkynes used in this work are shown in Schemes 4 and 5, respectively. In these schemes, a) indicates the known synthetic route, and b) shows how these routes are adapted for this work. With the water-soluble azides, only the substrate changes going from a) to b). In the synthesis of the ethynylated compounds, the only change is to the protecting group (TMS instead of TIPS).

Scheme 4 Synthesis of Water-Soluble Azide Compounds

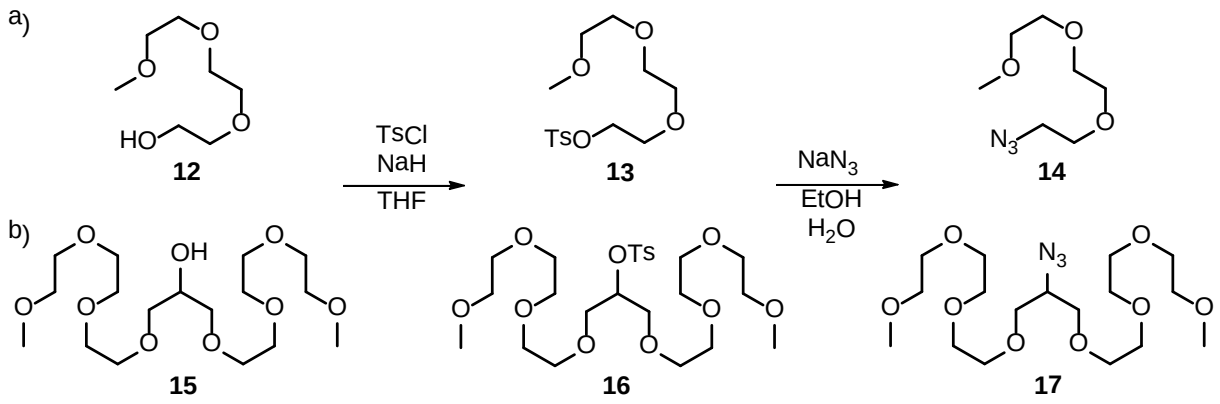

Scheme 5 Synthesis of Ethynylated Compounds

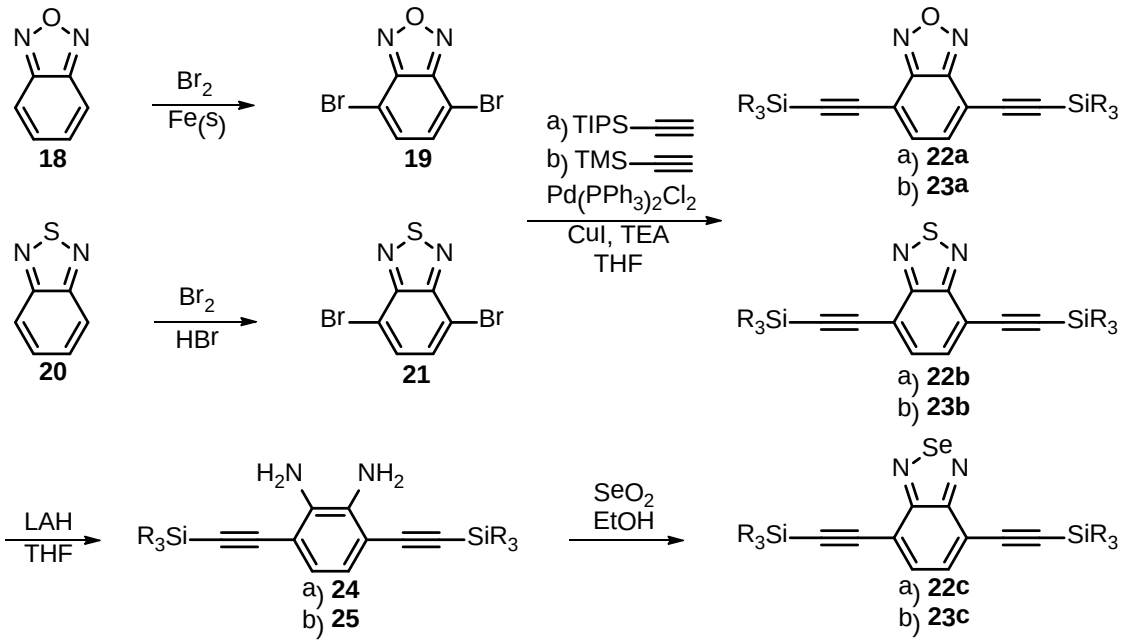

4.4.3 Other Small Molecules

Other small molecules that may work well in metal-binding schemes were also examined. Pyridine is a well-known metal ligand, and is able to coordinate metal ions in cooperation with the triazole ring.[119-121] Thiophene has also been proposed as capable of binding metal ions.[122] In particular, the softness of the sulfur may lead to selective binding of Hg^{2+} (a soft cation).[40,123] Boron-dipyrromethene (BODIPY) dyes may also be of interest. These dyes have been used in sensing applications and are prized for their photophysical properties, such as high quantum yields, absorption coefficients, and exceptional photostability.[124,125] All of these small molecules are easily accessible. A retrosynthetic plan to reach the bis-triazolyl cycloadducts is shown in Scheme 6

The final step is taken to be the cycloaddition, just as before. The chemistry is similar for the pyridine and thiophene. Synthesis of the ethynylated pyridine[126] and thiophene[127] are known, with the alkyne being introduced via Sonogashira coupling of the aryl bromides. The bromopyridine is commercially available, while the 2,5-dibromothiophene can be easily synthesized from thiophene with NBS. Two different BODIPY-containing cycloadducts may be synthesized. In the first, X represents OTEG chains, and R represents TEG, so the affixed phenyl

ring is trisubstituted with tri(ethylene glycol) chains. This should be beneficial for water-solubility. For the second, X represents hydrogen atoms, and R is a methyl group. The alkynylated precursors for these compounds are readily available, as they were synthesized by Sally Wagner (please refer to her Diplomarbeit for details on the synthesis of these alkynylated BODIPY derivatives).

Scheme 6 Retrosynthesis of Small Molecule Cycloadducts

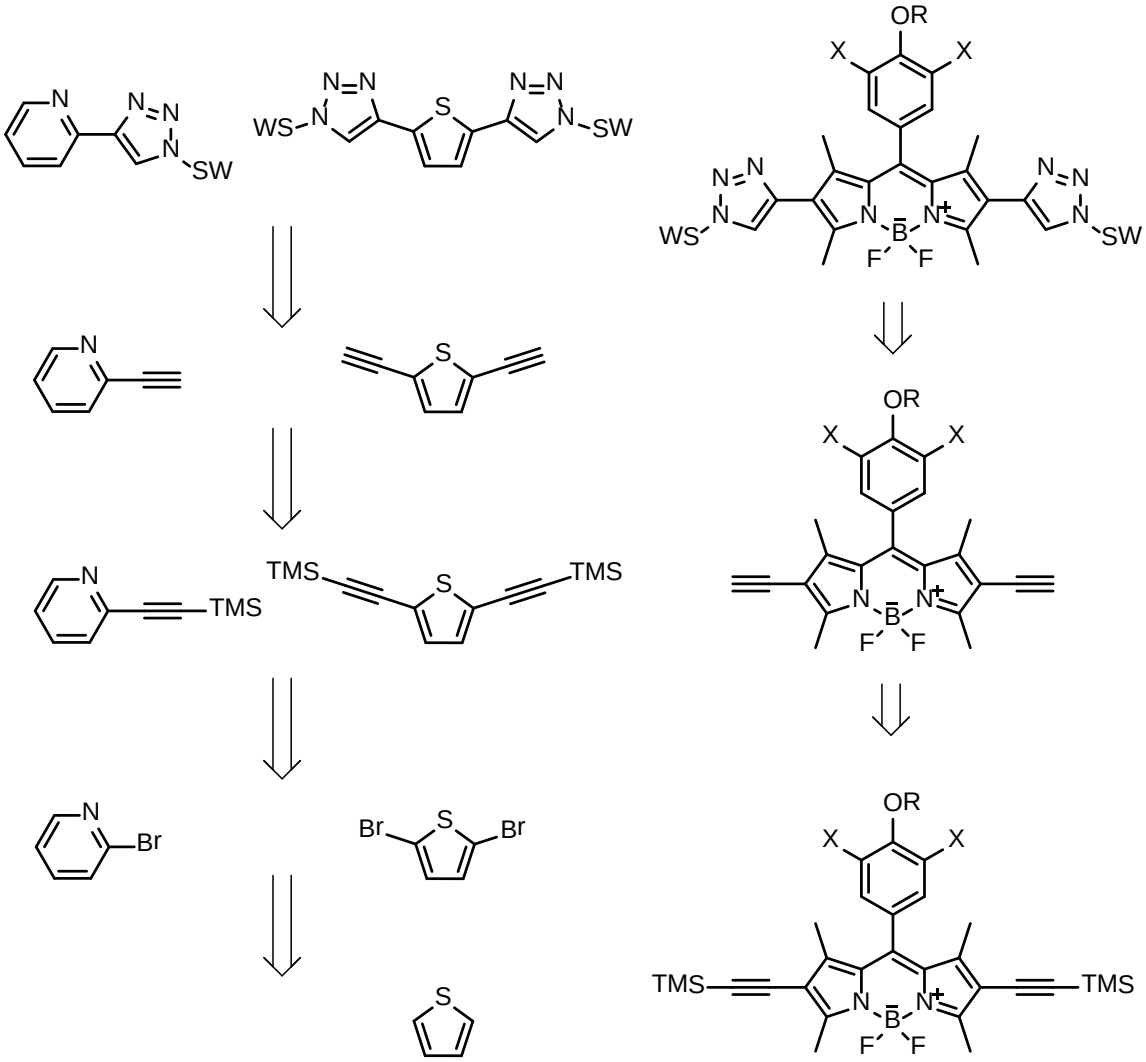

4.4.4 Polymers

Efforts are ongoing to incorporate the heretofore discussed properties and function into polymeric systems. It is well known that polymeric fluorescent sensors exhibit increased sensitivity towards analytes compared to their monomeric counterparts.[128,129] This effect is attributed to the conjugated polymer acting as a 'molecular wire' – upon excitation, the exciton is free to travel along the conjugation length until relaxation. This means that at any point along the conjugation length, a single analyte will be able to interact with the traveling exciton, and the entire conjugated polymer, instead of just one monomer. The amplification depends on the lifetime (how far the exciton is able to travel) – one study concludes that the exciton is able to travel over a hundred repeat units in a typical poly(phenyleneethynylene).[130]

When thinking about extending the small molecule concepts to polymeric systems, the first and simplest idea is an alternating copolymer of benzothiadiazole and triazole (Figure 22, top). Water-solubility could be provided either through hydrophilic substituents on the benzothiadiazole, or incorporation of a swallowtail-containing monomer. These polymers could be synthesized through CuAAC polymerization of the appropriate diazido and diethynyl monomers. There is one disadvantage here – it has been reported that in these types of polymers, the conjugation does not extend through the 1,2,3-triazole rings.[131]

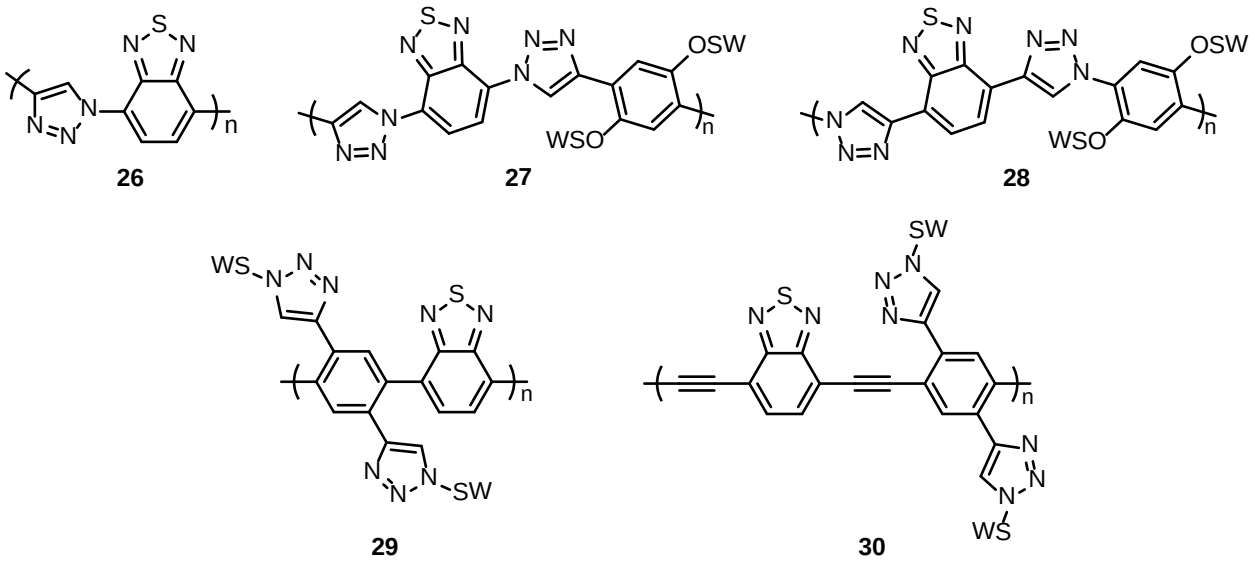

Figure 22 Possible copolymers containing benzothiadiazole and triazole.

Polymers with triazole in the main chain are envisioned as shown in Scheme 7. The CuAAC may be employed for the polymerization. Synthesis of the aryl azides may be modified from a known procedure.[132] The synthesis of the ethynylated benzothiadiazole has been discussed, and the ethynylated phenyl ring with swallowtail substituents has been previously synthesized.[52]

Scheme 7 Retrosynthesis of Click Polymers

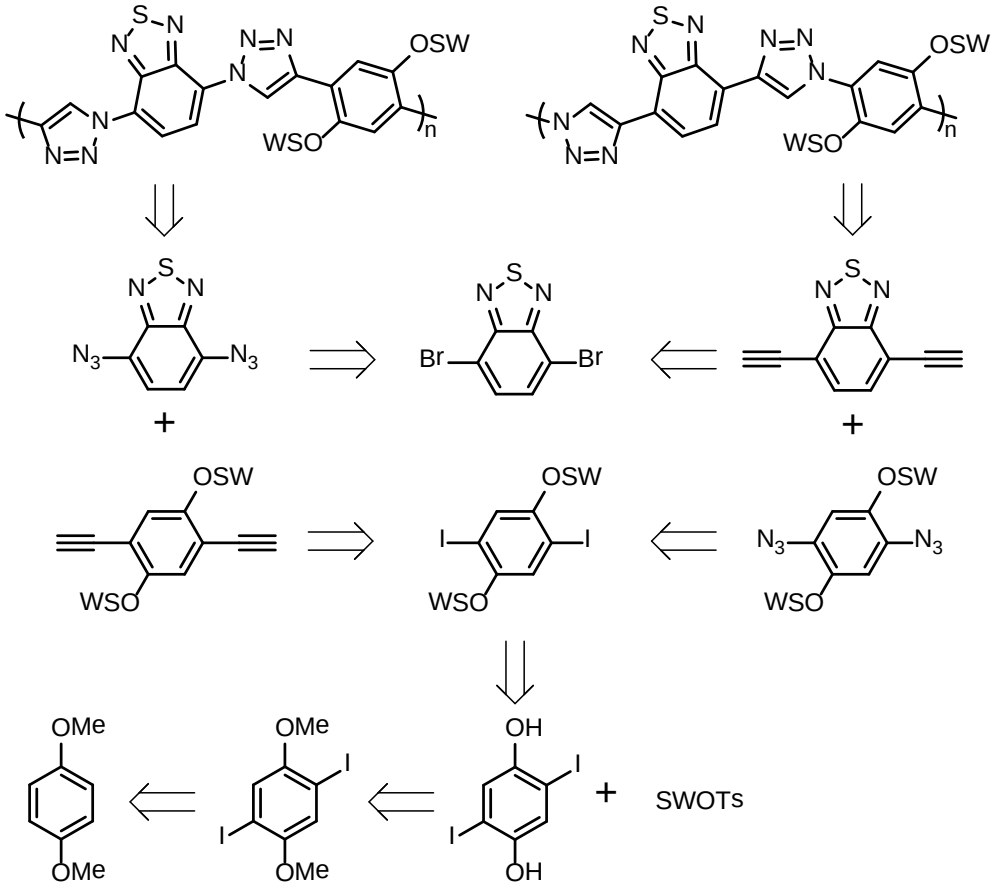

These polymers shown in Scheme 4.7 may not be fully conjugated. In the interest of retaining the conjugation, polymers with pendant triazoles may be considered (Figure 22, bottom). Much of the previous work on conjugated polymers with pendant triazole rings utilizes a nonconjugated spacer between the triazole and the polymer backbone. There are few examples of the triazole ring directly connected to the polymer chain, thereby participating in the conjugation.[133] As a

result of this cross-conjugation, we anticipate that these polymers may possess interesting optical properties. The question is, will they still bind metal ions?

The model compounds **31** and **32** (Figure 23) should suffice to answer the question of whether a binding pocket of the appropriate size is formed with triazole-functionalized polymers. Another interesting question is whether two properly placed triazole rings will do the same job. This may be answered by model compound **33**.

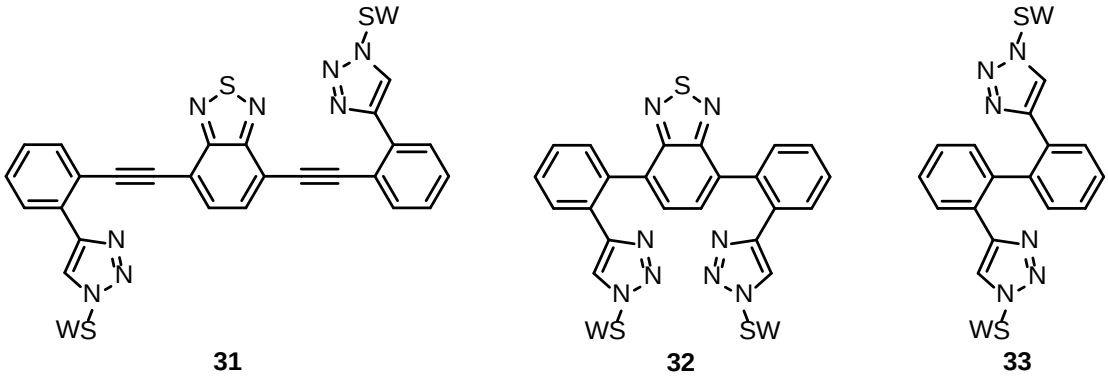

Figure 23 Proposed model compounds for metal-binding studies.

The synthesis of these model compounds is envisioned to proceed through metal-catalyzed couplings of the benzothiadiazole and triazol-4-ylbenzene monomers. For the alkyne-containing compound, Sonogashira coupling is the obvious answer. Suzuki coupling suggests itself for compound **32**, and **33** could be synthesized via Yamamoto coupling.

4.5 Poly(aryleneethynylene)s for Sensing Purposes

Some brief mention has been made of the potential for fluorescent molecules to serve as sensory scaffolds for more than just metal ions. Conjugated polymers are particularly promising materials in this field for their heightened sensitivity.[134] In this section the focus is on one particular type of conjugated polymer, poly(aryleneethynylene)s (PAEs).

PAEs made an appearance in the previous section and consist of alternating aryl and ethynyl units (see Figure 23 for an example). Poly(phenyleneethynylene) (PPE) is a common subset, featuring alternating phenyl and ethynyl goups. The synthesis can be accomplished through Sonogashira polymerization. The interested reader is referred to the excellent reviews penned regarding this useful reaction.[135-137]

The popular method for synthesizing water-soluble PAEs is functionalization of the aryl units with hydrophilic groups. Water-soluble PPEs have been studied extensively in the groups of Bunz[138,139] and Schanze.[140] Some representative examples (specifically, *para*-connected PAEs) are shown in Figure 24.

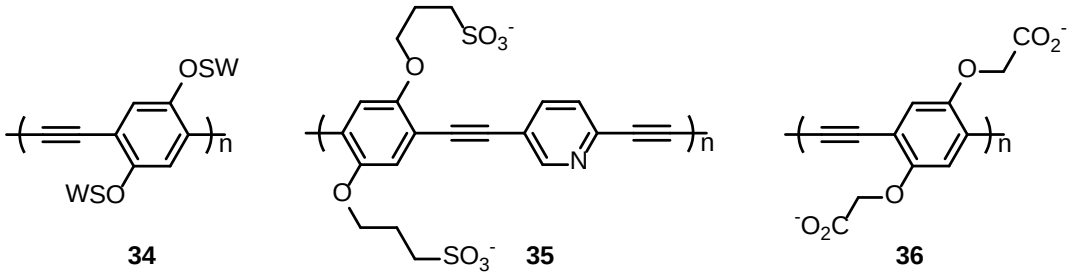

Figure 24 Examples of water-soluble PAEs.

The facile synthesis of these polymers, and their advantageous photophysical properties (high quantum efficiencies, photostability) have led to them finding use in sensing applications. Some examples with PPEs have already been discussed in section 4.1 for the detection of cancer cells and bacteria (Figures 4 and 7). Bunz and coworkers have also reported these materials in sensing schemes for biological molecules such as proteins[141] and pyrophosphate.[142]

Another feature of PAEs is their tunability. They may be synthesized as blue, green, or even longer wavelength emitters. The photophysical properties of these polymers depend on the

arylene units in the main chain, and also on the participation of conjugated side chains. Acceptor units such as benzothiadiazole are well known to red-shift the spectral properties of these polymers.[143] Emission in the red is attractive for cellular imaging, as the fluorescence of cellular species (blue or green) may be filtered out. Therefore, water-soluble PAEs may be useful as long-wavelength emitting fluorescent sensors.

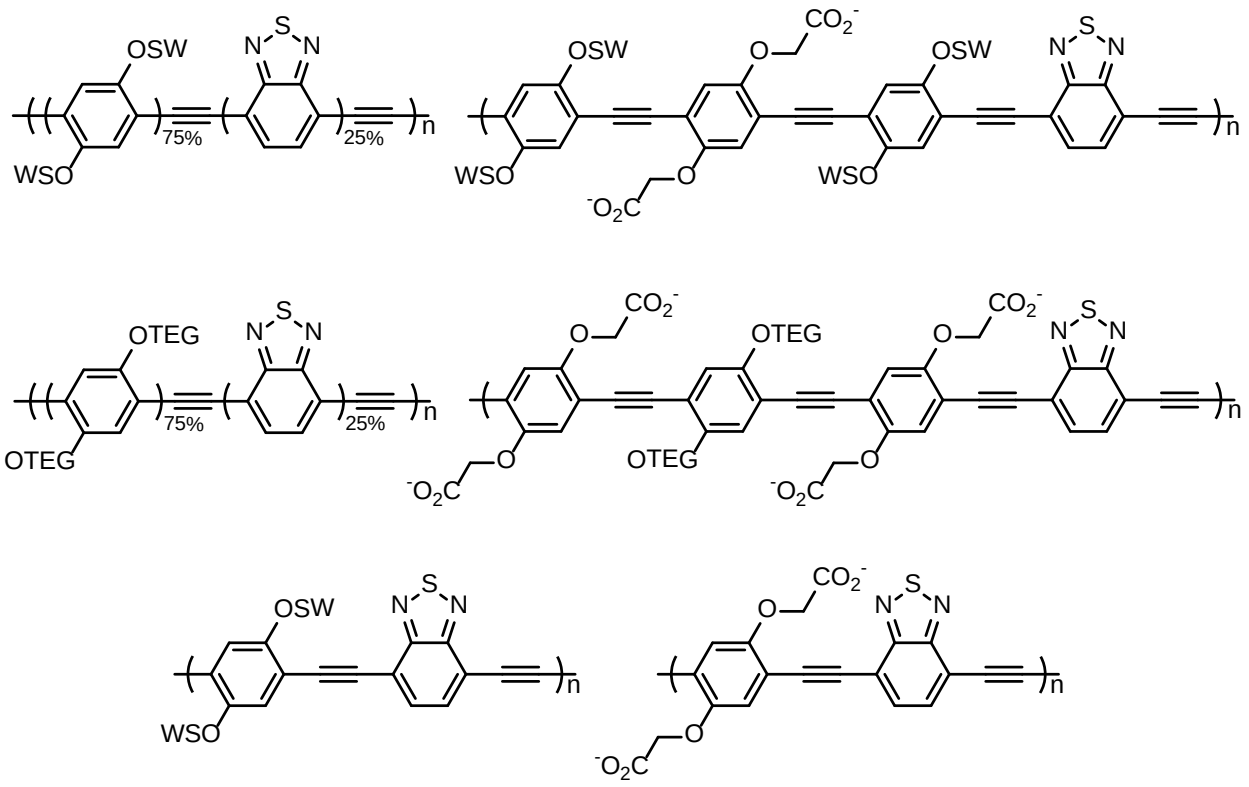

Figure 25 Proposed red-shifted water-soluble PAEs.

Proposed polymers are shown in Figure 25. The synthesis may be accomplished through Sonogashira polymerization of the monomers shown in Figure 26. The syntheses of these monomers are previously known in the Bunz lab. These polymers are anticipated to be soluble in water, and display red-shifted optical properties. Sensing of metals or biomolecules may be realized through specific interaction with the main chain benzothiadiazole, or through any perturbation of the polymer's conformation. A monomer containing an ester side chain is also included, as the carboxylate group should aid solubility in water, and may also contribute to the interaction with metal ions or other species.

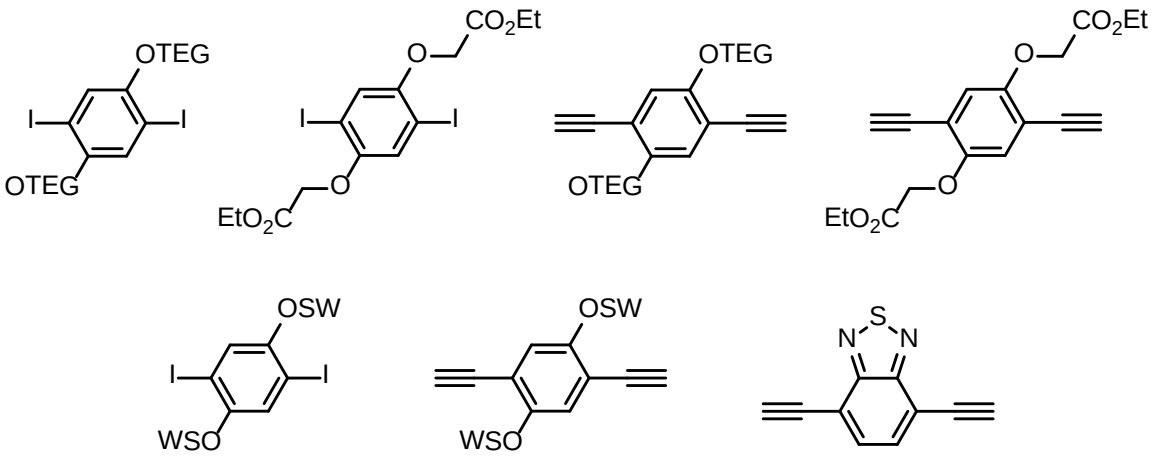

Figure 26 Monomers for the proposed PAEs.

5 Aim and Research Plan

The goal of this work is to synthesize novel fluorophores for aqueous metal ion sensing purposes, and to examine the effect of varying molecular structure on metal-binding activity. To achieve this, the copper-catalyzed azide-alkyne cycloaddition is used. Through this click chemistry, a water-solubilizing side chain is linked to a heteroaromatic core. This is proposed to function as a cooperative metal-binding system, with a binding pocket being formed between the heteroaromatic core and the triazole ring. By changing the core molecule, the effect on the metal-binding activity may also be studied. The series of fluorescent sensors to be synthesized is shown in Figure 27. The phenazine compounds are varied with a tetrahalogen substitution pattern, and the benzochalcogendiazoles differ in the chalcogen atom present.

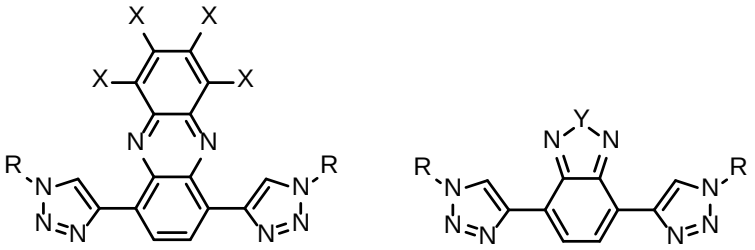

Figure 27 (*left*) Phenazine cycloadducts. X represents H, F, or Cl and R represents an oligo(ethylene glycol) substituent. (*right*) Benzochalcogendiazole cycloadducts. Y represents O, S, or Se and R represents an oligo(ethylene glycol) substituent.

The continuation of this work is the incorporation of these concepts into polymeric systems. Conjugated polymers containing triazole units may be capable of binding metal ions at higher sensitivities than small molecules. Further investigation into the biological activity of the phenazine compounds is also planned. These compounds have antibiotic properties, and may be useful *in vivo* imaging probes as well.

6 Results and Discussion

6.1 Phenazine-Triazole Cycloadducts as Selective Silver Ion Sensors

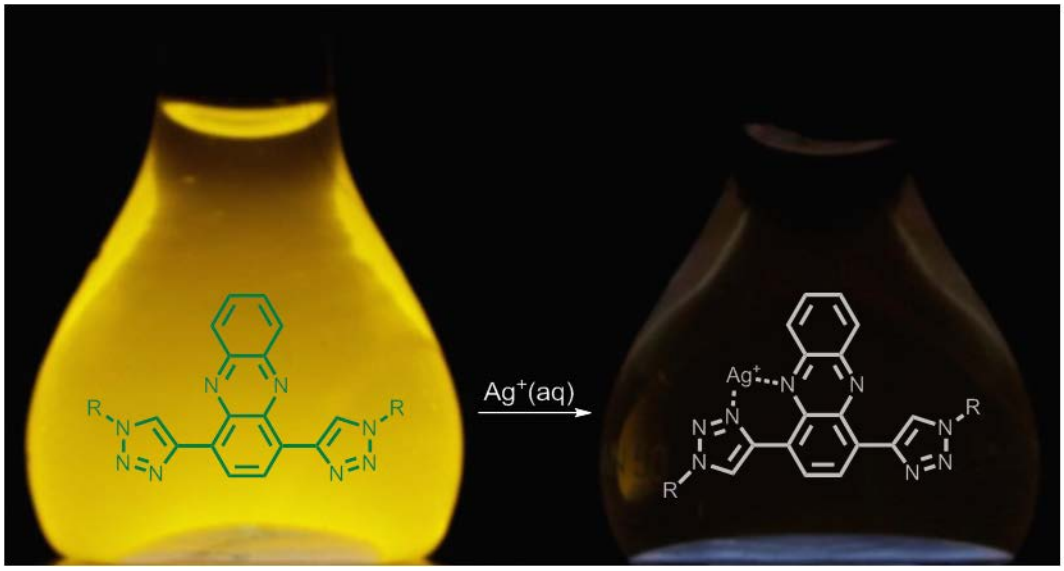

Figure 28 A picture of a swallowtail-substituted phenazine cycloadduct (left) and the same compound mixed with silver ion (right) irradiated under 365 nm light.

6.1.1 Synthesis

The synthesis of the phenazines and their corresponding 1,3-dipolar cycloaddition products is shown in Scheme 8. What is missing here is the synthesis of the benzenediamine precursor **25**. As discussed in the previous chapter, the synthesis of compound **24** is known. The same chemistry with a different protecting group gave **25**. **37c** and **37d** are commercially available. **37a** must be synthesized *in situ*, as it is highly unstable. **37b** is also synthesized immediately before use, according to a previously published procedure.[112] A 2:1 ratio of *para*- and *ortho*-fluoranil isomers was recovered, necessitating three equivalents without further purification. Alkynylated phenazines **38a-d** and **39a-d** were synthesized via condensation of **37a-d** with **24** or **25**. Ethanol was used as a solvent, but in the case of the fluorinated compounds, nucleophilic solvents had to be avoided, as they undergo substitution side reactions at the fluorinated carbons. In these cases, DCM was chosen as solvent. From the trimethylsilyl-protected phenazine core **39a-c**, deprotection with potassium carbonate gave **40a-c**. These ethynylated compounds are unstable; to avoid degradation of **40**, reaction with the azide was carried out immediately to give **41** or **42**.

The targets **42a-b** were obtained in 27-30% yield, while the TEG-substituted **41a** and **41c** formed in 46-61% yield.

Scheme 8 Synthesis of Cycloadducts **41** and **42**

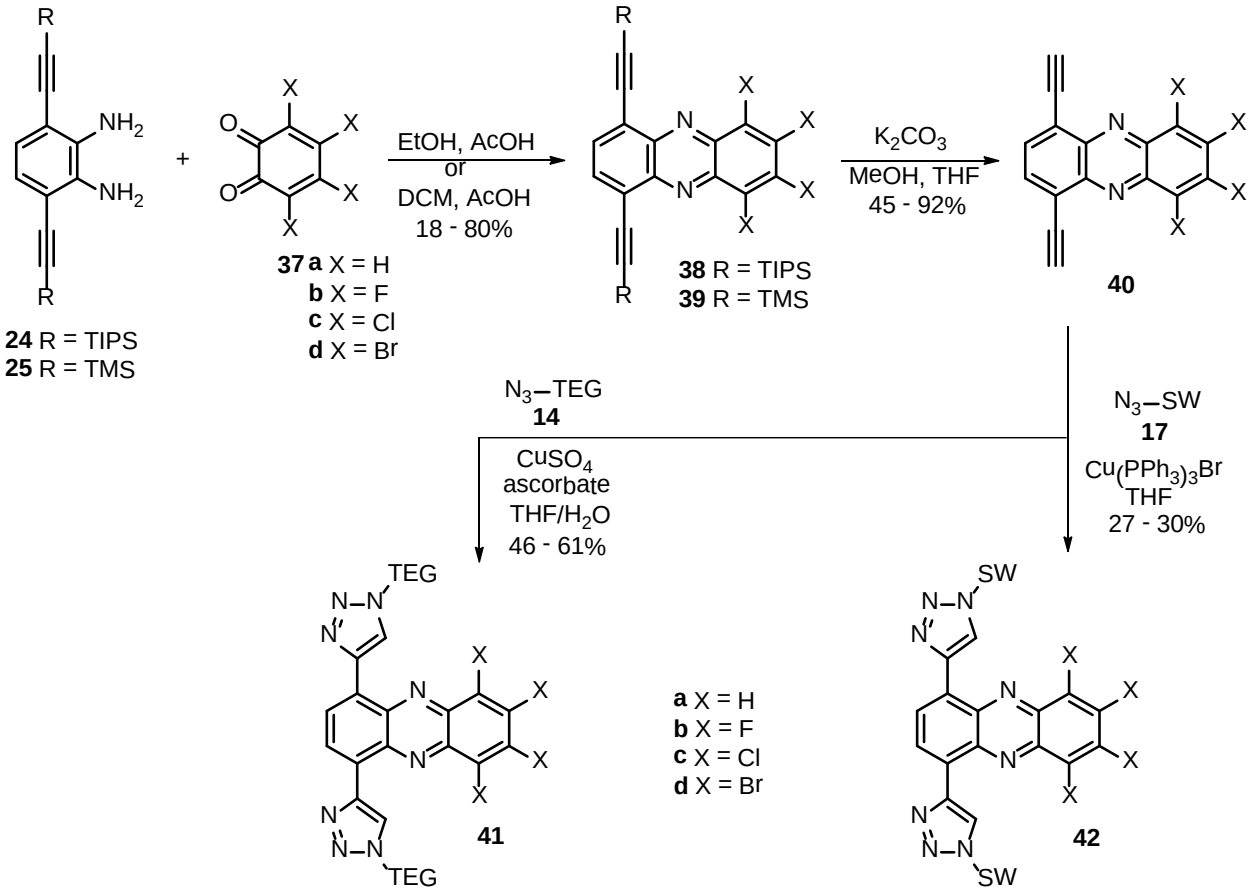

The unexpectedly low yields for this well-known reaction prompted us to vary the conditions slightly. Water has been postulated as an ideal solvent for stabilization of copper acetylide intermediates,[81] but the presence of water as co-solvent had no effect on our reaction (though it is necessary when using $CuSO_4$ as catalyst). Performing the reaction at elevated temperatures (50 ˚C) did not improve the yield, nor did variation of the copper catalyst ($Cu(PPh_3)_3Br$ or $CuSO_4$/ascorbate). Due to the reactive nature of the ethynylated species **40**, a one-pot deprotection/cycloaddition reaction would be ideal; however, such attempts turned out to be less reliable overall. In the best case, we were able to synthesize **42c** with this method in similar yield (35%).

After recovery of the products, no further experiments were done to optimize the yields. It is possible that they could be improved. One idea would be to use a Cu(I) stabilizing ligand in the reaction. This does not seem promising though, as the $Cu(PPh_3)_3Br$ catalyst employed contains a ligand which should serve that purpose to at least some degree. There are better options available, however.[91] The instability of the unprotected alkynes may also have something to do with the less than optimal yields. What is more obvious is the effect of the water-soluble substituent on the yields. The more bulky swallowtail group has a negative effect. This leads to the postulation that the problems with the yield arise from the purification, a notion also put forth by Hecht.[144] This idea is supported by the fact that there is no evidence of any remaining starting material; also, no clear side product could be isolated. The cycloadducts were purified by silica gel chromatography. These products are highly polar, making this type of purification difficult. These difficulties are exacerbated with the more polar swallowtail group compared to the TEG group. In future synthesis, alternative purification methods should be seriously considered, such as size exclusion or reverse phase chromatography.

6.1.2 Crystal Packing

TIPS-substitution facilitates crystal packing, and single crystals of **38a-d** were obtained (**38a**, **38c**, and **38d** were obtained by Yexiang Zhang). Crystal structures of the TMS-substituted or the terminal ethynyl phenazines were unattainable. Looking at the single crystals, halogen substitution forces the offset π-stacks of **38a** into a coplanar arrangement, which is more favorable for energy and electron transport.[145] In all the crystals, the molecules are slip-stacked to maximize hydrogen bonding interactions. This effect is seen to a greater extent in the halogenated species. For comparison, the crystal structures of **38a** and **38c** are shown in Figure 29. Packing of the fluoro- and bromo-substituted compounds are similar to that of the chloro-, with pi-stacking distances growing larger to accommodate larger halogens.

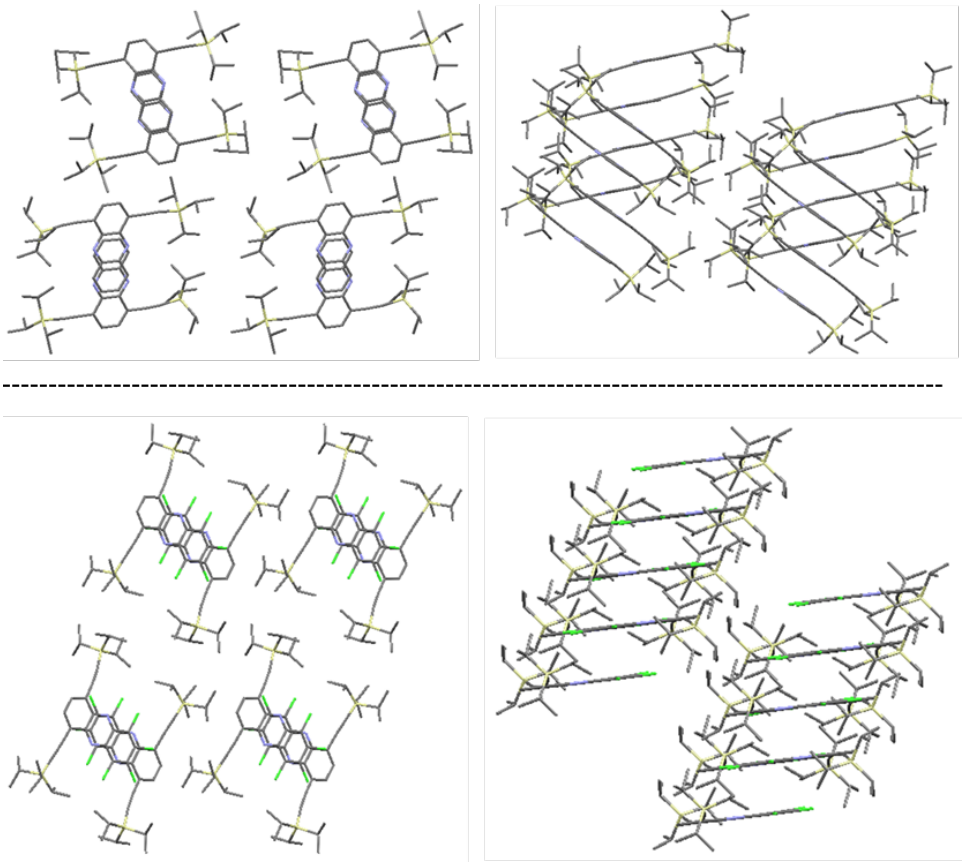

Figure 29 Crystal packing of **38a** (top) and **38c** (bottom). View along the *a* axis (left) and an approximate diagonal of the *a* and *c* axes (right). The hydrogen atoms are omitted for clarity.

6.1.3 Photophysical Properties

Figure 30 shows the absorption spectra of the ethynylated phenazines **38** and **40**. The TMS- and the TIPS-protected compounds show very similar absorption spectra, though the TIPS-substituted compounds show more distinct absorption maxima. Halogen substitution causes red-shifts which increase upon descending the group. The same effect is seen in the emission profiles (Figure 31), with the exception of the bromine-substituted phenazine. This compound is non-emissive due to the heavy atom effect of the bromine, and was not further explored. The optical properties of **38a-d** are summarized in Table 1 and are consistent with the previously reported properties of halogenated azaacenes[110] and pentacenes.[145]

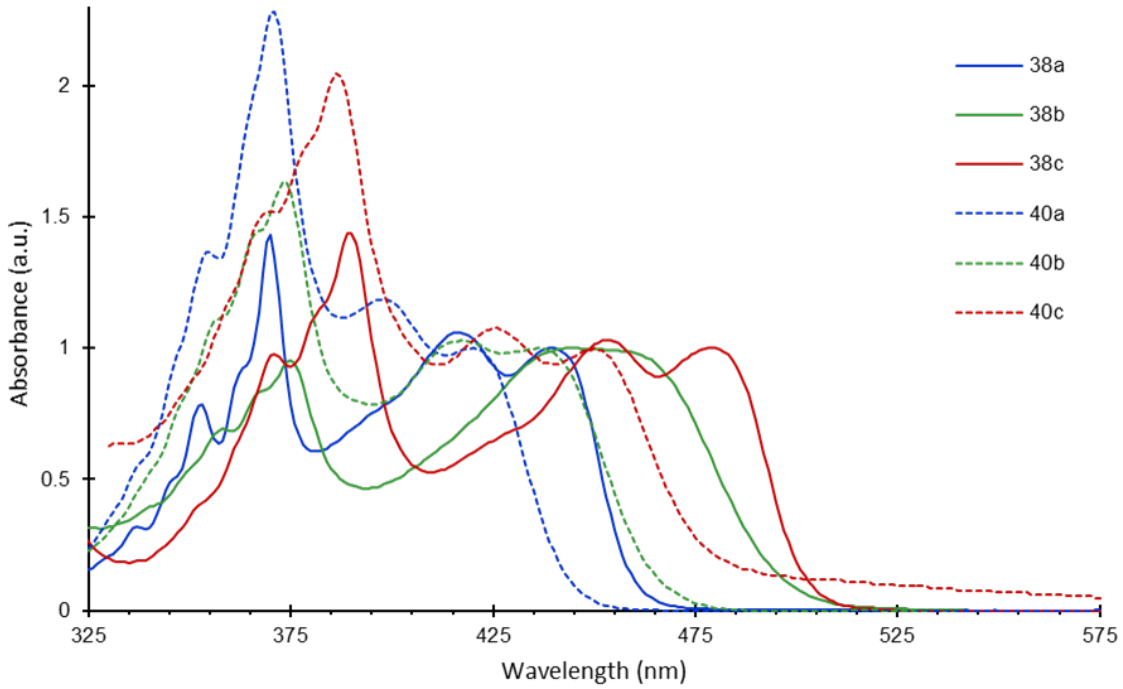

Figure 30 Absorption spectra of ethynylated phenazines **38a-c** and **40a-c** in DCM.

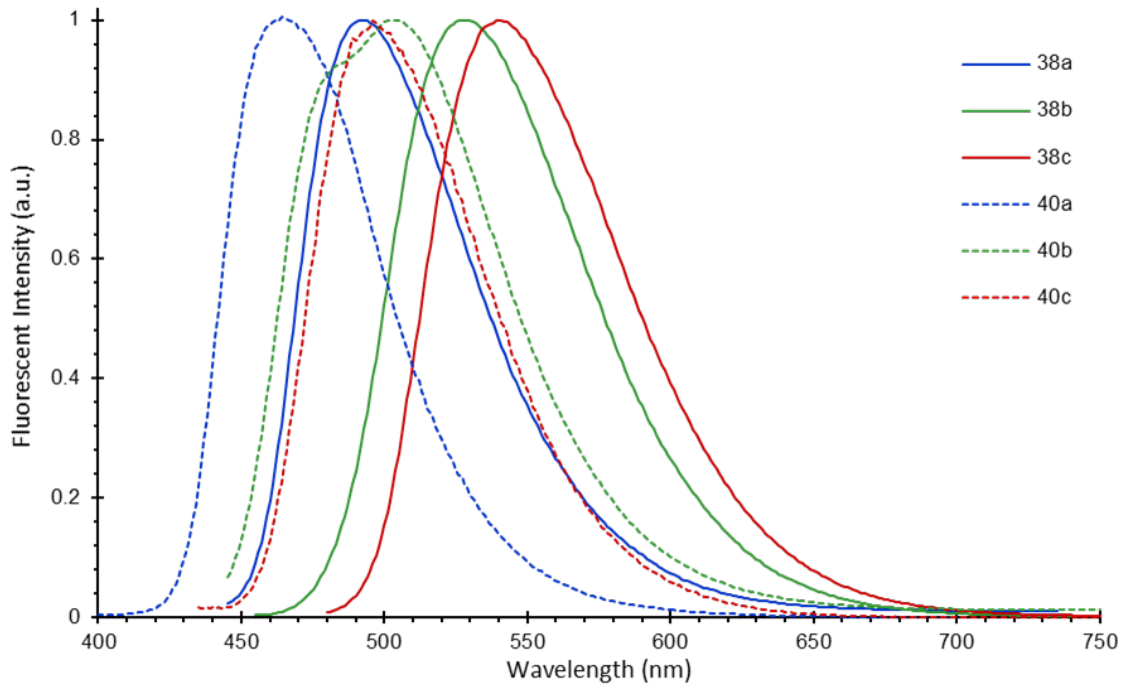

Figure 31 Fluorescence spectra of ethynylated phenazines **38a-c** and **40a-c** in DCM.

Table 1 Photophysical Properties Recorded for Compounds **38a-d** in DCM

Compound	Abs. λ_{max} (nm)	Em. λ_{max} (nm)	Stokes Shift (cm^{-1})	Φ_f	τ_f (ns)
38a	416	492	3710	0.02	0.37
38b	443	528	3630	0.50	10
38c	451	540	3650	0.11	2.5
38d	453	n/a	n/a	n/a	n/a

To gain further insight into the spectral properties of these compounds, we performed quantum chemical calculations. The calculated energies of the frontier orbitals and a comparison of the experimental and calculated band gaps are recorded in Table 2. Upon chlorination of the alkynylated phenazine, the LUMO is stabilized by 0.49 eV, whereas the HOMO is stabilized by only 0.30 eV. This results in a lowering of the optical gap by 0.19 eV, which agrees closely with the experimentally observed change of 0.20 eV. From the visual representations of the frontier molecular orbitals shown in Figure 32a, it is apparent that the coefficients of the HOMO on the halogenated ring are smaller than those of the LUMO. Therefore, the stabilizing effect of halogenation is greater for the LUMO than the HOMO, resulting in the observed bathochromic shifts. This effect is also seen in the cycloaddition products, where the HOMOs are located almost exclusively on the triazole-containing axis, resulting in even greater bathochromic shifts upon halogenation.

Table 2 Calculated and Experimental HOMO-LUMO Gaps

Compound	HOMO (eV)[a]	LUMO (eV)[a]	calc. gap (eV)	exp. gap (eV)[b]
40a	-6.24	-3.11	3.13	2.96
40b	-6.60	-3.60	3.00	2.85
40c	-6.54	-3.60	2.94	2.76
42a	-5.81	-3.01	2.80	2.76
42b	-6.13	-3.51	2.62	2.59
42c	-6.10	-3.56	2.54	2.53

[a]Calculated by SPARTAN 10 using the B3LYP method with the 6-311++G** basis set. [b]Acquired from the λ_{max} of absorption. [c]Ethylene glycol substituent approximated by a methyl group.

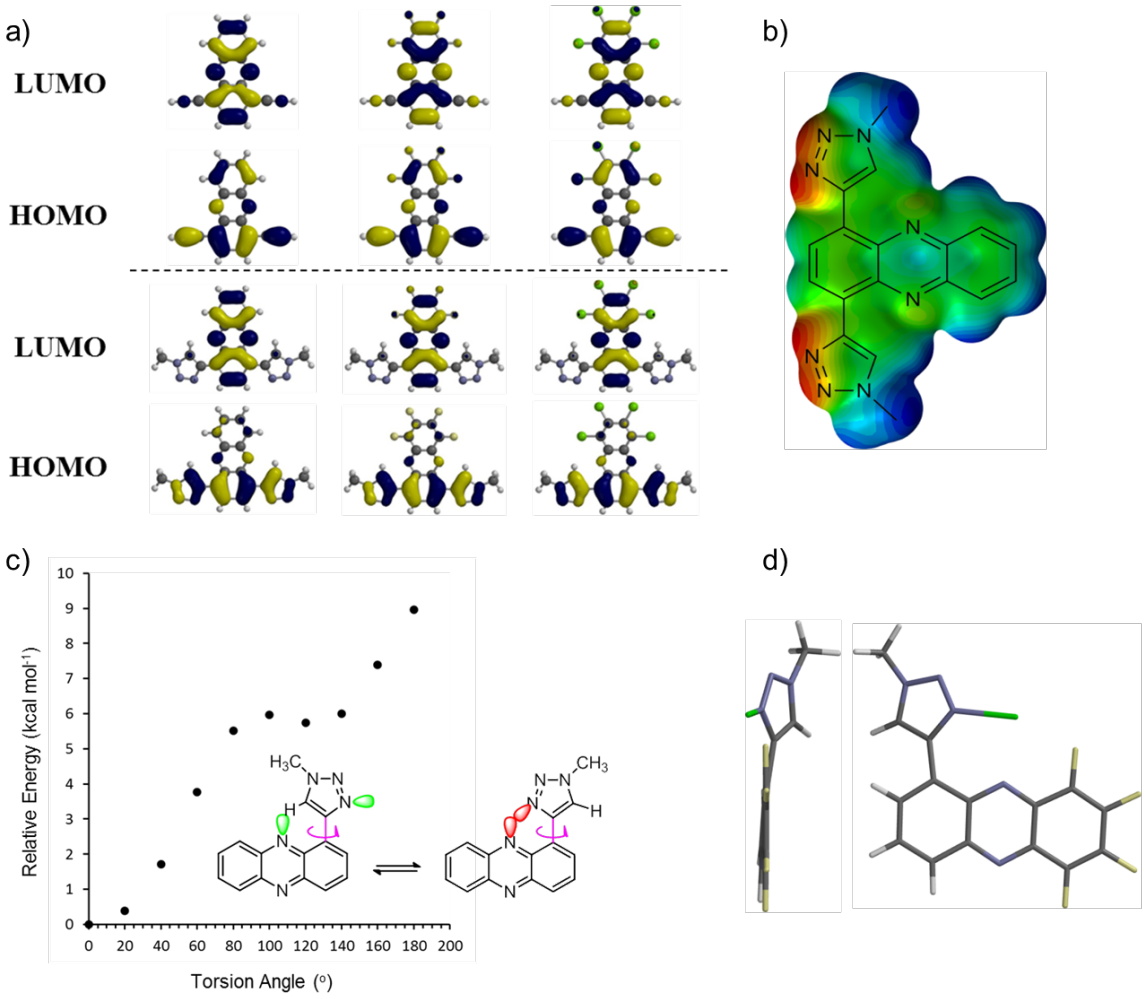

Figure 32 (a) Frontier orbitals for **40a-c** (top, left to right) and simplified models of **42a-c** (bottom, left to right). (b) Electrostatic potential map highlighting the localization of electron density on the nitrogen atoms, particularly those of the triazole ring. (c) Rotational profile of a simplified model of **41a** and **42a**. The left conformation (green) displays the lowest relative energy. The other conformation is 8.96 kcal mol^{-1} higher in energy. (d) Simplified model of **41b** and **42b** showing the predicted conformation when binding silver ion.

What is the conformation of the triazole unit with respect to the phenazine ring? Quantum chemical calculations always give the rotamer in which the C-H-group is close to the N-unit of the phenazine nucleus, and never the one in which the formal binding pocket is formed. To investigate this issue, we performed an analysis of the internal rotation around the C-C bond that connects the phenazine with the triazole rings (Figure 32b). From these quantum chemical

calculations (B3LYP 6-311++G**) it is clear that the rotamer forming the binding pocket is ca. 9 kcal mol^{-1} higher in energy. The reason for the energy difference is probably the mutual repulsion of the two adjacent electron pairs of the participating heterocyclic nitrogens. However, that is not an issue; upon coordination of silver, the binding pocket forms through rotation. We have calculated the structure of the Ag^{+} complex with the simplified model using the B3LYP 6-31G** basis set in the absence of further ligands (Figure 32c) and can see that the silver ion forces the ligand into a conformation that accommodates the cation optimally. This conformation is not planar but has a torsion angle of around 40°. Additionally, one can see that in the optimized structure the distance of the triazole nitrogen to the silver cation is 2.24 Å, while the distance to the phenazine nitrogen is 2.35 Å. Upon fluorination of the unsubstituted part of the phenazine, the geometry changes and the Ag-triazole distance is reduced to 2.21 Å, while the distance to the now much more electron poor phenazine is increased to 2.45 Å. As a consequence of the geometrical change the torsion angle is now only 35°. While these are only gas phase calculations without added ligands or counter ions, they are supported by 2D ^{1}H-^{1}H NOESY NMR (see Figure 37). In the absence of silver, the predicted rotamer is observed, with no interaction between the triazole hydrogen and the aromatic hydrogen of the nearest phenyl ring. After addition of silver ion, there is a clear interaction between these hydrogen atoms, made possible through the rotation of the triazole ring.

Figure 33 shows the absorption of **42a-c** in both water and dichloromethane. Though these compounds are soluble in both solvents, there is a considerable hypsochromic shift in the absorption profiles when going from organic to aqueous solvent, as much as 30 nm. This trend exists to a varying degree in each of the cycloadducts. The reverse occurs in the emission spectra (Figure 34), with aqueous solvent inducing either a bathochromic shift or none at all. This results in a much larger Stokes shift in water. Variation of the water-soluble triazole substituent does not have any appreciable effect on the absorption or emission. The spectra of **41** are nearly identical to those of **42** and are therefore not shown.

Comparing aqueous and organic solvent, the absorption profiles are hypsochromically shifted in water. Presumably the lowest-energy band is due to the n-π* transition, and the hydrogen-bonding interactions in water serve to stabilize the ground state, resulting in a negative

solvatochromism.[146] This effect is not seen with the higher energy absorption bands, which likely represent π-π* transitions.

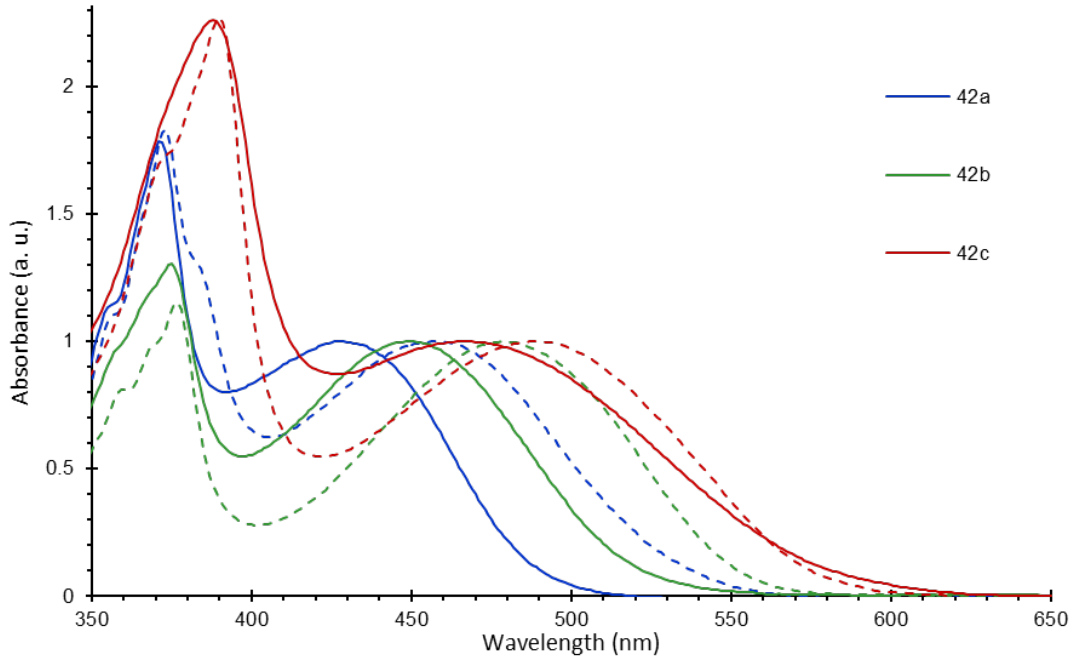

Figure 33 Absorption spectra **42a-c** in H_2O (solid line) and DCM (dashed line).

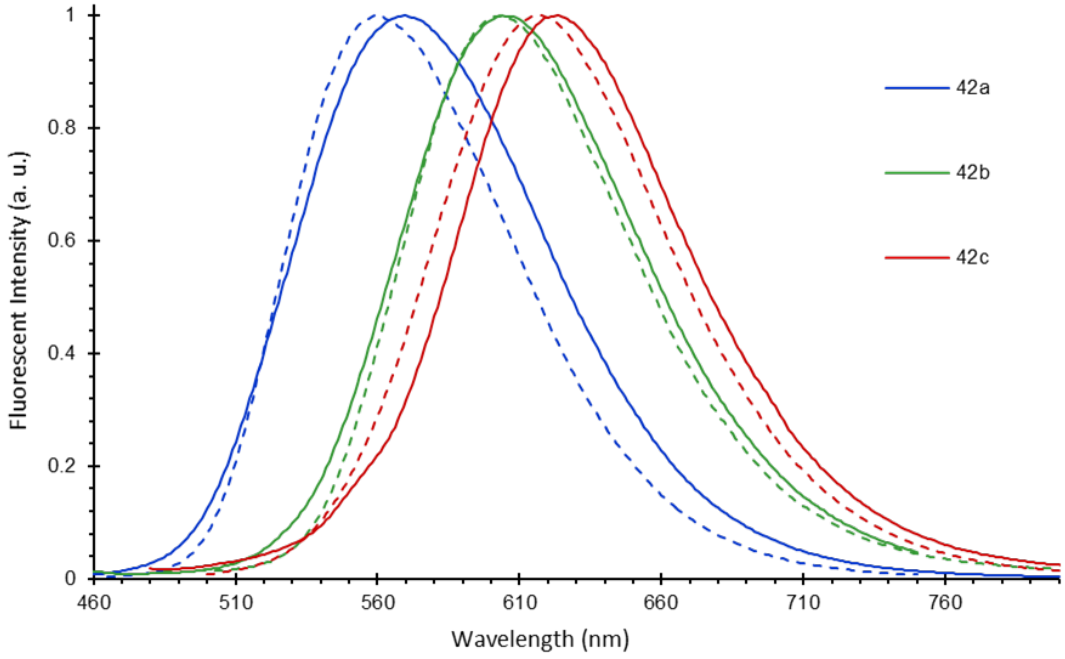

Figure 34 Fluorescence spectra of **42a-c** in H_2O (solid line) and DCM (dashed line).

Looking at the photophysical properties listed in Table 3, we see the phenazine cycloadducts possess rather long lifetimes (greater than 10 ns in organic solvent). It is unclear how much this is due to the phenazine core. The radiative rate of phenazine is very low; the dominant decay pathway from the excited singlet states is intersystem crossing to the triplet states.[147,148] The low quantum yield of alkynylated phenazine **38a** indicates that emission is still far outpaced by non-radiative decay. Further substitution of the phenazine ring (with halogens or triazole rings) increases the quantum yield, as well as the lifetime. The cycloadducts **41** and **42** have even longer lifetimes, suggesting that the presence of the triazole rings are at least partially responsible.

Table 3 Photophysical Data for **41** and **42**

Compound	Abs. λ_{max} (nm)		Em. λ_{max} (nm)		Stokes Shift (cm^{-1})		Φ_f		τ_f (ns)	
	DCM	H_2O	DCM	H_2O	DCM	H_2O	DCM	H_2O	DCM	H_2O
41a	450	433	559	573	4333	5643	0.31	0.01	19	1.7
42a	458	428	559	569	3945	5790	0.27	0.04	19	4.0
42b	479	448	603	604	4293	5765	0.04	<0.01	7.9	4.5
41c	496	486	610	619	3768	4421	0.06	<0.01[a]	16	6.8[a]
42c	490	465	617	624	4201	5480	0.02	<0.01	9.4	3.6

[a]determined in MeOH/H_2O

6.1.4 Metal-Binding Studies

The ready solubility of the bis-triazolylphenazines in water and the acceptable quantum yield of **42a** allow the examination of its metal binding properties in aqueous solution. Screened metals include Na^+, K^+, Li^+, Ag^+, Mg^{2+}, Ca^{2+}, Zn^{2+}, Cu^{2+}, Ni^{2+}, Hg^{2+}, Cd^{2+}, and Pb^{2+}. The halogenated fluorophores showed little if any response to metal ions. These compounds are so electron-poor as to preclude efficient metal binding in water. For the unsubstituted phenazine cycloadducts **41a** and **42a**, only minimal quenching upon exposure to Cu^{2+} and Hg^{2+} was observed. As seen in Figure 35, the fluorescence quenching by Ag^+ was pronounced, indicating that these compounds may serve as a fluorescent sensor for silver ions.

Due to the toxicity of silver and its increasing prevalence in industrial applications, the U.S. Environmental Protection Agency has set a secondary maximum contaminant level of 0.1 mg/L for silver.[6] As a result, there exists a desire for sensitive and selective methods of silver ion detection in aqueous media. As fluorescent sensors, these phenazine cycloadducts possess

attractive properties. Their Stokes shifts are quite large (>5000 cm^{-1}), allowing the excitation wavelength to be far removed from the emission wavelength. The auxochromic effect of the triazole units pushes the luminescence of these compounds from the blue/green region to the yellow and beyond, allowing cellular background fluorescence to be easily filtered out. The lifetimes are also relatively long, enabling such techniques as time-gated detection, though the lifetimes are lower in water than in dichloromethane.

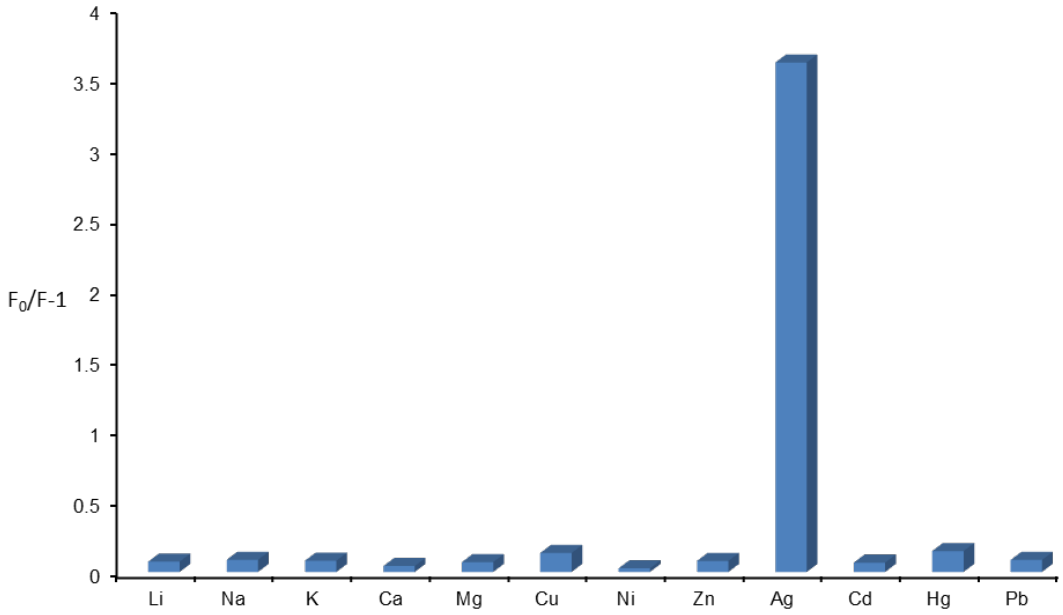

Figure 35 Relative fluorescence quenching of **42a** by metal ions in water.

Titrations of **41a** and **42a** with $AgNO_3$ were performed to determine the strength of the binding. Significant deviation from linearity occurred when the data were fitted to the typical Stern-Volmer equation. The data could be fitted well by equation 1.[149-152]

$$\Delta I = \frac{\alpha}{2}\left\{\left([F]+[Q]+\frac{1}{K}\right) \pm \sqrt{\left([F]+[Q]+\frac{1}{K}\right)^2 - 4[F][Q]}\right\} \quad (1)$$

ΔI is the change in fluorescent intensity, $[F]$ is the concentration of the fluorophore, $[Q]$ is the concentration of the quencher, and α is a constant. This equation is derived from the equilibrium expression (equation 2).

$$K = \frac{[F \cdot Q]}{[F]_f [Q]_f} \tag{2}$$

$[F \cdot Q]$ is the concentration of the complex, $[F]_f$ is the concentration of the uncomplexed, or free, fluorophore, and $[Q]_f$ is the concentration of the free quencher. A direct calculation of the association constant is not possible without a direct measurement of these values. If we assume a 1:1 binding ratio, the free concentrations can be rewritten in terms of the total concentrations (equations 3 and 4).

$$[F]_f = [F] - [F \cdot Q] \tag{3}$$

$$[Q]_f = [Q] - [F \cdot Q] \tag{4}$$

Assuming that the quencher is non-fluorescent, the fluorescent intensity can be defined by equation 5.

$$I = \alpha_f [F]_f + \alpha_{F \cdot Q} [F \cdot Q] \tag{5}$$

Substituting equation 3 into 5 gives

$$I = \alpha_f ([F] - [F \cdot Q]) + \alpha_{[F \cdot Q]} [F \cdot Q] \tag{6}$$

Here, α represents fluorescent proportionality constants. The initial fluorescence is defined as seen in equation 7, and the change in fluorescence is the difference between equations 6 and 7, which simplifies to equation 8.

$$I_0 = \alpha_f [F] \tag{7}$$

$$\Delta I = \alpha_{F \cdot Q} [F \cdot Q] - \alpha_f [F \cdot Q] = \alpha [F \cdot Q] \tag{8}$$

This shows what we would logically guess, that the change in the fluorescence is proportional to the concentration of the quencher-fluorophore complex. Substituting equations 3, 4, and 8 into the equilibrium expression and solving for ΔI results in equation 1.

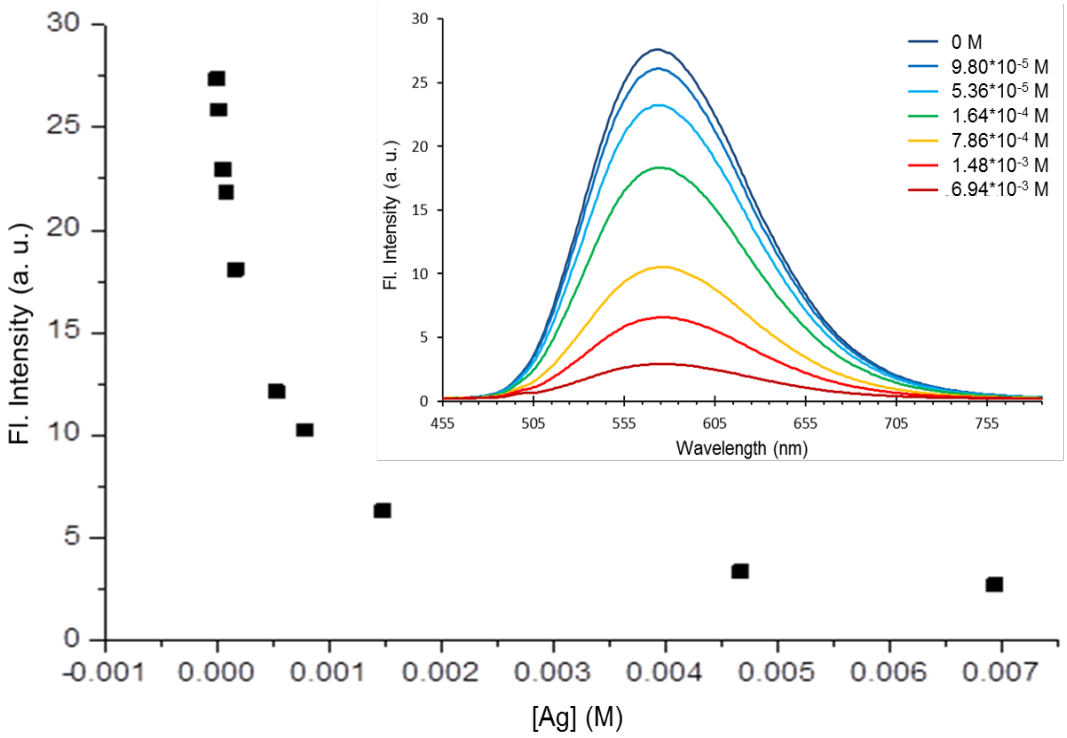

Figure 36 Representative titration (inset) and binding curve of **41a**.

The titration curve is shown in figure 36. The binding constant (or association constant) *K* can be extracted using a non-linear least-squares curve fitting of equation 1. The data can be fitted well by the 1:1 binding model, which is also supported by ^{1}H-^{1}H NOESY NMR (Figure 37). The binding constant for Ag^{+} was determined to be log(*K*) = 3.75 ± 0.09 for **41a** and log(*K*) = 2.84 ± 0.02 for **42a**.

Looking at the NMR spectra shown in figure 37, we see three aromatic signals for **42a**, which integrate to 2, 2, and 4 protons. Upon addition of silver ion, the four protons are split into two signals, indicating a disruption of symmetry. The ^{1}H-^{1}H NOESY spectrum of **42a** shows an interaction between the protons at the 2 and 3 positions. In the presence of silver ion, this interaction is still seen, along with a new interaction between the protons at the 1 and 2 positions, verifying the unsymmetrical 1:1 binding event.

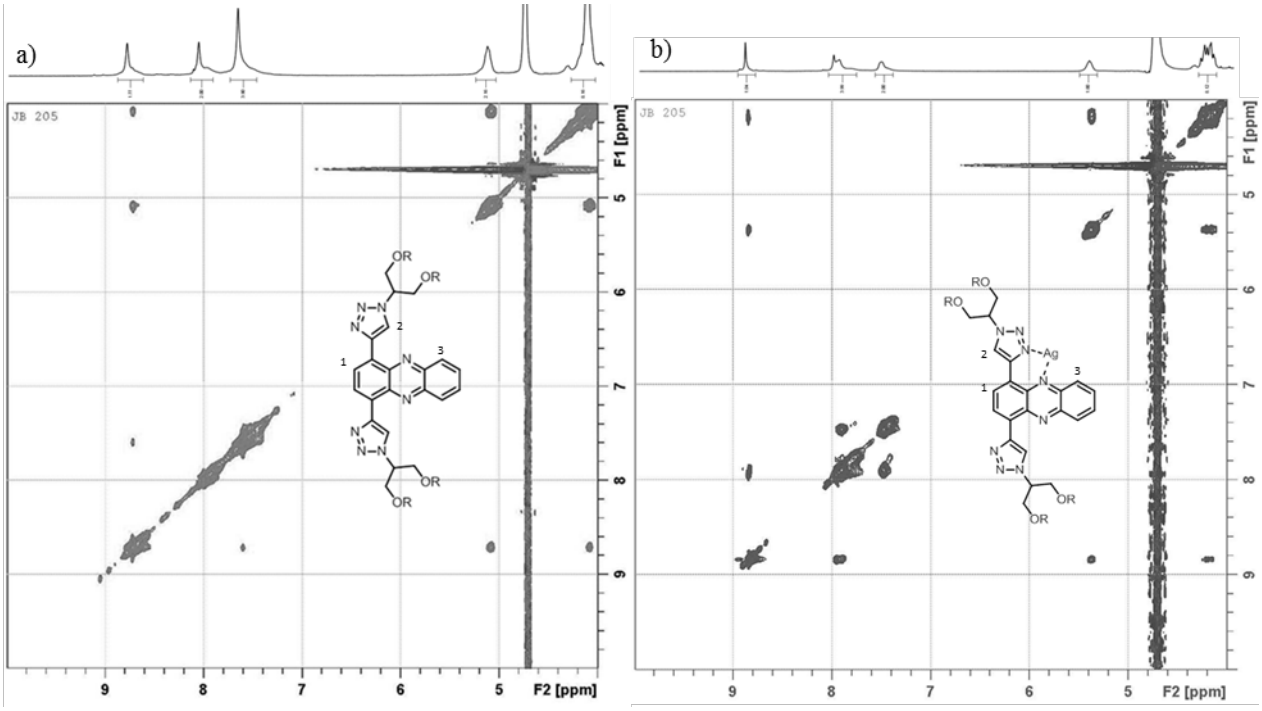

Figure 37 (a) ^{1}H-^{1}H NOESY NMR spectrum of **42a** (300 MHz in D_2O). (b) ^{1}H-^{1}H NOESY NMR spectrum of **42a** + Ag^{+} (300 MHz in D_2O).

Previous evidence that phenazine[107] and peralkynylated phenazine[108] are able to bind silver begs the question of whether the triazole is necessary for the binding event. For an answer, we investigated the interaction of bare phenazine and alkynylated phenazine **38a** with silver ion. Titrations of the three different phenazine compounds (including the cycloadduct **41a**) were performed in ethanol, which provides sufficient solubility and is somewhat comparable to water. Complex formation between silver ion and phenazine was observed only at excess concentrations of silver (>10^5 equivalents), and no binding constant was extracted. The binding constant for **41a** was determined to be log(K) = 3.44 ± 0.05, similar to the result obtained in water, while the value for **38a** was significantly lower (log(K) = 2.70 ± 0.02). These results demonstrate that the participation of the triazole ring serves to strengthen the binding of silver ion, though it is not strictly necessary. The selectivity of the phenazine cycloadducts for silver ion stems from the phenazine, and adjustment of the electronic properties of the phenazine core leads to changes in the metal-binding activity. The more electron-poor halogen-substituted phenazine compounds are unable to bind metal ions, despite the presence of the triazole. Interestingly, the cycloadduct **41a**

is more sensitive to Ag^+ than **42a**. This suggests that the ethylene glycol side chains interfere with the binding of silver in some way, but the exact nature of this interaction is not clear.

6.1.5 Biological and Antibiotic Activity

The data in this section (Figures 38 and 39) were provided by Steven Hayden from Georgia Institute of Technology.

The known anti-bacterial activity of phenazine prompted us to test their corresponding cycloadducts. Figure 38 shows the inhibition of bacterial growth when incubated with the cycloadducts **41a**, **42a**, and **42b**. Both of the non-halogenated phenazine cycloadducts **41a** and **42a** show antibacterial activity. **42a** contains the more bulky swallowtail, and is somewhat less potent than the TEG-substituted **41a**. Far less effective is the tetrafluorinated phenazine compound **42b**. This indicates that the antibiotic activity is a property of the phenazine core. These results can be compared with Tubermycin B, an efficient antibiotic with minimal inhibitory concentrations below 0.025 mM.[100]

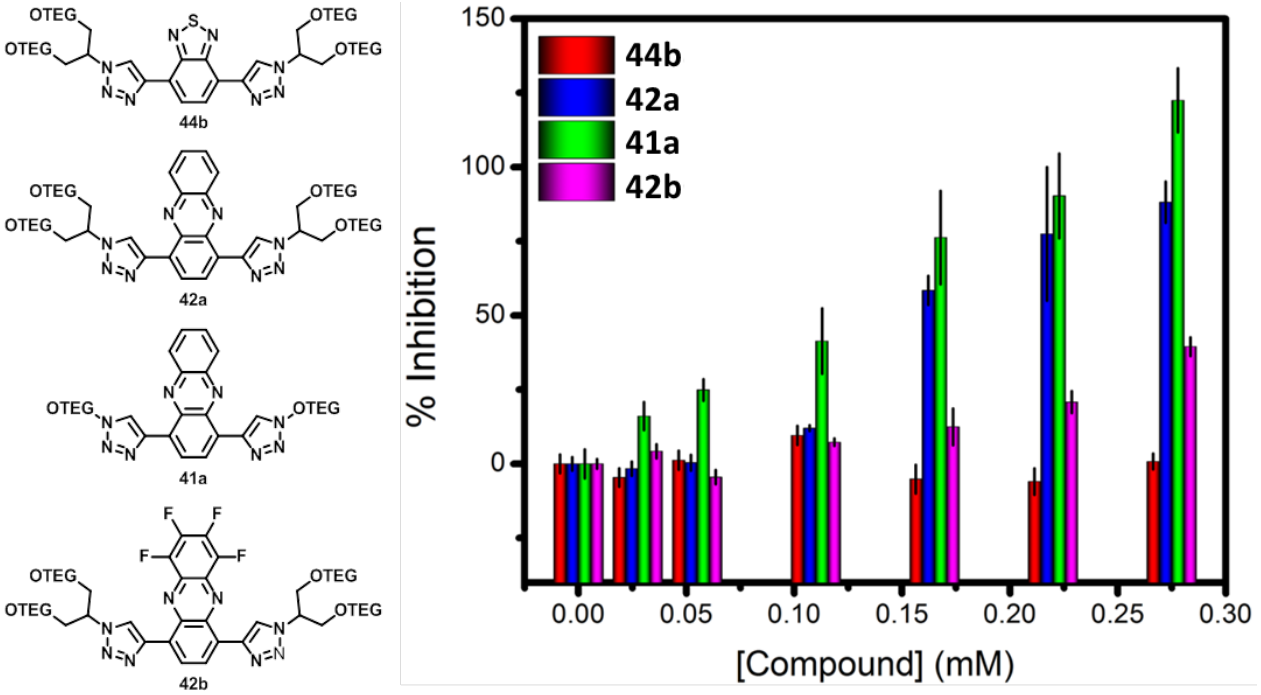

Figure 38 Inhibition of bacterial growth by bis-triazolyl cycloadducts.

There are some reports of triazole and other azole-containing compounds possessing antimicrobial activity.[153,154] The same inhibition studies were performed with the benzothiadiazole cycloadduct **44b** (discussed in the next section) to determine the source of the observed inhibition. No activity was seen with **44b**, confirming that the phenazine is the active ingredient, and not the triazole rings.

The utility of these cycloadducts is dependent on their overall cytotoxicity. Are they equally toxic to normal human cells? Such an antiobiotic would be useless. To answer this question, cycloadducts **41a**, **42a**, and **44b** were incubated with HaCat cells. The results are shown in Figure 39.

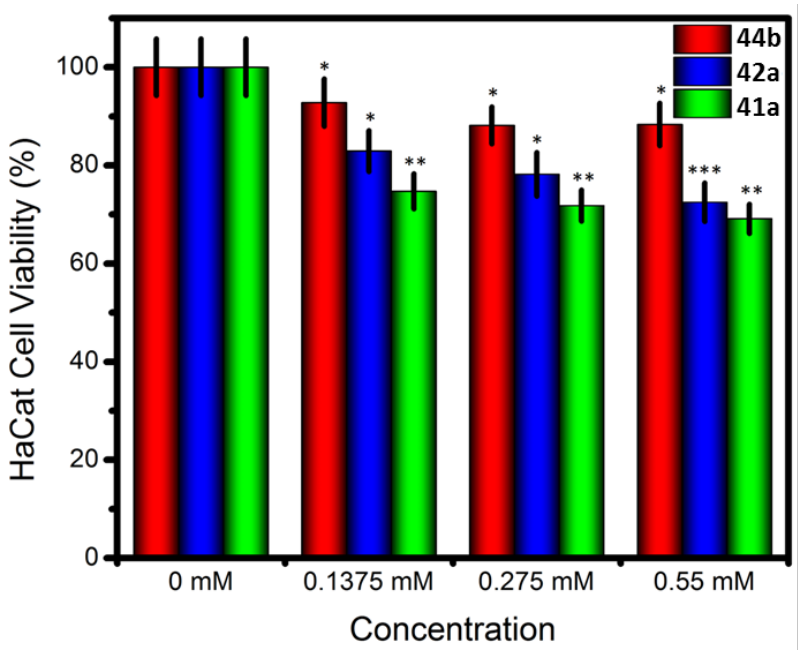

Figure 39 Cytotoxicity of bis-triazolyl cycloadducts.

More than 80% cell viability is seen with the phenazine cycloadduct containing swallowtail (**42a**), even at concentrations over 0.1 mM. The cycloadduct with TEG side chains (**41a**) is slightly less friendly. This trend in toxicity mirrors that seen in the bacteria studies. The compound without phenazine is the least toxic, indicating that phenazine plays at least a small role in the toxicity. These results beg the question of the mechanism of cell death, and the action of the phenazine. We hope that fluorescent microscopy images may shed some light on these areas.

6.2 Benzochalcogendiazole-Triazole Cycloadducts as Selective Metal Ion Sensors

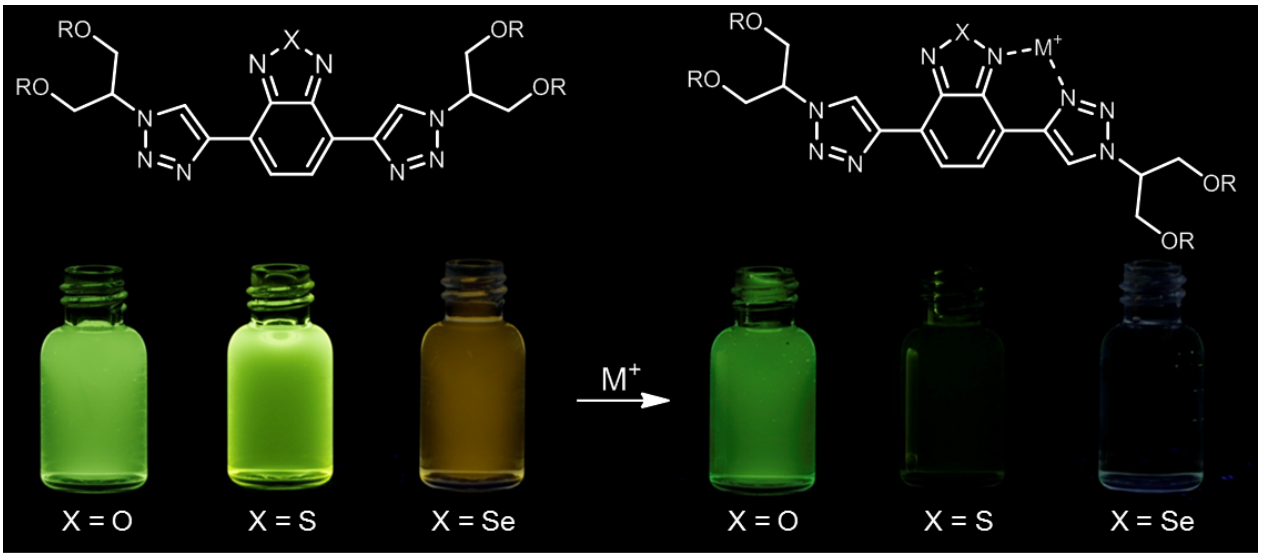

Figure 40 A picture of the series of benzochalcogendiazole cycloadducts irradiated under 365 nm light, showing the fluorescence without (left) and with Ni^{2+} ion (right).

6.2.1 Synthesis

The synthesis of these bis-triazolyl benzochalcogendiazoles is shown in Scheme 9. The starting materials **23a-b** can be easily reached as previously discussed. **23c** is synthesized from **23b** by first removing the sulfur with lithium aluminum hydride to reach the diamine, and then stirring with selenium dioxide. Removal of the silyl protecting group proceeded quickly using potassium carbonate for **23a** and **23b**, while TBAF was necessary for **23c**. The ethynylated compounds **43a-c** degrade rapidly, which made it necessary to use them immediately after purification. Stability of these compounds appeared to increase going from **43a** to **43c**. The products **44a-c** were then synthesized via copper-catalyzed azide-alkyne cycloaddition.[69,70] Attempts at a one-pot deprotection-cycloaddition synthesis from **23b** and **23c** failed to yield any product, so that it was required to first isolate **43a-c**. Yields for the cycloaddition were moderate, with the exception of **44c**. Using heat (50 ˚C) did not improve the yields. It seems the selenium-containing compound causes problems not only for Pd-catalyzed Sonogashira couplings, but also for the CuAAC. Due to the poor yield, the reaction was repeated under exactly the same conditions, to rule out human error. This second trial resulted in a 10% yield. Each time, the reaction developed a black color

which was not seen with the synthesis of **44a-b**. Unfortunately, no side reaction was identified, and no side product could be isolated.

Scheme 9 Synthesis of Cycloadducts **44a-c**

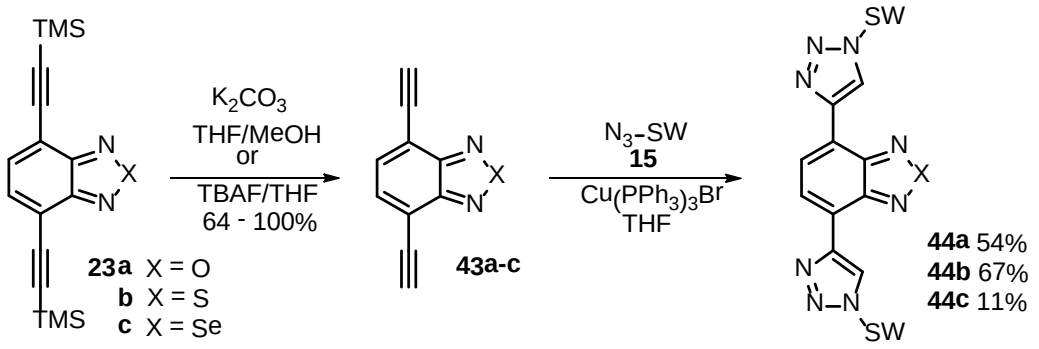

6.2.2 Photophysical Properties

44a-c are soluble in both organic and aqueous solvent. The absorption spectra are shown in Figure 41. Shifting the heteroatom down the periodic table from oxygen to selenium serves to red-shift the absorption bands; in particular, the lower-energy $S_0 \rightarrow S_1$ transition is shifted significantly more than the higher energy transitions. Similar to the phenazine cycloadducts, a negative solvatochromism is observed on moving from H_2O to DCM. Also of interest is the decrease in intensity of the lower-energy band upon moving to heavier chalcogen atoms, possibly indicating a decrease in charge transfer character.

Quantum chemical calculations were performed using SPARTAN molecular modeling software (Figure 42). For simplicity, the ethyleneglycol substituent is approximated by a methyl group. The HOMOs are localized mainly on the triazole axis, and the LUMOs predominantly on the benzochalcogendiazole axis. According to the calculated frontier orbital energies, destabilization of the HOMO is largely responsible for the observed red-shifts in the photophysical spectra. The change in the LUMO energies from **44a** (-2.96 eV) to **44b** (-2.89 eV) to **44c** (-3.01) indicates that multiple factors influence the energy, and thus the band gap. Treating these cycloadducts as donor-acceptor (D-A) systems, the more electronegative oxygen atom is expected to increase the D-A interaction, thus lowering the band gap. Experimental evidence shows the opposite trend;[155,156] it is thought that the lower ionization potential of the heavier chalcogen atoms, along

with the effect on the bond length alternation of the acceptor system (resulting in decreased aromatic character), trumps the D-A interaction, resulting in a lowering of the band gap on switching the chalcogen atom from oxygen to selenium.

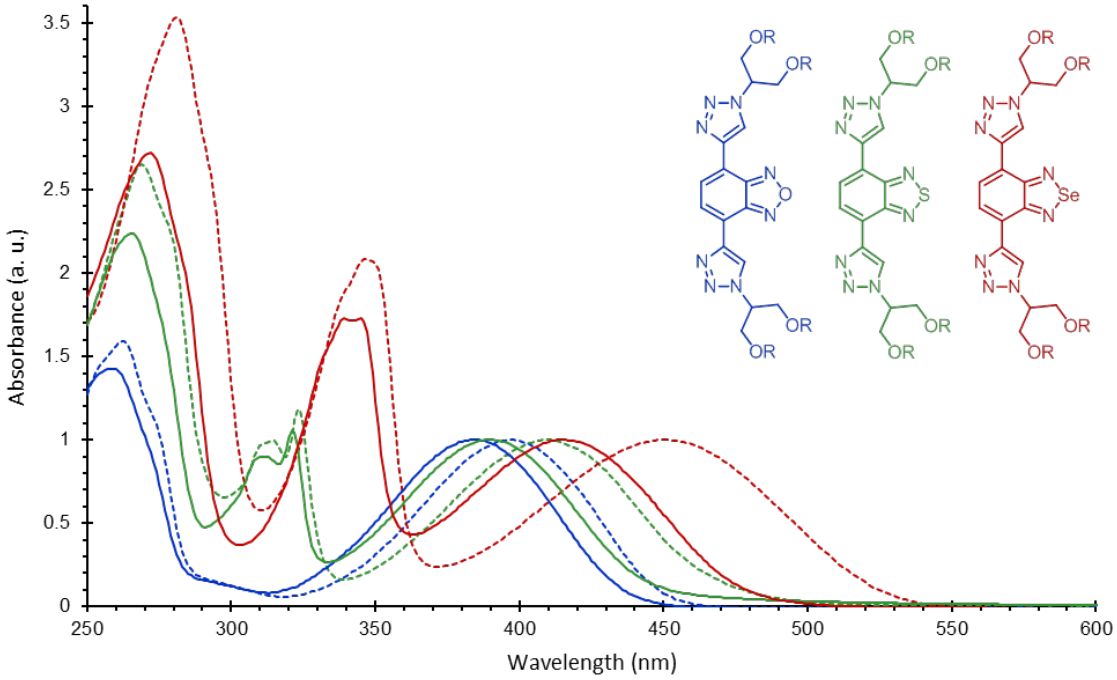

Figure 41 Absorption spectra of **44a-c** in H_2O (solid line) and DCM (dashed line).

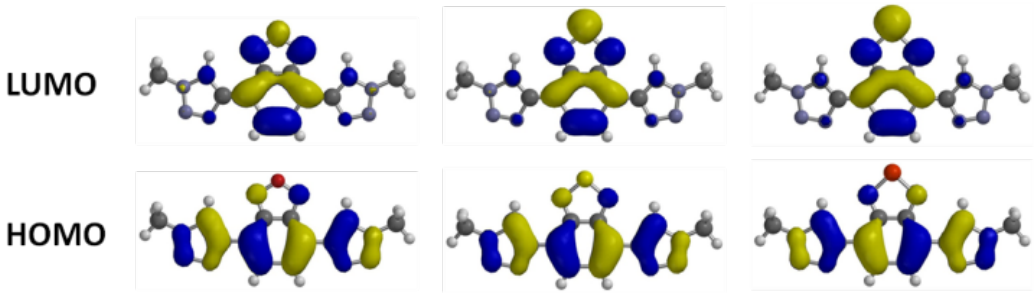

Figure 42 Calculated molecular orbitals for **44a-c** (left to right).

Table 4 Calculated and Experimental HOMO-LUMO Gaps

Compound	HOMO (eV)[a]	LUMO (eV)[a]	calc. gap (eV)	exp. gap (eV)[b]
44a	-6.18	-2.96	3.22	3.22
44b	-5.98	-2.89	3.09	3.18
44c	-5.91	-3.01	2.90	3.00

[a]Calculated with SPARTAN 10 using the B3LYP method with the 6-311++G** basis set. [b]Acquired from the λ_{max} of absorption in H_2O.

44a-c are yellow in solution, and their fluorescence ranges from blue-green to orange. The fluorescence spectra are shown in Figure 43. The fluorescence is slightly red-shifted in H_2O compared to DCM, resulting in large Stokes shifts in water. The emissive properties of these fluorophores make them attractive as sensors or *in vivo* imaging agents. **44a** and **44b** boast relatively high quantum yields in water (0.23 and 0.27, respectively), and their long lifetimes are ideal for such techniques as time-gated detection. Similarly long lifetimes were determined for the phenazine cycloadducts. Considering the lifetimes of the precursors **23a-c** (5.2, 8.5, and 1.6 ns), it is unclear to what extent the the heteroaromatic core determines the lifetime, as opposed to the triazole substituents. The fluorophore featuring selenium has a lower quantum yield than the other two congeners. This can be attributed to the selenium exerting a heavy atom effect, which is known to increase the rate of intersystem crossing.[157]

Table 5 Photophysical Data for **44a-c**

Compound	Abs. λ_{max} (nm)	Em. λ_{max} (nm)	Stoke's Shift (cm^{-1})	Φ_f	τ (ns)
44a (DCM)	397	510	5581	0.64	10
44b (DCM)	410	519	5122	0.66	15
44c (DCM)	450	559	4861	0.40	17
44a (H_2O)	385	525	6926	0.23	6.8
44b (H_2O)	390	528	6702	0.27	11
44c (H_2O)	414	576	6266	0.04	4.1

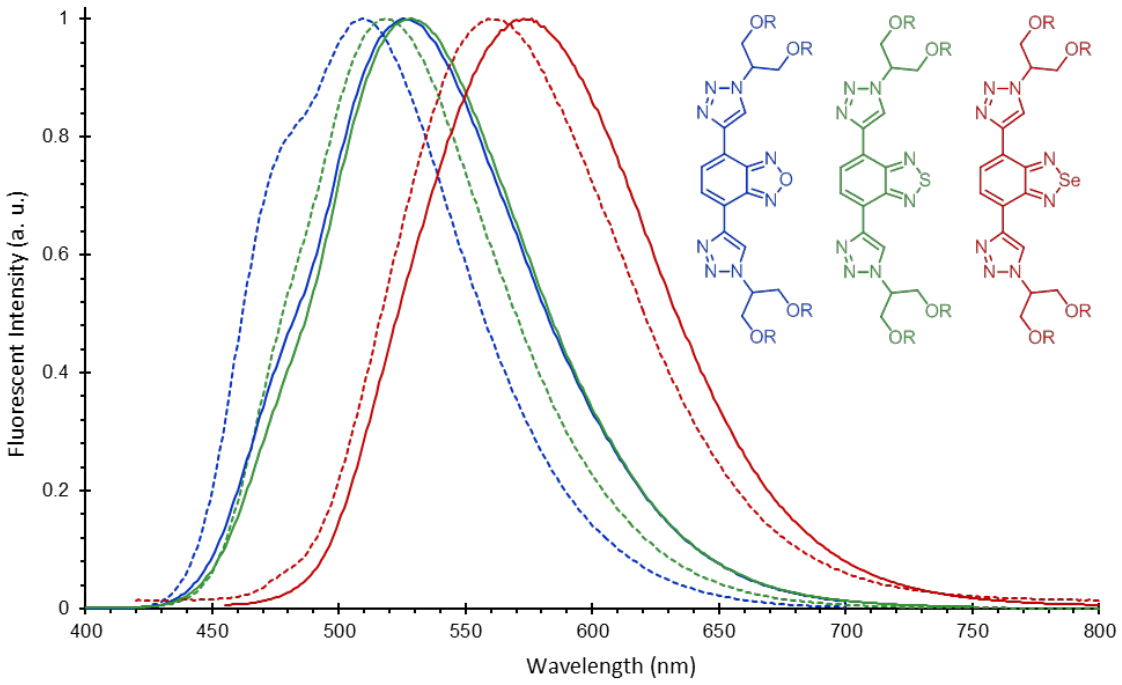

Figure 43 Fluorescence spectra of **44a-c** in H_2O (solid line) and DCM (dashed line).

6.2.3 Metal-Binding Studies

Next we examined the metal-binding properties of these cycloadducts in water. Screened metal ions include Na^+, K^+, Li^+, Mg^{2+}, Ca^{2+}, Cd^{2+}, Hg^{2+}, Pb^{2+}, Zn^{2+}, Cu^{2+}, Ni^{2+}, and Ag^+; the latter three acted as fluorescence quenchers. All three fluorophores exhibited a response to silver ions. Copper and nickel quenched the fluorescence of **44b** and **44c**, but the effect on **44a** was minimal. In order to quantify the binding strength, fluorescence titrations were performed with Ag^+, and also with Cu^{2+} and Ni^{2+} for **44b** and **44c**.

When the titration data were fitted to the standard Stern-Volmer equation, only the Cu^{2+} and Ni^{2+} data resulted in an acceptable fit. However, all the data were able to be fitted using equation 1.[149-152]

$$\Delta I = \frac{\alpha}{2}\left\{\left([F]+[Q]+\frac{1}{K}\right) - \sqrt{\left([F]+[Q]+\frac{1}{K}\right)^2 - 4[F][Q]}\right\} \quad (1)$$

ΔI is the change in fluorescent intensity, [F] is the concentration of the fluorophore, [Q] is the concentration of the quencher, and α is a fluorescence proportionality constant. The binding constant K can be determined through a least-squares curve fitting. Seeing that application of equation 1 for the Cu^{2+} and Ni^{2+} data resulted in binding constants very similar to what was determined from the Stern-Volmer analysis, this equation was used to determine the binding constants for all the data.

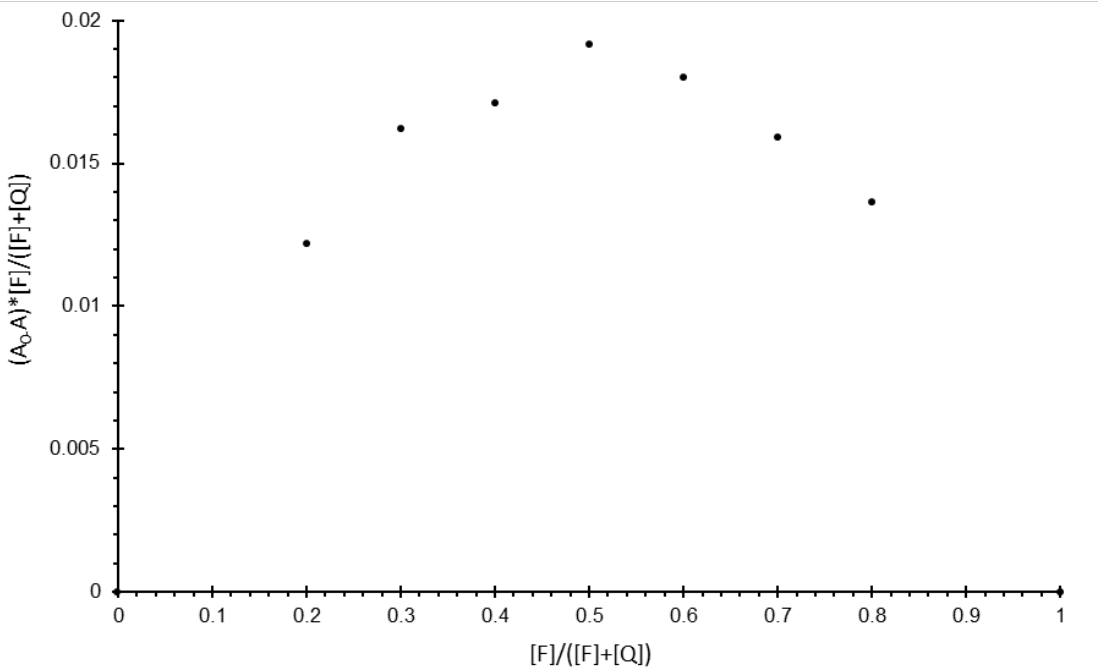

Figure 44 Job plot for **44b** with Ag^{+}.

One assumption inherent in this equation is a 1:1 stoichiometry in the metal-fluorophore complex. With the phenazine cycloadducts, this was verified by NMR spectroscopy. More commonly, the binding stoichiometry is determined through the method of continuous variations, also known as a Job plot. The concept here is to plot the change in the system as a function of the relative molar fractions. The binding stoichiometry is that where the largest change is seen. Figure 44 shows the Job plot for **44b** with silver ion. The greatest change is seen at a mole fraction of 0.5, indicating 1:1 complex formation. The x axis is the mole fraction of **44b**; the

number of moles of each species is varied, but the total number of moles is kept constant. On the y axis is plotted the change in the absorbance, multiplied by the mole fraction of **44b**. Simply plotting the change in absorbance will not work in this case, as it is proportional to the chromophore concentration. If there is a distinct peak arising from the formation of the metal-fluorophore complex, then it is a different story. A perusal of the literature reveals many Job plots, with many different ways of plotting the change in the signal on the y axis.

The binding constants are shown in Table 6. The values determined for **44b** are comparable to those found previously for a similar bis-triazolyl compound with triethylene glycol substituents.[110] Binding of copper and nickel ions is heavily influenced by the chalcogen heteroatom, with **44c** being the most sensitive. This increase in binding efficiency corresponds to a decrease in the electronegativity of the heteroatom. The binding to silver is unaffected by the chalcogen atom, resulting in similar binding constants for all three fluorophores. What is most unusual is the lack of fluorescence quenching upon binding of silver ion, especially considering that silver quenched the fluorescence of the phenazine cycloadducts. This implies that the binding mechanism is different in this case. Unlike the Stern-Volmer equation, formation of a non-fluorescent complex is not an assumption inherent in equation 1, and the binding constants are still able to be extracted from the fluorescence data.

Table 6 Binding Constants (Reported as log[*K*])

Compound	Cu^{2+}	Ni^{2+}	Ag^{+}
44a	-	-	3.80 ± 0.11
44b	2.40 ± 0.07	2.60 ± 0.04	3.73 ± 0.12
44c	4.25 ± 0.09	4.13 ± 0.07	4.08 ± 0.14

Limits of detection (LOD) for **44c** were calculated to be 3.8, 0.27, and 0.56 μM, for Ag^{+}, Cu^{2+}, and Ni^{2+}, respectively. These figures were calculated graphically, from a plot of the fluorescence change versus the metal ion concentration. The data were collected near the expected LOD. At these low concentrations, no quenching due to Ag^{+} was seen, so the absorbance data were used. Determining the LOD graphically means extracting the intercept from the plot – at what

concentration is no change seen? This calculation must take into account the standard deviation of the measurement, which can be calculated with the STEYX function in Excel (STFEHLERYX auf Deutsch). Multiply the standard deviation by three, then divide by the slope to get the LOD. The number three here is an arbitrary multiplier of the standard deviation – 3.3 is also often used.

A response from three different metals begs the question of whether some selectivity can be imparted. Examination of the UV-Vis spectra from the metal titrations reveals unique responses to each metal (Figure 45). Commercially available software SYSTAT13 enabled us to perform linear discriminant analysis (LDA) to analyze the differences in the absorption spectra, whereby each metal can be identified according to the characteristic response of the fluorophore. Absorbance titration data with Ag^{+}, Cu^{2+}, and Ni^{2+} were collected at a constant concentration of **42c**, with the metal ion concentration ranging from 6 to 600 µM. The collected spectral data were pre-processed by subtracting the initial absorption spectrum, where the concentration of metal is zero, so that the analysis was performed using the change in the absorbance. LDA is then able to classify each spectrum as belonging to one of the three metals, based on the unique spectral changes.

The results of the statistical analysis are shown in Figure 45. Each data point in the canonical scores plot represents an absorbance spectrum at a certain concentration of metal. To confirm the accuracy of this method, each individual spectrum can be treated as an unknown, and then classified as one of the three metals. Using this cross-validation technique, we found 100% classification accuracy for metal ion concentrations above 15 µM. Copper and nickel ions can be accurately discriminated from eachother at concentrations below 7 µM. Addition of silver ion to the analysis clouds the picture somewhat, and metal concentrations below 15 µM result in inaccuracies. The range of concentrations used in the titrations indicates that this identification technique is not dependent on concentration, and because the analysis is performed using the change in absorbance, it is largely independent of the fluorophore concentration as well. It should be noted that quantification of the metal ion concentration is a straightforward matter when the binding constant is known.

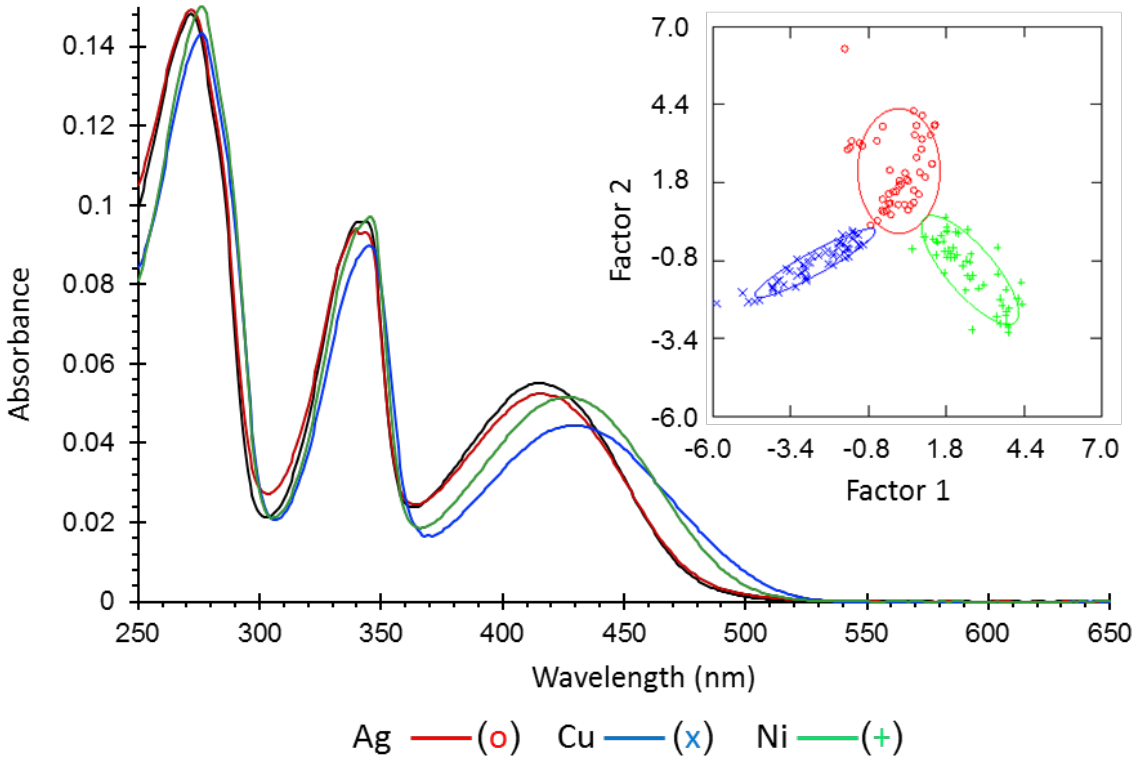

Figure 45 Absorption spectra of **44c** in H_2O without metal ion (black trace) and with different metal ions at 116 µM concentrations. (*inset*) The corresponding canonical scores plot generated from the linear discriminant analysis.

The analysis of the UV-Vis data was performed using SYSTAT 13. The absorbance data were collected as shown in Figure 46, at metal concentrations of 0, 6.58, 31.2, 58.8, 116, 333, and 579 µM. All titrations were performed at a constant fluorophore concentration of 8.8 µM. Three titrations were performed for each metal (Ag^+, Cu^{2+}, and Ni^{2+}). The absorbance data were carefully adjusted so that the absorbance past 600 nm was zero. The spectra were then subtracted from the spectrum taken at 0 M metal ion so that the change in absorbance could be analyzed. Analysis of the data revealed that the three metals could not be identified with 100% accuracy using the absorbance data from 6.58 µM Ag^+. Also, the analysis showed that data beyond 550 nm (only noise) affected the analysis and reduced the accuracy, so they were omitted. Three further titrations for each metal were then performed at metal ion concentrations of 6.40, 6.90, 7.39, 7.86, 8.33, 8.79, 9.24, 9.68, 10.1, 10.5, 15.6, 20.6, 25.5, 30.3, 44.1, 57.1, 104, 282, and 487 µM.

The analysis was performed using all trials. Omitting data recorded at lower metal ion concentrations resulted in more accurate classification. 100% cross-validation accuracy was seen when omitting data below 31.2, 15.6, and 20.6 µM for Ag^{+}, Cu^{2+}, and Ni^{2+}, respectively. 100% cross-validation accuracy was observed for only Cu^{2+} and Ni^{2+} when omitting data recorded below 6.58 and 6.90 µM for Cu^{2+} and Ni^{2+}, respectively.

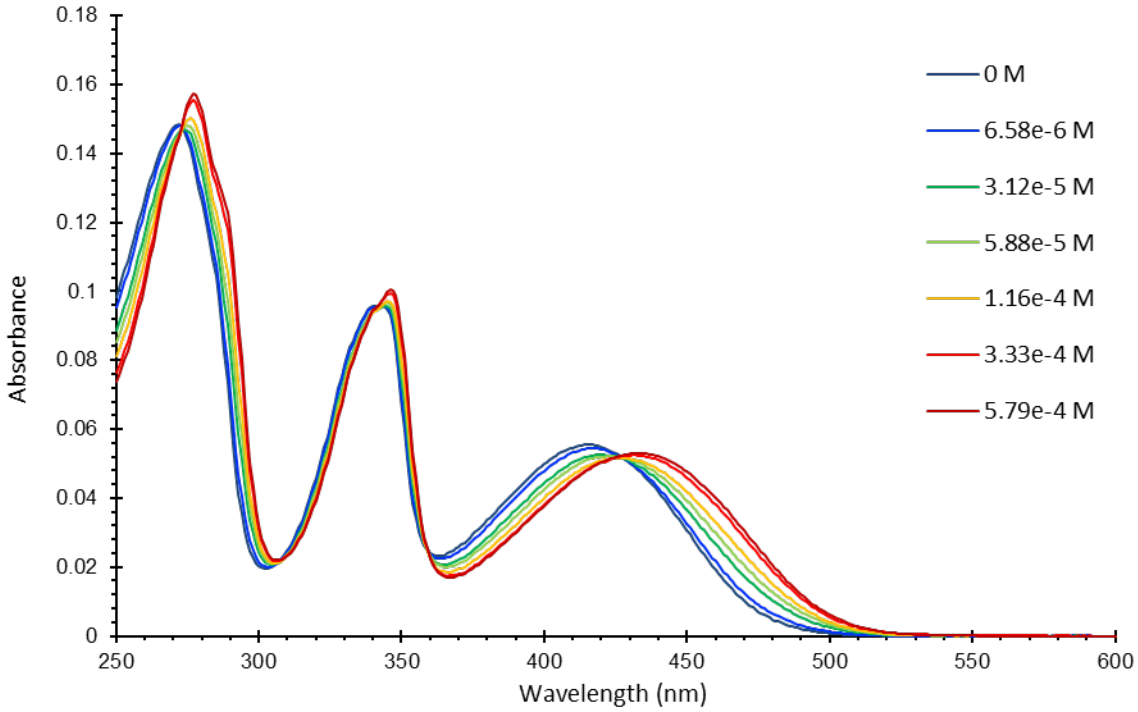

Figure 46 UV-Vis titration of **44c** with Ni^{2+}.

Cu^{2+} and Ni^{2+} can be differentiated at concentrations below 7 µM. Adding Ag^{+} lowers the accuracy. It is not clear why. It is clear that the problem lies with silver itself, and not the addition of a third metal. The accuracy is 100% above 15 µM with three metals, and it does not improve when differentiating silver and only one other metal. It only improves when silver ion is removed from consideration. The limit of detection of Ag^{+} is higher, but this may be due to the fact that it was gathered from absorbance data rather than fluorescence data.

6.3 Additional Small Molecule Cycloadducts

6.3.1 Cycloadducts of Thiophene and Pyridine

The synthesis of bis-triazolyl cycloadducts based on pyridine and thiophene is shown in Scheme 10. Synthesis of the pyridine cycloadduct was not carried through to completion; the synthesis proved to be troublesome, as ethynylated pyridines **51** and **52** were light-sensitive and degraded quickly.

Scheme 10 Synthesis of Thiophene and Pyridine Cycloadducts

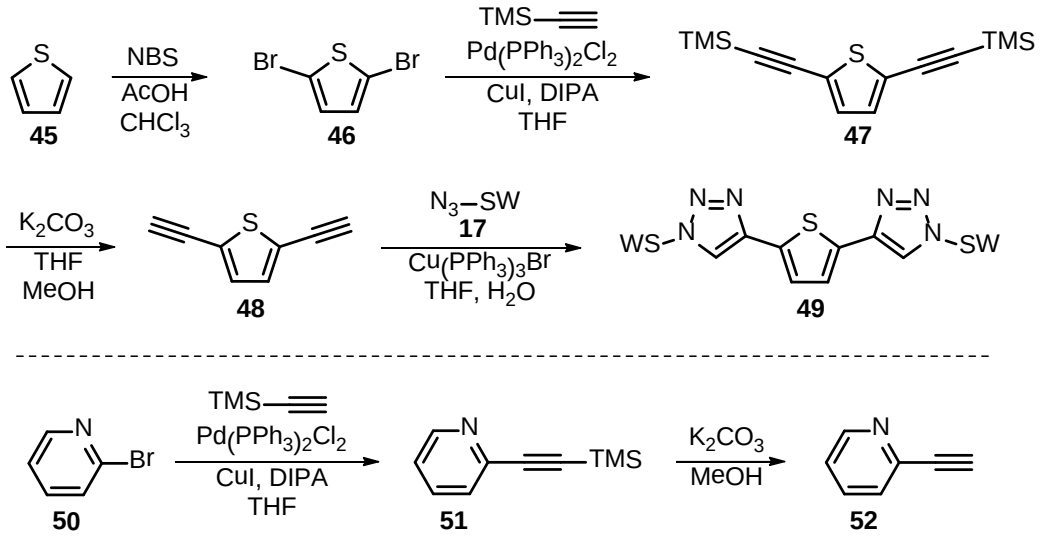

To briefly mention the results, the pyridine cycloadduct was not fully investigated, and the thiophene cycloadduct **49** was isolated as a water-soluble blue-fluorescent compound (Figure 47). **49** showed either very little or no response to the metal ions tested (Zn^{2+}, Mg^{2+}, K^{+}, Cu^{2+}, Ni^{2+}, Hg^{2+}, and Ag^{+}). The metal screening was done in water only. It is possible that some response would be observed in organic solvent. In particular, it is unfortunate that there was no response to Hg^{2+}.

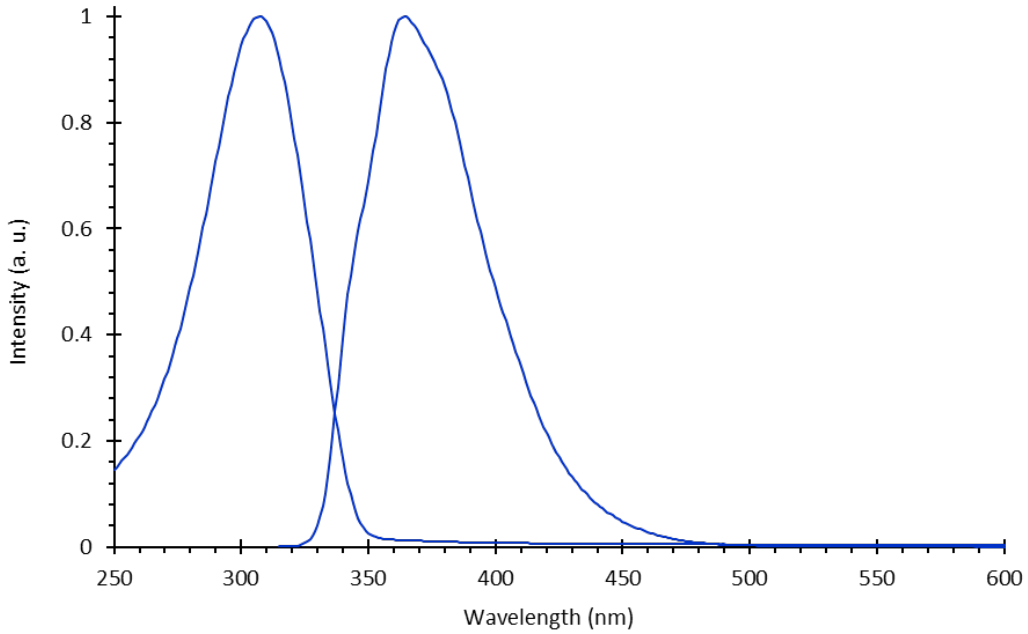

Figure 47 Absorption and emission spectra of **49** in H_2O.

6.3.2 Cycloadducts Containing Boron-Dipyrromethene (BODIPY)

BODIPY-containing cycloadducts **55a-b** were synthesized as shown in Scheme 11. Starting from **53a-b**, deprotection was accomplished with potassium fluoride dihydrate or potassium carbonate. For the cycloaddition, copper sulfate was used, as opposed to $Cu(PPh_3)_3Br$. **55a** was synthesized first, and the more bulky phosphine-ligated catalyst in THF was ineffective; no reaction was seen. Catalyst loading in this case was 10%, which was shown to be sufficient with the phenazine and benzochalcogendiazole substrates. A different catalyst ($CuSO_4$/ascorbate, 5 equiv.) was then added. Still, no progress was seen. Only after water was added as a co-solvent did the reaction proceed. So many equivalents were used in this case due to previous work demonstrating the necessity of more than one equivalent.[110] One advantage of the phosphine-containing catalyst is lower loading. To ensure that the catalyst is the problem and not the loading, **55b** was then synthesized using 1 equiv. $Cu(PPh_3)_3Br$. Again, no reaction was seen, and the $CuSO_4$/ascorbate system was required. The conclusion here is that $Cu(PPh_3)_3Br$ is too bulky to catalyze the cycloaddition to the BODIPY substrate. Also, the $CuSO_4$/ascorbate system is ineffective outside of aqueous systems.

Scheme 11 Synthesis of BODIPY Cycloadducts

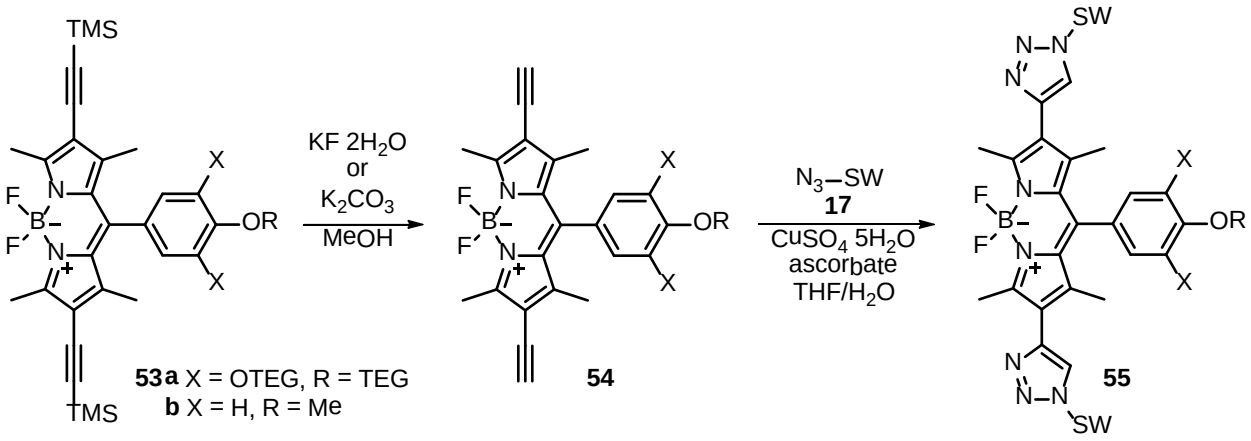

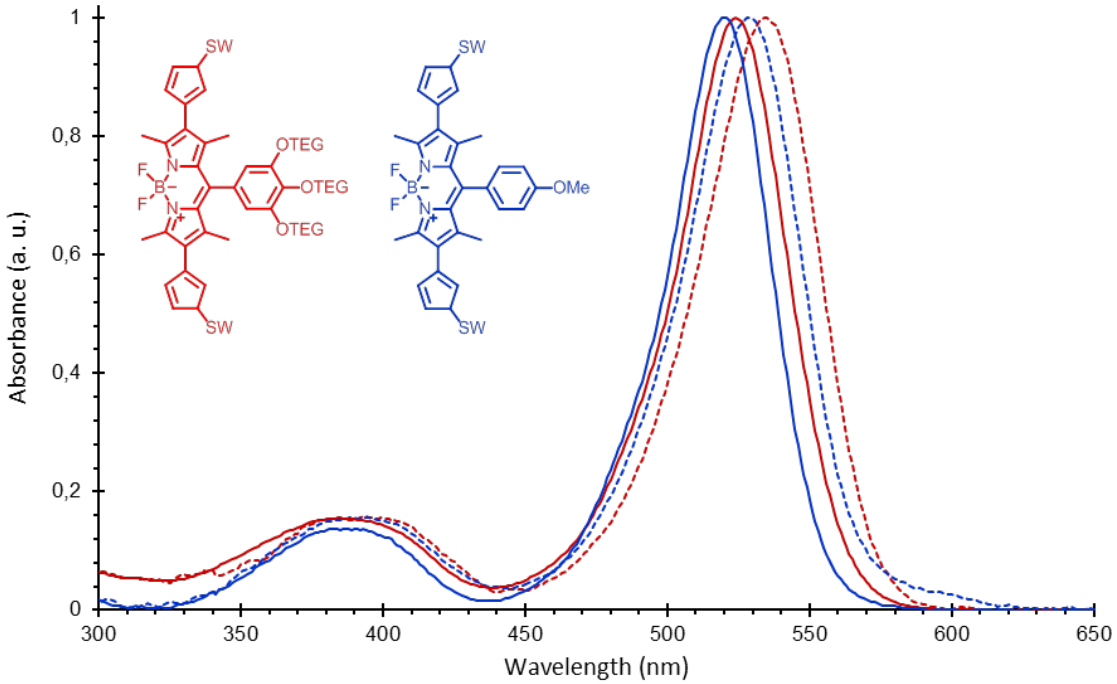

Figure 48 Absorption spectra of **55a-b** in H_2O (solid line) and DCM (dashed line).

The end result is two cycloadducts which are highly soluble in water and brightly fluorescent. The absorption and emission spectra are shown in Figures 48 and 49, respectively. Emission is in the orange, and the Stokes shifts are small, characteristic of BODIPY. Unlike the previous cycloadducts, no appreciable charge transfer character is evident in this case. The exceptional

aqueous quantum yields are attractive; unfortunately, no significant response to metal ions in water was seen. This is yet more evidence that the triazole ring alone is not enough to bind metal ions in water.

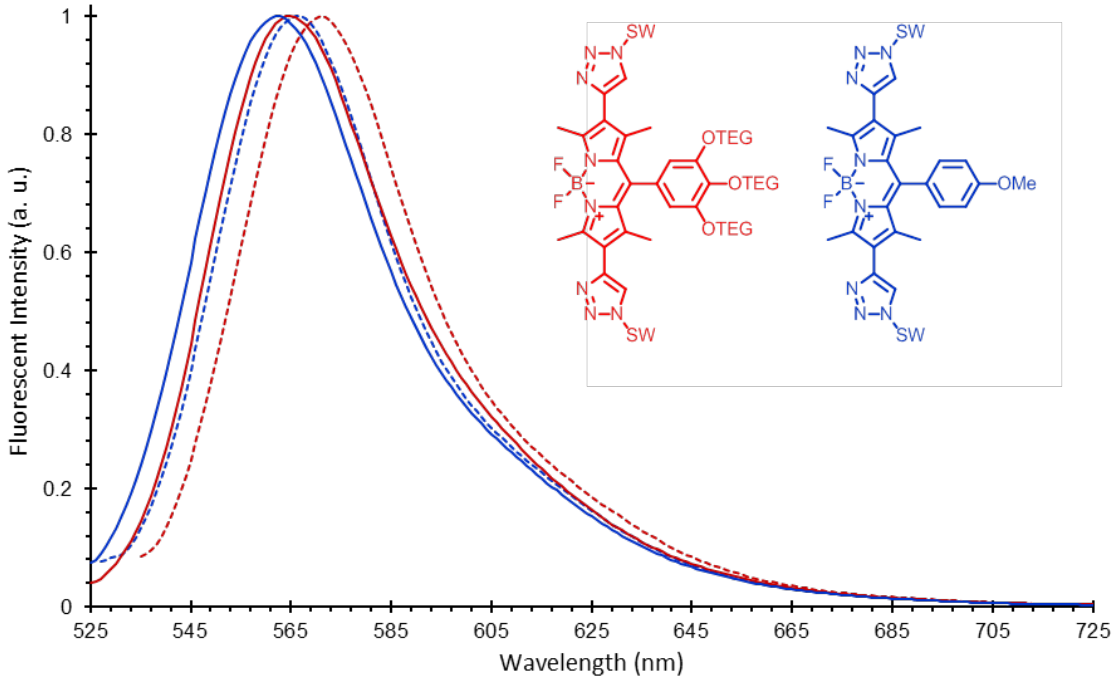

Figure 49 Fluorescence spectra of **55a-b** in H_2O (solid line) and DCM (dashed line).

The triazole rings do not seem to have a large effect on the photophysical properties in this case (Table 7). With the previous cycloadducts, the triazole exerted an auxochromic effect. Here, no significant red shifts are seen upon formation of the cycloadduct. Molecular orbital calculations (SPARTAN 10, B3LYP 6-311++G**) indicate the triazole rings do not participate in the conjugation (Figure 51).

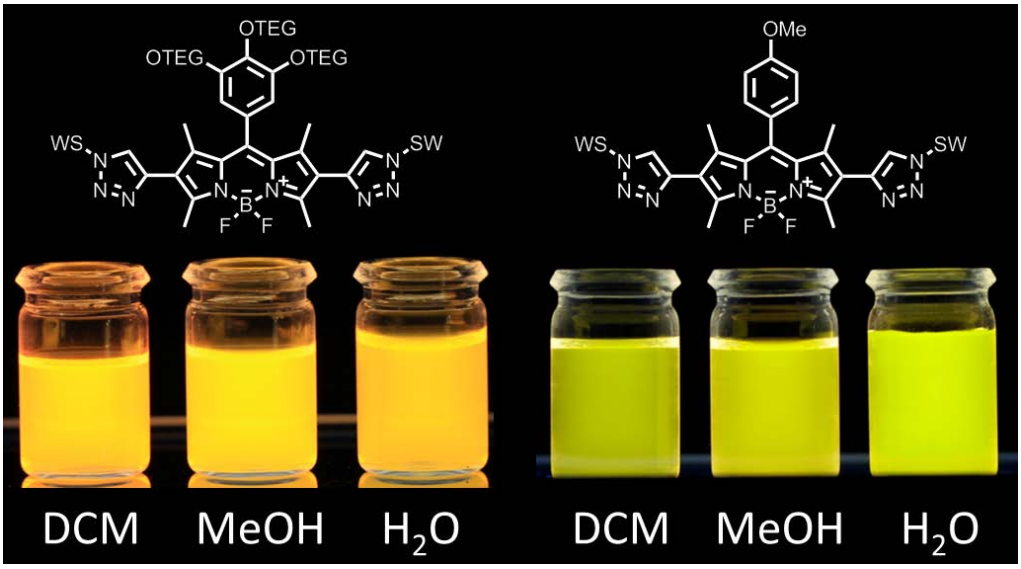

Figure 50 BODIPY cycloadducts in different solvents, illuminated under 365 nm light.

Table 7 Photophysical Properties of BODIPY Cycloadducts **55a-b**

Compound	Abs. λ_{max} (nm)		Em. λ_{max} (nm)		Stoke's Shift (cm^{-1})		Φ_f	
	DCM	H_2O	DCM	H_2O	DCM	H_2O	DCM	H_2O
55a	535	524	571	565	1178	1385	0.76	0.25
55b	529	520	566	562	1236	1437	0.80	0.63

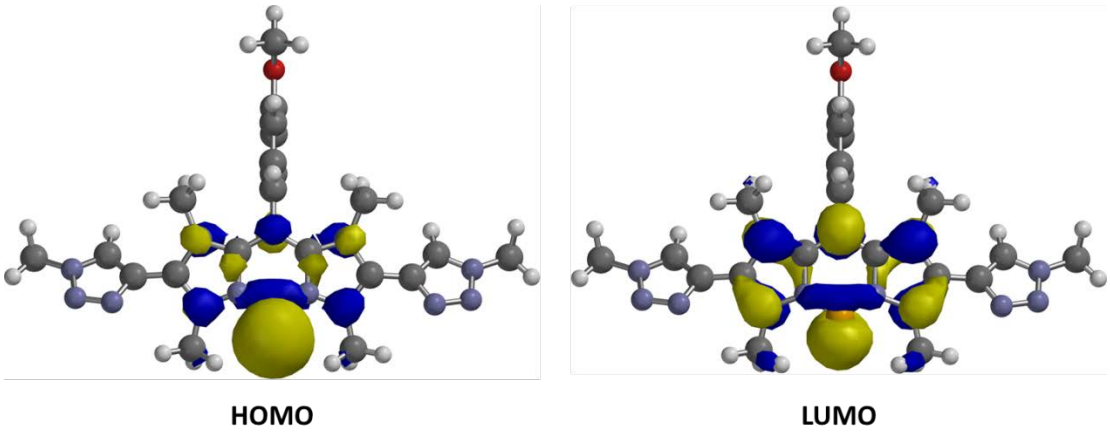

Figure 51 Calculated frontier molecular orbitals for **55b**.

6.4 Fluorescent Polymers for Metal Sensing

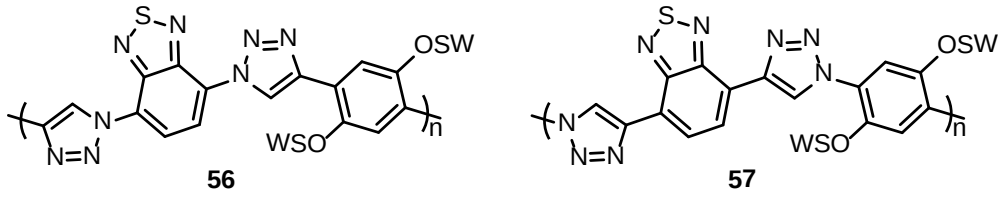

Figure 52 Click copolymers with benzothiadiazole.

Scheme 12 Synthesis of Monomers for Click Polymerization

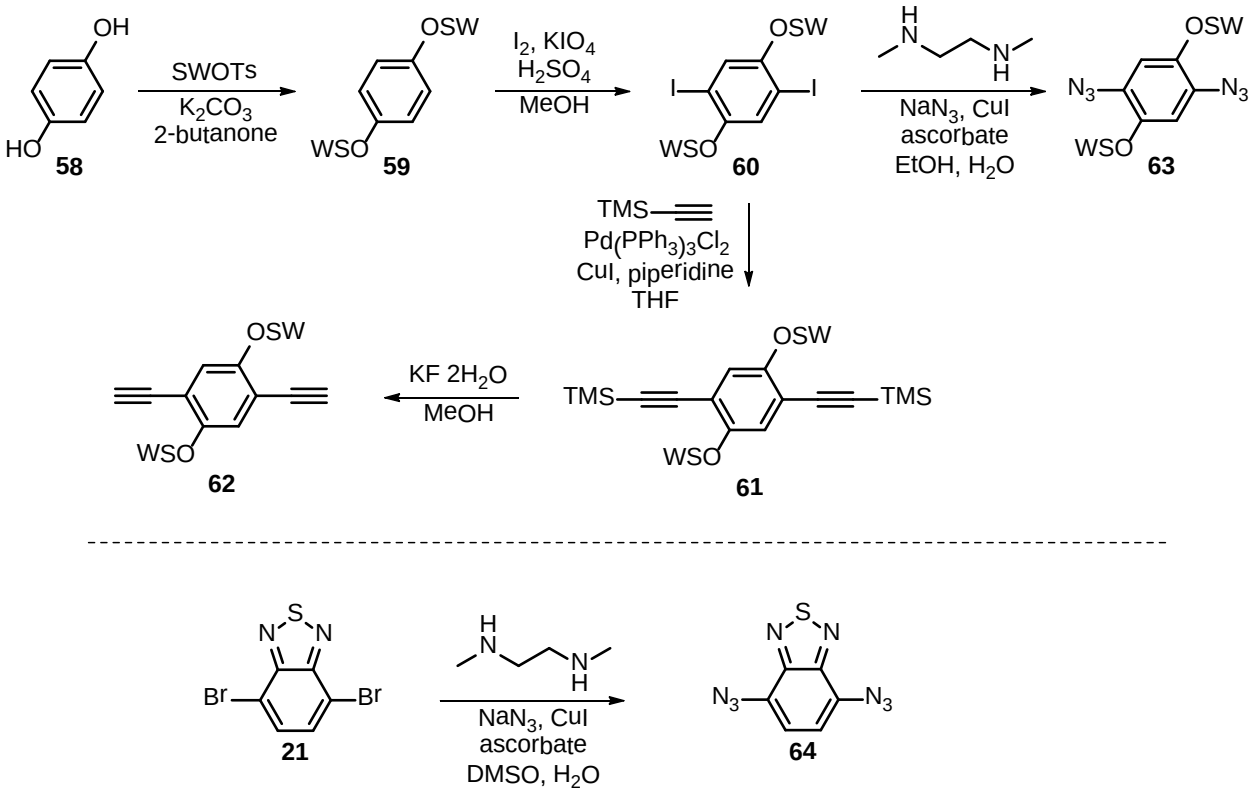

For the synthesis of polymers **56** and **57**, the monomers **62-64** and **43b** were attempted. The synthesis of **43b** has been mentioned already. The synthesis of monomers **62-64** is shown in Scheme 12. A slightly modified procedure was used for the synthesis of **60**, where the swallowtail was first added to the hydroquinone, followed by iodination, as opposed to the

iodination coming first. From there, monomer **62** was reached with a Sonogashira coupling, followed by deprotection. Problems were encountered in the syntheses of **63** and **64**. For **63**, the best conversion achieved was 18%, with 60% bearing only one azide group (according to ^{1}H NMR spectroscopy). The protocol used for **64** resulted in amination (not azidation) at only one of the brominated carbons. This result was found whether the reaction was run with or without heat. These issues with azidation prevented the synthesis of the target polymers.

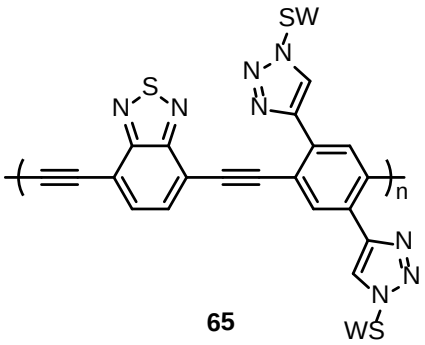

65

Figure 53 A PPE containing benzothiadiazole and triazole.

Scheme 13 Synthesis of an Alkyne-Functionalized PPE

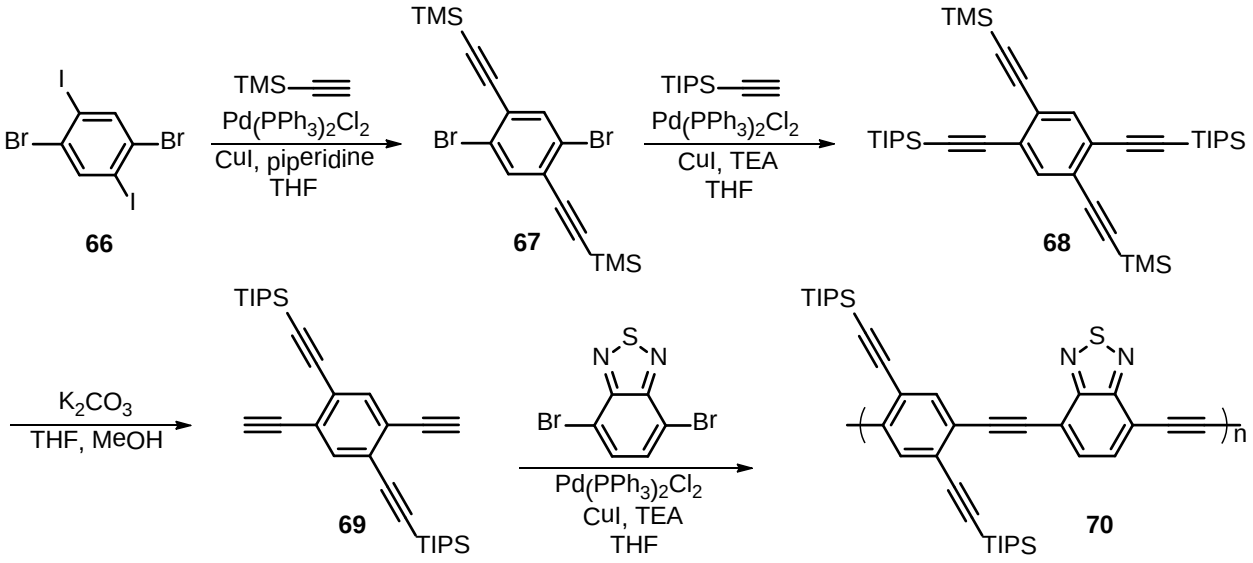

66 **67** **68** **69** **70**

A polymer with pendant triazole may possess interesting properties, in addition to being useful for sensing purposes. The synthesis of polymer **65** was attempted using a postfunctionalization

strategy. Scheme 13 shows the synthesis of precursor polymer **70**. With dibromobenzothiadiazole in hand, this synthesis can be achieved in four steps from the commercially available dibromo-diiodobenzene (**66**). The resulting polymer **710** suffered from poor solubility and high polydispersity. Postfunctionalization to polymer **65** via CuAAC was unsuccessful; in fact, no indication of a terminal alkyne was present after stirring **70** in THF with TBAF. Any further attempts at the synthesis of polymers with directly conjugated pendant triazoles must involve polymerization of the triazole-containing monomer.

Figure 54 shows the size exclusion chromatogram of **70**. Integrating from 17.5 to 28 min gives the number average molecular weight (M_n) as 13453 Da and the weight average molecular weight (M_w) as 50770 Da. This high polydispersity (PDI = M_w/M_n = 3.8) results from the presence of oligomeric species, which are seen in the chromatogram as the sharper peaks eluting after 25 min. Precipitation as a purification technique was not viable here due to low solubility. Soxhlet extraction met with only minimal success. In the end, this polymer was unable to be post-functionalized, and further efforts at purification were abandoned.

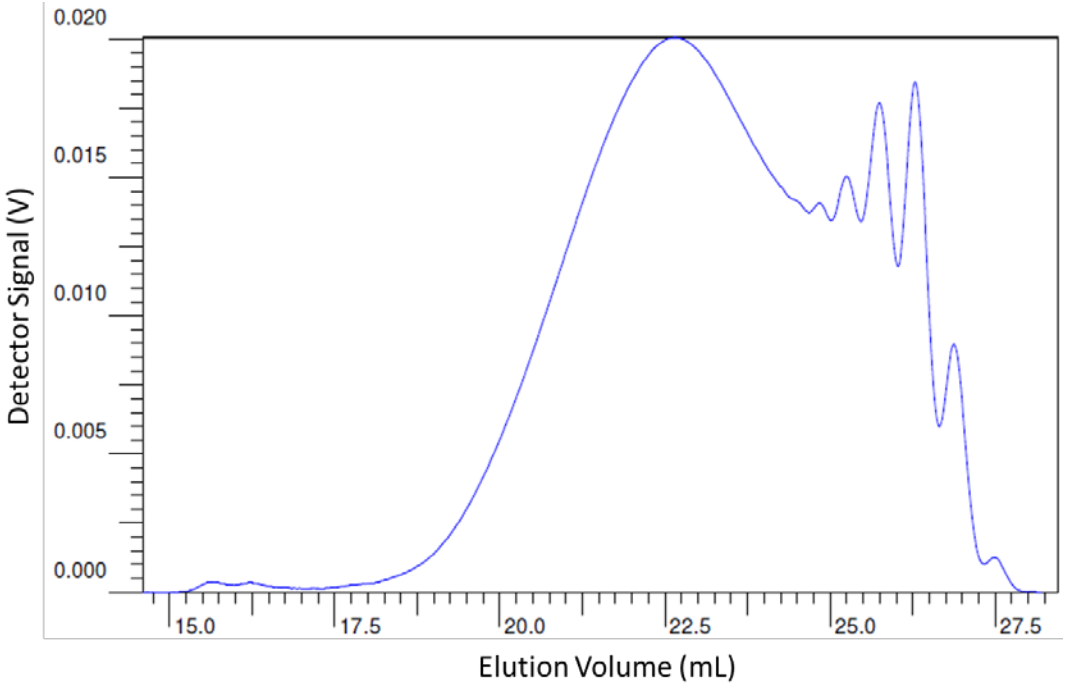

Figure 54 Size exclusion chromatogram of **70**.

The synthesis of triazole-containing monomers for polymerization has begun with the reaction shown in Scheme 14. The product **71** was recovered in 81% yield, and may be useful for future polymerizations.

Scheme 14 Synthesis of a Pre-Functionalized Monomer.

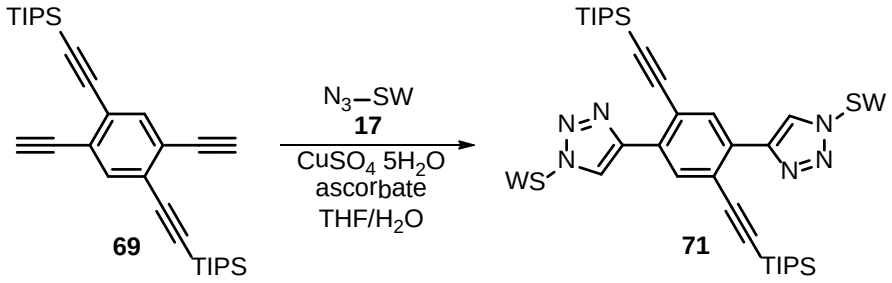

Another attempt at a triazole containing monomer was made with a thiophene. Scheme 15 shows the attempted synthesis of a thiophene with trimethylsilylethynyl groups at the 3 and 4 positions. From there, CuAAC would result in a monomer with two triazole rings. The thiophene is easily functionalized at the 2 and 5 positions to make reactive, polymerizable monomers. The first two reactions are known and **73** was synthesized without problem. However, the synthesis of **74** was unsuccessful, as the 3 and 4 positions are less reactive, and unresponsive towards Sonogashira coupling under the typical conditions employed.

Scheme 15 Attempted Synthesis of an Ethynylated Thiophene

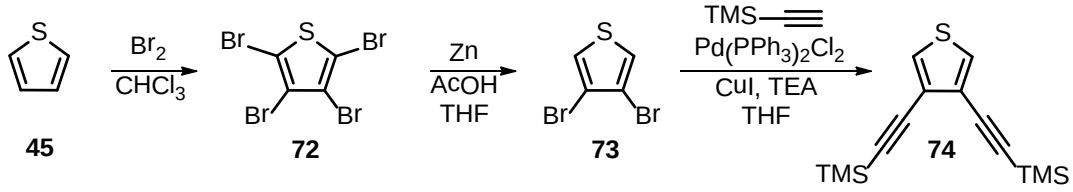

It is unknown whether such a thiophene monomer with two pendant triazole rings would be capable of binding metal ions. Will the two triazole rings cooperatively bind? Another pertinent question – is a sufficient binding pocket formed with pendant-triazole polymers such as **65**?

Model compounds such as those in Figure 55 will provide some answers to these questions, pointing towards likely candidates for metal binding polymers.

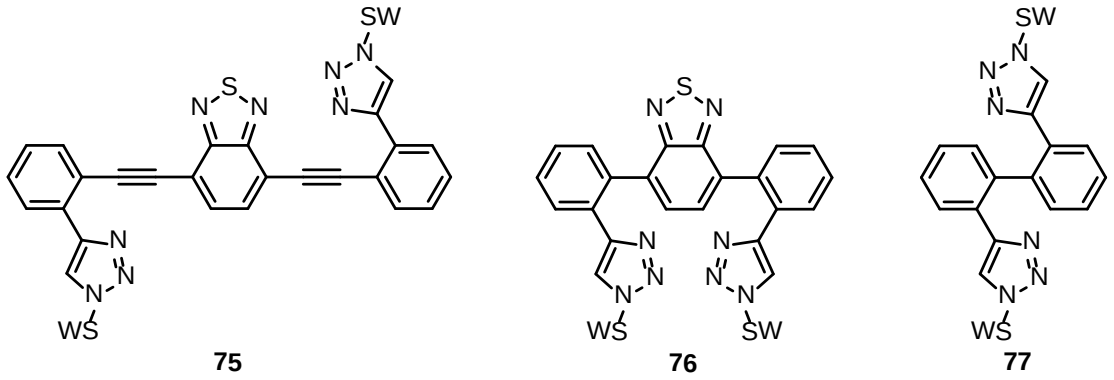

75 **76** **77**

Figure 55 Model compounds for metal-binding studies.

Scheme 16 Synthetic Strategy Towards Model Compounds

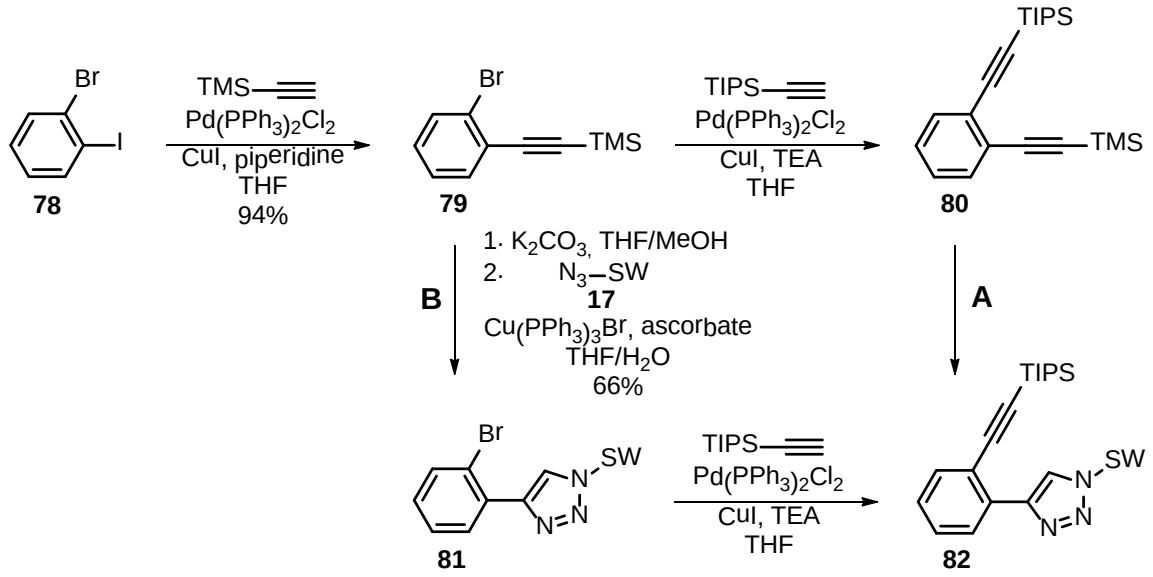

Scheme 16 shows a synthetic route towards these model compounds. Starting from commercially available 2-bromo-1-iodobenzene, compound **79** was synthesized in excellent yield. From there,

further alkynylation proved difficult. The Sonogashira reaction to reach **80** did not go to completion, and the product could not easily be separated from the starting material. The first attempt resulted in only 14% yield. This is in contrast to the symmetrical compound **81**, which can be isolated in greater than 70% yield.[158] Longer reaction times may be able to coax this reaction to completion. A separate route (**B**) was attempted in an effort to facilitate alkynylation at the brominated position. However, the synthesis of **82** from **81** was completely unsuccessful under the conditions employed, indicating that route **A** is preferable. Triazole-substituted **82** has yet to be synthesized, but it was determined that its counterpart **81** can be synthesized from **79** through a one-pot deprotection/cycloaddition reaction. An initial attempt in the synthesis of **81** was made which involved isolating and purifying the terminal ethynylated intermediate. This intermediate degraded rapidly and this reaction route resulted in a slightly lower yield.

6.5 Water-Soluble Poly(aryleneethynylene)s (PAEs)

6.5.1 Synthesis

The synthesized polymers are composed of a few different building blocks, shown in Figure 56. Polymerization was accomplished through Sonogashira coupling of the corresponding diiodo- and diethynyl- compounds. The polymers presented in this section were synthesized from the diethynylated benzothiadiazole, the synthesis of which was detailed previously in this chapter. For the other three phenylenes, both their diiodo and diethynyl versions were used. For each of these phenyl units, the diethynyl version is reached from the diiodo via Sonogashira coupling. The synthesis of the swallowtail-substituted monomer was discussed in the previous section. The tri(ethylene glycol)-substituted monomer is synthesized in the same manner. The last arylene sports ethyl ester groups. Post-polymerization, these esters are easily hydrolyzed to the carboxylate. The synthesis of the ester-containing monomers **86** and **88** is shown in Scheme 17.

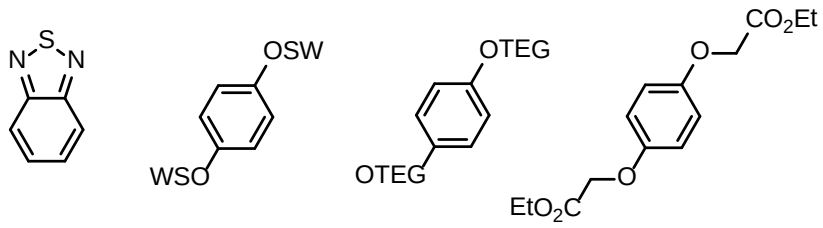

Figure 56 Arylenes used in the PAEs.

86 and **88** are synthesized in a fashion very similar to the other water-soluble monomers, with the substituent being added onto the benzene-1,4-diol, followed by ethynylation and deprotection. The order of the steps is slightly varied, with the iodination being performed first. Something worth mentioning is the reactivity of the ester group. Often, piperidine may be used in the synthesis of a compound such as **87**. In this case, piperidine should be avoided as it reacts with the ester. Tertiary amines must be used (triethylamine). In the deprotection step, methanol is a popular solvent choice to solubilize the carbonate salt. Methanol is a poor choice for the synthesis of **88**, however, as a Fischer esterification side reaction will result to some extent. This is not terribly important, as the end goal is to have the carboxylate (which can be reached from the ethyl or the methyl ester), but it may cause some confusion in the characterization of **88**.

Scheme 17 Synthesis of Ester Monomers **86** and **88**

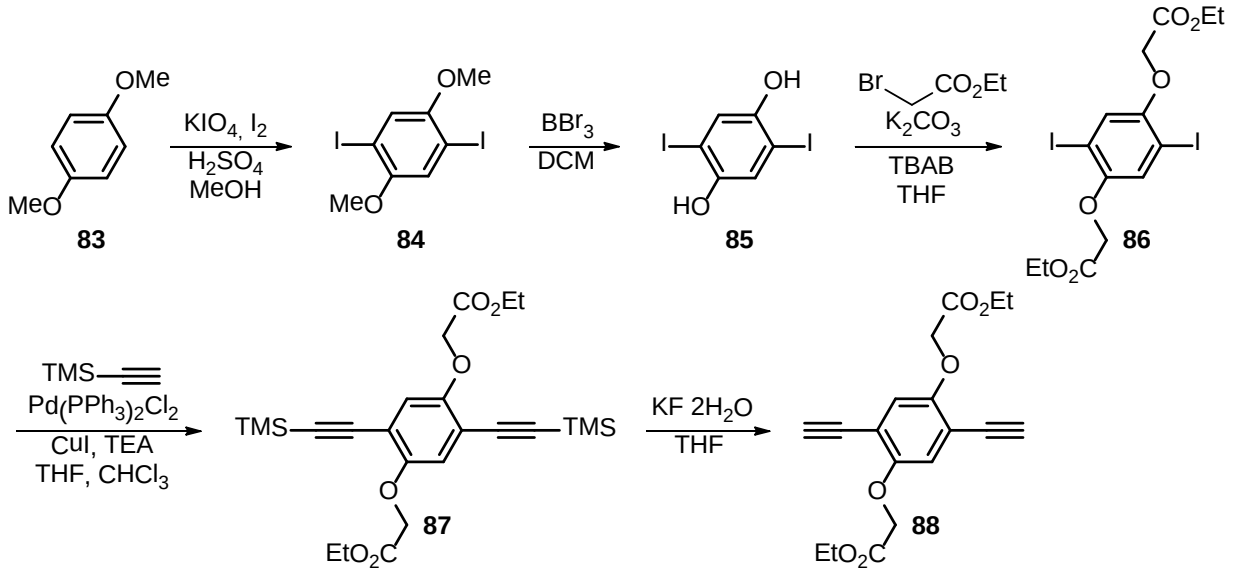

83 **84** **85** **86** **87** **88**

The synthesis of the polymers is shown in Scheme 18. All of the polymers containing the ester are hydrolyzed by sodium hydroxide to give the carboxylate. **92** and **93** are typical alternating copolymers. The others are statistical copolymers. **94** is synthesized so that there is a 3:1 ratio of TEG-containing monomer to benzothiadiazole, to aid solubility. Because of the nature of this polymerization, every other unit contains TEG side chains, but there is no guarantee that every fourth unit is benzothiadiazole. The same polymerization was performed with swallowtail-functionalized monomers to yield **95**. **96** and **97** are synthesized such that they contain benzothiadiazole, oligo(ethylene glycol) side chains, and the ester. This ester appears every other unit in **96**, while in **97** the swallowtail is present every other unit. For the purification of these polymers, precipitation in an appropriate solvent is common. Often, even multiple precipitations yield products which still contain some oligomers. Another option is dialysis, a purification technique made viable due to the water-solubility of these compounds. Placing the aqueous polymer solution into a dialysis membrane and stirring in water takes much longer (days) but is supremely effective at removing oligomeric products.

Scheme 18 Synthesis of PAEs

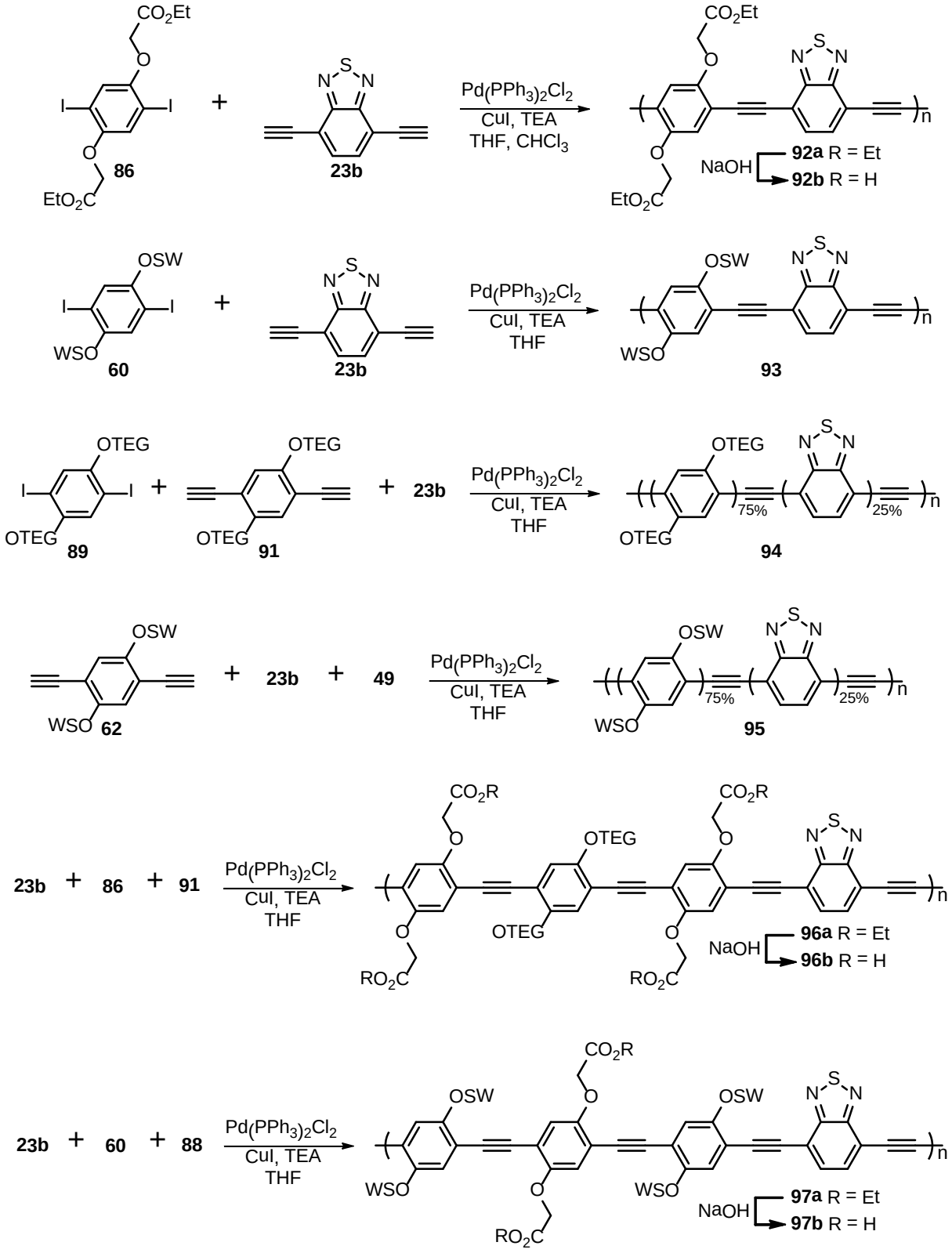

6.5.2 Size Distribution

One important consideration for the synthesis of these polymers is the stability of the ethynylated benzothiadiazole **23b**. Upon exposure to light, **23b** degrades rapidly, evidenced by its discoloration from orange to black. The importance of using this compound immediately after its isolation can be seen in the molecular weights of the resulting polymers. **93** and **97** were synthesized using freshly prepared **23b** as a monomer, and these two polymers show the highest molecular weight. This is most noticeable when comparing **93** and **95**. The use of extra swallowtail-substituted monomer in **95** should make this polymer more soluble, and we would expect a higher molecular weight, or at least something comparable. Instead, **93** is twice as large, and the only difference in the synthesis was the use of freshly prepared **23b**. The estimated molecular weights for the synthesized polymers are shown in Table 8, determined by gel permeation chromatography in THF, referenced to polystyrene standards. The degree of polymerization (DP) reported refers to the number of repeating aryleneethynylene units, and not to the number of benzothiadiazole units. The hydrolyzed polymers **92b**, **96b**, and **97b** were not characterized in this fashion, and are assumed to retain the degree of polymerization of their precursors.

Table 8 Polymer Size

Polymer	Mw (Da)	Mn (Da)	PDI	DP
92a	7330	3410	2.1	15
93	34600	19000	1.8	37
94	11030	6390	1.7	20
95	14100	9700	1.4	14
96a	12740	6140	2.1	21
97a	32500	16600	2.0	30

6.5.3 Physical and Spectral Properties

The absorption and emission spectra of all polymers is shown in Figures 57 and 58. The polymers synthesized without the swallowtail group (**92**, **94**, and **96**) displayed limited solubility in water. The spectra of **92a**, **94**, and **96a** were recorded only in organic solvent. Even the solubility of the hydrolyzed products **92b** and **96b** was very low; the absorption of **92b** was measured in water,

but the emission was measured in methanol due to a lack of solubility. **96b** is only sparingly soluble in water, and its quantum yield suffers greatly. The swallowtail group was incorporated in the other polymers to alleviate these problems. These swallowtail-containing polymers display much better solubility, though unfortunately, the quantum yields are still very low in water.

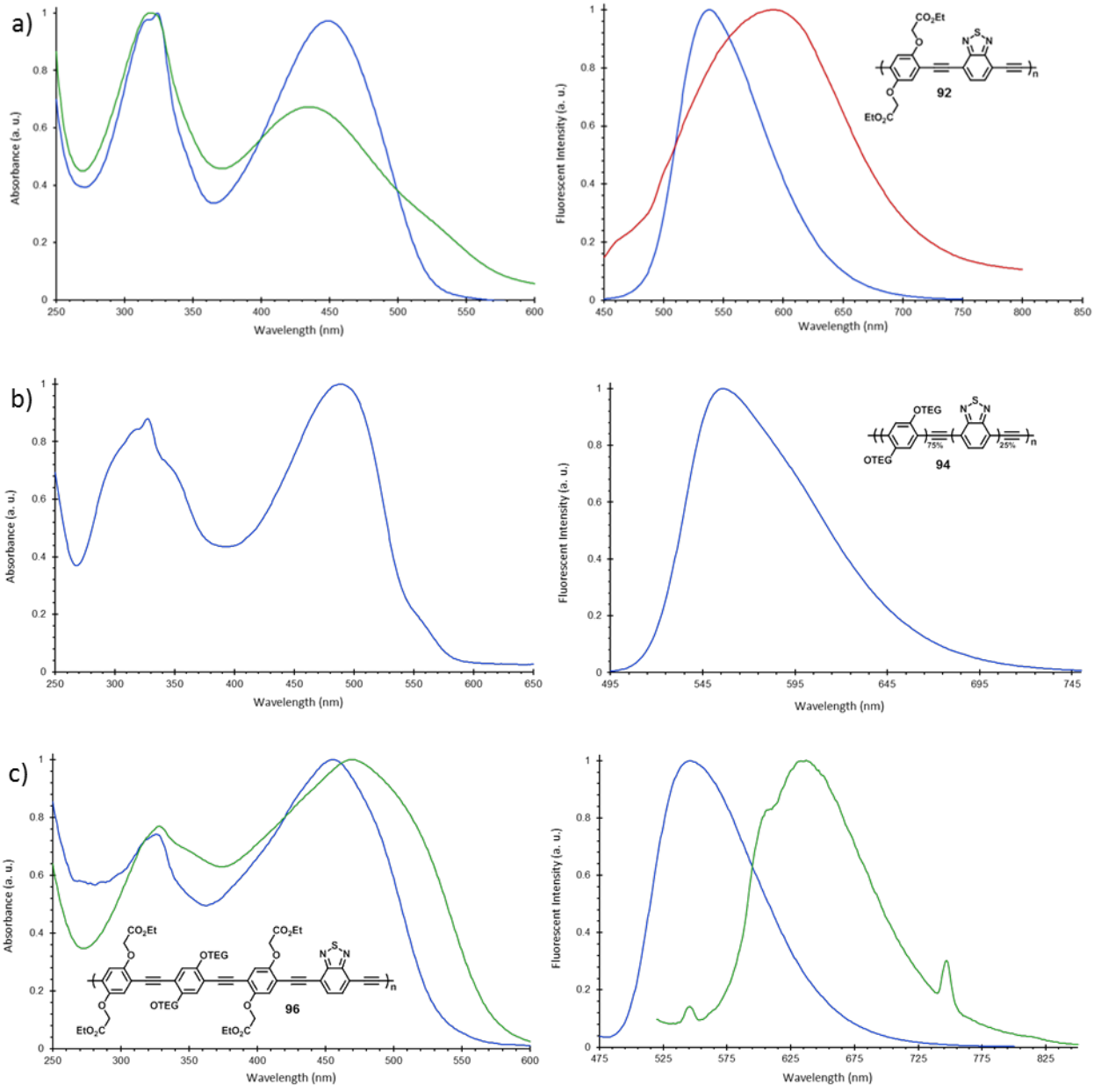

Figure 57 Absorption and emission spectra in DCM (blue trace), H_2O (green trace), and MeOH (red trace). a) **92a** (blue) and **92b** (green and red). b) **94**. c) **96a** (blue) and **96b** (green).

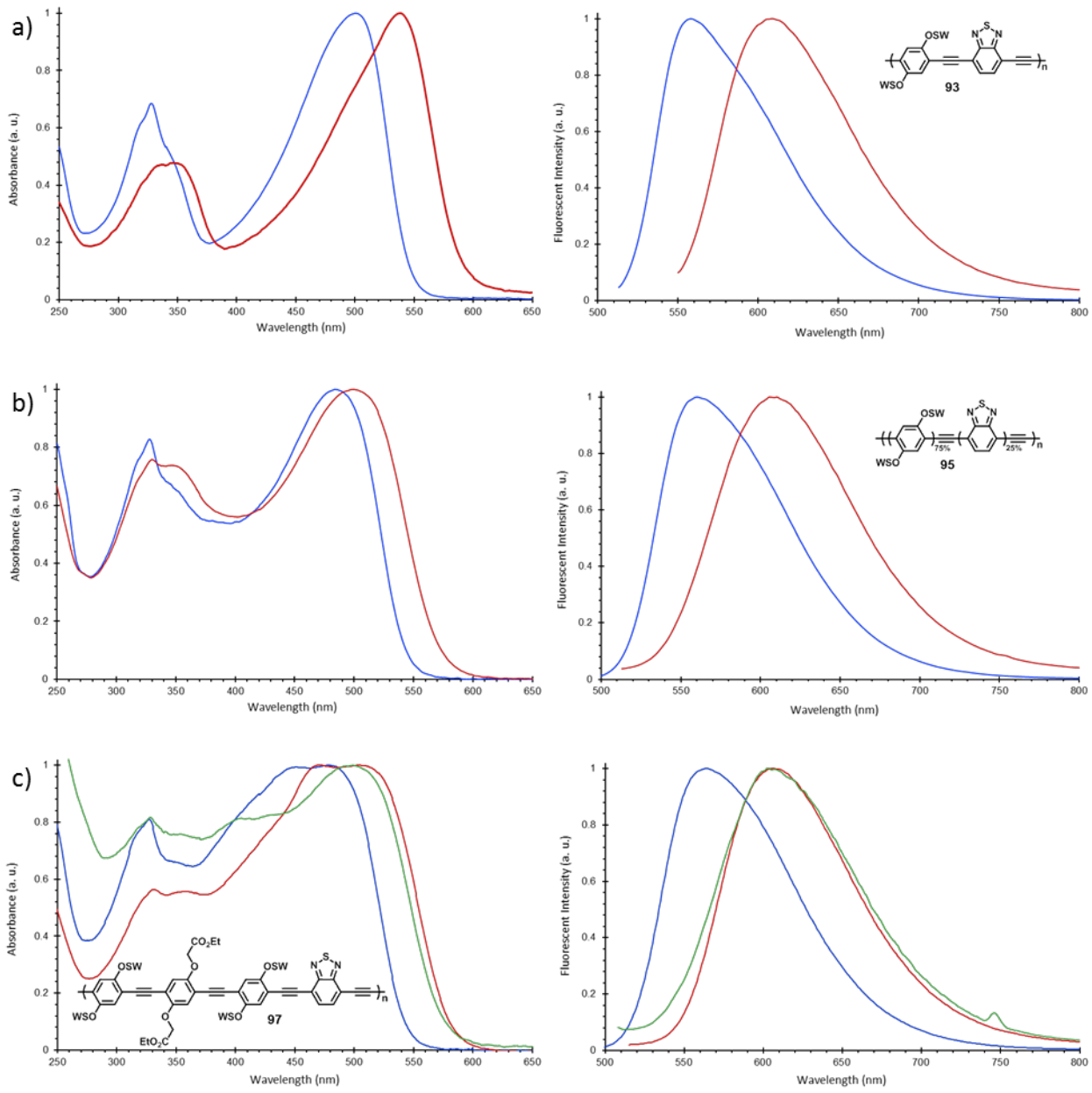

Figure 58 Absorption and emission spectra in DCM (blue trace) and H_2O (red and green traces). a) **93**. b) **95**. c) **97a** (red and blue) and **97b** (green).

It must be considered that polymers **96** and **97** are true random statistical copolymers only if the reactivity of the two diethynyl monomers is the same. A closer look at the optical spectra indicates that this may not be the case. Figure 59 shows the emission of **96a** in MeOH (blue trace) and DCM (red trace). The dominant peak present in dichloromethane is due to the presence of the benzothiadiazole. There is another peak, however, which is likely due to an entirely

different fluorescent species. Methanol is seen to quench the dominant peak seen in dichloromethane, leaving only the higher energy signal. Hydrolysis of the polymer gives **96b**, the fluorescence of which is also shown in Figure 57 (in water, green trace). Some fluorescence can be seen past 600 nm, but it is very weak. It is possible that polymerization occurs preferentially with one monomer, and then the other, resulting in two different polymers. The same thing was seen with **97a** – after hydrolysis to yield **97b**, not all of the product could be dissolved in water. The notion that there is a polymeric species present containing little to no benzothiadiazole would explain this, as well as the separate peaks, though elemental analysis of the pre-dialyzed product was unable to confirm this.

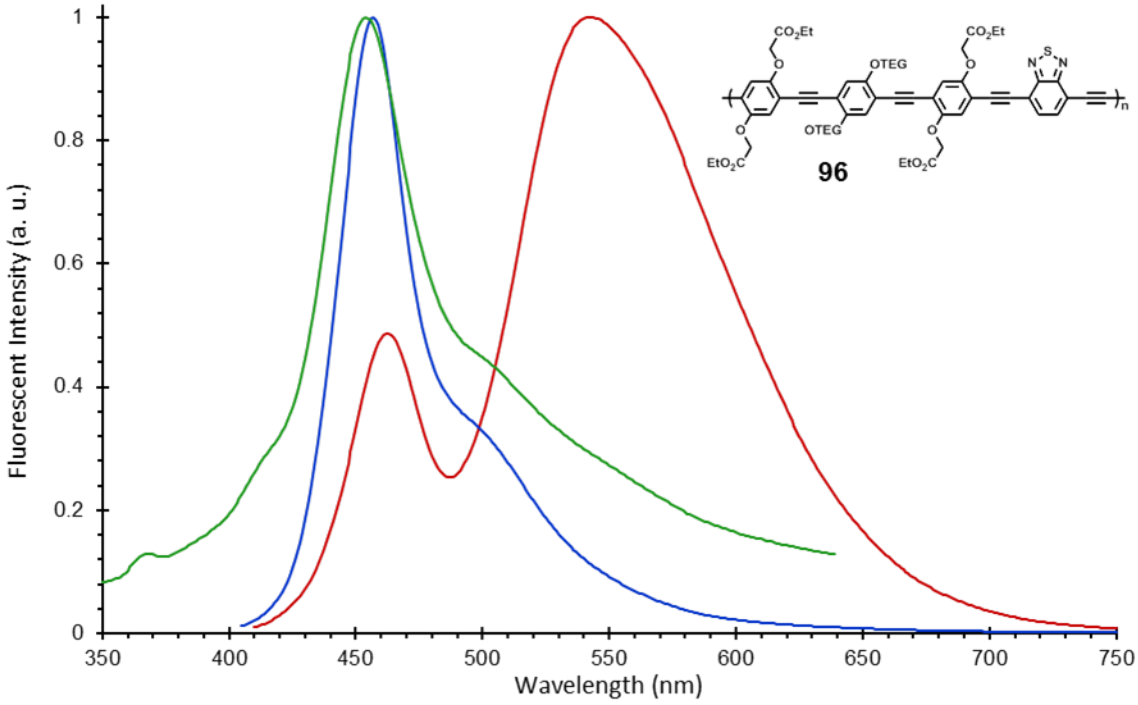

Figure 59 Emission spectra of **96a** in MeOH (blue) and DCM (red), and **96b** in H_2O (green).

The photophysical properties are summarized in Table 9. Little difference in the spectra occurs when the percentage of benzothiadiazole is varied (25% or 50%). The red-shifted spectra result from inclusion of the benzothiadiazole, though it is uncertain what percent is necessary to induce this effect. The extra red-shifting seen for **93** should be attributed to the extended conjugation

rather than the higher percentage of benzothiadiazole. The other polymers exhibiting emission further into the red (**92b** and **96b**) are likely experiencing aggregation to some degree.

Table 9 Photophysical Properties of PAEs **92-97**

Compound	Abs. λ_{max} (nm)		Em. λ_{max} (nm)		Stoke's Shift (cm^{-1})	
	DCM	H_2O	DCM	H_2O	DCM	H_2O
92a	449	-	538	-	3685	-
92b	-	435	-	613[a]	-	6676
93	500	539	558	609	2079	2133
94	489	-	556	-	2529	-
95	484	499	560	606	2804	3538
96a	456	-	546	-	3615	-
96b	-	470	-	633	-	5479
97a	478	474	563	606	3159	4595
97b	478	498	563	602	3159	3469

[a]593 nm in MeOH

These polymers have not yet been fully characterized – at this point, there are only a few conclusions that can be made. The swallowtail side chain has proven itself again to be an excellent agent for providing water-solubility. This is especially important here, as the benzothiadiazole, as well as the ester moiety, are poorly soluble even in common organic solvents. Polymers **92** and **96**, which contain the ester group every other arylene unit, were at best only slightly soluble in water, even after hydrolysis of the ester groups. This is compared to **97**, which contains swallowtail every other arylene unit, and is soluble in water even before the ester groups are hydrolyzed.

Not all of these spectra are pretty – the recovered polymers must be considered to be crude, even after precipitation. Purification by dialysis is ongoing, at which point it is expected to recover clean materials which may serve some sensory purpose. The polymers without swallowtail are unsuitable for these purposes due to their poor solubility. Preliminary metal-binding experiments with **97b** showed a response to Ag^{+} and Pb^{2+} in aqueous solution, indicating that this polymer may be useful as a metal ion sensor.

7 Conclusion and Outlook

Presented in this work is a method for the construction of fluorescent sensors utilizing click chemistry. These sensors are shown in Figure 60. The click reaction is used to introduce an oligo(ethylene glycol) substituent, giving products that are water-soluble and highly fluorescent. This reaction also produces a triazole ring, which serves multiple functions. The most important feature of the triazole in these molecules is its metal binding capacity. These sensors are constructed such that a binding pocket may be formed between the aromatic core and the triazole ring. The other function of the triazole is its contribution to the electronic properties. The rings serve to extend the conjugation, red-shifting the optical spectra. Additionally, the cycloadducts possess long lifetimes and large Stokes' shifts. These properties seem to stem from the triazole ring, implying that triazole-containing fluorophores may be useful for *in vivo* imaging.

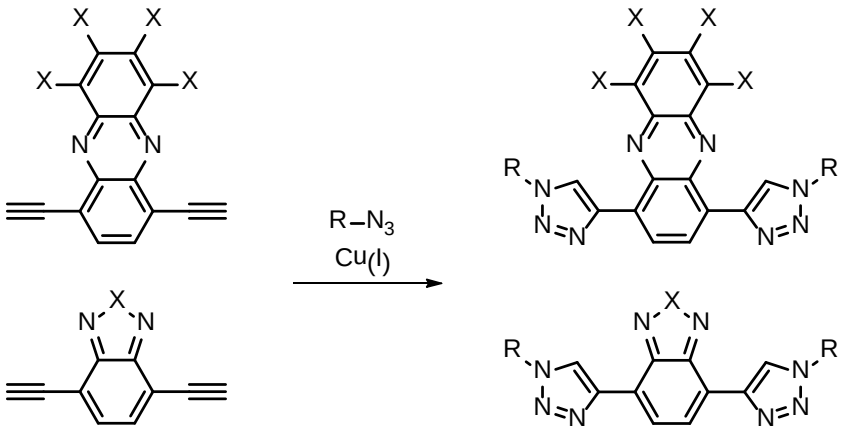

Figure 60 Click chemistry to synthesize fluorescence-based metal ion sensors. (*above*) Phenazine cycloadducts with a tetrahalogenated substitution pattern. X represents H, F, or Cl, and R represents an oligo(ethylene glycol) substituent. (*below*) Benzochalcogendiazole cycloadducts. X represents O, S, or Se and R represents an oligo(ethylene glycol) substituent.

The first series of bis-triazolyl cycloadducts was synthesized from ethynylated phenazines. The results show these compounds to be selective silver ion sensors. Next, the same chemistry was utilized to build a series of benzochalcogendiazole cycloadducts from the corresponding ethynylated compounds. These fluorophores proved capable of binding and discriminating copper, nickel, and silver ions.

The synthesis was designed such that it was possible to tune the electronic and optical properties of these fluorophores. The phenazines were synthesized with a tetrahalogenated substitution pattern, and the benzodiazole compounds were synthesized with different chalcogen atoms. The question of interest here is the effect of this variation in molecular architecture, not only on the electronic properties of the system, but also on the metal-binding activity.

The results obtained with the phenazine cycloadducts show that halogenation leads to a lowering of the band gap, and red-shifted absorption and emission spectra. According to DFT calculations, this can be attributed to a larger stabilization of the LUMO compared to the HOMO. These trends, at least with respect to N-heteroacenes, are already well-known. Less well-known, and therefore less predictable, is the concurrent effect on the metal-binding properties. Unsurprisingly, more electron rich π-systems facilitate more efficient binding. The more electron-poor halogenated phenazine cores are unable to bind metal ions in water. Also, the formation of only one binding pocket is observed in this symmetrical molecule, where there are two possible binding sites. This may also be due to an overall decrease in electron density upon binding the first metal ion, so that the system is too electron-deficient to bind a second.

With the benzochalcogendiazole cycloadducts, bathochromic shifts in the optical properties are seen on switching the chalcogen atom from oxygen to sulfur to selenium. In this case, DFT calculations indicate that the shifts are due to a destabilization of the HOMO. There also exists a clear trend in the binding affinity for copper and nickel ions in water; we observe an increase in the binding efficiency on moving down the chalcogen group. This may be due to a number of factors, including aromaticity and size, but the decreasing electronegativity of the chalcogen atom (going from O to Se) is the most likely suspect.

The phenazine cycloadducts were seen to bind silver only, while the benzochalcogendiazoles were able to bind copper, nickel, and silver. Based on these results, it can be concluded that any observed selectivity stems from the heteroaromatic core. It is notable that the triazole ring participates in the binding of metal ions (confirmed through NMR spectroscopy), but does not seem to dictate any selectivity.

The question of selectivity with regard to the benzochalcogendiazole compounds merited further exploration, as these compounds responded to more than one metal. Complex formation with

Cu^{2+}, Ni^{2+}, and Ag^{+} was observed through changes in the optical spectra. The variation in the spectral properties is dependent on the metal ion present. A statistical analysis of the spectrophotometric response can be performed to reveal which metal is being complexed (Figure 61). The benzoselenadiazole cycloadduct is the most sensitive, and the statistical analysis of its response to aqueous silver, copper, and nickel discriminates the three metals at concentrations as low as 15 µM.

The choice of solvent for these experiments is of utmost importance. The fact that these experiments are carried out in water is critical. Solvent effects in this area of metal-fluorophore interactions are very complex and cannot be predicted. It cannot be assumed that metal sensing results obtained in organic solvent will be valid in aqueous solvent. The world of aqueous solution is of course much broader than water. Solvent experiments were not performed here for the most part, leaving interesting questions regarding the performance of these molecules in buffered solutions, at varying pH, or under physiological conditions.

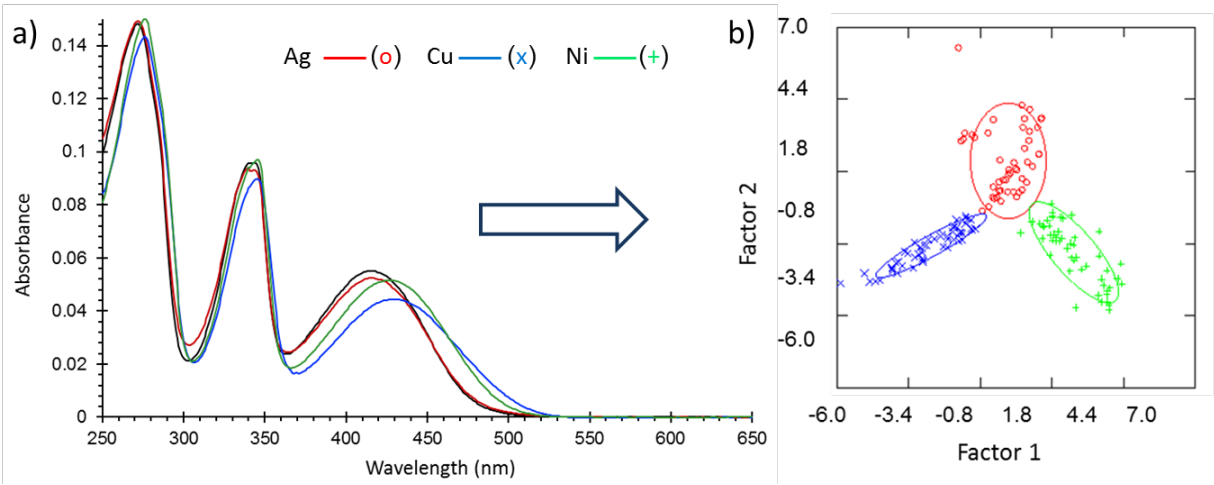

Figure 61 a) Absorbance curves of **44c** in the presence of different metal ions. b) Differentiation of the unique absorbance curves through linear discriminant analysis.

Many questions remain as to the most efficient construction of metal ion sensors, and the best methods of imparting selectivity. The results given here regarding tunable metal-binding properties provide some chapters to the manual on fluorescence detection, and should be useful towards the future construction of highly sensitive and specific metal ion sensors.

Our immediate future direction is to apply our results to polymeric systems. We anticipate polymers with interesting features, as well as improved sensitivity towards metal ions when compared to small molecule systems. Also of interest is the application of these molecules in biological systems. The phenazine cycloadducts synthesized here show promising antibacterial properties, and the bright fluorescence and long lifetimes of these compounds may prove useful for *in vivo* imaging.

8 Experimental

8.1 Materials and Methods

All reagents and solvents were obtained from Fisher Scientific, ABCR, Alfa Aesar, Sigma-Aldrich, or VWR, and used without further purification unless otherwise noted. All absolute solvents were dried by a MB SPS-800 using drying columns. Preparation of air- and moisture-sensitive materials was carried out in oven-dried flasks under an atmosphere of nitrogen using Schlenk techniques. For thin layer chromatography, Polygram Sil G/UV 254 plates from Macherey, Nagel & Co. KG, Düren (Germany) were used and examined under UV-light irradiation (254 nm and 365 nm). Flash column chromatography was performed on silica gel from Macherey, Nagel & Co. KG, Düren (pore size 0.04-0.063 mm). Melting points were determined with a Melting Point Apparatus MEL-TEMP (Electrothermal, Rochford, UK) and are uncorrected. ^{1}H-NMR and ^{13}C-NMR spectra were recorded on a Bruker Avance 300 (300 MHz) or a Bruker 400 (400 MHz) spectrometer. Chemical shifts (δ) are reported in parts per million (ppm) relative to proton traces of the deuterated solvent.[159] All NMR spectra were integrated and processed using MestReNova. MS spectra were recorded on a Vakuum Generators ZAB-2F, Finnigan MAT TSQ 700 or JEOL JMS-700 spectrometer. Crystal structure analysis was accomplished on Bruker Smart CCD or Bruker APEX diffractometer. Infrared (IR) spectra were recorded on a Jasco FT/IR-4100 spectrometer. Absorption spectra were recorded on a Jasco UV-VIS V-660 or Jasco UV-VIS V-670. Emission spectra were recorded on a Jasco FP-6500. Elemental analysis was performed by the Microanalytical Laboratory of the University of Heidelberg using an Elementar Vario EL machine. Quantum yield measurements were measured relative to an appropriate standard (quinine sulfate in dilute sulfuric acid, or fluorescein in dilute sodium hydroxide solution). Time-correlated single photon counting lifetime measurements were made with a pulsed laser diode. GPC measurements were recorded by a Jasco UV-2075 Plus detector. The samples were separated on Polymer Standards Service polystyrene columns in THF, calibrated according to polystyrene standards.

8.2 Ethyleneglycol Compounds 13-17

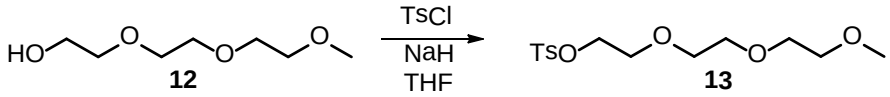

2-(2-(2-Methoxyethoxy)ethoxy)ethyl 4-methylbenzenesulfonate (**13**)

12 (50.0 g, 0.304 mol) and tosyl chloride (116 g, 0.609 mol) were stirred into THF (200 mL). The reaction mixture was then cooled to 0 ˚C, and aqueous NaOH (36.5 g, 0.913 mol) was added. After stirring overnight, the solution was extracted with $CHCl_3$ (3 x 100 mL). The organic fractions were collected and dried over magnesium sulfate, and the solvent was evaporated. Purification by silica gel chromatography (9:1 hexanes:EtOAc for excess TsCl, followed by 1:1 hexanes:EtOAc), yielded **13** as a colorless oil (71.3 g, 0.224 mol, 74%). ^{1}H NMR (300 MHz, $CDCl_3$): δ = 7.66 (d, 2H, J = 8 Hz), 7.23 (d, 2H, J = 8 Hz), 4.03 (t, 2H, J = 5 Hz), 3.55 (t, 2H, J = 5 Hz), 3.46 (m, 6H), 3.39 (m, 2H), 3.23 (s, 3H), 2.32 (s, 3H). ^{13}C NMR (75 MHz, $CDCl_3$): δ = 144.4, 132.5, 129.4, 127.5, 71.4, 70.22, 70.06, 70.05, 68.9, 68.2, 58.5, 21.2.

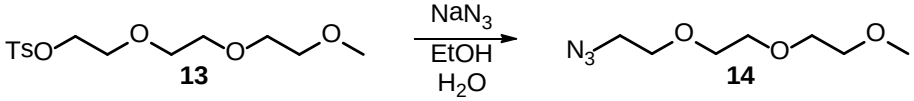

1-Azido-2-(2-(2-methoxyethoxy)ethoxy)ethane (**14**)

13 (12.9 g, 40.5 mmol) and NaN_3 (5.27 g, 81.0 mmol) were stirred into 1:1 H_2O:MeOH (100 mL). The reaction was heated to reflux and stirred overnight (16 h). The reaction mixture was cooled, and extracted with DCM (2 x 70 mL). The organic fractions were collected, dried over magnesium sulfate, and the solvent was removed under reduced pressure. Purification by silica gel chromatography (1:1 hexanes:EtOAc) gave **14** as a pale yellow oil (6.76 g, 35.7 mmol, 88%). IR (cm^{-1}): 2872, 2097, 1453, 1284, 1106, 934, 851; ^{1}H NMR (300 MHz, $CDCl_3$): δ = 3.67 (m, 8H), 3.55 (m, 2H), 3.38 (t, J = 5.1 Hz, 2H), 3.37 (s, 3H); ^{13}C NMR (75 MHz, $CDCl_3$): δ = 72.0, 70.8, 70.8, 70.7, 70.1, 59.1, 50.8.

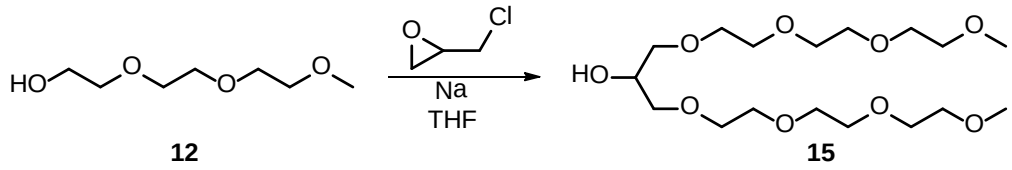

12 **15**

2,5,8,11,15,18,21,24-Octaoxapentacosan-13-ol (**15**)

Sodium metal (10. g, 0.43 mol) was stirred in **12** (190 mL) in a dry flask at 100 ˚C for 2 h, until completely dissolved. The temperature was then reduced to 65 ˚C, and epichlorohydrin (32 mL, 0.41 mol) was added dropwise. The reaction was reheated to 100 ˚C and allowed to stir for 24 h, after which time NH_4Cl (22 g, 0.41 mol) was added. The reaction mixture was stirred for another hour and then filtered through celite with DCM. The solvent was evaporated, and the product was purified by vacuum distillation, yielding **15** as a colorless oil (average yield of two reactions = 79 g, 0.20 mol, 50%). IR (cm^{-1}): 3456, 2870, 1643, 1455, 1351, 1293, 1248, 1199, 1097, 937, 849, 753, 516; ^1H NMR (300 MHz, $CDCl_3$): δ = 3.76 (quin, J = 6.0 Hz, 1H), 3.47 (m, 20H), 3.36 (m, 9H), 3.19 (s, 6H); ^{13}C NMR (75 MHz, $CDCl_3$): δ = 72.7, 72.0, 70.78, 70.62, 70.59, 70.54, 70.53, 69.4, 59.0; MS (ESI) *m/z*: $[M + H]^+$ Calcd for $C_{17}H_{37}O_9$ = 385.2; Found = 385.3.

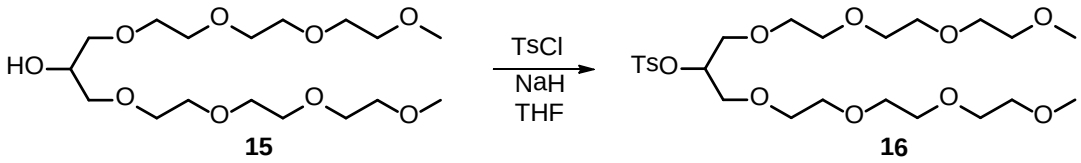

15 **16**

2,5,8,11,15,18,21,24-Octaoxapentacosan-13-yl 4-methylbenzenesulfonate (**16**)

NaH (1.35 g, 56.2 mmol) was slowly added to a dry flask containing compound **15** (18.0 g, 46.8 mmol) and dry THF (50 mL). Tosyl chloride (17.8 g, 93.6 mmol) was added and the reaction was stirred at room temperature overnight. Excess NaH was quenched by slowly adding H_2O (50 mL). The product was then extracted with $CHCl_3$ (3 x 50 mL). The solvent was evaporated and the residue was purified by silica gel chromatography (EtOAc) to yield **16** as a colorless oil (19.5 g, 36.0 mmol, 77%). IR (cm^{-1}): 2872, 1456, 1354, 1095, 924; ^1H NMR (300 MHz, $CDCl_3$): δ = 7.76 (d, J = 8.4 Hz, 2H), 7.28 (d, J = 8.4 Hz, 2H), 4.63 (quin, J = 6.0 Hz, 1H), 3.62-3.46 (m, 29H), 3.32 (s, 6H), 2.39 (s, 3H); ^{13}C NMR (75 MHz, $CDCl_3$): δ = 144.6, 134.2, 129.6, 128.1,

79.7, 72.0, 70.97, 70.66, 70.58, 70.42, 69.73, 59.1, 21.7; MS (ESI) *m/z*: $[M + Na]^+$ Calcd for $C_{24}H_{42}O_{11}SNa$ = 561.2; Found = 561.2.

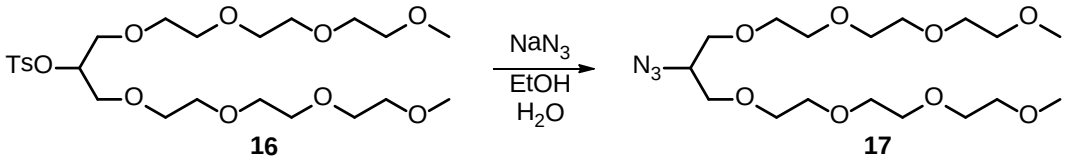

16 **17**

13-Azido-2,5,8,11,15,18,21,24-octaoxapentacosane (**17**)

16 (12.1 g, 22.5 mmol) and NaN_3 (4.38, 67.4 mmol) were stirred into 1:1 H_2O:EtOH (250 mL). The reaction was heated to reflux and stirred for 4 h. The reaction mixture was cooled, and extracted with saturated aqueous NaCl (100 mL) and DCM (3 x 100 mL). The solvent was removed under reduced pressure and the residue was purified by silica gel chromatography (EtOAc) gave **17** as a pale yellow oil (8.50 g, 20.8 mmol, 92%). IR (cm^{-1}): 2866, 2092, 1455, 1269, 1098, 849, 731; ^1H NMR (300 MHz, $CDCl_3$): δ = 3.48-3.35 (m, 29H), 3.20 (s, 6H); ^{13}C NMR (75 MHz, $CDCl_3$): δ = 71.67, 70.64, 70.38, 70.35, 70.28, 70.24, 60.3, 58.7; HRMS (ESI) *m/z*: $[M + Na]^+$ Calcd for $C_{17}H_{35}N_3O_8Na$ = 432.2322; Found = 432.2319.

8.3 Benzochalcogendiazoles and Benzenediamines 19-25

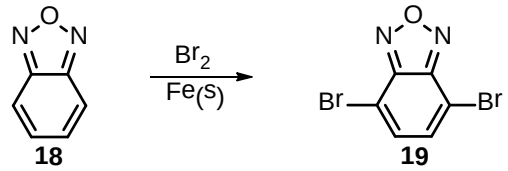

18 **19**

4,7-Dibromobenzo[c][1,2,5]oxadiazole (**19**)

Benzofurazan (2.50 g, 20.8 mmol) and iron powder (0.232 g, 4.16 mmol) were mixed in a three-neck round-bottom flask equipped with a condenser. The mixture was heated to 90 ˚C, and bromine (9.98 g, 62.4 mmol) was added dropwise over a period of 2 hours. The mixture was stirred at 90 ˚C for two additional hours and then cooled to room temperature. The dark and sticky product was quenched with saturated aqueous NaS_2O_3 (50 mL) and stirred overnight. The product was then dissolved in THF, extracted with DCM (3 x 100 mL), and washed with saturated aqueous $NaHCO_3$ (2 x 50 mL). The organic phase was dried over $MgSO_4$ and the solvent was removed under reduced pressure. The yellow solid was purified by silica gel chromatography (19:1 hexanes:EtOAc) and afterwards purified by recrystallization from ethanol to give the product **19** as yellow needles (2.30 g, 8.22 mmol, 39%). mp: 94-95 ˚C; IR (cm^{-1}): 3005, 2966, 1874, 1716, 1696, 1605, 1517; ^1H NMR (300 MHz, $CDCl_3$): δ = 7.50 (s, 2H); ^{13}C NMR (75 MHz, $CDCl_3$): δ = 149.4, 134.3, 108.7; MS (EI) *m/z*: $[M]^+$ Calcd for $C_6H_2N_2OBr_2$ = 275.85; Found = 275.85.

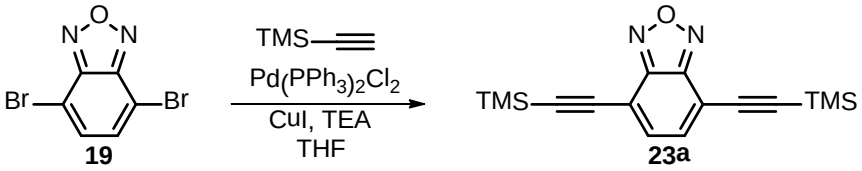

19 **23a**

4,7-Bis(trimethylsilyl)ethynylbenzo[c][1,2,5]oxadiazole (**23a**)

19 (94 mg, 0.34 mmol), $Pd(PPh_3)_2Cl_2$ (2.4 mg, 0.0034 mmol), and CuI (1.3 mg, 0.0068 mmol) were dissolved in THF (4 mL) and triethylamine (1 mL) in a Schlenk tube. The solution was then deoxygenated by freezing and evacuating (3x). After warming to room temperature and sealing the Schlenk tube under nitrogen gas, trimethylsilyl acetylene (0.13 g, 1.4 mmol) was added via

syringe. The reaction was then stirred at room temperature for 18 hours. The solids were filtered, and the solution was extracted with saturated aqueous NH_4Cl (25 mL) and DCM (2 x 25 mL). The organic fractions were collected and dried over magnesium sulfate, the solvent was evaporated, and the product was purified by silica gel chromatography (100:1 hexanes:EtOAc) to yield **23a** as a yellow solid (64 mg, 0.20 mmol, 60%). mp: 86-88 ˚C; IR (cm^{-1}): 2957, 2898, 2156, 1592, 1550, 1530, 1378, 1250, 1065, 1004, 838, 761, 699; ^1H NMR (300 MHz, $CDCl_3$): δ = 7.46 (s, 2H), 0.30 (s, 18H); ^{13}C NMR (75 MHz, $CDCl_3$): δ = 149.4, 135.0, 112.9, 106.0, 98.3, -0.2; HRMS (EI) *m/z*: $[M]^+$ Calcd for $C_{16}H_{20}N_2OSi_2$ = 312.1114; Found = 312.1130.

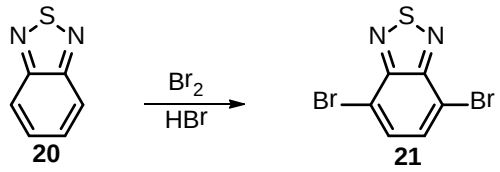

4,7-Dibromobenzo[c][1,2,5]thiadiazole (**21**) was provided by Benjamin D. Lindner

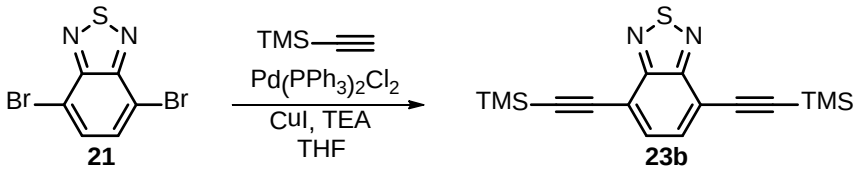

4,7-Bis(trimethylsilyl)ethynylbenzo[c][1,2,5]thiadiazole (**23b**)

21 (2.0 g, 68 mol), $Pd(PPh_3)_2Cl_2$ (0.19 g, 0.27 mmol), and CuI (0.10 g, 0.27 mmol) were dissolved in THF (40 mL) and triethylamine (10 mL) in a Schlenk tube. The solution was then deoxygenated by freezing and evacuating (3x). After warming to room temperature and sealing the Schlenk tube under nitrogen, trimethylsilyl acetylene (2.0 g, 20. mol) was added via syringe. The reaction was then stirred at room temperature for 48 hours. The solids were filtered, the solvent was evaporated, and purification by silica gel chromatography (200:1 hexanes:EtOAc) gave **23b** as a light tan solid (1.8 g, 5.5 mmol, 81%). mp: 114-115 ˚C; IR (cm^{-1}): 2955, 2898, 2153, 1560, 1539, 1491, 1338, 1245, 1031, 836, 758, 640; ^1H NMR (300 MHz, $CDCl_3$): δ = 7.70 (s, 2H), 0.33 (s, 18H); ^{13}C NMR (75 MHz, $CDCl_3$): δ = 154.4, 133.3, 117.4, 103.8, 100.2, 0.03; HRMS (EI) *m/z*: $[M]^+$ Calcd for $C_{16}H_{20}N_2SSi_2$ = 328.0886; Found = 328.0898.

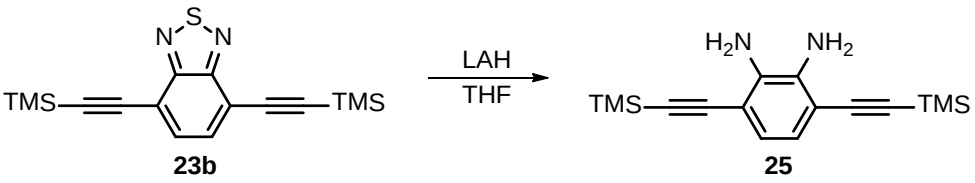

23b **25**

3,6-Bis((trimethylsilyl)ethynyl)benzene-1,2-diamine (**25**)

23b (5.19 g, 15.8 mmol) and dry THF (50 mL) were added to an oven dried Schlenk flask, which was purged with nitrogen gas and cooled to 0 ˚C. Lithium aluminum hydride (1.50 g, 39.5 mmol) was slowly added to the reaction mixture over a period of 30 minutes. The reaction was then allowed to stir for 30 minutes under nitrogen, at which point it was slowly quenched with saturated aqueous NH_4Cl (30 mL) at 0 ˚C. The resulting product was extracted with diethyl ether (3 x 200 mL), dried over magnesium sulfate, and the solvent was removed under reduced pressure. Purification by silica gel chromatography (9:1 hexanes:Et_2O) gave **25** as an air-sensitive yellow solid (4.31 g, 14.3 mmol, 91% yield). mp = 140-144 ˚C; IR (cm^{-1}): 3425, 3420, 3335, 3075, 2956, 2897, 2788, 2142, 1616, 1608, 1451, 1411, 1247, 1245, 1184, 1123; ^{1}H NMR (400 MHz, $CDCl_3$): δ = 6.77 (s, 2H), 3.94 (s, 4H), 0.26 (s, 18H); ^{13}C NMR (100 MHz, $CDCl_3$): δ = 136.9, 122.4, 110.0, 102.1, 101.3, 0.4; HRMS (EI) *m/z*: $[M]^+$ Calcd for $C_{16}H_{24}N_2Si_2$ = 300.1478; Found = 300.1472.

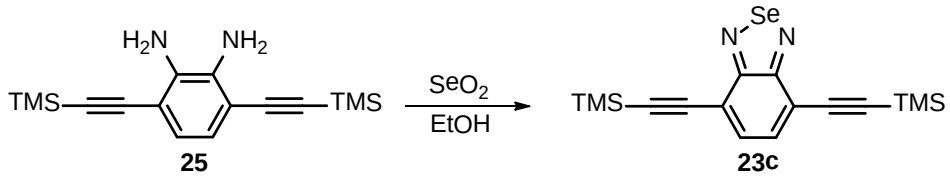

25 **23c**

4,7-Bis(trimethylsilyl)ethynylbenzo[c][1,2,5]selenodiazole (**23c**)

A solution of selenium dioxide (0.185 g, 1.66 mmol) in hot H_2O (1 mL) was added to a solution of **25** (0.100 g, 0.333 mmol) in EtOH (15 mL) at 60 ˚C. The reaction was stirred until full conversion was reached according to TLC. The reaction mixture was then filtered, and the precipitate was washed with water. Purification by silica gel chromatography (hexanes → 50:1 hexanes:EtOAc) gave **23c** as a yellow crystalline solid (0.113 g, 0.301 mmol, 90%). mp: 172-175 ˚C; IR (cm^{-1}): 2960, 2898, 2148, 1560, 1520, 1474, 1354, 1245, 1037, 1014, 833, 758, 633; ^{1}H NMR (300 MHz, $CDCl_3$): δ = 7.60 (s, 2H), 0.31 (s, 18H); ^{13}C NMR (75 MHz, $CDCl_3$): δ = 159.2,

133.6, 119.1, 103.5, 100.7, 0.06; HRMS (EI) *m/z*: $[M]^+$ Calcd for $C_{16}H_{20}N_2SeSi_2$ = 376.0330; Found = 376.0334; Correct isotope distribution: Calcd for $C_{16}H_{20}N_2SeSi_2$ = C 51.18, H 5.37, N 7.46; Found = C 50.97, H 5.52, N 7.56.

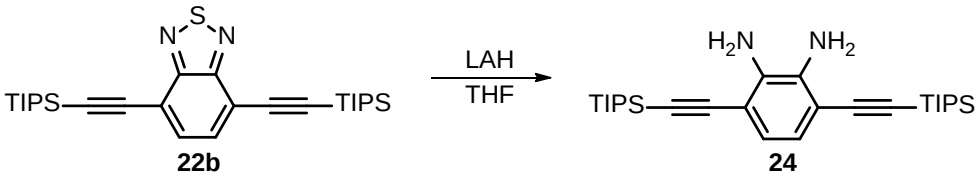

22b **24**

3,6-Bis((triisopropylsilyl)ethynyl)benzene-1,2-diamine (**24**)

22b[111,160,161] (3.26 g, 6.56 mmol) and dry THF (50 mL) were added to an oven dried Schlenk flask, which was purged with nitrogen gas and cooled to 0 ˚C. Lithium aluminum hydride (0.622 g, 16.4 mmol) was slowly added to the reaction mixture over a period of 30 minutes. The reaction was then allowed to stir for 12 hours under nitrogen, at which point it was slowly quenched with saturated aqueous NH_4Cl (30 mL) at 0 ˚C. The resulting product was extracted with diethyl ether (3 x 200 mL), dried over magnesium sulfate, and the solvent was removed under reduced pressure. Purification by silica gel chromatography (9:1 hexanes:Et_2O) gave **24** as an air-sensitive light yellow solid (2.92 g, 6.23 mmol, 95% yield). mp = 127-129 ˚C; IR (cm^{-1}): 3436, 3328, 3070, 2954, 2862, 2715, 2611, 2140, 1612, 1481, 1269, 1384, 1361, 1253, 1184; ^1H NMR (400 MHz, $CDCl_3$): δ = 6.80 (s, 2H), 3.97 (s, 4H), 1.14 (s, 42H); ^{13}C NMR (75 MHz, $CDCl_3$): δ = 136.7, 122.3, 110.1, 103.8, 97.3, 18.9, 11.4; HRMS (EI) *m/z:* $[M]^+$ Calcd for $C_{28}H_{48}N_2Si_2$ = 468.3356; Found = 468.3359.

8.4 Phenazines 38-42

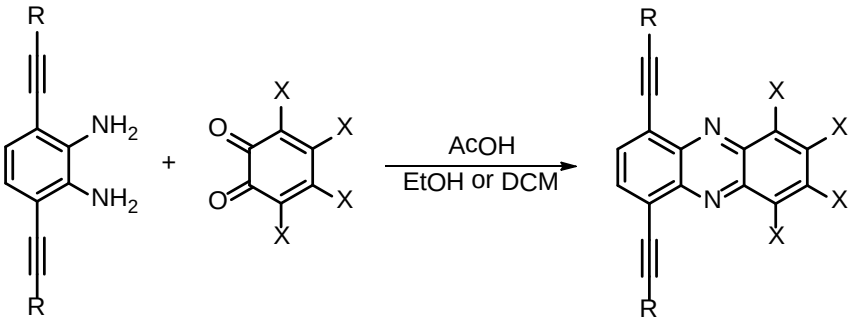

General Procedure 1

Diamine **24** or **25** was added to a solution of the *ortho*-benzoquinone in EtOH (10 mL) or DCM (50 mL), along with AcOH (3 mL). The reaction mixture was heated and stirred overnight (~16 h). The solution was then extracted with saturated aqueous $NaHCO_3$ (50 mL) and DCM (2 x 50 mL). The organic fractions were collected and dried over sodium sulfate, the solvent was removed under reduced pressure, and the product was purified by silica gel chromatography.

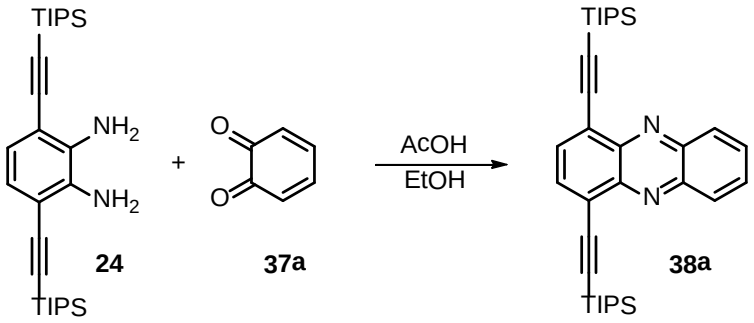

1,4-Bis((triisopropylsilyl)ethynyl)phenazine (**38a**)

ortho-Benzoquinone **37a** was freshly prepared by stirring a solution of catechol (0.692 g, 6.40 mmol) in $CHCl_3$ (200 mL) into a solution of $K_2Cr_2O_7$ (3.76 g, 12.8 mmol) in 1 M H_2SO_4 (100 mL). After stirring for 10 min. at room temperature, the organic fraction was collected and the solvent was removed under reduced pressure. **24** (1.00 g, 2.13 mmol) was then added, and the mixture was reacted according to general procedure 1, using EtOH as solvent. The reaction mixture was heated to reflux and stirred overnight. Purification by silica gel chromatography (3:1 hexanes:DCM) gave the product **38a** as a yellow solid (0.480 g, 0.887 mmol, 42%). mp = 96-98

˚C; IR (cm^{-1}): 3062, 2962, 2864, 2756, 2723, 2154, 1946, 1886, 1568, 1521, 1461, 1409, 1257, 1118; ^{1}H NMR (300 MHz, $CDCl_3$): δ = 8.24 (dd, *J* = 3.4 Hz, *J* = 6.7 Hz, 2H), 7.94 (s, 2H), 7.84 (dd, *J* = 3.4 Hz, *J* = 6.7 Hz, 2H), 1.26 (s, 42H); ^{13}C NMR (75 MHz, $CDCl_3$): δ = 143.73, 143.55, 133.7, 130.97, 130.30, 124.6, 103.8, 100.8, 19.0, 11.7; HRMS (EI) *m/z*: $[M]^+$ Calcd for $C_{34}H_{48}N_2Si_2$ = 540.3356; Found = 540.3354.

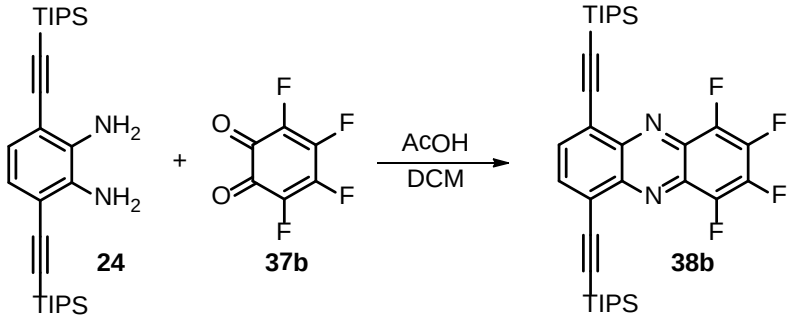

1,2,3,4-Tetrafluoro-6,9-bis((triisopropylsilyl)ethynyl)phenazine (**38b**)

The tetrafluoro-*ortho*-benzoquinone **37b** was freshly prepared before use, according to a previously published procedure.[112] **24** (0.500 g, 1.07 mmol) and **37b** (0.576 g, 3.20 mmol) were reacted according to general procedure 1, using DCM as solvent. The reaction mixture was heated to reflux and stirred overnight. Purification by silica gel chromatography (10:1 hexanes:DCM) yielded **38b** as a yellow solid (152 mg, 0.248 mmol, 23%). mp = 107-108 ˚C; IR (cm^{-1}): 2939, 2891, 2864, 2159, 1675, 1595, 1536, 1480, 1341, 1260, 1076, 993, 881, 809, 678, 453; ^{1}H NMR (300 MHz, $CDCl_3$): δ = 8.03 (s, 2H), 1.24 (s, 42H); ^{13}C NMR (75 MHz, $CDCl_3$): δ = 143.3, 135.3, 124.6, 102.56, 102.35, 18.8, 11.6 (the carbons next to the fluorine atoms could not be identified); ^{19}F NMR (300 MHz, $CDCl_3$): δ = -148.80 (dd, *J* = 15.0 Hz, *J* = 3.0 Hz, 2F), -149.91 (dd, *J* = 16.2 Hz, *J* = 3.6 Hz, 2F); HRMS (ESI) *m/z*: $[M + H]^+$ Calcd for $C_{34}H_{45}F_4N_2Si_2$ = 613.3052; Found = 613.3067.

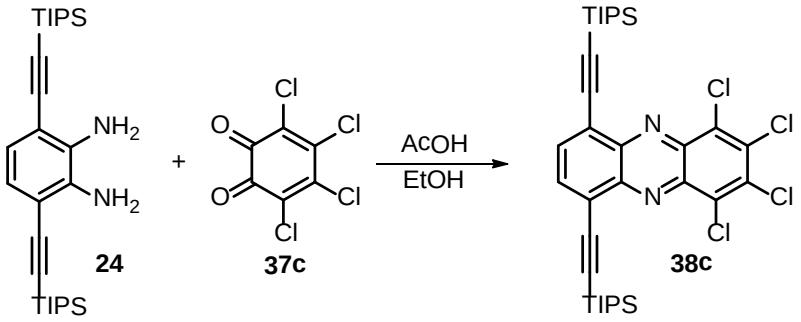

1,2,3,4-Tetrachloro-6,9-bis-((triisopropylsilyl)ethynyl)phenazine (**38c**)

24 (0.200 g, 0.427 mmol) and **37c** (0.115 g, 0.469 mmol) were reacted according to general procedure 1, using EtOH as solvent. The reaction mixture was heated to reflux and stirred overnight. Purification by silica gel chromatography (20:1 hexanes:DCM) yielded **38c** as a yellow solid (54.0 mg, 0.0796 mmol, 19%). mp = 100-102 ˚C; IR (cm^{-1}): 2964, 2866, 2725, 2156, 1949, 1458, 1369, 1263, 1107, 1031; ^{1}H NMR (400 MHz, $CDCl_3$): δ = 8.02 (s, 2H), 1.21 (s, 42H); ^{13}C NMR (100 MHz, $CDCl_3$): δ = 143.3, 138.8, 135.9, 133.7, 132.2, 124.5, 102.4, 102.0, 18.8, 11.4; HRMS (EI) *m/z*: $[M]^+$ Calcd for $C_{34}H_{44}Cl_4N_2Si_2$ = 676.1797; Found = 676.1776.

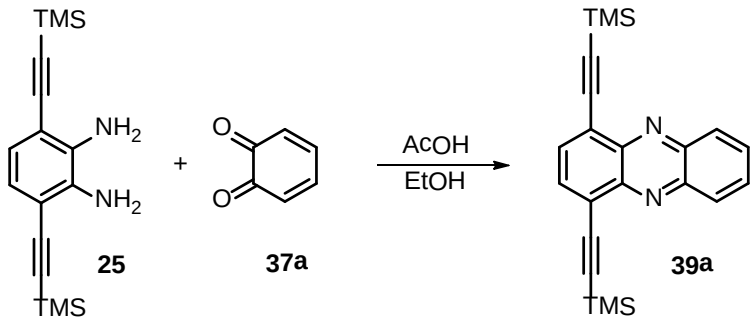

1,4-Bis((trimethylsilyl)ethynyl)phenazine (**39a**)

ortho-Benzoquinone **37a** was freshly prepared by stirring a solution of catechol (1.10 g, 9.98 mmol) in $CHCl_3$ (200 mL) into a solution of $K_2Cr_2O_7$ (5.88 g, 20.0 mmol) in 1 M H_2SO_4 (100 mL). After stirring for 10 min. at room temperature, the organic fraction was collected, and the solvent was removed under reduced pressure. **25** (1.00 g, 3.33 mmol) was then added and the mixture was reacted according to general procedure 1, using EtOH as solvent. The reaction mixture was heated to 40 ˚C and stirred overnight. Purification by silica gel chromatography (3:1

hexanes:DCM) gave the product **39a** as a yellow solid (780. mg, 2.09 mmol, 63%). mp = 166-168 ˚C; IR (cm^{-1}): 3089, 3040, 2963, 2954, 2897, 2152, 1919, 1518, 1473, 1406, 1281, 1138, 1118, 1025; ^{1}H NMR (400 MHz, $CDCl_3$): δ = 8.29 (dd, *J* = 3.4 Hz, *J* = 6.7 Hz, 2H), 7.95 (s, 2H), 7.83 (dd, *J* = 3.4 Hz, *J* = 6.7 Hz, 2H), 0.35 (s, 18H); ^{13}C NMR (100 MHz in $CDCl_3$): δ = 143.6, 143.0, 134.4, 131.2, 130.3, 124.3, 104.2, 101.6, 0.1; HRMS (EI) *m/z*: $[M]^+$ Calcd for $C_{22}H_{24}N_2Si_2$ = 372.1478; Found = 372.1488.

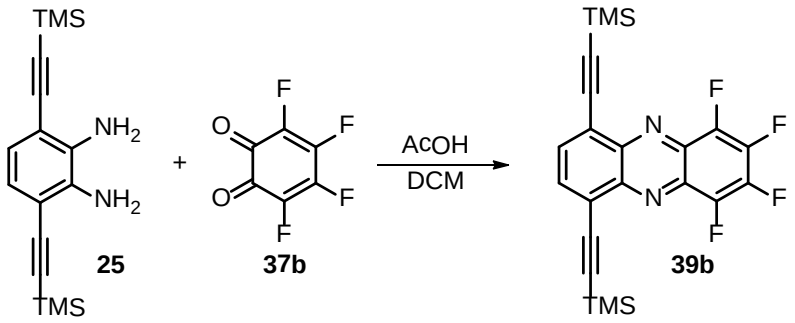

1,2,3,4-Tetrafluoro-6,9-bis((trimethylsilyl)ethynyl)phenazine (**39b**)

The tetrafluoro-*ortho*-benzoquinone **37b** was freshly prepared before use according to a previously published procedure.[112] **25** (1.10 g, 3.66 mmol) and **37b** (2.00 g, 11.1 mmol) were reacted according to general procedure 1, using DCM as solvent. The reaction mixture was heated to reflux and stirred overnight. Purification by silica gel chromatography (10:1 hexanes:DCM) yielded **39b** as a yellow solid (292 mg, 0.657 mmol, 18%). mp = 207-210 ˚C; IR (cm^{-1}): 2957, 2901, 2853, 2153, 1675, 1595, 1536, 1485, 1341, 1245, 1073, 833, 755, 686, 625, 464; ^{1}H NMR (300 MHz, $CDCl_3$): δ = 8.03 (s, 2H), 0.38 (s, 18H); ^{13}C NMR (75 MHz, $CDCl_3$): δ = 142.9, 135.5, 124.3, 106.1, 100.3, -0.04 (the carbons next to the fluorine atoms could not be identified); ^{19}F NMR (300 MHz, $CDCl_3$): δ = -149.61 (dd, *J* = 16.2 Hz, *J* = 3.6 Hz, 2F), -150.34 (dd, *J* = 15.0 Hz, *J* = 3.0 Hz, 2F); HRMS (ESI) *m/z*: $[M + H]^+$ Calcd for $C_{22}H_{21}F_4N_2Si_2$ = 445.1174; Found = 445.1180.

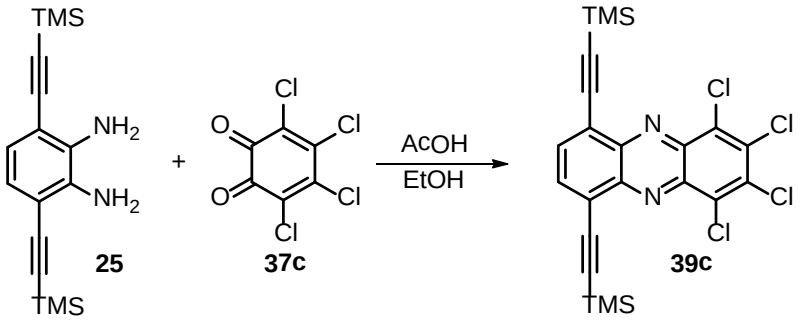

1,2,3,4-Tetrachloro-6,9-bis-((trimethylsilyl)ethynyl)phenazine (**39c**)

25 (0.600 g, 2.00 mmol) and **37c** (0.982 g, 3.99 mmol) were reacted according to general procedure 1, using EtOH as solvent. The reaction mixture was heated to 40 ˚C and stirred overnight. Purification by silica gel chromatography (20:1 hexanes:DCM) yielded **39c** as a yellow solid (819 mg, 1.60 mmol, 80%). mp = 201-203 ˚C; IR (KBr, cm^{-1}): 2958, 2899, 2152, 1573, 1551, 1488, 1454, 1371, 1245, 1132, 1050; ^{1}H NMR (400 MHz, $CDCl_3$): δ = 8.02 (s, 2H), 0.36 (s, 18H); ^{13}C NMR (100 MHz, $CDCl_3$): δ = 143.3, 138.7, 135.4, 135.1, 132.2, 124.3, 105.8, 100.2, -0.1; HRMS (EI) *m/z*: $[M]^+$ Calcd for $C_{22}H_{20}Cl_4N_2Si_2$ = 507.9919; Found = 507.9918.

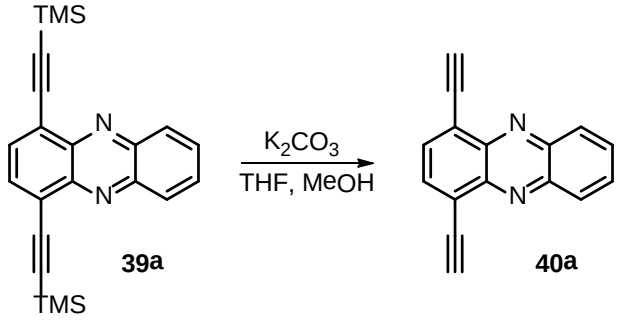

1,4-Diethynylphenazine (**40a**)

39a (0.186 g, 0.499 mmol) was dissolved in 1:1 THF:MeOH (20 mL), to which K_2CO_3 (0.190 g, 4.99 mmol) was added. The solution was stirred for 30 min at room temperature. The product mixture was then poured over H_2O (50 mL) and extracted with DCM (2 x 50 mL). The resulting solution was dried over sodium sulfate, and the solvent was removed under reduced pressure. Purification by silica gel chromatography (10:1 hexanes:EtOAc) gave **40a** as a yellow solid (0.105 g, 0.460 mmol, 92%). mp = 80 ˚C (decomposition); IR (cm^{-1}): 3298, 3270, 3232, 3205, 2101, 1521, 1473, 1334, 1112, 1034; ^{1}H NMR (400 MHz, $CDCl_3$): δ = 8.36 (dd, J = 10.2 Hz, J =

3.3 Hz, 2H), 8.01 (s, 2H), 7.87 (dd, *J* = 10.2 Hz, *J* = 3.3 Hz, 2H), 3.76 (s, 2H); ^{13}C NMR (100 MHz, $CDCl_3$): δ = 144.0, 143.2, 134.9, 131.7, 130.4, 124.0, 86.1, 80.6; HRMS (EI) *m/z*: $[M]^+$ Calcd for $C_{16}H_8N_2$ = 228.0687; Found = 228.0690.

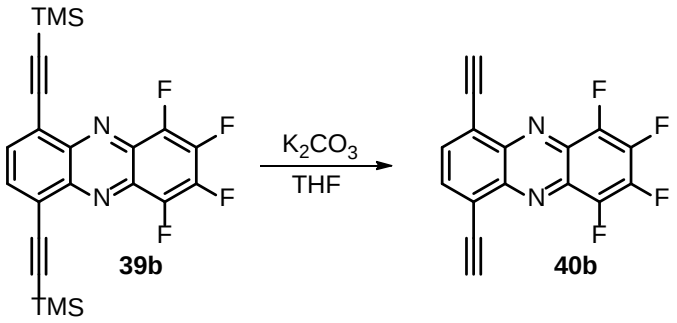

1,2,3,4-Tetrafluoro-6,9-diethynylphenazine (**40b**)

39b (59 mg, 0.13 mmol) was dissolved in THF (10 mL), to which K_2CO_3 (0.18 g, 1.3 mmol) was added. The solution was stirred for 2 hours at room temperature. The reaction did not go to completion, and no progress was seen after 2 hours, even after 24 hours. The product mixture was then poured over H_2O (50 mL) and extracted with DCM (2 x 50 mL). The resulting solution was dried over sodium sulfate, and the solvent was removed under reduced pressure. Purification by silica gel chromatography (20:1 hexanes:EtOAc) gave **40b** as a yellow solid (0.018 g, 0.060 mmol, 45%). mp = 51 ˚C (decomposition); IR (cm^{-1}): 3263, 2955, 2923, 2356, 2036, 1615, 1489, 1261, 1069, 800; ^{1}H NMR (300 MHz, $CDCl_3$): δ = 8.11 (s, 2H), 3.79 (s, 2H); ^{13}C NMR (75 MHz, $CDCl_3$): δ = 137.2, 136.2, 124.0, 87.1, 79.2 (the carbons next to the fluorine atoms could not be identified); ^{19}F NMR (300 MHz): δ = -148.80 (dd, *J* = 16.2 Hz, *J* = 3.6 Hz, 2F), -149.91 (dd, *J* = 15 Hz, *J* = 3.0 Hz, 2F); HRMS (FAB) *m/z*: $[M + H]^+$ Calcd for $C_{16}H_5N_2F_4$ = 301.0383; Found = 301.0419.

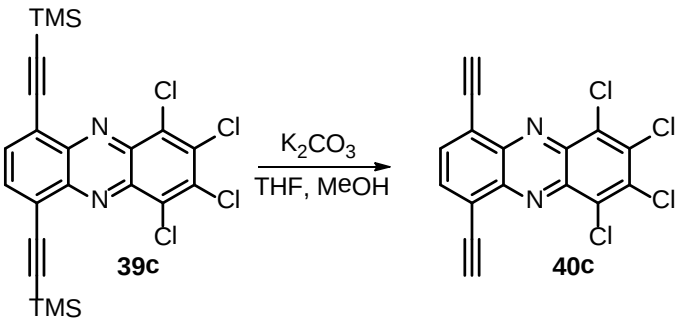

1,2,3,4-Tetrachloro-6,9-diethynylphenazine (**40c**)

39c (0.200 g, 0.392 mmol) was dissolved in 1:1 THF:MeOH (20 mL), to which K_2CO_3 (0.542 g, 3.92 mmol) was added. The solution was stirred for 30 min at room temperature. The product mixture was then poured over H_2O (50 mL) and extracted with DCM (2 x 50 mL). The resulting solution was dried over sodium sulfate, and the solvent was removed under reduced pressure. Purification by silica gel chromatography (20:1 hexanes:EtOAc) gave **40c** as a yellow solid (0.119 g, 0.325 mmol, 83%). mp = 40 ˚C (decomposition); IR (cm^{-1}): 3269, 2958, 2954, 2924, 2109, 1727, 1549, 1454, 1368, 1287, 1247, 1051, 1039; ^{1}H NMR (400 MHz, $CDCl_3$): δ = 8.09 (s, 2H), 3.77 (s, 2H); ^{13}C NMR (100 MHz, $CDCl_3$): δ = 143.1, 138.9, 136.1, 135.4, 132.1, 124.0, 86.8, 79.2; HRMS (EI) *m/z*: $[M]^+$ Calcd for $C_{16}H_4Cl_4N_2$ = 363.9129; Found = 363.9133.

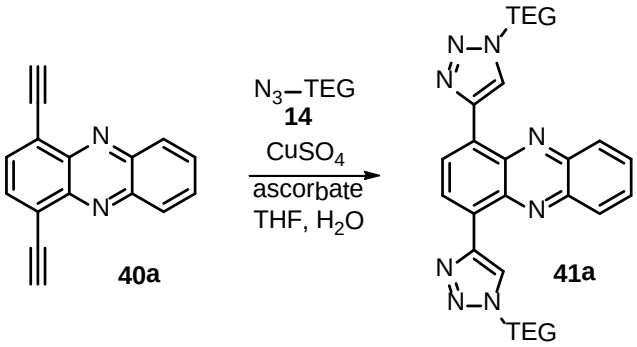

1,4-Bis(1-(2-(2-(2-methoxyethoxy)ethoxy)ethyl)-1H-1,2,3-triazol-4-yl)phenazine (**41a**)

40a (0.300 g, 1.31 mmol) and **14** (0.746 g, 3.94 mmol) were dissolved in a 5:1 THF:H_2O solution (20 mL) and deoxygenated via the freeze-pump-thaw method (3x). Under a flow of nitrogen, $CuSO_4$•$5H_2O$ (0.820 g, 3.29 mmol) and sodium ascorbate (0.651 g, 3.29 mmol) were added, and the reaction was sealed and stirred overnight at room temperature. The crude mixture was then

filtered through celite with DCM, and the solvent was dried with sodium sulfate and removed in vacuo. The product **41a** was purified via silica gel flash chromatography (DCM, followed by EtOAc), and isolated as an orange oil (487 mg, 0.803 mmol, 61%). IR (cm^{-1}): 2942, 2921, 2871, 2783, 2772, 2739, 2739, 1751, 1653, 1647, 1558, 1447, 1430, 1352, 1332, 1229, 1108, 1098, 1064, 1030; ^{1}H NMR (300 MHz, $CDCl_3$): δ = 9.20 (s, 2H), 8.96 (s, 2H), 8.32 (dd, *J* = 10.2 Hz, *J* = 3.3 Hz, 2H), 7.88 (dd, *J* = 10.2 Hz, *J* = 3.3 Hz, 2H), 4.74 (t, *J* = 5.4 Hz, 4H), 4.04 (t, *J* = 5.4 Hz, 4H), 3.68 (m, 8H), 3.57 (m, 9H), 3.25 (s, 6H); ^{13}C NMR (100 MHz, $CDCl_3$): δ = 143.1, 142.0, 140.2, 130.5, 129.6, 128.6, 128.0, 126.4, 71.78, 70.77, 70.53, 70.50, 69.74, 58.9, 50.4; HRMS (EI) *m/z*: $[M]^+$ Calcd for $C_{30}H_{38}N_8O_6$ = 606.2914; Found = 606.2903.

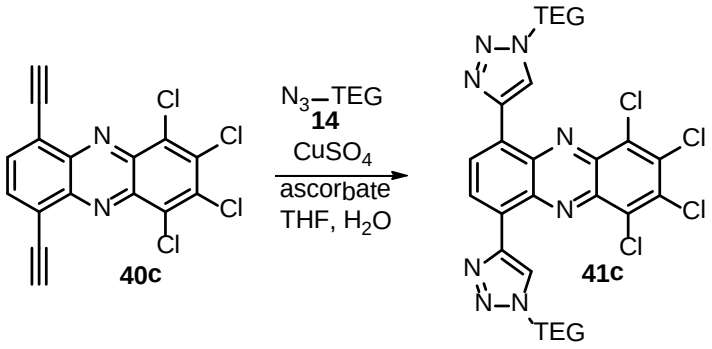

1,2,3,4-Tetrachloro-6,9-bis(1-(2-(2-(2-methoxyethoxy)ethoxy)ethyl)-1H-1,2,3-triazol-4-yl)phenazine (**41c**)

40c (0.080 g, 0.22 mmol) and **14** (0.12 g, 0.66 mmol) were dissolved in a 5:1 THF:H_2O solution (20 mL) and deoxygenated via the freeze-pump-thaw method (3x). Under a flow of nitrogen, $CuSO_4$•$5H_2O$ (0.14 g, 0.55 mmol) and sodium ascorbate (0.11 g, 0.55 mmol) were added, and the reaction was then sealed and stirred overnight at room temperature. The crude mixture was then filtered through celite with DCM, and the solvent was dried with sodium sulfate and removed in vacuo. The product **41c** was purified via silica gel flash chromatography (DCM followed by EtOAc) and isolated as a red oil (75 mg, 0.10 mmol, 46%). IR (cm^{-1}): 2904, 2883, 2869, 2854, 1734, 1653, 1558, 1457, 1374, 1252, 1108, 1099; ^{1}H NMR (400 MHz, $CDCl_3$): δ = 9.15 (s, 2H), 8.98 (s, 2H), 4.70 (t, 4H), 4.00 (t, 4H), 3.64 (m, 8H), 3.49 (m, 8H), 3.21 (s, 6H); ^{13}C NMR (100 MHz, $CDCl_3$): δ = 141.8, 138.9, 136.4, 134.3, 131.4, 129.5, 128.2, 126.3, 71.86, 70.77, 70.56,

69.58, 59.0, 50.5; HRMS (EI) *m/z*: $[M]^+$ Calcd for $C_{30}H_{34}Cl_4N_8O_6$ = 742.1355; Found = 742.1333.

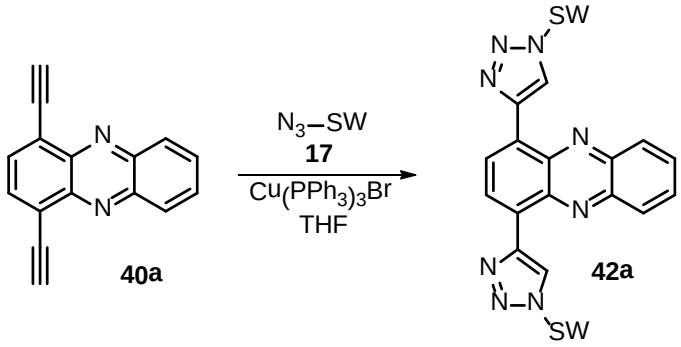

1,4-Bis(1-(2,5,8,11,15,18,21,24-octaoxapentacosan-13-yl)-1H-1,2,3-triazol-4-yl)phenazine (**42a**)

40a (48 mg, 0.21 mmol) and **17** (190 mg, 0.46 mmol) were stirred together in H_2O (1 mL) and THF (5 mL). The solution was then deoxygenated via the freeze-pump-thaw method (3x). Under a flow of nitrogen, $Cu(PPh_3)_3Br$ (0.020 g, 0.021 mmol) was added. The reaction was sealed under the inert atmosphere and stirred at 50 ˚C for 2 d. The reaction mixture was then extracted with saturated aqueous NH_4Cl (25 mL) and DCM (5 x 25 mL), the organic fractions were collected and dried over sodium sulfate, and the solvent was removed under reduced pressure. Purification by silica gel chromatography (gradient elution, EtOAc → EtOAc:MeOH 20:1 → 10:1) gave **42a** as an orange oil (66 mg, 0.063 mmol, 30%). IR (cm^{-1}): 2870, 1717, 1584, 1435, 1218, 1095, 851, 767; ^{1}H NMR (300 MHz, $CDCl_3$): δ = 9.27 (s, 2H), 9.00 (s, 2H), 8.32 (dd, *J* = 10.2 Hz, *J* = 3.3 Hz, 2H), 7.89 (dd, *J* = 10.2 Hz, *J* = 3.3 Hz, 2H), 5.09 (quin, *J* = 6.0 Hz, 2H), 4.09 (d, *J* = 6.3 Hz, 8H), 3.70-3.40 (m, 48H), 3.30 (s, 12H); ^{13}C NMR (75 MHz, $CDCl_3$): δ = 143.0, 142.3, 140.6, 130.7, 130.0, 128.9, 128.4, 125.9, 71.95, 71.11, 70.68, 70.65, 70.56, 70.55, 70.43, 61.1, 59.1; HRMS (ESI) *m/z*: $[M + H]^+$ Calcd for $C_{50}H_{79}N_8O_{16}$ = 1047.5609; Found = 1047.5618.

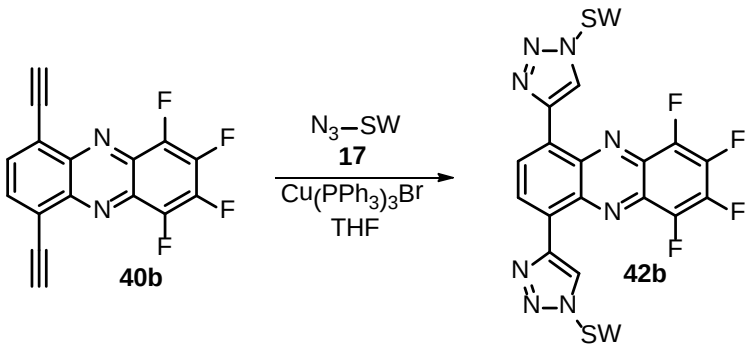

6,9-Bis(1-(2,5,8,11,15,18,21,24-octaoxapentacosan-13-yl)-1H-1,2,3-triazol-4-yl)-1,2,3,4-tetrafluorophenazine (**42b**)

40b (18 mg, 0.060 mmol) and **17** (61 mg, 0.15 mmol) were stirred together in H_2O (1 mL) and THF (5 mL). The solution was then deoxygenated via the freeze-pump-thaw method (3x). Under a flow of nitrogen, $Cu(PPh_3)_3Br$ (0.011 g, 0.012 mmol) was added. The reaction was sealed under the inert atmosphere and stirred at 50 ˚C for 2 d. The reaction mixture was then extracted with saturated aqueous NH_4Cl (25 mL) and DCM (5 x 25 mL), the organic fractions were collected and dried over sodium sulfate, and the solvent was removed under reduced pressure. Purification by silica gel chromatography (gradient elution, EtOAc → EtOAc:MeOH 20:1 → 10:1) gave **42b** as a red oil (18 mg, 0.016 mmol, 27%). IR (cm^{-1}): 2923, 2856, 1737, 1456, 1260, 1092, 198, 464; ^{1}H NMR (300 MHz, $CDCl_3$): δ = 9.24 (s, 2H), 9.15 (s, 2H), 5.11 (quin, J = 6.0 Hz, 2H), 4.09 (d, J = 6.3 Hz, 8H), 3.70-3.55 (m, 41H), 3.48 (m, 8H), 3.33 (s, 12H); ^{13}C NMR (75 MHz, $CDCl_3$): δ = 142.2, 140.2, 130.1, 129.1, 125.8, 72.02, 71.16, 70.73, 70.71, 70.61, 70.39, 61.2, 59.1 (the carbons next to the fluorine atoms could not be identified); ^{19}F NMR (300 MHz, $CDCl_3$): δ = -150.88 (dd, J = 16.2 Hz, J = 3.6 Hz, 2F), -152.06 (dd, J = 15.0 Hz, J = 3.0 Hz, 2F); HRMS (ESI) *m/z*: $[M + H]^+$ Calcd for $C_{50}H_{75}F_4N_8O_{16}$ = 1119.5232; Found = 1119.5230.

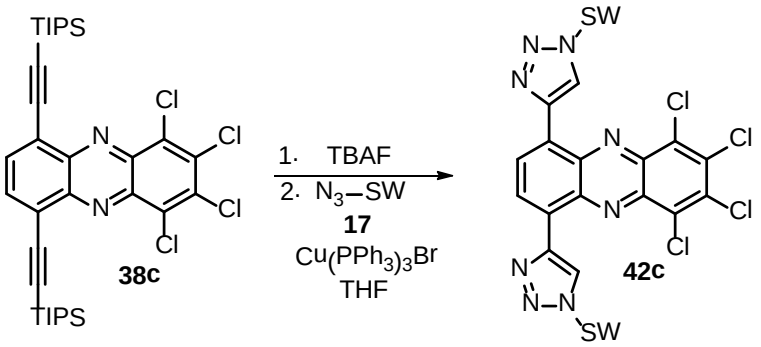

6,9-Bis(1-(2,5,8,11,15,18,21,24-octaoxapentacosan-13-yl)-1H-1,2,3-triazol-4-yl)-1,2,3,4-tetrachlorophenazine (**42c**)

38c (0.020 g, 0.039 mmol) and **17** (0.080 g, 0.20 mmol) were stirred into THF (10 mL). The reaction mixture was then deoxygenated via the freeze-pump-thaw method (3x). $CuSO_4 \cdot 5H_2O$ (0.049 g, 0.20 mmol), $KF \cdot 2H_2O$ (0.037 g, 0.39 mmol), and sodium ascorbate (0.039 g, 0.20 mmol) were dissolved in a separate solution of H_2O (3 mL), which was deoxygenated (3x) and added to the reaction mixture under a flow of nitrogen. The reaction was sealed and stirred at room temperature for 3 d. The solution was extracted with saturated aqueous NH_4Cl (25 mL) and DCM (3 x 25 mL). The organic fractions were collected, the solvent was evaporated, and purification by silica gel chromatography (19:1 EtOAc:MeOH) gave **42c** as a red oil (0.016 g, 0.014 mmol, 35%). ^{1}H NMR (300 MHz, $CDCl_3$): δ = 9.50 (s, 2H), 9.16 (s, 2H), 5.13 (quin, J = 6.0 Hz, 2H), 4.09 (d, J = 6.3 Hz, 4H), 3.54 – 3.70 (m, 63H), 3.47 (m, 9H), 3.32 (s, 13H); ^{13}C NMR (75 MHz, $CDCl_3$): δ = 142.5, 140.6, 137.7, 134.8, 130.4, 129.3, 126.4, 72.21, 71.36, 70.92, 70.89, 70.81, 70.80, 70.61, 61.3, 59.3; HRMS (ESI) *m/z*: $[M + H]^+$ Calcd for $C_{50}H_{75}Cl_4N_8O_{16}$ = 1183.4050; Found = 1183.4109.

8.5 Benzochalcogendiazoles 43-44

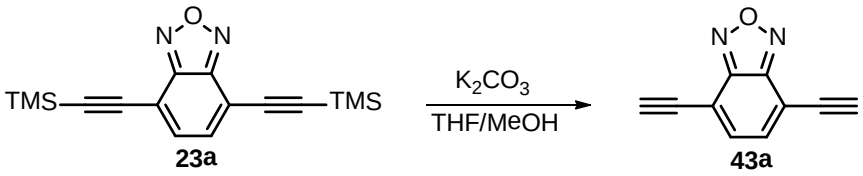

23a **43a**

4,7-Diethynylbenzo[c][1,2,5]oxadiazole (**43a**)

23a (64 mg, 0.20 mmol) and K_2CO_3 (0.28 g, 2.0 mmol) were stirred into 1:1 MeOH:THF (10 mL) for 15 min. The solids were then filtered, the solvent was evaporated, and the residue was purified by silica gel chromatography (50:1 hexanes:EtOAc) to give **43a** as a faint yellow, light-sensitive solid (33 mg, 0.20 mmol, 100%). mp: 82 ˚C (decomposition); IR (cm^{-1}): 3313, 3269, 2923, 2853, 2106, 1767, 1552, 993, 866, 618; ^1H NMR (300 MHz, $CDCl_3$): δ = 7.55 (s, 2H), 3.70 (s, 2H); ^{13}C NMR (75 MHz, $CDCl_3$): δ = 149.7, 135.6, 112.8, 87.4, 77.6; HRMS (EI) *m/z*: $[M]^+$ Calcd for $C_{10}H_4N_2O$ = 168.0324; Found = 168.0327.

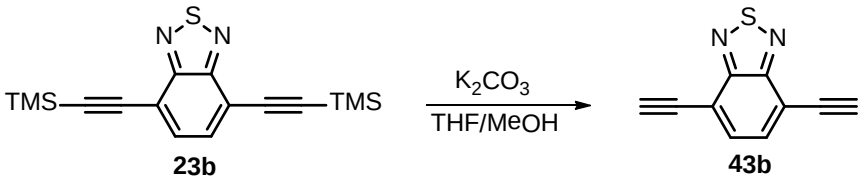

23b **43b**

4,7-Diethynylbenzo[c][1,2,5]thiadiazole (**43b**)

23b (1.61 g, 4.78 mmol) was dissolved in a 1:1 THF:MeOH solution (50 mL). K_2CO_3 (3.3 g, 24 mmol) was added as a solution in H_2O (10 mL) and the reaction mixture was stirred overnight (16 h). The solution was extracted with H_2O (40 mL) and DCM (3 x 50 mL). Purification by silica gel chromatography (50:1 hexanes:EtOAc) gave **43b** as an orange, light-sensitive solid (0.560 g, 3.04 mmol, 64%). mp: 114 °C (decomposition); IR (cm^{-1}): 3276, 3053, 2108, 1892, 1541, 1489, 1478, 881, 848, 670, 611; ^1H NMR (300 MHz, $CDCl_3$): δ = 7.75 (s, 2H), 3.67 (s, 2H); ^{13}C NMR (75 MHz, $CDCl_3$): δ = 154.5, 133.4, 116.9, 85.5, 79.0; MS (EI) *m/z*: $[M]^+$ Calcd for $C_{10}H_4N_2S$ = 184.0; Found = 184.0.

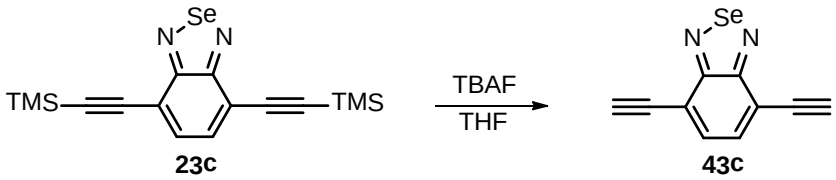

23c **43c**

4,7-Diethynylbenzo[c][1,2,5]selenadiazole (**43c**)

23c (0.100 g, 0.266 mmol) was dissolved in THF (10 mL). A 1.0 M solution of tetra-butylammoniumfluoride in THF (1.7 mL, 1.7 mmol) was added very slowly and the reaction was stirred for five minutes. The solvent was then removed under reduced pressure, and purification by silica gel chromatography (1:1 $CHCl_3$:hexanes) afforded43**2c** as a yellow-orange solid (0.0480 g, 0.208 mmol, 78%). mp: 109 ˚C (decomposition); IR (cm^{-1}): 3266, 3045, 2129, 2100, 1885, 1698, 1523, 1483, 847, 610; ^{1}H NMR (300 MHz, $CDCl_3$): δ = 7.67 (s, 2H), 3.67 (s, 2H); ^{13}C NMR (75 MHz, $CDCl_3$): δ = 159.2, 133.6, 118.7, 85.3, 79.5; HRMS (EI) *m/z*: $[M]^+$ Calcd for $C_{10}H_4N_2Se$ = 231.9540; Found = 231.9540.

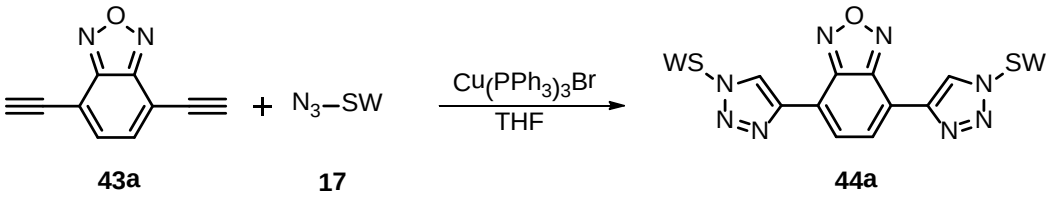

43a **17** **44a**

4,7-Bis(1-(2,5,8,11,15,18,21,24-octaoxapentacosan-13-yl)-1H-1,2,3-triazol-4-yl)benzo[c][1,2,5]oxadiazole (**44a**)

43a (0.017 g, 0.10 mmol) and **17** (0.10 g, 0.25 mmol) were dissolved in THF (2 mL). The mixture was degassed via the freeze/pump/thaw method (3x) and $Cu(PPh_3)_3Br$ (0.0090 g, 0.010 mmol) was added under a flow of nitrogen. The solution was then stirred at room temperature overnight (16 h), during which time a green fluorescence developed. The solution was extracted with saturated aqueous NH_4Cl (30 mL) and DCM (3 x 50 mL). Purification by silica gel chromatography (9:1 EtOAc:MeOH) yielded **44a** as an orange oil (0.054 g, 0.055 mmol, 54%). IR (cm^{-1}): 2918, 2870, 1450, 1349, 1236, 1097, 937, 873; ^{1}H NMR (300 MHz, $CDCl_3$): δ = 8.65 (s, 2H), 8.40 (s, 2H), 5.05 (quin, *J* = 6.0 Hz, 2H), 4.02 (m, 4H), 3.66-3.56 (m, 41H), 3.50 (m, 8H), 3.33 (s, 12H); ^{13}C NMR (75 MHz, $CDCl_3$): δ = 147.6, 141.5, 127.2, 124.4, 118.6, 72.01,

71.10, 70.74, 70.71, 70.59, 70.14, 61.3, 59.1; HRMS (ESI) *m/z*: $[M + H]^+$ Calcd for $C_{44}H_{75}N_8O_{17}$ = 987.5250; Found = 987.5246.

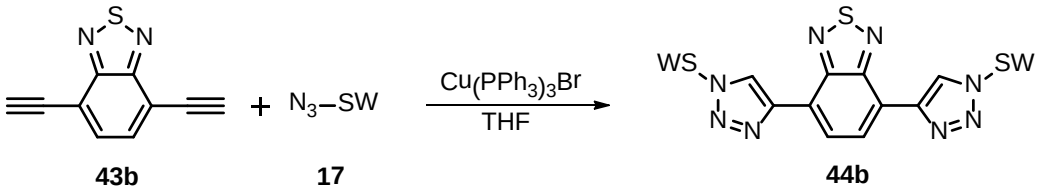

43b **17** **44b**

4,7-Bis(1-(2,5,8,11,15,18,21,24-octaoxapentacosan-13-yl)-1H-1,2,3-triazol-4-yl)benzo[c][1,2,5]thiadiazole (**44b**)

43b (0.090 g, 0.49 mmol) and **17** (0.50 g, 1.2 mmol) were dissolved in THF (10 mL). The mixture was degassed via the freeze/pump/thaw method (3x) and $Cu(PPh_3)_3Br$ (0.045 g, 0.049 mmol) was added under a flow of nitrogen. The solution was then stirred at 50 ˚C overnight (16 h), during which time a green color and intense green fluorescence developed. The solution was extracted with H_2O (70 mL) and DCM (5 x 20 mL) until the aqueous phase was no longer fluorescent. The organic portions were collected and washed with saturated aqueous NH_4Cl (25 mL). Purification by silica gel chromatography (5:1 EtOAc:MeOH) yielded **44b** as an orange oil (0.33 g, 0.33 mmol, 68%). IR(cm^{-1}): 2870, 1704, 1447, 1352, 1236, 1095, 878, 847; ^1H NMR (300 MHz, $CDCl_3$): δ = 8.87 (s, 2H), 8.61 (s, 2H), 5.03 (m, 2H), 4.01 (d, 8H, J = 6.0 Hz), 3.65-3.51 (m, 41H), 3.46 (m, 8H), 3.29 (s, 12H); ^{13}C NMR (75 MHz, $CDCl_3$): δ = 152.3, 142.7, 125.9, 124.3, 122.8, 71.86, 70.96, 70.58, 70.56, 70.45, 70.14, 61.0, 59.0; HRMS (ESI) *m/z*: $[M + H]^+$ Calcd for $C_{44}H_{75}N_8O_{16}S$ = 1003.5022; Found = 1003.5030.

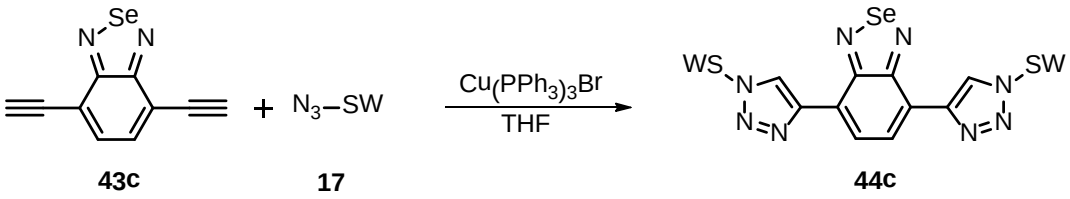

4,7-Bis(1-(2,5,8,11,15,18,21,24-octaoxapentacosan-13-yl)-1H-1,2,3-triazol-4-yl)benzo[c][1,2,5]selenadiazole (**44c**)

43c (0.048 g, 0.21 mmol) and **17** (0.21 g, 0.52 mmol) were dissolved in THF (10 mL). The mixture was degassed via the freeze/pump/thaw method (3x) and $Cu(PPh_3)_3Br$ (0.020 g, 0.021 mmol) was added under a flow of nitrogen. The solution was then stirred at 50 ˚C overnight (16 h). The solution turned black and intensely green fluorescent after only 3 h. The solution was extracted with H_2O (30 mL) and DCM (5 x 50 mL) until the aqueous phase was no longer fluorescent. The organic portions were collected and washed with saturated aqueous NH_4Cl (25 mL). Purification by silica gel chromatography (9:1 EtOAc:MeOH) yielded **44c** as an orange oil (0.023 g, 0.022 mmol, 11%). IR (cm^{-1}): 2870, 2097, 1723, 1637, 1453, 1352, 1250, 1200, 1097, 934, 849, 542; ^1H NMR (300 MHz, $CDCl_3$): δ = 8.87 (s, 2H), 8.56 (s, 2H), 5.03 (quin, 2H, J = 6.0 Hz), 4.03 (d, 7H, J = 6.0 Hz), 3.65-3.55 (m, 48H), 3.49 (m, 8H), 3.33 (s, 13H); ^{13}C NMR (75 MHz, $CDCl_3$): δ = 158.0, 143.1, 126.4, 124.9, 124.3, 72.00, 71.09, 70.72, 70.69, 70.59, 70.57, 70.29, 61.1, 59.1; HRMS (ESI) *m/z*: $[M + H]^+$ Calcd for $C_{44}H_{75}N_8O_{16}Se$ = 1051.4466; Found = 1051.4489.

8.6 Pyridine Compounds 51-52

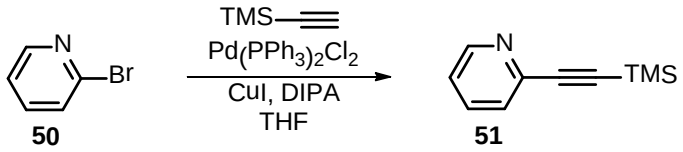

50 **51**

2-((Trimethylsilyl)ethynyl)pyridine (**51**)

50 (1.00 g, 6.33 mmol), $Pd(PPh_3)_2Cl_2$ (44 mg, 0.063 mmol), and CuI (24 mg, 0.12 mmol) were dissolved in a degassed mixture of THF (2 mL) and morpholine (0.5 mL). After stirring for a few minutes at room temperature, trimethylsilyl acetylene (1.24 g, 12.7 mmol) was added slowly via syringe. A color change from yellow to green/blue to brown/yellow was observed. The reaction was then stirred overnight. The next day, the reaction was incomplete according to TLC, so the reaction was heated to 50 ˚C, more trimethylsilyl acetylene (1.24 g, 12.67 mmol) was added, and the reaction was stirred at 50 ˚C another day. The mixture was then extracted with EtOAc (3 x 100 mL), at which point the precipitation of a dark solid was observed. The solid was removed by filtration. After drying with magnesium sulfate and evaporation of the solvent under reduced pressure, the crude mixture was purified by silica gel chromatography (hexanes:EtOAc 9:1) to give **51** as a yellow, light-sensitive oil (760. mg, 4.34 mmol, 69%). IR (cm^{-1}): 2960, 2897, 2164, 1578, 1560, 1456, 1423; ^1H NMR (300 MHz, $CDCl_3$): δ = 8.52 (dq, J = 4.9 Hz, J = 0.8 Hz, 1H), 7.58 (dt, J = 7.7 Hz, J = 1.7 Hz, 1H), 7.40 (dt, J = 7.8 Hz, J = 0.8 Hz, 1H), 7.17 (ddd, J = 7.6 Hz, J = 4.9 Hz, J = 1.1 Hz, 1H), 0.23 (s, 9H); ^{13}C NMR (75 MHz, $CDCl_3$): δ = 150.1, 143.3, 136.2, 127.4, 123.2, 103.9, 94.9, 0.1; MS (EI) *m/z*: $[M]^+$ Calcd for $C_{10}H_{13}NSi$ = 175.1; Found = 175.1.

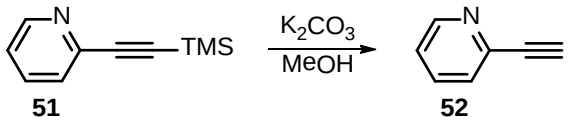

51 **52**

2-Ethynylpyridine (**52**)

51 (760. mg, 4.34 mmol) and K_2CO_3 (1.2 g, 8.7 mmol) were dissolved in MeOH (10 mL) in a round bottom flask. The reaction was kept in the dark by covering the flask with aluminum foil and stirred overnight. The pale brown reaction mixture was then extracted with DCM (3 x 20 mL), the solvent removed under reduced pressure, and the product was purified by silica gel

chromatography (DCM:MeOH (98:2) to give **52** as a yellow, light-sensitive oil (111 mg, 1.08 mmol, 25%). IR (cm^{-1}): 3291, 3217, 2109, 1582, 1561, 1461, 1427, 1244; ^{1}H NMR (300 MHz, $CDCl_3$): δ = 8.57 (d, J = 4.8 Hz, 1H), 7.64 (d, J = 7.7 Hz, J = 1.7 Hz, 1H), 7.46 (dt, J = 7.8 Hz, 1H), 7.24 (ddd, J = 7.7 Hz, J = 4.8 Hz, J = 1.0 Hz, 1H), 3.14 (s, 9H); ^{13}C NMR (75 MHz, $CDCl_3$): δ = 150.3, 142.6, 136.4, 127.7, 123.6, 83.0, 77.3; MS (EI) *m/z*: $[M]^+$ Calcd for C_7H_5N = 103.0; Found = 103.1.

8.7 BODIPY Compounds 54-55

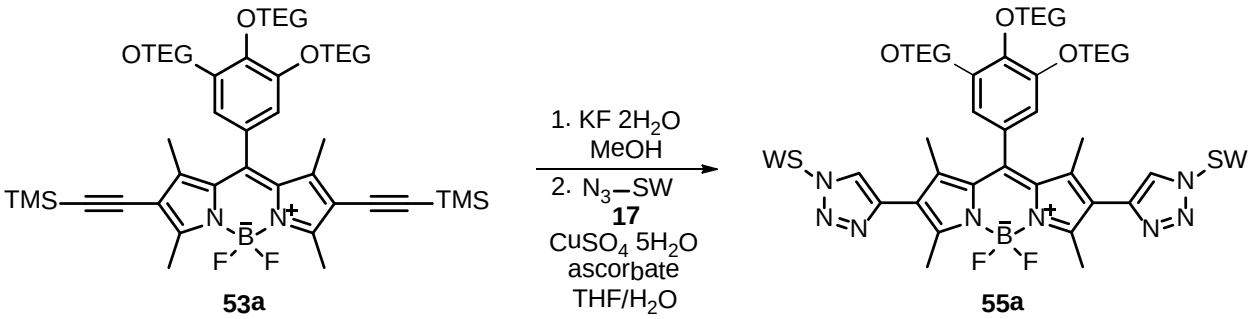

53a **55a**

4,4'-Difluoro-8-(3,4,5-tris(2-(2-(2-methoxyethoxy)ethoxy)ethoxy)phenyl)-2,6-bis-(1-(2,5,8,11,15,18,21,24-octaoxapentacosan-13-yl)-1H-1,2,3-triazol-4-yl)-1,3,5,7-tetramethyl-4-bora-3a,4a-diaza-s-indacene (**55a**)

53a (24 mg, 0.024 mmol) was stirred into MeOH (15 mL). KF•$2H_2O$ (11 mg, 0.12 mmol) was then added as a solution in MeOH (15 mL). The reaction was stirred at room temperature for 20 minutes. The reaction mixture was then extracted with DCM and H_2O. Purification was accomplished with a short silica gel column (19:1 EtOAc:MeOH) to yield **54a** as a dark red oil (20. mg, 0.023 mmol, 97%) which was immediately dissolved in THF (2 mL) along with **17** (60. mg, 0.15 mmol). The solution was deoxygenated three times by freezing and evacuating, and $Cu(PPh_3)_3Br$ (2 mg, 0.003 mmol) was added under a flow of nitrogen gas. The reaction vessel was sealed under the inert atmosphere and stirred overnight at room temperature. No progress was evidenced the next day, and the reaction was then heated to 40 ˚C and stirred another night. After still no progress being observed, $CuSO_4$•$5H_2O$ (18 mg, 0.12 mmol) and sodium ascorbate (23 mg, 0.12 mmol) were added under nitrogen gas and the reaction was stirred at 40 ˚C overnight. Again, no reaction was observed, so deoxygenated H_2O (1 mL) was added. The reaction was then stirred overnight at room temperature, at which point no starting material remained. The mixture was extracted with saturated aqueous NH_4Cl (30 mL) and DCM (5 x 50 mL). The organic fractions were collected and dried over magnesium sulfate. The solvent was evaporated, and the residue was purified by silica gel chromatography (9:1 EtOAc:MeOH) to give **55a** as a red oil (14 mg, 0.0083 mmol, 36%). IR (cm^{-1}): 2870, 1704, 1536, 1450, 1349, 1325, 1245, 1189, 1095, 1012, 940, 849, 560; ^1H NMR (300 MHz, $CDCl_3$): δ = 7.74 (s, 2H), 6.59 (s, 2H), 4.95 (quin, J = 5.7 Hz, 2H), 4.22 (t, J = 4.8 Hz, 2H), 4.12 (t, J = 4.5 Hz, 4H), 3.96 (d, J = 5.7

Hz, 8H), 3.84 (m, 8H), 3.69-3.50 (m, 93H), 3.36 (m, 25H), 2.66 (s, 6H), 1.60 (s, 6H); ^{13}C NMR (75 MHz, $CDCl_3$): δ = 154.0, 151.6, 139.97, 139.32, 135.9, 131.4, 130.1, 128.4, 125.6, 123.0, 107.8, 72.07, 72.01, 70.96, 70.81, 70.75, 70.69, 70.65, 70.61, 70.55, 70.06, 69.80, 69.35, 60.8, 59.1, 34.3, 21.3, 14.2, 13.1; MS (ESI) *m/z*: $[M + K]^+$ Calcd for $C_{78}H_{131}BF_2KN_8O_{28}$ = 1715.8; Found = 1715.8.

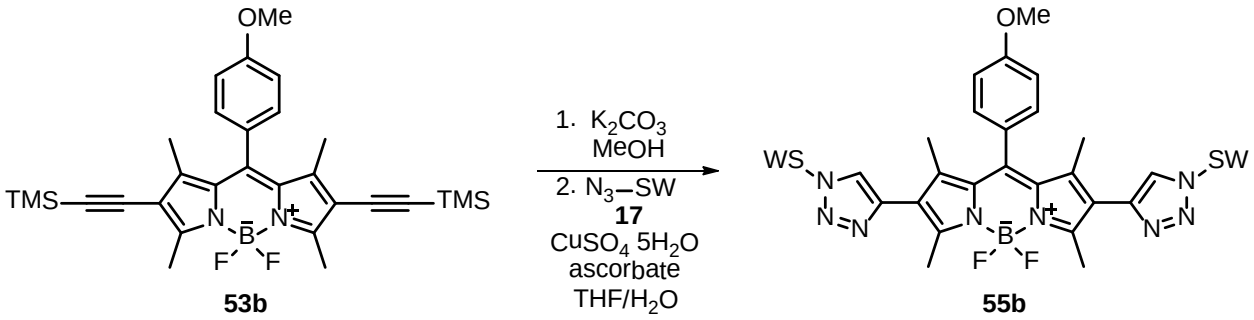

4,4'-Difluoro-8-(4-methoxyphenyl)-2,6-bis-(1-(2,5,8,11,15,18,21,24-octaoxapentacosan-13-yl)-1H-1,2,3-triazol-4-yl)-1,3,5,7-tetramethyl-4-bora-3a,4a-diaza-s-indacene (**55b**)

53b (25 mg, 0.046 mmol) was dissolved in MeOH (10 mL). $KF•2H_2O$ (17 mg, 0.18 mmol) was added as a solution in MeOH (10 mL). After stirring at room temperature for 30 minutes, no reaction was observed. K_2CO_3 (0.10 g, 0.72 mmol) was then added, and the reaction was stirred for a further 10 minutes, at which point full conversion was seen by TLC. The reaction mixture was then extracted with brine (50 mL) and EtOAc (30 mL). The organic portion was dried over magnesium sulfate, the solvent was evaporated, and the residue was purified by silica gel chromatography (50:1 hexanes:EtOAc) to give **54b** as a red solid (13 mg, 0.032 mmol, 71%) which was immediately dissolved in THF (3 mL) along with **17** (40. mg, 0.097 mmol). The solution was deoxygenated three times by freezing and evacuating. $Cu(PPh_3)_3Br$ (30. mg, 0.032 mmol) was added under nitrogen gas. The reaction vessel was sealed under the inert atmosphere and stirred at room temperature overnight. No reaction progress was seen the next day, so $CuSO_4•5H_2O$ (24 mg, 0.097 mmol) and sodium ascorbate (19 mg, 0.097 mmol) were added under a flow of nitrogen gas. The reaction was then stirred overnight at room temperature, after which time it was extracted with brine (25 mL) and DCM (5 x 25 mL). The organic fractions were collected and dried over magnesium sulfate. The solvent was evaporated, and the residue was purified by silica gel chromatography (9:1 EtOAc:MeOH) to yield **55b** as a red oil (25 mg,

0.020 mmol, 63%). IR (cm^{-1}): 2870, 1603, 1533, 1453, 1349, 1322, 1250, 1189, 1103, 1012, 937, 844, 560; ^{1}H NMR (300 MHz, $CDCl_3$): δ = 7.74 (s, 2H), 7.23 (d, J = 8.4 Hz, 2H), 7.03 (d, J = 8.7 Hz, 2H), 4.94 (quin, J = 5.4 Hz, 2H), 3.95 (d, J = 5.4 Hz, 8H), 3.87 (s, 3H), 3.60-3.50 (m, 56H), 3.34 (s, 12H), 2.67 (s, 6H), 1.51 (s, 6H); ^{13}C NMR (75 MHz, $CDCl_3$): δ = 160.5, 132.0, 129.5, 127.2, 123.11, 122.76, 115.11, 114.86, 72.01, 70.97, 70.70, 70.67, 70.62, 70.53, 70.05, 60.9, 59.1, 55.5, 13.86, 13.41; HRMS (ESI) *m/z*: Calcd for $C_{58}H_{91}BF_2N_8O_{17}$ =1220.6563; Found = 2509.8062 (100%), 2309.1822 (50.6%), 976.1033 (36.4%), 2075.7043 (27.6%).

8.8 Click Polymerization Compounds 59-71

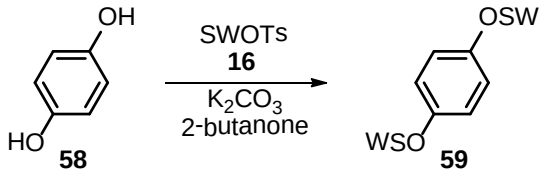

1,4-Bis(2,5,8,11,15,18,21,24-octaoxapentacosan-13-yloxy)benzene (**59**)

To a solution of **16** (23.3 g, 43.3 mmol) in 2-butanone (100 mL) under an inert nitrogen atmosphere, K_2CO_3 (14.9 g, 108 mmol) and **58** (1.99 g, 18.0 mmol) were added. The mixture was stirred at reflux for 5 days. The precipitate was filtered off, the filtrate was dried over $MgSO_4$, and then filtered through Celite. The solvent was removed under reduced pressure, and the brown crude product was purified by silica gel chromatography (gradient elution, EtOAc → EtOAc:MeOH 98:2 → 95:5 → 90:10) to yield **59** as a colorless oil (10.2 g, 12.1 mmol, 67%). IR (cm^{-1}): 2868, 1504, 1455, 1215, 1098, 944, 847; ^{1}H NMR (300 MHz, $CDCl_3$): δ = 6.72 (s, 4H), 4.21 (quin, J = 5.0 Hz, 2H), 3.55-3.32 (m, 56H), 3.18 (s, 12H); ^{13}C NMR (75 MHz, $CDCl_3$): δ = 152.8, 117.7, 77.9, 71.91, 71.00, 70.60, 70.59, 70.50, 70.41, 59.0; MS (ESI) *m/z*: $[M + Na]^+$ Calcd for $C_{40}H_{74}NaO_{18}$ = 865.5; Found = 865.5.

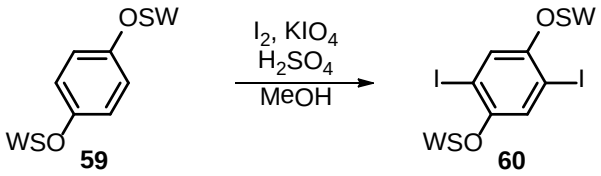

13,13'-((2,5-Diiodo-1,4-phenylene)bis(oxy))bis(2',5',8',11',15',18',21',24'-octaoxapentacosane) (**60**)

KIO_4 (1.82 g, 7.93 mmol) was added to a solution of iodine (3.76 g, 14.8 mmol) in MeOH (200 mL). The mixture was stirred at room temperature for 15 minutes, and concentrated sulfuric acid (5 mL) and **59** (10.0 g, 11.9 mmol) were added. The reaction was stirred at reflux overnight, and then quenched with aqueous Na_2SO_3 until the color faded. The mixture was then extracted with DCM (6 x 70 mL). The organic fractions were collected and dried over magnesium sulfate. The solvent was evaporated and the residue was purified by silica gel chromatography (gradient

elution, EtOAc → EtOAc:MeOH 98:2 → 95:5) to give **60** as a slightly yellow oil (9.80 g, 8.95 mmol, 75%). IR (cm^{-1}): 2868, 1462, 1348, 1200, 1098, 849, 776; ^{1}H NMR (300 MHz, $CDCl_3$): δ = 7.38 (s, 2H), 4.32 (quin, J = 5.2 Hz, 2H), 3.70-3.42 (m, 58H), 3.30 (s, 12H); ^{13}C NMR (75 MHz, $CDCl_3$): δ = 153.4, 126.1, 88.0, 80.9, 72.0, 71.27, 70.91, 70.75, 70.72, 70.67, 70.59, 59.1; MS (ESI) *m/z*: $[M + NH_4]^+$ Calcd for $C_{40}H_{76}I_2NO_{18}$ = 1112.3; Found = 1112.1.

((2,5-Bis(2,5,8,11,15,18,21,24-octaoxapentacosan-13-yloxy)-1,4-phenylene)bis(ethyne-2,1-diyl))bis(trimethylsilane) (**61**)

60 (4.6 g, 4.2 mmol) was dissolved in THF (5 mL) and piperidine (5 mL). The reaction mixture was degassed by bubbling nitrogen through it for 10 minutes. $Pd(PPh_3)_2Cl_2$ (29 mg, 0.042 mmol) and CuI (8 mg, 0.04 mmol) were subsequently added under a flow of nitrogen. The reaction mixture was sealed and trimethylsilylacetylene (2.42 mL, 16.8 mmol) was added via syringe. The reaction was stirred at room temperature for 2 days. The solids were then filtered off, the solvent was evaporated, and the residue was purified by silica gel chromatography (19:1 EtOAc:MeOH) to give **61** as a light yellow oil (3.57 g, 3.44 mmol, 82%). IR (cm^{-1}): 2869, 2153, 1489, 1249, 1199, 1102, 841, 760, 627; ^{1}H NMR (300 MHz, $CDCl_3$): δ = 7.05 (s, 2H), 4.40 (quin, J = 5.1 Hz, 2H), 3.78-3.47 (m, 56H), 3.35 (s, 12H), 0.22 (s, 18H); ^{13}C NMR (75 MHz, $CDCl_3$): δ = 154.0, 121.5, 116.0, 101.2, 100.1, 79.9, 72.03, 71.27, 70.74, 70.72, 70.67, 70.63, 70.61, 59.1, 0.07; MS (ESI) *m/z*: $[M + NH_4]^+$ Calcd for $C_{50}H_{94}NO_{18}Si_2$ = 1052.6; Found = 1052.5.

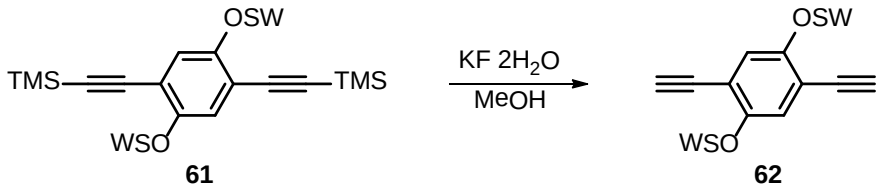

13,13'-((2,5-Diethynyl-1,4-phenylene)bis(oxy))bis(2',5',8',11',15',18',21',24'-octaoxapentacosane) (**62**)

61 (2.58 g, 2.49 mmol) was dissolved in MeOH (25 mL). KF•$2H_2O$ (0.94 g, 9.97 mmol) was added as a solution in MeOH (25 mL). The reaction mixture was stirred for 3 hours at room temperature, then poured into water (25 mL) and extracted with DCM (3 x 50 mL). The organic fractions were collected and dried over magnesium sulfate. The crude product was then purified by silica gel chromatography (gradient elution, EtOAc → 19:1 EtOAc:MeOH) to give **62** as a slightly yellow oil (2.12 g, 2.38 mmol, 96%). IR (cm^{-1}): 3239, 2869, 1490, 1199, 1098, 948, 849; ^{1}H NMR (300 MHz, $CDCl_3$): δ = 7.13 (s, 2H), 4.41 (quin, J = 5.1 Hz, 2H), 3.80-3.44 (m, 56H), 3.35 (s, 12H), 3.30 (s, 2H); ^{13}C NMR (75 MHz, $CDCl_3$): δ = 154.2, 121.6, 115.1, 82.8, 80.1, 79.8, 72.00, 71.23, 70.70, 70.63, 70.57, 59.1; MS (ESI) *m/z*: $[M + NH_4]^+$ Calcd for $C_{44}H_{78}NO_{16}$ = 908.5; Found = 908.5.

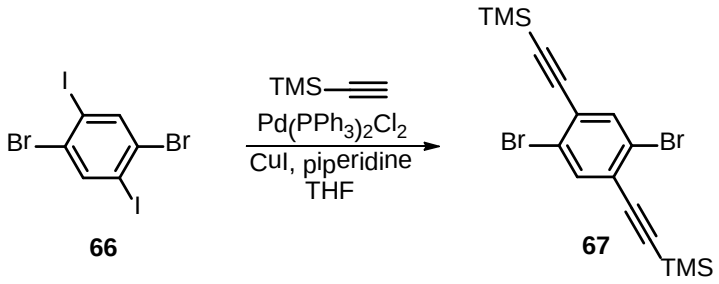

((2,5-Dibromo-1,4-phenylene)bis(ethyne-2,1-diyl))bis(trimethylsilane) (**67**)

66 (1.00 g, 2.05 mmol) was stirred into THF (10 mL) and diisopropylamine (10 mL) along with $Pd(PPh_3)_2Cl_2$ (86 mg, 0.12 mmol) and CuI (47 mg, 0.25 mmol). The mixture was deoxygenated three times via the freeze/pump/thaw method. After warming to room temperature and filling with nitrogen gas, trimethylsilylacetylene (442 mg, 4.50 mmol) was added with a syringe and the reaction was stirred at room temperature for 12 hours. The mixture was then filtered through Celite with hexanes, and purified by silica gel chromatography (hexanes) to give **67** as a colorless

crystalline compound (606 mg, 1.42 mmol, 70%). mp: 130 ˚C; IR (cm^{-1}): 2956, 2158, 1458, 1245, 833; ^{1}H NMR (300 MHz, $CDCl_3$): δ = 7.67 (s, 2H), 0.27 (s, 19H); ^{13}C NMR (75 MHz, $CDCl_3$): δ = 136.4, 126.4, 123.7, 103.0, 101.3, -0.3; MS (EI) *m/z*: $[M]^+$ Calcd for $C_{16}H_{20}Br_2Si_2$ = 427.9; Found = 428.0.

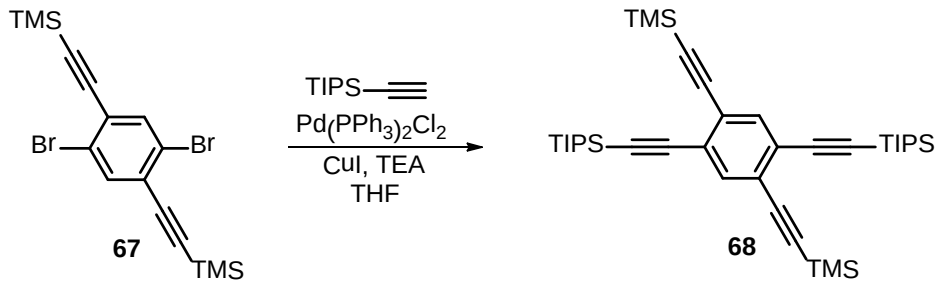

((2,5-Bis((triisopropylsilyl)ethynyl)-1,4-phenylene)bis(ethyne-2,1-diyl))bis(trimethylsilane) (**68**)

To a deoxygenated solution of THF (8 mL) and diisopropylamine (8 mL) was added **67** (0.900 g, 2.10 mmol), $Pd(PPh_3)_4$ (72 mg, 0.063 mmol) and CuI (24 mg, 0.13 mmol) under nitrogen gas. Triisopropylsilylacetylene (1.08 mL, 4.62 mmol) was then added through a septum. The reaction was stirred for 18 hours at 60 ˚C. The mixture was then filtered through Celite with hexanes, and purified by silica gel chromatography (hexanes) to give **68** as a yellow oil (0.921 g, 1.46 mmol, 70%). IR (cm^{-1}): 2942, 2864, 2160, 1479, 1249, 839; ^{1}H NMR (300 MHz, $CDCl_3$): δ = 7.53 (s, 2H), 1.14 (s, 45H), 0.24 (s, 18H); ^{13}C NMR (75 MHz, $CDCl_3$): δ = 137.0, 125.19, 125.09, 104.0, 102.2, 100.4, 97.3, 18.8, 11.3, -0.2; MS (EI) *m/z*: $[M]^+$ Calcd for $C_{38}H_{62}Si_4$ = 630.4; Found = 630.4.

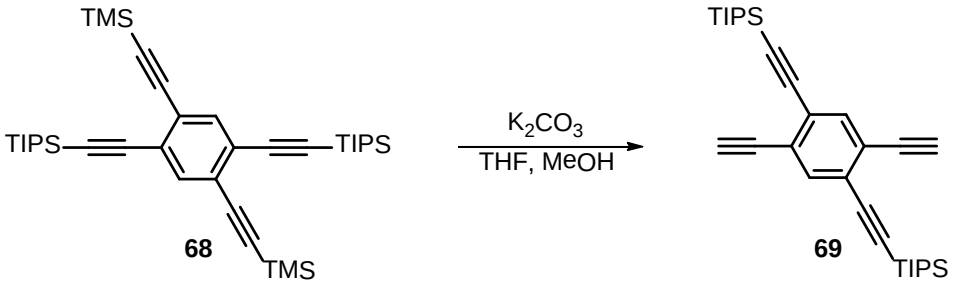

((2,5-Diethynyl-1,4-phenylene)bis(ethyne-2,1-diyl))bis(triisopropylsilane) (**69**)

68 (921 mg, 1.46 mmol) was dissolved in a 3:1 THF:MeOH solution (80 mL). K_2CO_3 (1.21 g, 8.76 mmol) was added, and the reaction was stirred for 22 hours at room temperature. The

solution was then extracted with saturated aqueous NH_4Cl and Et_2O. The solvent was removed and the residue was purified by silica gel chromatography (hexanes) to give **69** as a colorless solid (494 mg, 1.01 mmol, 70%). mp: 174-175 ˚C; IR (cm^{-1}): 3284, 2941, 2863, 2158, 1479, 1190, 996, 837, 661; ^1H NMR (300 MHz, $CDCl_3$): δ = 7.58 (s, 2H), 3.32 (s, 2H), 1.14 (s, 43H); ^{13}C NMR (75 MHz, $CDCl_3$): δ = 136.1, 126.0, 124.9, 103.5, 98.1, 83.0, 81.1, 18.6, 11.2; MS (EI) *m/z*; $[M]^+$ Calcd for $C_{32}H_{46}Si_2$ = 486.3, Found = 486.3.

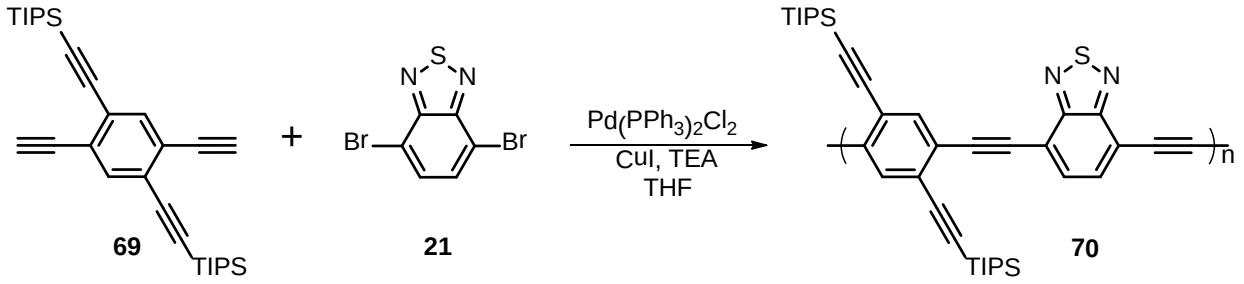

Poly(2,5-bis((triisopropylsilyl)ethynyl)phenylene-1,4-ethynylene-alt-benzo[c][1,2,5]thiadiazole-2,5-ethynylene) (**70**)

69 (300. mg, 0.616 mmol) and **21** (181 mg, 0.616 mmol) were dissolved in THF (3.5 mL) and TEA (3.5 mL). The solution was deoxygenated three times by freezing and evacuating. Under a flow of nitrogen, $Pd(PPh_3)_2Cl_2$ (2 mg, 0.003 mmol) and CuI (2 mg, 0.006 mmol) were added. The reaction was then stirred at 50 ˚C for 3 days, during which time the solution turned brightly fluorescent. The reaction was extracted with saturated aqueous NH_4Cl and DCM. The organic fractions were collected and concentrated, and the polymer was precipitated into MeOH three times, and then extracted with Et_2O via Soxhlet for 7 days. **70** was recovered as a red solid (362 mg, 0.55 mmol, 89%). This must be considered a crude yield, for the purification techniques used were insufficient. As a result, this polymer was not fully characterized. IR (cm^{-1}): 3128, 3043, 2940, 2862, 2154, 1769, 1402, 1184, 995, 674; GPC ($CHCl_3$, polystyrene): M_w = 50770 Da, M_n = 13453 Da.

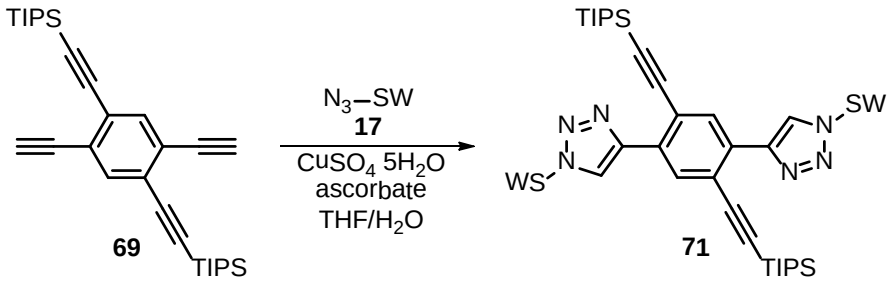

4,4'-(2,5-Bis((triisopropylsilyl)ethynyl)-1,4-phenylene)bis(1-(2,5,8,11,15,18,21,24-octaoxapentacosan-13-yl)-1H-1,2,3-triazole) (**71**)

69 (145 mg, 0.290 mmol) and **17** (600. mg, 1.50 mmol) were added to a 5:1 THF:H_2O solution (12 mL). The solution was then deoxygenated via the freeze/pump/thaw method. Under nitrogen gas, $CuSO_4$•$5H_2O$ (82.5 mg, 0.330 mmol) and sodium ascorbate (13 mg, 0.360 mmol) were added. The reaction was stirred at room temperature for 24 hours. At this point, complete conversion was not observed, so another equivalent of Cu was added. The reaction was then stirred for a further 3 days. The reaction mixture was extracted with saturated aqueous NH_4Cl and $CHCl_3$ until the aqueous phase was no longer fluorescent. The organic fractions were collected and the solvent was removed to give **71** as a red, viscous oil (308 mg, 0.236 mmol, 81%). IR (cm^{-1}): 3616, 2863, 2108, 1459, 1103, 677; ^{1}H NMR (300 MHz, $CDCl_3$): δ = 8.61 (s, 2H), 8.49 (s, 2H), 4.87 (quin, 2H), 3.98 (s, 8H), 3.58 (m, 48H), 3.34 (s, 12H), 1.59 (s, 12H), 1.16 (s, 50H); ^{13}C NMR (75 MHz, $CDCl_3$): δ = 144.0, 133.4, 130.8, 123.4, 120.2, 106.5, 98.2, 71.9, 70.6, 61.26, 60.6, 59.0, 18.83, 11.4; HRMS (ESI) *m/z*: $[M + K]^+$ Calcd for $C_{66}H_{116}KN_6O_{16}Si_2$ = 1343.7623; Found = 1343.7632.

8.9 Thiophenes 46-49 and 72-73

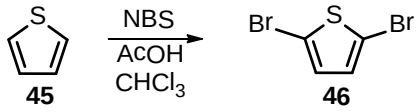

2,5-Dibromothiophene (**46**)

45 (8.7 g, 0.10 mol) was dissolved in $CHCl_3$ (100 mL) and AcOH (50 mL). The solution was cooled to 0 ˚C and NBS (40. g, 0.23 mol) was added. The reaction was warmed to room temperature and stirred overnight. The reaction was then slowly quenched with saturated aqueous Na_2SO_3 (30 mL) and extracted with H_2O and $CHCl_3$. The solvent was evaporated and the crude mixture was purified by silica gel chromatography (hexanes) to give **46** as a colorless oil (22.2 g, 0.092 mol, 92%). IR (cm^{-1}): 3094, 1517, 1411, 1201, 980, 945, 779, 464, 416; ^1H NMR (300 MHz, $CDCl_3$): δ = 6.84 (s); ^{13}C NMR (75 MHz, $CDCl_3$): δ = 130.5, 111.7.

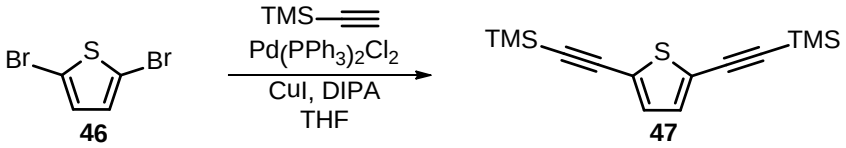

2,5-Bis((trimethylsilyl)ethynyl)thiophene (**47**)

To a degassed solution of **46** (5.0 g, 21 mmol) in THF (10 mL) and diisopropylamine (5 mL) were added $Pd(PPh_3)_2Cl_2$ (290 mg, 0.42 mmol) and CuI (80. mg, 0.42 mmol). The mixture was heated to 40 ˚C and stirred for a few minutes. Trimethylsilyl acetylene (4.9 g, 50. mmol) was then added in three portions through a septum. After the first mL the solution became considerably thicker. It was then diluted by adding THF (20 mL) and $CHCl_3$ (5 mL). 4 mL and 2 mL of trimethylsilyl acetylene were added to the brownish suspension within half an hour. The next day another aliquot of trimethylsilyl acetylene (1.38 g, 14.2 mmol) was added to the suspension, which was stirred for another day at 40 ˚C. The suspension was then quenched with H_2O (100 mL) and extracted with EtOAc (3 x 100 mL). The organic fractions were dried over magnesium sulfate and the solvent was evaporated under reduced pressure. The raw product was purified by silica gel chromatography (hexanes) to give **47** as a pale brown solid (3.4 g, 12 mmol, 60%). mp: 77-80 ˚C; IR (cm^{-1}): 2952, 2897, 2851, 2143, 1509, 1437, 1408, 1245, 1170; ^1H NMR (300 MHz,

$CDCl_3$): δ = 7.02 (s, 2H), 0.24 (s, 18H); ^{13}C NMR (75 MHz, $CDCl_3$): δ = 132.5, 124.8, 100.2, 97.1, 0.03; MS (EI) *m/z*: $[M]^+$ Calcd for $C_{14}H_{20}SSi_2$ = 276.08; Found = 276.09.

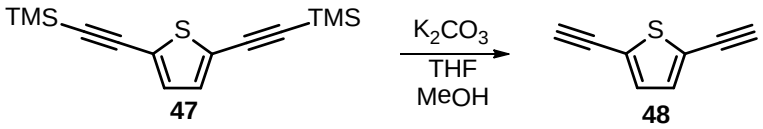

2,5-Diethynylthiophene (**48**)

47 (1.0 g, 3.6 mmol) and K_2CO_3 (1.5 g, 11 mmol) were dissolved in MeOH (20 mL) and THF (5 mL) and stirred for two hours. The solvent was then evaporated under reduced pressure and the crude product was adsorbed on celite and loaded onto a silica gel column. The product was eluted with hexanes to give **48** as a pale brown oil (0.35 g, 2.6 mmol 73%). IR (cm^{-1}): 3289, 3097, 2105, 1779, 1613 1515, 1435, 1210, 1132, 1028; ^1H NMR (300 MHz, $CDCl_3$): δ = 7.12 (s, 2H), 3.36 (s, 2H); ^{13}C NMR (75 MHz, $CDCl_3$): δ = 133.0, 124.0, 82.5, 76.6; MS (EI) *m/z*: $[M]^+$ Calcd for C_8H_4S = 132.0; Found = 132.0.

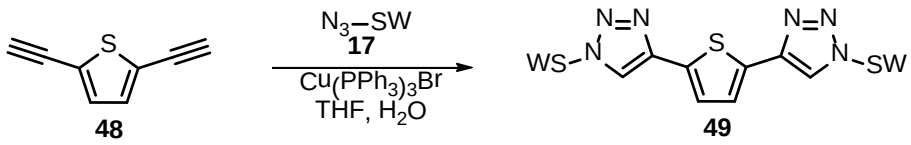

2,5-Bis(1-(2,5,8,11,15,18,21,24-octaoxapentacosan-13-yl)-1H-1,2,3-triazol-4-yl)thiophene (**49**)

48 (200. mg, 1.51 mmol), **17** (1.19 g, 2.91 mmol), and $Cu(PPh_3)_3Br$ (135 mg, 0.145 mmol) were dissolved in a 5:1 THF:H_2O (12 mL). The solution was deoxygenated by freezing and evacuating. The reaction was then sealed under an inert nitrogen atmosphere, heated to 50 ˚C, and stirred for 2 days. The mixture was then extracted with DCM (3 x 20 mL), dried with $MgSO_4$ and purified by silica gel chromatography (gradient elution, EtOAc:acetone 1:1 → acetone) to give **49** as a yellow oil (91 mg, 0.096 mmol, 6%). IR (cm^{-1}): 3120, 2871, 1735, 1638; ^1H NMR (300 MHz, $CDCl_3$): δ = 7.96 (s, 2H), 7.32 (s, 2H), 4.92 (quin, *J* = 5.6 Hz, 2H), 3.93 (m, 8H), 3.58 (m, 48H), 3.31 (s, 6H); ^{13}C NMR (75 MHz, $CDCl_3$): δ = 142.3, 132.7, 124.5, 120.0, 72.0, 71.01, 70.74, 70.72, 70.64, 70.57, 70.05, 61.01, 59.12; MS (ESI) *m/z*: $[M + H]^+$ Calcd for $C_{42}H_{75}N_6O_{16}S$ = 951.5; Found = 951.4.

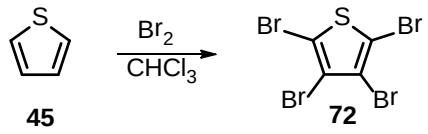

45 **72**

Perbromothiophene (**72**)

45 (10.0 g, 0.119 mol) was stirred into $CHCl_3$ (100 mL). Bromine (79.8 g, 25.7 mL, 0.500 mol) was added dropwise while maintaining the temperature at 10-15 ˚C. The reaction was then warmed to room temperature and stirred for three hours, after which time the reaction was heated to reflux and stirred overnight. The reaction at this point showed 92% tribromothiophene by GC-MS, so Br_2 (28.5 g, 9.18 mL, 0.178 mol) was added dropwise, and the mixture was heated to reflux and stirred for 36 hours. The reaction was then quenched with aqueous sodium hydroxide until the color faded. The solid was filtered and dried to yield **72** as a pale beige powder (38,3 g, 0.0958 mol, 80%). mp: 115-117 ˚C; IR (cm^{-1}): 1743, 1714, 1643, 1523, 1480, 1406, 1270, 1206, 1087, 1007, 855, 730; ^{13}C NMR (75 MHz, $CDCl_3$): δ = 117.1, 110.4.

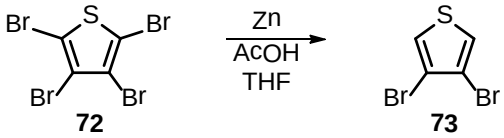

72 **73**

3,4-Dibromothiophene (**73**)

72 (25.0 g, 62.5 mmol) was stirred into THF (750 mL) and AcOH (150 mL). Zn powder was added slowly. The reaction was stirred for hours until complete. At first, 2.2 equiv. of Zn was used, then more, until full conversion was seen by GC-MS. At that point, the solution was extracted with EtOAc, then washed with H_2O (3 x 50 mL) and saturated aqueous $NaHCO_3$ (2 x 50 mL). The crude material was purified by vacuum distillation to yield **73** as a colorless oil (10.9 g, 45.0 mmol, 72%). IR (cm^{-1}): 3110, 1474, 1391, 1328, 1114, 907, 847, 779, 649, 459; ^1H NMR (300 MHz, $CDCl_3$): δ = 7.22 (s); ^{13}C NMR (75 MHz, $CDCl_3$): δ = 115.0, 123.8.

8.10 Phenylethynyl Compounds 79-81

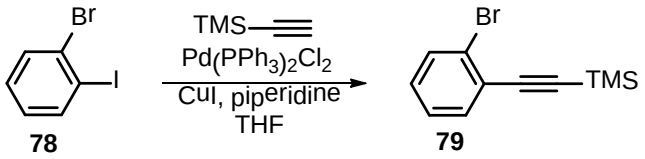

((2-Bromophenyl)ethynyl)trimethylsilane (**79**)

78 (3.01 g, 10.6 mmol) was stirred into a mixture of THF (1 mL) and piperidine (1 mL). $Pd(PPh_3)_2Cl_2$ (74.7 mg, 0.106 mmol) and CuI (20.3 mg, 0.106 mmol) were added to the mixture, which was then deoxygenated via the freeze/pump/thaw method (3x). After warming to room temperature, trimethylsilylacetylene (1.66 mL, 11.7 mmol) was added slowly through a syringe over a period of 60 min. The reaction was then stirred for 16 hours at room temperature. The mixture was extracted with H_2O (30 mL) and toluene (2 x 25 mL). The solvent was evaporated and filtered through silica gel with hexanes to yield **79** as a light yellow oil (2.53 g, 10.0 mmol, 94%). ^{1}H NMR (300 MHz, $CDCl_3$): δ = 7.46 (dd, J = 7.8 Hz, J = 1.2 Hz, 1H), 7.39 (dd, J = 7.5 Hz, J = 1.8 Hz, 1H), 7.12 (td, J = 7.5 Hz, J = 1.2 Hz, 1H), 7.03 (td, J = 7.8 Hz, J = 1.8 Hz, 1H), 0.20 (s, 9H); ^{13}C NMR (300 MHz, $CDCl_3$): δ = 133.7, 132.4, 129.6, 127.0, 125.8, 125.4, 103.2, 99.7, -0.02.

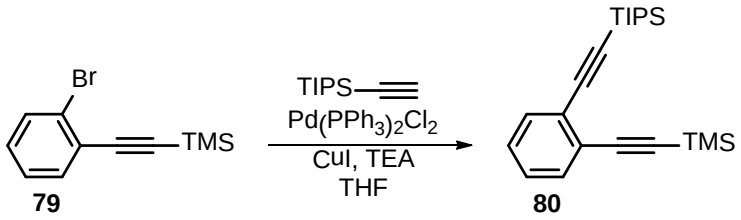

Triisopropyl((2-((trimethylsilyl)ethynyl)phenyl)ethynyl)silane (**80**)

79 (1.50 g, 5.92 mmol) was stirred into a mixture of THF (1.5 mL) and TEA (1.5 mL). The solution was deoxygenated via the freeze/pump/thaw method (3x) and $Pd(PPh_3)_2Cl_2$ (41.6 mg, 0.0592 mmol) and CuI (11.3 mg, 0.0592 mmol) were added under a flow of nitrogen gas. Triisopropylsilylacetylene (1.60 mL, 7.11 mmol) was then added through a syringe, and the reaction was stirred for 16 hours at room temperature. The mixture was extracted with saturated aqueous NH_4Cl (30 mL) and EtOAc (2 x 25 mL). Purification by silica gel chromatography

(hexanes) gave **80** as a pale orange oil (0.255 g, 0.85 mmol, 14%). IR (cm^{-1}): 2957, 2942, 2894, 2864, 2159, 1714, 1643, 1523, 1474, 1406, 1270, 1204, 871, 838, 788, 755, 678, 664; ^{1}H NMR (300 MHz, $CDCl_3$): δ = 7.48 (m, 2H), 7.23 (m, 2H), 1.19 (s, 21H), 0.27 (s, 9H); ^{13}C NMR (300 MHz, $CDCl_3$): δ = 133.04, 133.02, 128.08, 127.94, 126.08, 125.81, 105.5, 103.6, 98.2, 95.0, 18.9, 11.5, 0.07; HRMS (EI) *m/z*: $[M]^+$ Calcd for $C_{22}H_{34}Si$ = 354.2199; Found = 354.2186.

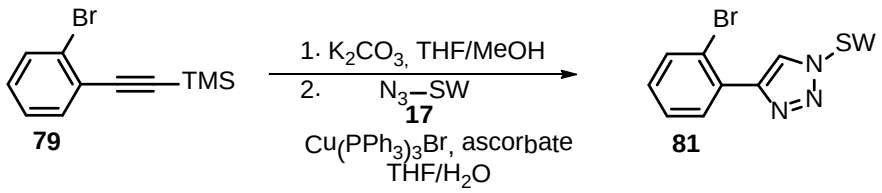

4-(2-Bromophenyl)-1-(2,5,8,11,15,18,21,24-octaoxapentacosan-13-yl)-1H-1,2,3-triazole (**81**)

79 (498 mg, 1.97 mmol) was stirred into a 1:1 THF:MeOH mixture (10 mL). K_2CO_3 (544 mg, 3.93 mmol) was added and the reaction was stirred at room temperature for 30 min. The solids were then filtered and washed with THF. The solvent was removed, and THF (2 mL) and **17** (886 mg, 2.16 mmol) were added to the residue. The solution was deoxygenated via the freeze/pump/thaw method (3x) and $Cu(PPh_3)_3Br$ (183 mg, 0.197 mmol) and sodium ascorbate (195 mg, 0.983 mmol) were added under a flow of nitrogen gas. The reaction was then sealed under an inert nitrogen atmosphere and stirred for 48 hours at room temperature. The mixture was extracted with saturated aqueous NH_4Cl (20 mL) and DCM (4 x 25 mL). The organic fractions were collected and the solvent was evaporated. Purification by silica gel chromatography (19:1 EtOAc:MeOH) gave **81** as an orange oil (763 mg, 1.29 mmol, 66%). IR (cm^{-1}): 2870, 1483, 1406, 1353, 1270, 1207, 1087, 1007, 855, 765, 736; ^{1}H NMR (300 MHz, $CDCl_3$): δ = 8.31 (s, 1H), 7.94 (d, *J* = 7.5 Hz, 1H), 7.48 (dd, *J* = 8.1 Hz, *J* = 1.2 Hz, 1H), 7.24 (t, *J* = 7.2 Hz, 1H), 7.03 (t, *J* = 7.8 Hz, 1H), 4.84 (quin, *J* = 5.7 Hz, 1H), 3.85 (m, 4H), 3.50-3.35 (m, 27H), 3.18 (s, 6H); ^{13}C NMR (300 MHz, $CDCl_3$): δ = 133.1, 131.2, 130.2, 128.8, 127.3, 123.3, 120.8, 71.5, 70.57, 70.21, 70.19, 70.07, 69.61, 60.5, 58.6.

8.11 Monomers 84-91

83 **84**

1,4-Diiodo-2,5-dimethoxybenzene (**84**)

I_2 (68.9, 0.271 mol) and KIO_4 (33.3 g, 0.145 mol) were stirred in MeOH (600 mL) and concentrated H_2SO_4 (6 mL). **83** (30.0 g, 0.217 mol) was then added, and the mixture was stirred at reflux for 4 hours. The reaction was then quenched by stirring in Na_2SO_3 (34 g) until the solution turned yellow. The precipitate was filtered and washed with copious amounts of water and dried to give **84** as an off-white crystalline powder (84.4 g, 0.216 mol, 100%). mp: 170-173 ˚C; IR (cm^{-1}): 3091, 3025, 3006, 2957, 2931, 2897, 2832, 1480, 1442, 1346, 1271, 1212, 1063, 1014, 851, 836, 744; ^{1}H NMR (300 MHz, $CDCl_3$): δ = 7.18 (s, 2H), 3.82 (s, 6H); ^{13}C NMR (75 MHz, $CDCl_3$): δ = 153.2, 121.5, 85.4, 57.1.

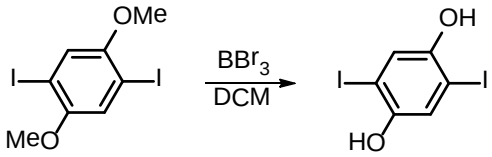

84 **85**

2,5-Diiodobenzene-1,4-diol (**85**)

84 (20.0 g, 51.3 mmol) was dissolved in dry CH_2Cl_2 (500 mL), and the solution was cooled to 0 ˚C. BBr_3 (9.7 mL, 0.102 mol) was added under N_2(g). After the reaction was stirred at room temperature overnight, it was slowly quenched with H_2O. The solid product crashed out, and was filtered and dried, yielding **85** as a fluffy off-white powder (16.2 g, 44.7 mmol, 87%). m.p. 198-201 ˚C; IR (cm^{-1}): 3431, 3113, 2862, 2755, 1637, 1506, 1388, 1322, 1226, 1189, 1049, 871, 851, 791; ^{1}H NMR (300 MHz, DMSO): δ = 9.80 (s, 2H), 7.12 (s, 2H); ^{13}C NMR (75 MHz, DMSO): δ = 150.4, 123.5, 84.3.

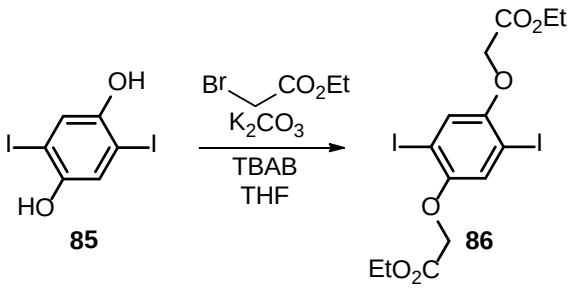

Diethyl 2,2'-((2,5-diiodo-1,4-phenylene)bis(oxy))diacetate (**86**)

K_2CO_3 (33 g, 0.24 mol) and tetra-butylammonium bromide (4 g, 0.01 mol) were stirred in hot THF (150 mL) for 15 minutes. **85** (17.6 g, 48.6 mmol) was added to the mixture, followed by bromoethyl acetate (13.5 mL, 122 mmol). After the reaction mixture was stirred at reflux for 2 d, an aqueous solution of $NaSO_3$ (100 mL) was used to quench the reaction. After extraction with CH_2Cl_2 (3 x 100 mL), the solvent was evaporated, and the product was recrystallized from EtOAc to yield **86** as a colorless solid (21.8 g, 40.9 mmol, 83%). mp: 121-124 ˚C; ^{1}H NMR (300 MHz, $CDCl_3$): δ = 7.14 (s, 2H), 4.60 (s, 4H), 4.25 (q, J = 7 Hz, 4H), 1.29 (t, J = 7 Hz, 6H); ^{13}C NMR (75 MHz, $CDCl_3$): δ = 167.9, 152.6, 123.5, 86.1, 67.2, 61.5, 14.1.

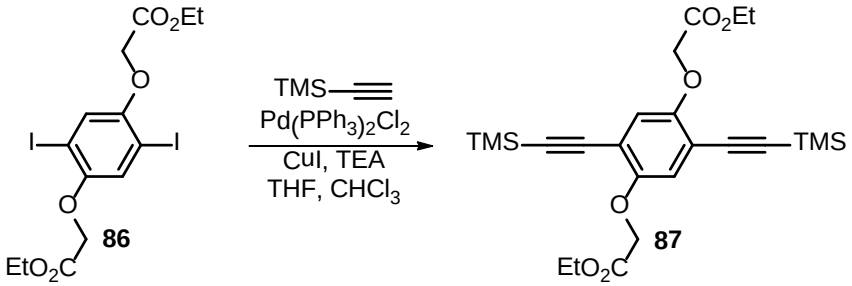

Diethyl 2,2'-((2,5-bis((trimethylsilyl)ethynyl)-1,4-phenylene)bis(oxy))diacetate (**87**)

86 (4.9 g, 9.2 mmol) was stirred into THF (3 mL), TEA (1 mL) and $CHCl_3$ (30 mL). $Pd(PPh_3)_2Cl_2$ (64 mg, 0.092 mmol) and CuI (35 mg, 0.18 mmol) were added to the solution, which was then deoxygenated via the freeze/pump/thaw method (3x). The reaction was sealed under an inert nitrogen atmosphere and trimethylsilyl acetylene (3.6 g, 5.2 mL, 37 mmol) was added through a septum. The reaction was stirred at room temperature for 2 days, after which time the mixture was washed with saturated aqueous NH_4Cl. The solvent was evaporated and purified by silica gel chromatography (19:1 hexanes:EtOAc) to give **87** as a slightly yellow,

fluffy solid (3.52 g, 7.4 mmol, 81%). mp: 127-128 ˚C; IR (cm^{-1}): 2957, 2901, 2153, 1768, 1498, 1440, 1408, 1284, 1247, 1186, 1082, 1031, 907, 865, 836, 758, 699, 625; ^{1}H NMR (300 MHz, $CDCl_3$): δ = 6.90 (s, 2H), 4.63 (s, 4H), 4.28 (q, J = 8.4 Hz, 4H), 1.30 (t, J = 8.7 Hz, 6H), 0.25 (s, 18H); ^{13}C NMR (75 MHz, $CDCl_3$): δ = 168.5, 156.9, 153.9, 118.9, 83.7, 79.0, 67.0, 61.6, 52.5, 14.3.

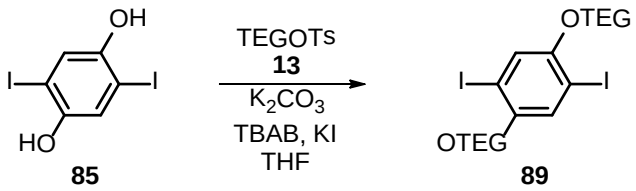

1,4-Diiodo-2,5-bis(2-(2-(2-methoxyethoxy)ethoxy)ethoxy)benzene (**89**)

K_2CO_3 (29.6 g, 214 mmol) and tetra-butylammonium bromide (3 g, 10 mmol) were stirred into acetone (150 mL) for ten minutes. **85** (12.9 g, 35.6 mmol) and KI (0.6 g, 4 mmol) were then added to the mixture, followed by **13** (25.0 g, 78.5 mmol). The reaction was stirred at reflux for 3 days. The solids were then filtered through Celite with DCM, the solvent was evaporated, and the residue was purified by silica gel chromatography (3:1 hexanes:EtOAc for excess **13**, EtOAc for product) to give **89** as a pale yellow oil which eventually solidified into a nearly colorless solid (18.4 g, 28.2 mmol, 79%). mp: 34-36 ˚C; IR (cm^{-1}): 2883, 1485, 1464, 1360, 1330, 1221, 1197, 1141, 1117, 1090, 1063, 1031, 969, 931, 881, 857, 833, 798; ^{1}H NMR (300 MHz, $CDCl_3$): δ = 7.18 (s, 2H), 4.05 (t, 4H, J =5 Hz), 3.82 (t, 4H, J = 5 Hz), 3.74 (m, 4H), 3.62 (m, 8H), 3.50 (m, 4H), 3.32 (s, 6H); ^{13}C NMR (75 MHz, $CDCl_3$): δ = 153.0, 123.4, 86.4, 71.90, 71.10, 70.71, 70.54, 70.23, 69.56, 59.0.

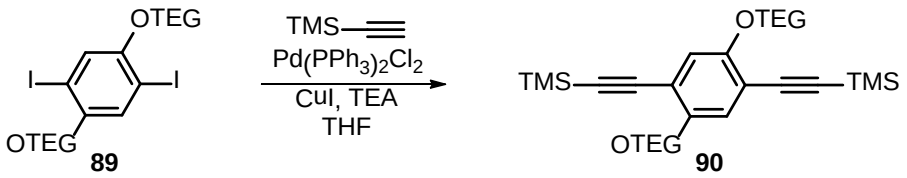

((2,5-Bis(2-(2-(2-methoxyethoxy)ethoxy)ethoxy)-1,4-phenylene)bis(ethyne-2,1-diyl))bis(trimethylsilane) (**90**)

89 (11.3 g, 17.3 mmol) and TEA (1 mL) were stirred in THF (20 mL) under N_2(g) for 15 min. $Pd(PPh_3)_2Cl_2$ (0.12 g, 0.17 mmol) and CuI (0.065 g, 0.34 mmol) were added under N_2(g). The reaction was sealed, and trimethylsilyl acetylene (12.3 mL, 86.4 mmol) was added via syringe. The reaction was stirred for 2 days, and then extracted with H_2O and $CHCl_3$ (3 x 50 mL). The product was purified by silica gel chromatography (5:1 hexanes:EtOAc), yielding **90** as a light tan powder (7.41 g, 12.4 mmol, 72%). ^{1}H NMR (300 MHz, $CDCl_3$): δ = 6.90 (s, 2H), 4.11 (t, 4H, J = 5 Hz), 3.86 (t, 4H, J = 5 Hz), 3.76 (m, 4H), 3.65 (m, 8H), 3.55 (m, 4H), 3.36 (s, 6H), 0.23 (s, 18H); ^{13}C NMR (75 MHz, $CDCl_3$): δ = 153.8, 117.7, 114.1, 100.78, 100.32, 71.88, 71.11, 70.74, 70.50, 69.63, 69.46, 59.0, -0.1.

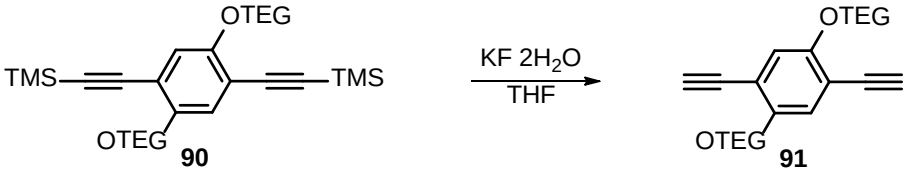

1,4-Diethynyl-2,5-bis(2-(2-(2-methoxyethoxy)ethoxy)ethoxy)benzene (**91**)

90 (1.1 g, 1.8 mmol) was dissolved in MeOH (20 mL). KF•2H_2O (1.0 g, 11 mmol) was dissolved in MeOH (20 mL) and added to the mixture. The reaction was stirred at room temperature for 5 minutes, and then extracted with H_2O and $CHCl_3$. The organic portion was washed with saturated aqueous NH_4Cl and dried over magnesium sulfate. The solvent was evaporated and the residue was purified through a short silica gel plug (4:1 EtOAc:hexanes) to give **91** as a light beige powder (0.82 g, 1.8 mmol, 98%). mp: 50-51 ˚C; ^{1}H NMR (300 MHz, $CDCl_3$): δ = 6.99 (s, 2H), 4.14 (t, 4H, J = 5 Hz), 3.86 (t, 4H, J = 5 Hz), 3.77 (m, 4H), 3.66 (m, 8H), 3.54 (m, 4H), 3.37 (s, 6H), 3.32 (s, 2H); ^{13}C NMR (75 MHz, $CDCl_3$): δ = 154.0, 118.2, 113.5, 82.8, 79.5, 71.92, 71.03, 70.68, 70.54, 69.56, 69.45, 59.0.

8.12 Polymers 92-97

The reported yields in this section should be taken as crude yields, as the polymers have not yet been sufficiently purified.

General Saponification Procedure

The polymer was dissolved in a 1:1 MeOH:H_2O solution, along with 5 eq. of NaOH (s). The reaction was stirred overnight at room temperature. To remove oligomeric species, the aqueous polymer solution was sealed inside dialysis tubing and stirred in deionized H_2O for 5 days, where fresh deionized H_2O was used every day. The aqueous solvent was then removed via lyophilization.

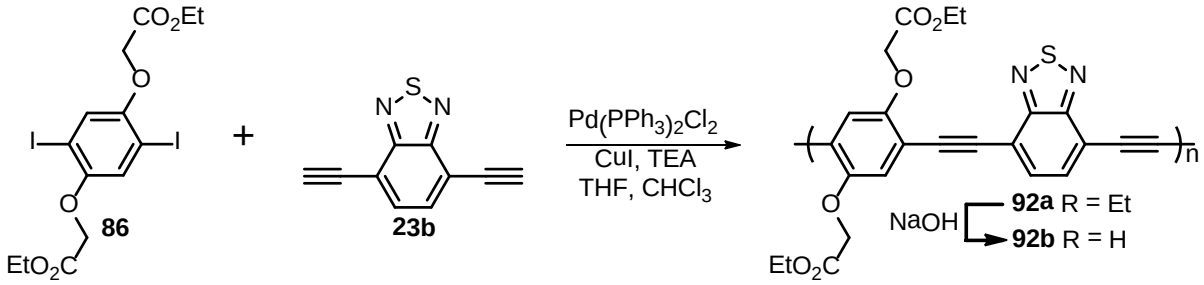

Poly(2,5-bis(ethylacet-1-yloxy)phenylene-1,4-ethynylene-alt-benzo[c][1,2,5]thiadiazole-1,4-ethynylene) (**92**)

86 (289 mg, 0.541 mmol) and **23b** (100. mg, 0.541 mmol) were dissolved in $CHCl_3$ (5 mL) along with TEA (1 mL) and THF (1 mL). The mixture was deoxygenated via the freeze/pump/thaw method (3x), and $Pd(PPh_3)_2Cl_2$ (3.8 mg, 0.0054 mmol) and CuI (2.0 mg, 0.011 mmol) were added under a flow of nitrogen. The reaction was sealed under the inert gas and stirred at room temperature for 2 days. The reaction mixture was then dropped into Et_2O (300 mL). This was insufficient to cause precipitation, so hexanes (200 mL) was added. The solid precipitate was filtered to give **92a** as a burnt orange solid (370 mg, 0.800 mmol, 74%). GPC (polystyrene, THF): Mn = 3410; Mw = 7330.

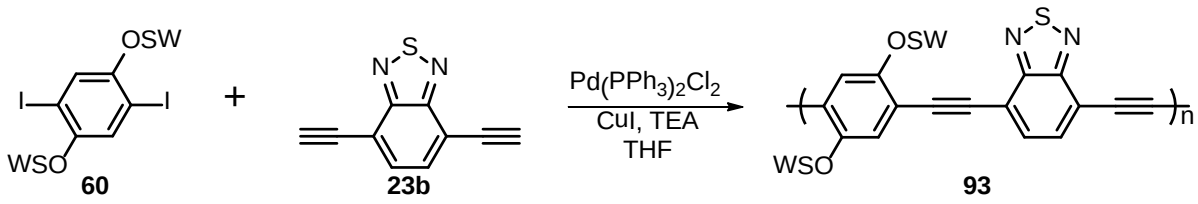

Poly(2,5-bis(2,5,8,11,15,18,21,24-octaoxapentacosan-13-yloxy)phenylene-1,4-ethynylene-alt-benzo[c][1,2,5]thiadiazole-1,4-ethynylene) (**93**)

60 (297 mg, 0.271 mmol) and **23b** (50.0 mg, 0.271 mmol) were dissolved in THF (2 mL) and TEA (2 mL). After thorough deoxygenation by freezing and evacuating, $Pd(PPh_3)_2Cl_2$ (1.9 mg, 2.7 mmol) and CuI (0.5 mg, 3 mmol) were added under a flow of nitrogen. The reaction was sealed under the inert atmosphere and stirred for 48 hours at room temperature. After dilution with EtOAc (50 mL) and filtration, the filtrate was poured into saturated aqueous NH_4Cl (100 mL) and extracted with DCM (1 x 150 mL, 3 x 50 mL). The combined organic phases were dried over magnesium sulfate and the solvent was removed under reduced pressure. The residue was re-dissolved in DCM (3 mL) and the polymer solution was precipitated into Et_2O (450 mL). The precipitate was filtered and dried under vacuum to obtain **93** as a red solid exhibiting a green-gold luster (209 mg, 74%). GPC (polystyrene, THF): Mn = 19000; Mw = 34600.

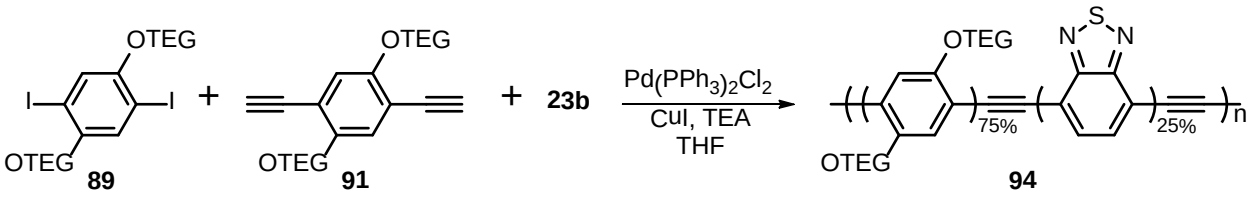

Poly(2,5-bis(2-(2-(2-methoxyethoxy)ethoxy)ethoxy)phenylene-1,4-ethynylene-co-benzo[c][1,2,5] thiadiazole-1,4-ethynylene) (**94**)

89 (700. mg, 1.07 mmol), **91** (241 mg, 0.535 mmol), and **23b** (98.0 mg, 0.535 mmol) were dissolved in THF (5 mL) and TEA (1 mL). The mixture was deoxygenated by freezing and evacuating (3x) and $Pd(PPh_3)_2Cl_2$ (8 mg, 0.01 mmol) and CuI (4 mg, 0.02 mmol) were added under a flow of nitrogen. The reaction was sealed under the inert atmosphere and stirred overnight at room temperature. The reaction was then precipitated into Et_2O (300 mL) and

filtered to give **94** as a red solid (249 mg, 32%). GPC (polystyrene, THF): Mn = 6390; Mw = 11030.

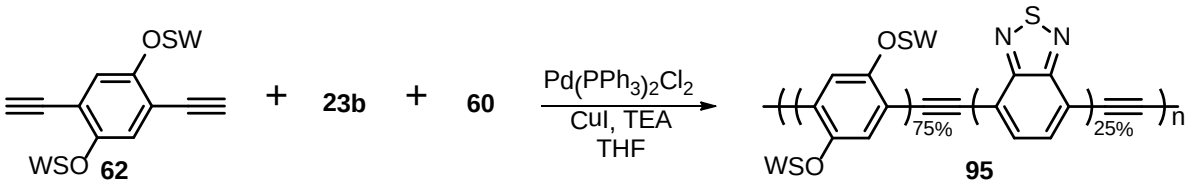

Poly(2,5-bis(2,5,8,11,15,18,21,24-octaoxapentacosan-13-yloxy)phenylene-1,4-ethynylene-co-benzo[c][1,2,5]thiadiazole-1,4-ethynylene) (**95**)

60 (475 mg, 0.434 mmol), **23b** (40.0 mg, 0.217 mmol) and **62** (193 mg, 0.217 mmol) were dissolved in THF (2 mL) and TEA (2 mL). After thorough deoxygenation by freezing and evacuating, $Pd(PPh_3)_2Cl_2$ (3.0 mg, 4.3 mmol) and CuI (0.8 mg, 4 mmol) were added under a flow of nitrogen. The reaction was sealed under the inert atmosphere and stirred for 48 hours at room temperature. After dilution with EtOAc (50 mL) and filtration, the filtrate was poured into saturated aqueous NH_4Cl (75 mL) and extracted with DCM (1 x 100 mL, 3 x 25 mL). The combined organic phases were dried over magnesium sulfate and the solvent was removed under reduced pressure. The residue was re-dissolved in DCM (3 mL) and the polymer solution was precipitated into a mixture of Et_2O (300 mL) and PE (100 mL). The precipitate was filtered, washed with pentane, and dried under vacuum to obtain **95** as a red solid exhibiting a green-gold luster (327 mg, 55%). GPC (polystyrene, THF): Mn = 9700; Mw = 14100.

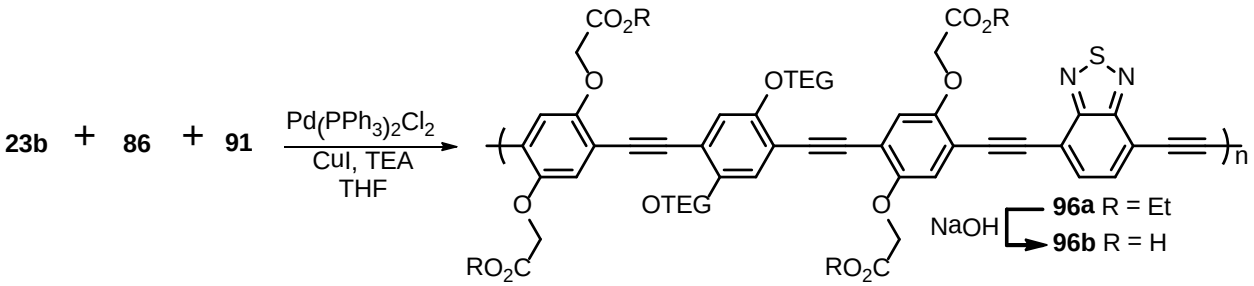

Poly(2,5-bis(2-(2-(2-methoxyethoxy)ethoxy)ethoxy)phenylene-1,4-ethynylene-co-benzo[c][1,2,5] thiadiazole-1,4-ethynylene-alt-2,5-bis(ethylacet-1-yloxy)phenylene-1,4-ethynylene) (**96**)

23b (86 mg, 0.47 mmol), **86** (0.50 g, 0.94 mmol), and **91** (210 mg, 0.47 mmol) were dissolved in THF (6 mL) and TEA (1 mL). The solution was deoxygenated by freezing and evacuating (3x), and $Pd(PPh_3)_2Cl_2$ (6 mg, 0.009 mmol) and CuI (4 mg, 0.02 mmol) were added under a flow of nitrogen. The reaction was sealed under the inert atmosphere and stirred for 20 hours at room temperature. The solution was then precipitated into Et_2O (300 mL) and filtered to give **96** as a red solid (620 mg, 92%). GPC (polystyrene, THF): Mn = 6140; Mw = 12740.

Poly(2,5-bis(ethylacet-1-yloxy)phenylene-1,4-ethynylene-co-benzo[c][1,2,5]thiadiazole-1,4-ethynylene-alt-2,5-bis(2,5,8,11,15,18,21,24-octaoxapentacosan-13-yloxy)phenylene-1,4-ethynylene) (**97**)

60 (475 mg, 0.434 mmol), **23b** (40.0 mg, 0.217 mmol) and **88** (71.7 mg, 0.217 mmol) were dissolved in THF (2 mL) and TEA (2 mL). After thorough deoxygenation by freezing and evacuating, $Pd(PPh_3)_2Cl_2$ (3.0 mg, 4.3 mmol) and CuI (0.8 mg, 4 mmol) were added under a flow of nitrogen. The reaction was sealed under the inert atmosphere and stirred for 48 hours at room temperature. After dilution with EtOAc (75 mL) and filtration, the filtrate was poured into

saturated aqueous NH_4Cl (100 mL) and extracted with DCM (1 x 100 mL, 3 x 25 mL). The combined organic phases were dried over magnesium sulfate and the solvent was removed under reduced pressure. The residue was re-dissolved in DCM (2 mL) and precipitated into a mixture of Et_2O (250 mL) and PE (150 mL). The precipitate was filtered, then dissolved in DCM (3 mL) and poured into a mixture of MeOH (250 mL) and H_2O (100 mL). The solvent was removed under reduced pressure and the aqueous phase was extracted with DCM (3 x 100 mL). The combined organic phases were dried over magnesium sulfate. The solvent was removed under reduced pressure to yield **97a** as a red solid exhibiting a green-gold luster (465 mg, 98%). GPC (polystyrene, THF): Mn = 16600; Mw = 32500.

9 Appendix

9.1 Single Crystal Data for 38b

Table 10 Crystal Data and Structure Refinement for **38b**

Identification code	**38b**	
Empirical formula	$C_{34}H_{44}F_4N_2Si_2$	
Formula weight	612.89	
Temperature	200(2) K	
Wavelength	0.71073 Å	
Crystal system	triclinic	
Space group	P&^-&B1	
Z	2	
Unit cell dimensions	a = 8.344(4) Å	α =106.28(1) deg.
	b = 13.194(6) Å	β = 94.079(11) deg.
	c = 17.228(7) Å	γ =107.054(10) deg.
Volume	1716.1(12) $Å^3$	
Density (calculated)	1.19 g/cm^3	
Absorption coefficient	0.15 mm^{-1}	
Crystal shape	needle	
Crystal size	0.19 x 0.11 x 0.08 mm^3	
Crystal colour	yellow	
Theta range for data collection	1.7 to 24.7 deg.	
Index ranges	-9≤h≤9, -15≤k≤15, -20≤l≤20	
Reflections collected	13720	
Independent reflections	5846 (R(int) = 0.0883)	
Observed reflections	3396 (I >2σ(I))	
Absorption correction	Semi-empirical from equivalents	
Max. and min. transmission	0.99 and 0.97	
Refinement method	Full-matrix least-squares on F^2	
Data/restraints/parameters	5846 / 289 / 407	
Goodness-of-fit on F^2	0.98	
Final R indices (I>2σ(I))	R1 = 0.075, wR2 = 0.164	
Largest diff. peak and hole	0.29 and -0.30 $eÅ^{-3}$	

Table 11 Atomic Coordinates and Equivalent Isotropic Displacement Parameters ($Å^2$) for **38b** (U_{eq} is defined as one third of the trace of the orthogonalized U_{ij} tensor)

Atom	x	y	z	U_{eq}
C1	0.3349(5)	0.7417(3)	0.7680(2)	0.0451(10)
C2	0.2681(5)	0.7496(3)	0.8282(2)	0.0532(11)

C3	0.6157(4)	0.7347(3)	0.4755(2)	0.0358(8)
C4	0.6623(5)	0.7394(3)	0.4120(2)	0.0413(9)
C11	0.4119(5)	0.7358(3)	0.6960(2)	0.0379(9)
C12	0.3416(4)	0.6407(3)	0.6242(2)	0.0347(9)
N13	0.2081(4)	0.5565(2)	0.6267(2)	0.0355(7)
C14	0.1468(4)	0.4689(3)	0.5580(2)	0.0360(9)
C15	0.0037(5)	0.3782(3)	0.5563(2)	0.0420(9)
C16	-0.0604(5)	0.2893(3)	0.4876(3)	0.0477(10)
C17	0.0142(5)	0.2852(3)	0.4163(2)	0.0484(10)
C18	0.1482(5)	0.3712(3)	0.4147(2)	0.0401(9)
C19	0.2202(4)	0.4663(3)	0.4853(2)	0.0331(8)
N20	0.3526(3)	0.5508(2)	0.4823(2)	0.0337(7)
C21	0.4140(4)	0.6381(3)	0.5508(2)	0.0321(8)
C22	0.5537(4)	0.7331(3)	0.5507(2)	0.0341(8)
C23	0.6176(5)	0.8203(3)	0.6214(2)	0.0417(9)
C24	0.5493(5)	0.8220(3)	0.6934(2)	0.0423(9)
F15	-0.0693(3)	0.3807(2)	0.6232(1)	0.0578(6)
F16	-0.1960(3)	0.2029(2)	0.4842(2)	0.0641(7)
F17	-0.0534(3)	0.1945(2)	0.3508(2)	0.0658(7)
F18	0.2160(3)	0.3669(2)	0.3464(1)	0.0525(6)
Si1	0.1647(2)	0.7692(1)	0.9190(1)	0.0585(4)
C41	0.0570(6)	0.8756(4)	0.9180(2)	0.0705(13)
C42	-0.0961(7)	0.8322(6)	0.8488(3)	0.119(2)
C43	0.1817(8)	0.9844(5)	0.9166(3)	0.0930(17)
C44	0.3424(6)	0.8281(4)	1.0082(2)	0.0697(13)
C45	0.4460(8)	0.7503(5)	1.0117(3)	0.1020(19)
C46	0.2929(9)	0.8721(6)	1.0910(3)	0.119(2)
C47	-0.0213(17)	0.6378(8)	0.9040(9)	0.075(4)
C48	-0.122(3)	0.644(2)	0.9736(13)	0.099(6)
C49	0.018(3)	0.5305(13)	0.8733(14)	0.108(7)
Si2	0.6977(1)	0.7461(1)	0.3090(1)	0.0410(3)
C51	0.5542(5)	0.8207(3)	0.2807(2)	0.0550(11)
C52	0.5984(7)	0.9394(4)	0.3392(4)	0.0908(17)
C53	0.3670(6)	0.7566(5)	0.2748(4)	0.0864(16)
C54	0.6462(6)	0.5971(3)	0.2403(2)	0.0588(11)
C55	0.6289(9)	0.5879(5)	0.1494(3)	0.104(2)
C56	0.4943(6)	0.5132(4)	0.2560(3)	0.0753(14)
C57	0.9291(5)	0.8240(4)	0.3137(3)	0.0568(11)
C58	1.0150(6)	0.9125(4)	0.3953(3)	0.0828(15)
C59	0.9632(6)	0.8737(5)	0.2441(3)	0.0807(16)
C47B	0.057(2)	0.6247(10)	0.9267(9)	0.080(4)
C48B	-0.081(4)	0.627(2)	0.981(2)	0.154(15)
C49B	-0.024(3)	0.5432(16)	0.8403(10)	0.110(7)

Table 12 Hydrogen Coordinates and Isotropic Displacement Parameters ($Å^2$) for **38b**

Atom	x	y	z	U_{eq}
H23	0.7117	0.8822	0.6218	0.050
H24	0.5992	0.8842	0.7415	0.051
H41	0.0122	0.8923	0.9708	0.085
H42A	-0.1748	0.7622	0.8516	0.178
H42B	-0.0569	0.8188	0.7957	0.178
H42C	-0.1544	0.8879	0.8548	0.178
H43A	0.2779	1.0099	0.9613	0.139
H43B	0.1250	1.0409	0.9234	0.139
H43C	0.2230	0.9728	0.8640	0.139
H44	0.4229	0.8948	0.9988	0.084
H45A	0.4798	0.7247	0.9582	0.153
H45B	0.3766	0.6856	1.0253	0.153
H45C	0.5478	0.7907	1.0537	0.153
H46A	0.2289	0.9228	1.0879	0.179
H46B	0.3958	0.9126	1.1324	0.179
H46C	0.2222	0.8094	1.1063	0.179
H47	-0.1018	0.6356	0.8572	0.091
H48A	-0.1221	0.7207	0.9972	0.149
H48B	-0.0698	0.6215	1.0160	0.149
H48C	-0.2390	0.5936	0.9530	0.149
H49A	0.0926	0.5362	0.8323	0.162
H49B	-0.0882	0.4685	0.8485	0.162
H49C	0.0745	0.5169	0.9194	0.162
H51	0.5713	0.8266	0.2251	0.066
H52A	0.7184	0.9805	0.3416	0.136
H52B	0.5784	0.9367	0.3941	0.136
H52C	0.5270	0.9772	0.3194	0.136
H53A	0.3392	0.6810	0.2363	0.130
H53B	0.2969	0.7954	0.2554	0.130
H53C	0.3445	0.7520	0.3290	0.130
H54	0.7468	0.5741	0.2524	0.071
H55A	0.7288	0.6417	0.1402	0.157
H55B	0.5263	0.6039	0.1332	0.157
H55C	0.6204	0.5120	0.1167	0.157
H56A	0.5079	0.5198	0.3144	0.113
H56B	0.4866	0.4375	0.2234	0.113
H56C	0.3903	0.5281	0.2404	0.113
H57	0.9885	0.7671	0.3065	0.068
H58A	0.9962	0.8795	0.4396	0.124

H58B	0.9670	0.9735	0.4039	0.124
H58C	1.1373	0.9418	0.3952	0.124
H59A	0.9092	0.8158	0.1915	0.121
H59B	1.0861	0.9022	0.2452	0.121
H59C	0.9163	0.9350	0.2510	0.121
H47B	0.1437	0.5989	0.9511	0.096
H48D	-0.0276	0.6743	1.0372	0.232
H48E	-0.1408	0.5512	0.9806	0.232
H48F	-0.1615	0.6579	0.9597	0.232
H49D	0.0648	0.5420	0.8058	0.165
H49E	-0.1098	0.5676	0.8163	0.165
H49F	-0.0769	0.4681	0.8436	0.165

Table 13 Anisotropic Displacement Parameters ($Å^2$) for **38b** (The anisotropic displacement factor exponent takes the form: $-2\ pi^2\ (h^2\ a^{*2}\ U_{11} + ... + 2\ h\ k\ a^*\ b^*\ U_{12})$)

Atom	U_{11}	U_{22}	U_{33}	U_{23}	U_{13}	U_{12}
C1	0.059(3)	0.049(3)	0.036(2)	0.0161(19)	0.0187(19)	0.024(2)
C2	0.070(3)	0.054(3)	0.037(2)	0.013(2)	0.019(2)	0.022(2)
C3	0.036(2)	0.041(2)	0.037(2)	0.0207(17)	0.0124(17)	0.0131(18)
C4	0.047(2)	0.043(2)	0.043(2)	0.0214(19)	0.0163(18)	0.0179(19)
C11	0.049(2)	0.043(2)	0.0300(19)	0.0135(18)	0.0131(17)	0.025(2)
C12	0.043(2)	0.046(2)	0.0308(19)	0.0211(18)	0.0173(16)	0.027(2)
N13	0.0394(18)	0.043(2)	0.0388(17)	0.0224(16)	0.0201(14)	0.0218(16)
C14	0.038(2)	0.041(2)	0.041(2)	0.0214(19)	0.0123(17)	0.0217(19)
C15	0.041(2)	0.050(3)	0.050(2)	0.030(2)	0.0181(19)	0.020(2)
C16	0.036(2)	0.047(3)	0.068(3)	0.033(2)	0.009(2)	0.011(2)
C17	0.051(3)	0.041(3)	0.053(3)	0.014(2)	0.001(2)	0.016(2)
C18	0.044(2)	0.043(2)	0.039(2)	0.0154(19)	0.0105(18)	0.020(2)
C19	0.033(2)	0.040(2)	0.037(2)	0.0185(18)	0.0096(16)	0.0202(18)
N20	0.0350(17)	0.0414(19)	0.0319(16)	0.0159(15)	0.0108(13)	0.0177(15)
C21	0.036(2)	0.038(2)	0.0324(19)	0.0170(17)	0.0134(16)	0.0206(18)
C22	0.038(2)	0.039(2)	0.034(2)	0.0171(18)	0.0138(16)	0.0180(18)
C23	0.047(2)	0.041(2)	0.043(2)	0.019(2)	0.0162(18)	0.016(2)
C24	0.052(2)	0.042(2)	0.036(2)	0.0112(18)	0.0126(18)	0.018(2)
F15	0.0532(14)	0.0682(16)	0.0656(15)	0.0395(13)	0.0303(12)	0.0176(13)
F16	0.0505(14)	0.0551(16)	0.0861(18)	0.0349(14)	0.0099(12)	0.0050(13)
F17	0.0671(16)	0.0487(16)	0.0648(16)	0.0095(13)	0.0014(13)	0.0049(13)
F18	0.0646(15)	0.0533(14)	0.0369(12)	0.0104(10)	0.0139(11)	0.0177(12)
Si1	0.0810(9)	0.0618(8)	0.0345(6)	0.0131(6)	0.0325(6)	0.0227(7)
C41	0.078(3)	0.106(4)	0.037(2)	0.012(3)	0.023(2)	0.051(3)

C42	0.103(4)	0.175(7)	0.073(4)	0.019(4)	-0.003(3)	0.062(4)
C43	0.121(5)	0.091(4)	0.095(4)	0.037(3)	0.028(3)	0.067(4)
C44	0.102(4)	0.078(3)	0.042(2)	0.019(2)	0.018(2)	0.045(3)
C45	0.144(5)	0.108(5)	0.080(4)	0.038(3)	0.011(4)	0.073(4)
C46	0.161(6)	0.172(7)	0.037(3)	0.009(3)	0.015(3)	0.096(5)
C47	0.066(7)	0.084(6)	0.074(8)	0.018(6)	0.039(6)	0.021(5)
C48	0.082(9)	0.115(13)	0.093(10)	0.039(11)	0.052(7)	0.006(10)
C49	0.131(16)	0.068(7)	0.133(16)	0.037(10)	0.045(12)	0.032(8)
Si2	0.0463(6)	0.0515(7)	0.0368(6)	0.0239(5)	0.0204(5)	0.0203(5)
C51	0.064(3)	0.068(3)	0.054(2)	0.034(2)	0.023(2)	0.034(2)
C52	0.100(4)	0.066(3)	0.128(5)	0.038(3)	0.032(4)	0.049(3)
C53	0.053(3)	0.109(4)	0.124(5)	0.063(4)	0.020(3)	0.040(3)
C54	0.079(3)	0.062(3)	0.044(2)	0.015(2)	0.017(2)	0.036(2)
C55	0.174(6)	0.087(4)	0.045(3)	0.009(3)	0.030(3)	0.041(4)
C56	0.093(4)	0.055(3)	0.078(3)	0.020(3)	0.011(3)	0.025(3)
C57	0.055(2)	0.073(3)	0.065(3)	0.043(2)	0.029(2)	0.028(2)
C58	0.062(3)	0.093(4)	0.082(3)	0.045(3)	0.005(3)	-0.005(3)
C59	0.076(3)	0.110(4)	0.082(3)	0.065(3)	0.048(3)	0.025(3)
C47B	0.064(9)	0.083(7)	0.108(9)	0.046(7)	0.042(7)	0.024(6)
C48B	0.17(3)	0.153(19)	0.21(2)	0.115(17)	0.15(2)	0.079(16)
C49B	0.093(13)	0.062(9)	0.148(13)	0.026(9)	0.021(11)	-0.008(8)

Table 14 Bond Lengths (Å) and Angles (deg) for **38b**

C1-C2	1.206(5)
C1-C11	1.429(5)
C2-Si1	1.832(4)
C3-C4	1.199(4)
C3-C22	1.432(4)
C4-Si2	1.841(4)
C11-C24	1.372(5)
C11-C12	1.430(5)
C12-N13	1.336(4)
C12-C21	1.435(4)
N13-C14	1.342(5)
C14-C15	1.413(5)
C14-C19	1.429(5)
C15-F15	1.338(4)
C15-C16	1.351(6)
C16-F16	1.334(4)
C16-C17	1.411(5)
C17-F17	1.334(4)
C17-C18	1.348(5)

C18-F18	1.336(4)
C18-C19	1.418(5)
C19-N20	1.336(4)
N20-C21	1.337(4)
C21-C22	1.440(5)
C22-C23	1.361(5)
C23-C24	1.399(5)
C23-H23	0.9500
C24-H24	0.9500
Si1-C44	1.868(5)
Si1-C41	1.879(5)
Si1-C47	1.895(9)
Si1-C47B	1.902(11)
C41-C43	1.514(7)
C41-C42	1.535(6)
C41-H41	1.0000
C42-H42A	0.9800
C42-H42B	0.9800
C42-H42C	0.9800
C43-H43A	0.9800
C43-H43B	0.9800
C43-H43C	0.9800
C44-C46	1.518(5)
C44-C45	1.535(6)
C44-H44	1.0000
C45-H45A	0.9800
C45-H45B	0.9800
C45-H45C	0.9800
C46-H46A	0.9800
C46-H46B	0.9800
C46-H46C	0.9800
C47-C49	1.506(12)
C47-C48	1.510(11)
C47-H47	1.0000
C48-H48A	0.9800
C48-H48B	0.9800
C48-H48C	0.9800
C49-H49A	0.9800
C49-H49B	0.9800
C49-H49C	0.9800
Si2-C51	1.876(4)
Si2-C57	1.886(4)
Si2-C54	1.891(4)

C51-C53	1.524(6)
C51-C52	1.525(6)
C51-H51	1.0000
C52-H52A	0.9800
C52-H52B	0.9800
C52-H52C	0.9800
C53-H53A	0.9800
C53-H53B	0.9800
C53-H53C	0.9800
C54-C56	1.517(6)
C54-C55	1.528(5)
C54-H54	1.0000
C55-H55A	0.9800
C55-H55B	0.9800
C55-H55C	0.9800
C56-H56A	0.9800
C56-H56B	0.9800
C56-H56C	0.9800
C57-C58	1.516(6)
C57-C59	1.526(5)
C57-H57	1.0000
C58-H58A	0.9800
C58-H58B	0.9800
C58-H58C	0.9800
C59-H59A	0.9800
C59-H59B	0.9800
C59-H59C	0.9800
C47B-C48B	1.531(12)
C47B-C49B	1.536(13)
C47B-H47B	1.0000
C48B-H48D	0.9800
C48B-H48E	0.9800
C48B-H48F	0.9800
C49B-H49D	0.9800
C49B-H49E	0.9800
C49B-H49F	0.9800
C2-C1-C11	177.8(4)
C1-C2-Si1	176.6(4)
C4-C3-C22	176.6(4)
C3-C4-Si2	170.4(3)
C24-C11-C1	121.1(3)
C24-C11-C12	118.9(3)
C1-C11-C12	119.9(3)

N13-C12-C11	118.9(3)
N13-C12-C21	121.5(3)
C11-C12-C21	119.6(3)
C12-N13-C14	116.9(3)
N13-C14-C15	119.6(3)
N13-C14-C19	121.5(3)
C15-C14-C19	118.9(4)
F15-C15-C16	119.8(3)
F15-C15-C14	119.7(4)
C16-C15-C14	120.5(3)
F16-C16-C15	121.8(4)
F16-C16-C17	117.5(4)
C15-C16-C17	120.7(4)
F17-C17-C18	121.5(4)
F17-C17-C16	117.9(4)
C18-C17-C16	120.6(4)
F18-C18-C17	120.0(3)
F18-C18-C19	119.3(3)
C17-C18-C19	120.7(3)
N20-C19-C18	119.8(3)
N20-C19-C14	121.8(3)
C18-C19-C14	118.4(3)
C19-N20-C21	116.8(3)
N20-C21-C12	121.6(3)
N20-C21-C22	119.4(3)
C12-C21-C22	119.0(3)
C23-C22-C3	122.2(3)
C23-C22-C21	118.8(3)
C3-C22-C21	118.9(3)
C22-C23-C24	122.2(4)
C22-C23-H23	118.9
C24-C23-H23	118.9
C11-C24-C23	121.4(4)
C11-C24-H24	119.3
C23-C24-H24	119.3
C2-Si1-C44	105.0(2)
C2-Si1-C41	107.19(19)
C44-Si1-C41	109.5(2)
C2-Si1-C47	108.5(4)
C44-Si1-C47	123.2(6)
C41-Si1-C47	102.6(5)
C2-Si1-C47B	106.9(4)
C44-Si1-C47B	101.4(6)

C41-Si1-C47B	125.1(6)
C47-Si1-C47B	25.0(4)
C43-C41-C42	111.4(5)
C43-C41-Si1	111.6(3)
C42-C41-Si1	113.1(4)
C43-C41-H41	106.8
C42-C41-H41	106.8
Si1-C41-H41	106.8
C41-C42-H42A	109.5
C41-C42-H42B	109.5
H42A-C42-H42B	109.5
C41-C42-H42C	109.5
H42A-C42-H42C	109.5
H42B-C42-H42C	109.5
C41-C43-H43A	109.5
C41-C43-H43B	109.5
H43A-C43-H43B	109.5
C41-C43-H43C	109.5
H43A-C43-H43C	109.5
H43B-C43-H43C	109.5
C46-C44-C45	110.7(4)
C46-C44-Si1	115.2(4)
C45-C44-Si1	113.7(3)
C46-C44-H44	105.4
C45-C44-H44	105.4
Si1-C44-H44	105.4
C44-C45-H45A	109.5
C44-C45-H45B	109.5
H45A-C45-H45B	109.5
C44-C45-H45C	109.5
H45A-C45-H45C	109.5
H45B-C45-H45C	109.5
C44-C46-H46A	109.5
C44-C46-H46B	109.5
H46A-C46-H46B	109.5
C44-C46-H46C	109.5
H46A-C46-H46C	109.5
H46B-C46-H46C	109.5
C49-C47-C48	114.6(14)
C49-C47-Si1	114.7(12)
C48-C47-Si1	114.1(10)
C49-C47-H47	103.8
C48-C47-H47	103.8

Si1-C47-H47	103.8
C47-C48-H48A	109.5
C47-C48-H48B	109.5
H48A-C48-H48B	109.5
C47-C48-H48C	109.5
H48A-C48-H48C	109.5
H48B-C48-H48C	109.5
C47-C49-H49A	109.5
C47-C49-H49B	109.5
H49A-C49-H49B	109.5
C47-C49-H49C	109.5
H49A-C49-H49C	109.5
H49B-C49-H49C	109.5
C4-Si2-C51	105.17(17)
C4-Si2-C57	108.95(18)
C51-Si2-C57	112.31(18)
C4-Si2-C54	106.75(17)
C51-Si2-C54	114.5(2)
C57-Si2-C54	108.9(2)
C53-C51-C52	110.1(4)
C53-C51-Si2	112.4(3)
C52-C51-Si2	112.3(3)
C53-C51-H51	107.2
C52-C51-H51	107.2
Si2-C51-H51	107.2
C51-C52-H52A	109.5
C51-C52-H52B	109.5
H52A-C52-H52B	109.5
C51-C52-H52C	109.5
H52A-C52-H52C	109.5
H52B-C52-H52C	109.5
C51-C53-H53A	109.5
C51-C53-H53B	109.5
H53A-C53-H53B	109.5
C51-C53-H53C	109.5
H53A-C53-H53C	109.5
H53B-C53-H53C	109.5
C56-C54-C55	110.5(4)
C56-C54-Si2	115.0(3)
C55-C54-Si2	112.2(3)
C56-C54-H54	106.1
C55-C54-H54	106.1
Si2-C54-H54	106.1

C54-C55-H55A	109.5
C54-C55-H55B	109.5
H55A-C55-H55B	109.5
C54-C55-H55C	109.5
H55A-C55-H55C	109.5
H55B-C55-H55C	109.5
C54-C56-H56A	109.5
C54-C56-H56B	109.5
H56A-C56-H56B	109.5
C54-C56-H56C	109.5
H56A-C56-H56C	109.5
H56B-C56-H56C	109.5
C58-C57-C59	109.8(4)
C58-C57-Si2	114.7(3)
C59-C57-Si2	113.8(3)
C58-C57-H57	105.9
C59-C57-H57	105.9
Si2-C57-H57	105.9
C57-C58-H58A	109.5
C57-C58-H58B	109.5
H58A-C58-H58B	109.5
C57-C58-H58C	109.5
H58A-C58-H58C	109.5
H58B-C58-H58C	109.5
C57-C59-H59A	109.5
C57-C59-H59B	109.5
H59A-C59-H59B	109.5
C57-C59-H59C	109.5
H59A-C59-H59C	109.5
H59B-C59-H59C	109.5
C48B-C47B-C49B	109.8(16)
C48B-C47B-Si1	110.7(13)
C49B-C47B-Si1	109.0(12)
C48B-C47B-H47B	109.1
C49B-C47B-H47B	109.1
Si1-C47B-H47B	109.1
C47B-C48B-H48D	109.5
C47B-C48B-H48E	109.5
H48D-C48B-H48E	109.5
C47B-C48B-H48F	109.5
H48D-C48B-H48F	109.5
H48E-C48B-H48F	109.5
C47B-C49B-H49D	109.5

C47B-C49B-H49E	109.5
H49D-C49B-H49E	109.5
C47B-C49B-H49F	109.5
H49D-C49B-H49F	109.5
H49E-C49B-H49F	109.5

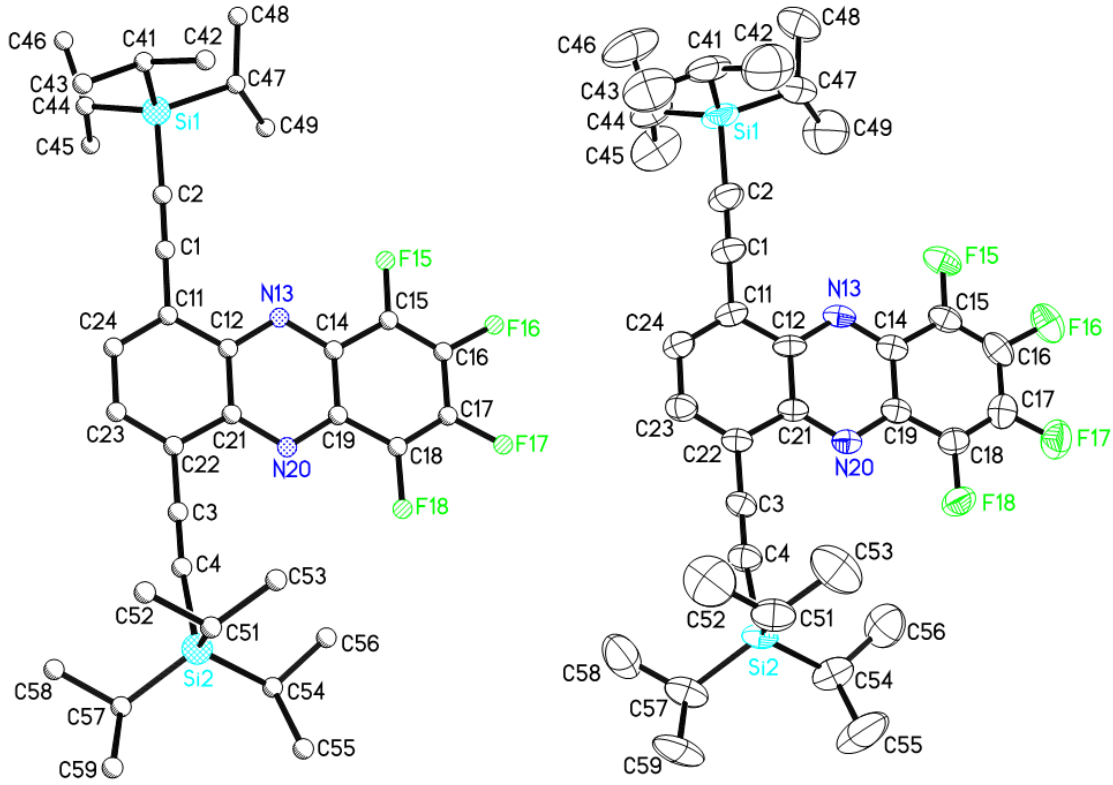

Figure 62 Single molecule of **38b**.

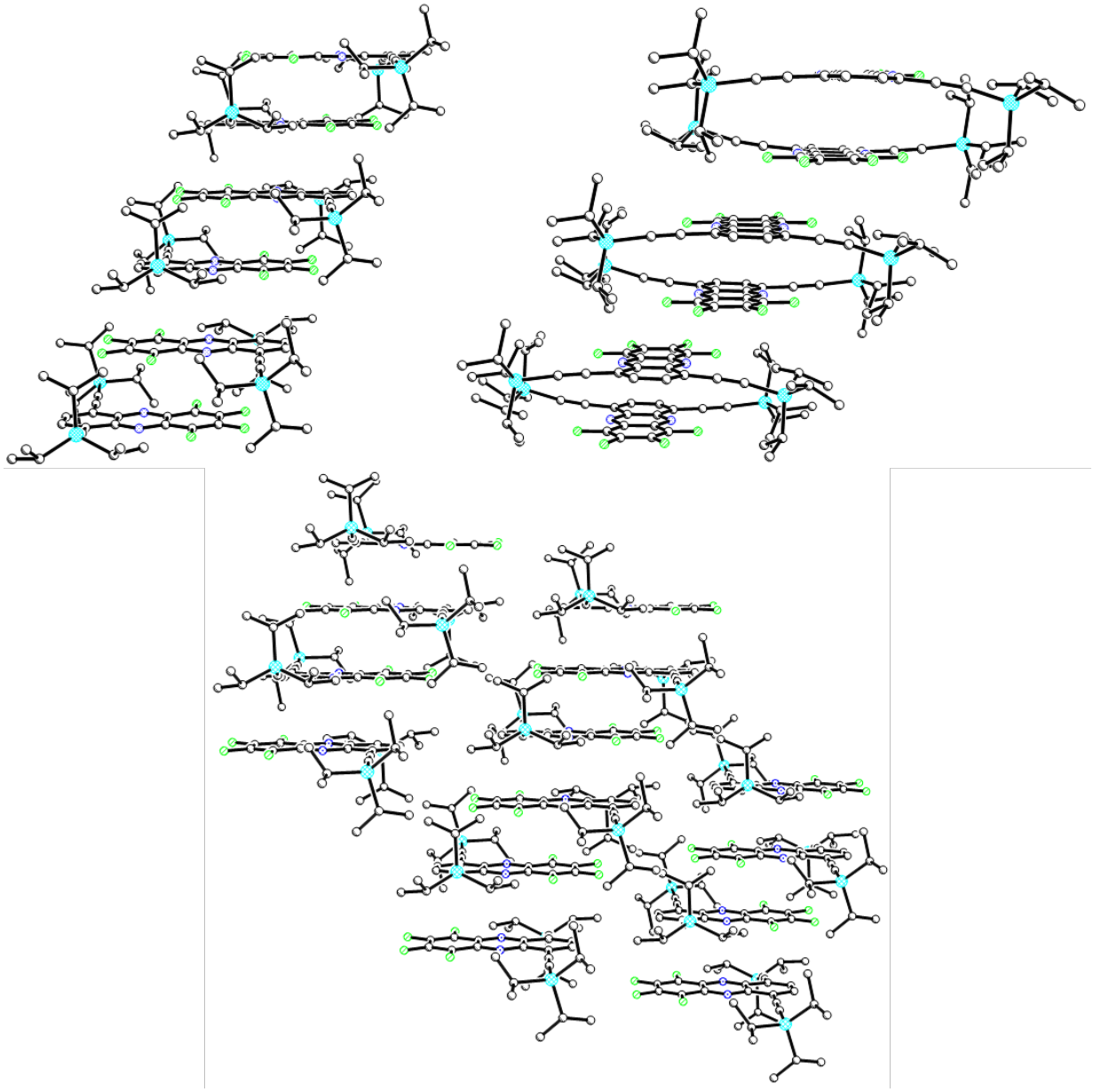

Figure 63 Crystal packing of **38b**.

9.2 Cartesian Coordinates for Calculations

Table 15 Cartesian Coordinates of Computational Data for **40a**

C	-0.720826	0.000000	1.646936
C	0.720826	0.000000	1.646936
C	-1.415646	0.000000	2.893361
C	1.415646	0.000000	2.893361
C	0.713572	0.000000	4.066458
C	-0.713572	0.000000	4.066458
N	1.412367	0.000000	0.501189
N	-1.412367	0.000000	0.501189
C	-0.722243	0.000000	-0.640923
C	0.722243	0.000000	-0.640923
C	1.434535	0.000000	-1.897353
C	-1.434535	0.000000	-1.897353
C	0.706028	0.000000	-3.070361
H	1.233019	0.000000	-4.016512
C	-0.706028	0.000000	-3.070361
H	-1.233019	0.000000	-4.016512
C	2.856271	0.000000	-1.919286
C	4.059657	0.000000	-1.973279
C	-2.856271	0.000000	-1.919286
C	-4.059657	0.000000	-1.973279
H	-2.498691	0.000000	2.868122
H	-1.240659	0.000000	5.013771
H	1.240659	0.000000	5.013771
H	2.498691	0.000000	2.868122
H	-5.121660	0.000000	-2.007028
H	5.121660	0.000000	-2.007028

Table 16 Cartesian Coordinates of Computational Data for **40b**

C	-0.721496	0.000000	0.766624
C	0.721496	0.000000	0.766624
C	-1.412581	0.000000	2.015205
C	1.412581	0.000000	2.015205
C	0.711867	0.000000	3.186450
C	-0.711867	0.000000	3.186450
N	1.409957	0.000000	-0.373623
N	-1.409957	0.000000	-0.373623
C	-0.722212	0.000000	-1.517024
C	0.722212	0.000000	-1.517024

C	1.437386	0.000000	-2.770578
C	-1.437386	0.000000	-2.770578
C	0.706189	0.000000	-3.941977
H	1.232135	0.000000	-4.888618
C	-0.706189	0.000000	-3.941977
H	-1.232135	0.000000	-4.888618
C	2.858107	0.000000	-2.787343
C	4.061589	0.000000	-2.829156
C	-2.858107	0.000000	-2.787343
C	-4.061589	0.000000	-2.829156
H	-5.124173	0.000000	-2.850736
H	5.124173	0.000000	-2.850736
F	2.744717	0.000000	2.038005
F	1.336038	0.000000	4.364386
F	-1.336038	0.000000	4.364386
F	-2.744717	0.000000	2.038005

Table 17 Cartesian Coordinates of Computational Data for **40c**

C	-0.719687	0.000000	-0.149204
C	0.719687	0.000000	-0.149204
C	-1.421488	0.000000	-1.400728
C	1.421488	0.000000	-1.400728
C	0.720102	0.000000	-2.582958
C	-0.720102	0.000000	-2.582958
N	1.402048	0.000000	0.994223
N	-1.402048	0.000000	0.994223
C	-0.720610	0.000000	2.140310
C	0.720610	0.000000	2.140310
C	1.437105	0.000000	3.392180
C	-1.437105	0.000000	3.392180
C	0.705945	0.000000	4.564223
H	1.232038	0.000000	5.510846
C	-0.705945	0.000000	4.564223
H	-1.232038	0.000000	5.510846
C	2.857773	0.000000	3.409931
C	4.061068	0.000000	3.458201
C	-2.857773	0.000000	3.409931
C	-4.061068	0.000000	3.458201
H	-5.123592	0.000000	3.483470
H	5.123592	0.000000	3.483470
Cl	3.152868	0.000000	-1.368180
Cl	1.562200	0.000000	-4.099209

Cl	-1.562200	0.000000	-4.099209
Cl	-3.152868	0.000000	-1.368180

Table 18 Cartesian Coordinates of Computational Data for Model Compound Representing **42a**

C	0.001648	-2.410057	-0.705385
H	0.001659	-3.356042	-1.231642
C	0.001350	-1.247755	-1.446689
C	0.001159	0.001473	-0.728050
C	0.001159	0.001473	0.728050
C	0.001350	-1.247755	1.446689
C	0.001648	-2.410057	0.705385
H	0.001659	-3.356042	1.231642
N	0.000751	1.153519	-1.405756
N	0.000751	1.153519	1.405756
C	0.000139	2.303348	-0.718174
C	0.000139	2.303348	0.718174
C	-0.000649	3.549988	-1.411789
H	-0.000675	3.530785	-2.495190
C	-0.001438	4.725692	-0.712775
H	-0.002106	5.671945	-1.241697
C	-0.000649	3.549988	1.411789
H	-0.000675	3.530785	2.495190
C	-0.001438	4.725692	0.712775
H	-0.002106	5.671945	1.241697
C	0.000609	-1.324700	-2.909344
C	0.001304	-0.351034	-3.893096
H	0.003104	0.720335	-3.832027
N	-0.001769	-1.038297	-5.058401
N	-0.003681	-2.369966	-4.826125
N	-0.002483	-2.543175	-3.542640
C	0.000609	-1.324700	2.909344
C	0.001304	-0.351034	3.893096
H	0.003104	0.720335	3.832027
N	-0.001769	-1.038297	5.058401
N	-0.003681	-2.369966	4.826125
N	-0.002483	-2.543175	3.542640
C	0.002522	-0.533646	6.421265
H	-0.037570	-1.396079	7.083876
H	-0.868561	0.100856	6.594661
H	0.914557	0.033775	6.616515
C	0.002522	-0.533646	-6.421265
H	0.914557	0.033775	-6.616515

H	-0.868561	0.100856	-6.594661
H	-0.037570	-1.396079	-7.083876

Table 19 Cartesian Coordinates of Computational Data for Model Compound Representing **42b**

C	0.003244	-3.136675	-0.705639
H	0.003069	-4.083027	-1.231420
C	0.002799	-1.975048	-1.450194
C	0.002803	-0.730995	-0.728364
C	0.002803	-0.730995	0.728364
C	0.002799	-1.975048	1.450194
C	0.003244	-3.136675	0.705639
H	0.003069	-4.083027	1.231420
N	0.002236	0.421994	-1.403422
N	0.002236	0.421994	1.403422
C	0.001418	1.565036	-0.718168
C	0.001418	1.565036	0.718168
C	0.000173	2.813010	1.407447
C	-0.001185	3.987212	0.711636
C	0.000173	2.813010	-1.407447
C	-0.001185	3.987212	-0.711636
C	0.001213	-2.043375	-2.912066
C	0.002435	-1.063156	-3.890503
H	0.005969	0.009039	-3.829452
C	0.001213	-2.043375	2.912066
C	0.002435	-1.063156	3.890503
H	0.005969	0.009039	3.829452
N	-0.003673	-1.745526	-5.057511
N	-0.007420	-3.078671	-4.831998
N	-0.004863	-3.258685	-3.549768
N	-0.003673	-1.745526	5.057511
N	-0.007420	-3.078671	4.831998
N	-0.004863	-3.258685	3.549768
C	0.003437	-1.233269	-6.418537
H	-0.849967	-0.572250	-6.578222
H	-0.068026	-2.090207	-7.085520
H	0.929906	-0.691691	-6.618042
C	0.003437	-1.233269	6.418537
H	-0.849967	-0.572250	6.578222
H	0.929906	-0.691691	6.618042
H	-0.068026	-2.090207	7.085520
F	0.000111	2.831084	2.744643
F	-0.002659	5.164239	1.339278

F	-0.002659	5.164239	-1.339278
F	0.000111	2.831084	-2.744643

Table 20 Cartesian Coordinates of Computational Data for Model Compound Representing **42c**

C	-0.002421	-3.710605	-0.705238
H	-0.002273	-4.656774	-1.231315
C	-0.002187	-2.548826	-1.449929
C	-0.002154	-1.304938	-0.727401
C	-0.002154	-1.304938	0.727401
C	-0.002187	-2.548826	1.449929
C	-0.002421	-3.710605	0.705238
H	-0.002273	-4.656774	1.231315
N	-0.001871	-0.149342	-1.396532
N	-0.001871	-0.149342	1.396532
C	-0.001367	0.997552	0.717428
C	-0.001367	0.997552	-0.717428
C	-0.000707	2.249833	-1.414767
C	-0.000707	2.249833	1.414767
C	0.000075	3.435395	0.719018
C	0.000075	3.435395	-0.719018
C	-0.000979	-2.622347	-2.911109
C	-0.000979	-2.622347	2.911109
C	0.000678	-1.645191	-3.891568
H	0.000658	-0.573013	-3.831389
C	0.000678	-1.645191	3.891568
H	0.000658	-0.573013	3.831389
N	0.003144	-2.330573	5.056925
N	0.000311	-3.839816	3.545278
N	0.002599	-3.663418	4.827855
N	0.003144	-2.330573	-5.056925
N	0.000311	-3.839816	-3.545278
N	0.002599	-3.663418	-4.827855
C	0.002373	-1.822482	6.419349
H	-0.903370	-1.244023	6.610400
H	0.880366	-1.197696	6.591931
C	0.002373	-1.822482	-6.419349
H	-0.903370	-1.244023	-6.610400
H	0.880366	-1.197696	-6.591931
H	0.031432	-2.683887	-7.083833
H	0.031432	-2.683887	7.083833
Cl	-0.000829	2.229417	3.152559
Cl	0.001066	4.951000	1.563286

Cl	0.001066	4.951000	-1.563286
Cl	-0.000829	2.229417	-3.152559

Table 21 Cartesian Coordinates of Computational Data for the Model Phenazine Cycloadduct with Ag^+

H	0.543632	-4.893560	-0.829927
C	0.240651	-3.880458	-0.586622
H	-1.875808	-4.288635	-0.539825
C	-1.078997	-3.560194	-0.435453
C	0.946755	-1.562187	-0.111804
C	-1.454327	-2.217308	-0.135676
C	1.233529	-2.883191	-0.415921
C	-0.446063	-1.178552	-0.005055
N	-2.761238	-1.960425	0.004167
H	2.272898	-3.172961	-0.535463
C	-3.136964	-0.709513	0.282734
C	-4.523233	-0.409953	0.451636
C	-2.163341	0.351305	0.383886
H	-1.884345	2.470227	0.770890
N	-0.849036	0.092453	0.215360
C	-4.920602	0.874140	0.710812
H	-5.228021	-1.229977	0.363804
H	-5.972611	1.106241	0.842211
C	-3.957981	1.923075	0.814682
H	-4.295379	2.931955	1.031916
C	-2.618892	1.671896	0.655067
C	2.108814	-0.693105	0.165333
C	3.310826	-1.074893	0.742582
H	3.644214	-2.010387	1.164165
N	4.086782	0.033721	0.726957
C	5.457841	0.201834	1.207237
H	5.733725	1.242418	1.039764
H	6.128362	-0.455350	0.648987
H	5.506514	-0.030742	2.273359
Ag	0.453768	1.929088	-0.438932
N	3.440630	1.069403	0.189117
N	2.252369	0.631575	-0.153796

Table 22 Cartesian Coordinates of Computational Data for the Tetrafluorinated Model Phenazine Cycloadduct with Ag^+

H	1.722801	-5.032038	-0.535760
C	1.308384	-4.040748	-0.384366

H	-0.756972	-4.664047	-0.382060
C	-0.042654	-3.851424	-0.306703
C	1.763271	-1.632859	-0.060680
C	-0.558606	-2.534903	-0.130359
C	2.189181	-2.936275	-0.259175
C	0.336056	-1.391489	-0.035565
N	-1.889940	-2.400536	-0.064785
H	3.254878	-3.129500	-0.329531
C	-2.392657	-1.177339	0.082044
C	-3.810820	-1.001460	0.166328
C	-1.527987	-0.023918	0.136959
N	-0.192411	-0.155614	0.074111
C	-4.344977	0.254253	0.289527
C	-3.493246	1.397478	0.326704
C	-2.133370	1.255558	0.252031
C	2.818993	-0.628234	0.181353
C	4.062879	-0.861522	0.751898
H	4.505830	-1.744959	1.184761
N	4.708815	0.325771	0.713154
C	6.055387	0.655118	1.180569
H	6.209693	1.718020	0.997788
H	6.792172	0.070167	0.625677
H	6.135825	0.444337	2.249244
Ag	0.987447	1.927744	-0.434140
N	3.945850	1.273360	0.168916
N	2.809761	0.700874	-0.155014
F	-1.355458	2.372027	0.280252
F	-4.048721	2.594378	0.432943
F	-5.653673	0.450503	0.367996
F	-4.599606	-2.063995	0.119696

Table 23 Cartesian Coordinates of the Internal Rotation Experiment of the Model Phenazine Cycloadduct – Starting Conformer Structure Optimization

H	0.850570	-4.386015	0.003567
C	0.505830	-3.358058	0.000507
H	-1.589010	-3.852071	0.007767
C	-0.830747	-3.078588	0.002945
C	1.127194	-0.977307	-0.010912
C	-1.261385	-1.722058	-0.000747
C	1.466425	-2.315359	-0.006369
C	-0.285097	-0.648176	-0.006957
N	-2.578240	-1.472596	0.002176

H	2.511306	-2.601879	-0.008669
C	-2.967899	-0.193685	-0.000356
C	-4.358621	0.129613	0.002434
C	-1.999464	0.873494	-0.005348
H	-1.706282	3.008770	-0.010915
N	-0.686506	0.623441	-0.008579
C	-4.754944	1.437809	0.000461
H	-5.069430	-0.688361	0.006161
H	-5.811005	1.683990	0.002640
C	-3.795920	2.495577	-0.004321
H	-4.143679	3.522538	-0.005856
C	-2.455698	2.226393	-0.007143
C	2.203483	0.030361	-0.019281
C	3.571472	-0.213174	-0.023308
H	4.156742	-1.116402	-0.021479
N	4.146620	1.006844	-0.032003
N	3.198455	1.971567	-0.034893
N	2.039167	1.391670	-0.027204
C	5.554846	1.366586	-0.042750
H	6.052175	0.997404	0.855961
H	5.604254	2.453447	-0.065954
H	6.046004	0.961112	-0.929153

Table 24 Cartesian Coordinates of the Internal Rotation Experiment of the Model Phenazine Cycloadduct – End Conformer Structure Optimization

H	0.662415	-4.553968	0.000130
C	0.386247	-3.505493	0.000127
H	-1.736234	-3.865829	0.000077
C	-0.930602	-3.141873	0.000097
C	1.148063	-1.176614	0.000185
C	-1.277377	-1.760082	0.000083
C	1.416006	-2.529136	0.000166
C	-0.232703	-0.754383	0.000115
N	-2.572009	-1.421065	0.000037
H	2.450981	-2.846941	0.000220
C	-2.874646	-0.117772	0.000015
C	-4.241985	0.291351	-0.000030
C	-1.840989	0.885747	0.000036
H	-1.428053	3.006061	0.000028
N	-0.544035	0.546441	0.000088
C	-4.560287	1.620806	-0.000047
H	-5.000046	-0.482932	-0.000047

H	-5.598994	1.931435	-0.000081
C	-3.537603	2.615103	-0.000028
H	-3.819351	3.662116	-0.000042
C	-2.216272	2.262284	0.000011
C	2.264616	-0.226087	0.000329
C	2.307351	1.157172	0.000380
H	1.524768	1.891808	0.000267
N	3.625767	1.460557	0.000631
N	4.373820	0.334839	0.000764
N	3.561817	-0.674241	0.000466
C	4.267904	2.764385	0.000842
H	3.988385	3.328049	-0.891263
H	5.342693	2.593398	0.000971
H	3.988133	3.327874	0.892977

Table 25 Cartesian Coordinates of the Phenazine Model Compound for Electrostatic Map

H	-0.000705	-3.355752	1.231904
C	-0.000825	-2.409958	0.705356
C	-0.000765	-1.247487	1.446564
C	-0.000765	-1.247487	-1.446564
C	-0.000906	0.001772	0.728022
C	-0.000825	-2.409958	-0.705356
C	-0.000906	0.001772	-0.728022
N	-0.000860	1.153879	1.405842
H	-0.000705	-3.355752	-1.231904
C	-0.000983	2.303695	0.718216
C	-0.000957	3.550245	1.411825
C	-0.000983	2.303695	-0.718216
H	-0.000960	3.530947	-2.495173
N	-0.000860	1.153879	-1.405842
C	-0.000858	4.725868	0.712813
H	-0.000960	3.530947	2.495173
H	-0.000641	5.672060	1.241809
C	-0.000858	4.725868	-0.712813
H	-0.000641	5.672060	-1.241809
C	-0.000957	3.550245	-1.411825
C	-0.000391	-1.324718	-2.909223
C	0.001206	-0.351327	-3.893290
H	0.002389	0.720041	-3.832578
C	-0.000391	-1.324718	2.909223
C	0.001206	-0.351327	3.893290
H	0.002389	0.720041	3.832578

N	0.000445	-1.038851	-5.058593
N	-0.001661	-2.370367	-4.825883
N	-0.002303	-2.543407	-3.542294
N	-0.002303	-2.543407	3.542294
N	-0.001661	-2.370367	4.825883
N	0.000445	-1.038851	5.058593
C	0.003393	-0.535805	-6.422270
H	-0.882978	0.074055	-6.605896
H	-0.007040	-1.400274	-7.083194
H	0.901594	0.056128	-6.609155
C	0.003393	-0.535805	6.422270
H	-0.882978	0.074055	6.605896
H	0.901594	0.056128	6.609155
H	-0.007040	-1.400274	7.083194

Table 26 Cartesian Coordinates of Computational Data for Model Compound Representing **44a**

C	-0.713158	0.000220	1.630607
H	-1.228571	0.000645	2.583091
C	-1.471795	0.000210	0.481475
C	-0.719243	-0.000045	-0.739156
C	0.713158	-0.000220	1.630607
H	1.228571	-0.000645	2.583091
C	1.471795	-0.000210	0.481475
C	0.719243	0.000045	-0.739156
N	1.136465	0.000084	-1.988798
N	-1.136465	-0.000084	-1.988798
O	0.000000	0.000000	-2.746617
C	2.926818	-0.000905	0.494493
C	-2.926818	0.000905	0.494493
C	3.828557	0.003240	-0.555669
H	3.687186	0.008672	-1.622582
C	-3.828557	-0.003240	-0.555669
H	-3.687186	-0.008672	-1.622582
N	-5.041803	0.003018	0.040536
N	-4.910864	0.009567	1.387300
N	-3.644708	0.008815	1.660974
N	5.041803	-0.003018	0.040536
N	4.910864	-0.009567	1.387300
N	3.644708	-0.008815	1.660974
C	6.363738	0.010201	-0.565884
H	6.529881	0.947702	-1.099795
H	6.470921	-0.829085	-1.254752

H	7.088664	-0.083447	0.240234
C	-6.363738	-0.010201	-0.565884
H	-6.470921	0.829085	-1.254752
H	-7.088664	0.083447	0.240234
H	-6.529881	-0.947702	-1.099795

Table 27 Cartesian Coordinates of Computational Data for Model Compound Representing **44b**

C	-0.708825	-0.000056	1.769175
H	-1.229285	-0.000412	2.718789
C	-1.462501	0.000135	0.613535
C	-0.727254	0.000282	-0.616877
C	0.727254	-0.000282	-0.616877
C	1.462501	-0.000135	0.613535
C	0.708825	0.000056	1.769175
H	1.229285	0.000412	2.718789
N	-1.251149	0.000555	-1.845972
N	1.251149	-0.000555	-1.845972
S	0.000000	0.000000	-2.906418
C	-2.920318	-0.000505	0.651695
C	2.920318	0.000505	0.651695
C	3.851532	-0.002935	-0.372311
H	3.737779	-0.007730	-1.441295
C	-3.851532	0.002935	-0.372311
H	-3.737779	0.007730	-1.441295
N	-5.048949	-0.003318	0.256476
N	-4.882361	-0.009098	1.598661
N	-3.608910	-0.007906	1.837130
N	3.608910	0.007906	1.837130
N	5.048949	0.003318	0.256476
N	4.882361	0.009098	1.598661
C	-6.385847	0.008733	-0.314530
H	-7.089640	-0.082597	0.510493
H	-6.512127	-0.832261	-0.998310
H	-6.566796	0.944803	-0.846520
C	6.385847	-0.008733	-0.314530
H	7.089640	0.082597	0.510493
H	6.512127	0.832261	-0.998310
H	6.566796	-0.944803	-0.846520

Table 28 Cartesian Coordinates of Computational Data for Model Compound Representing **44c**

C	-0.710001	0.000444	2.081449
H	-1.229983	0.001031	3.031365
C	0.710001	-0.000444	2.081449
H	1.229983	-0.001031	3.031365
C	1.462055	-0.000675	0.929599
C	0.736524	-0.000184	-0.317330
C	-1.462055	0.000675	0.929599
C	-0.736524	0.000184	-0.317330
N	1.316310	-0.000250	-1.507937
N	-1.316310	0.000250	-1.507937
Se	0.000000	0.000000	-2.746276
C	2.920728	-0.001505	0.980510
C	3.867281	0.002166	-0.029337
H	3.768977	0.006809	-1.099438
C	-2.920728	0.001505	0.980510
C	-3.867281	-0.002166	-0.029337
H	-3.768977	-0.006809	-1.099438
N	5.055769	-0.003571	0.616652
N	3.593476	-0.008377	2.175830
N	4.870068	-0.009138	1.956147
N	-5.055769	0.003571	0.616652
N	-3.593476	0.008377	2.175830
N	-4.870068	0.009138	1.956147
C	6.400200	0.009935	0.064222
H	7.092931	-0.080884	0.898563
H	6.587496	0.946227	-0.465108
H	6.536926	-0.830636	-0.618208
C	-6.400200	-0.009935	0.064222
H	-6.587496	-0.946227	-0.465108
H	-6.536926	0.830636	-0.618208
H	-7.092931	0.080884	0.898563

10 References

(1) Reginald H. Garrett, C. M. G. *Biochemistry*; 3rd ed.; Brooks/Cole, 2004.
(2) Stohs, S. J.; Bagchi, D. *Free Radical Biol. Med.* **1995**, *18*, 321.
(3) Nriagu, J. O.; Pacyna, J. M. *Nature* **1988**, *333*, 134.
(4) Quang, D. T.; Kim, J. S. *Chem. Rev.* **2010**, *110*, 6280.
(5) Qian, X.; Xiao, Y.; Xu, Y.; Guo, X.; Qian, J.; Zhu, W. *Chem. Commun.* **2010**, *46*, 6418.
(6) Tan, S. S.; Teo, Y. N.; Kool, E. T. *Org. Lett.* **2010**, *12*, 4820.
(7) Jeong, Y.; Yoon, J. *Inorg. Chim. Acta* **2012**, *381*, 2.
(8) Winkler, J. D.; Bowen, C. M.; Michelet, V. *J. Am. Chem. Soc.* **1998**, *120*, 3237.
(9) Zhang, J. F.; Zhou, Y.; Yoon, J.; Kim, J. S. *Chem. Soc. Rev.* **2011**, *40*, 3416.
(10) Veale, E. B.; Gunnlaugsson, T. *Annu. Rep. Prog. Chem. B* **2010**, *106*, 376.
(11) Hong, J. W.; Hemme, W. L.; Keller, G. E.; Rinke, M. T.; Bazan, G. C. *Adv. Mater.* **2006**, *18*, 878.
(12) Wang, S.; Gaylord, B. S.; Bazan, G. C. *J. Am. Chem. Soc.* **2004**, *126*, 5446.
(13) Woo, H. Y.; Vak, D.; Korystov, D.; Mikhailovsky, A.; Bazan, G. C.; Kim, D.-Y. *Adv. Funct. Mater.* **2007**, *17*, 290.
(14) Zhao, J.; Fyles, T. M.; James, T. D. *Angew. Chem., Int. Ed.* **2004**, *43*, 3461.
(15) Zhao, J.; Davidson, M. G.; Mahon, M. F.; Kociok-Koehn, G.; James, T. D. *J. Am. Chem. Soc.* **2004**, *126*, 16179.
(16) Pickup, J. C.; Hussain, F.; Evans, N. D.; Rolinski, O. J.; Birch, D. J. S. *Biosens. Bioelectron.* **2005**, *20*, 2555.
(17) Miranda, O. R.; You, C.-C.; Phillips, R.; Kim, I.-B.; Ghosh, P. S.; Bunz, U. H. F.; Rotello, V. M. *J. Am. Chem. Soc.* **2007**, *129*, 9856.
(18) De, M.; Rana, S.; Akpinar, H.; Miranda, O. R.; Arvizo, R. R.; Bunz, U. H. F.; Rotello, V. M. *Nat. Chem.* **2009**, *1*, 461.
(19) Yu, D.; Zhang, Y.; Liu, B. *Macromolecules* **2008**, *41*, 4003.
(20) Rhee, H.-W.; Lee, C.-R.; Cho, S.-H.; Song, M.-R.; Cashel, M.; Choy, H. E.; Seok, Y.-J.; Hong, J.-I. *J. Am. Chem. Soc.* **2008**, *130*, 784.
(21) Ma, G.; Cheng, Q. *Langmuir* **2006**, *22*, 6743.
(22) Phillips, R. L.; Miranda, O. R.; You, C.-C.; Rotello, V. M.; Bunz, U. H. F. *Angew. Chem., Int. Ed.* **2008**, *47*, 2590.
(23) Hoffman, R. M. *Nat. Rev. Cancer* **2005**, *5*, 796.
(24) Wang, Y. M.; Judkewitz, B.; DiMarzio, C. A.; Yang, C. *Nat. Commun.* **2012**, *3*, 928.
(25) Stadler, A. L.; Delos, S. J. O.; Stensrud, E. S.; Dembska, A.; Silva, G. L.; Liu, S.; Shank, N. I.; Kunttas-Tatli, E.; Sobers, C. J.; Gramlich, P. M. E.; Carell, T.; Peteanu, L. A.; McCartney, B. M.; Armitage, B. A. *Bioconjugate Chem.* **2011**, *22*, 1491.
(26) Disney, M. D.; Zheng, J.; Swager, T. M.; Seeberger, P. H. *J. Am. Chem. Soc.* **2004**, *126*, 13343.
(27) Kim, I.-B.; Shin, H.; Garcia, A. J.; Bunz, U. H. F. *Bioconjugate Chem.* **2007**, *18*, 815.
(28) Lakowicz, J. R. *Principles of Fluorescence Spectroscopy*; 4th ed.; Springer, 2006.
(29) Phillips, R. L.; Kim, I.-B.; Carson, B. E.; Tidbeck, B. r.; Bai, Y.; Lowary, T. L.; Tolbert, L. M.; Bunz, U. H. F. *Macromolecules* **2008**, *41*, 7316.
(30) Birks, J. B. *Photophysics of Aromatic Molecules*; Wiley: London, 1970.
(31) Fan, C.; Wang, S.; Hong, J. W.; Bazan, G. C.; Plaxco, K. W.; Heeger, A. J. *Proc. Nat. Acad. Sci. USA* **2003**, *100*, 6297.
(32) Luo, J.; Xie, Z.; Lam, J. W. Y.; Cheng, L.; Chen, H.; Qiu, C.; Kwok, H. S.; Zhan, X.; Liu, Y.; Zhu, D.; Tang, B. Z. *Chem. Commun.* **2001**, 1740.
(33) Hong, Y.; Lam, J. W. Y.; Tang, B. Z. *Chem. Soc. Rev.* **2011**, *40*, 5361.

(34) Tour, J. M. *Adv. Mater.* **1994**, *6*, 190.
(35) Tong, H.; Hong, Y.; Dong, Y.; Hau; Lam, J. W. Y.; Li, Z.; Guo, Z.; Guo, Z.; Tang, B. Z. *Chem. Commun.* **2006**, 3705.
(36) Gaylord, B. S.; Heeger, A. J.; Bazan, G. C. *Proc. Nat. Acad. Sci. USA* **2002**, *99*, 10954.
(37) Zucchero, A. J.; McGrier, P. L.; Bunz, U. H. F. *Acc. Chem. Res.* **2010**, *43*, 397.
(38) Zucchero, A. J.; Wilson, J. N.; Bunz, U. H. F. *J. Am. Chem. Soc.* **2006**, *128*, 11872.
(39) Wilson, J. N.; Bunz, U. H. F. *J. Am. Chem. Soc.* **2005**, *127*, 4124.
(40) Sun, H.-B.; Liu, S.-J.; Ma, T.-C.; Song, N.-N.; Zhao, Q.; Huang, W. *New J. Chem.* **2011**, *35*, 1194.
(41) Formica, M.; Fusi, V.; Giorgi, L.; Micheloni, M. *Coord. Chem. Rev.* **2012**, *256*, 170.
(42) Kim, H. N.; Ren, W. X.; Kim, J. S.; Yoon, J. *Chem. Soc. Rev.* **2012**, *41*, 3210.
(43) Tolosa, J.; Zucchero, A. J.; Bunz, U. H. F. *J. Am. Chem. Soc.* **2008**, *130*, 6498.
(44) Bao, Y.; Wang, H.; Li, Q.; Liu, B.; Li, Q.; Bai, W.; Jin, B.; Bai, R. *Macromolecules* **2012**, *45*, 3394.
(45) Li, C.; Zhou, C.; Zheng, H.; Yin, X.; Zuo, Z.; Liu, H.; Li, Y. *J. Polym. Sci. A Pol. Chem.* **2008**, *46*, 1998.
(46) Kim, I. B.; Erdogan, B.; Wilson, J. N.; Bunz, U. H. F. *Chem.- Eur. J.* **2004**, *10*, 6247.
(47) Lutz, J.-F. *J. Polym. Sci. A Pol. Chem.* **2008**, *46*, 3459.
(48) Lutz, J.-F. *Adv. Mater.* **2011**, *23*, 2237.
(49) Oishi, M.; Nagasaki, Y. *Nanomedicine - UK* **2010**, *5*, 451.
(50) Hucknall, A.; Rangarajan, S.; Chilkoti, A. *Adv. Mater.* **2009**, *21*, 2441.
(51) Khan, A.; Muller, S.; Hecht, S. *Chem. Commun.* **2005**, 584.
(52) Kim, I.-B.; Phillips, R.; Bunz, U. H. F. *Macromolecules* **2007**, *40*, 5290.
(53) Lee, Y. H.; Lee, M. H.; Zhang, J. F.; Kim, J. S. *J. Org. Chem.* **2010**, *75*, 7159.
(54) Kim, S. H.; Kim, J. S.; Park, S. M.; Chang, S.-K. *Org. Lett.* **2006**, *8*, 371.
(55) Moore, D. S.; Robinson, S. D. *Adv. Inorg. Chem.* **1988**, *32*, 171.
(56) Kwong, H.-L.; Yeung, H.-L.; Yeung, C.-T.; Lee, W.-S.; Lee, C.-S.; Wong, W.-L. *Coord. Chem. Rev.* **2007**, *251*, 2188.
(57) Atilgan, S.; Ozdemir, T.; Akkaya, E. U. *Org. Lett.* **2008**, *10*, 4065.
(58) Zhu, X.; Fu, S.; Wong, W.-K.; Wong, W.-Y. *Tet. Lett.* **2008**, *49*, 1843.
(59) Rochford, J.; Chu, D.; Hagfeldt, A.; Galoppini, E. *J. Am. Chem. Soc.* **2007**, *129*, 4655.
(60) Liao, M.-S.; Scheiner, S. *J. Chem. Phys.* **2002**, *117*, 205.
(61) Constable, E. C.; Thompson, A. M. W. C. *J. Chem. Soc., Dalton Trans.* **1992**, 3467.
(62) Schluetter, F.; Wild, A.; Winter, A.; Hager, M. D.; Baumgaertel, A.; Friebe, C.; Schubert, U. S. *Macromolecules* **2010**, *43*, 2759.
(63) Winter, A.; Friebe, C.; Chiper, M.; Hager, M. D.; Schubert, U. S. *J. Polym. Sci. A Pol. Chem.* **2009**, *47*, 4083.
(64) Aromi, G.; Barrios, L. A.; Roubeau, O.; Gamez, P. *Coord. Chem. Rev.* **2011**, *255*, 485.
(65) Hoffman, H. L.; Ernst, E. J.; Klepser, M. E. *Expert Opin. Invest. Drugs* **2000**, *9*, 593.
(66) Michael, A. *Journal für Praktische Chemie* **1893**, *48*, 94.
(67) Huisgen, R.; Knorr, R.; Möbius, L.; Szeimies, G. *Chem. Ber.* **1965**, *98*, 4014.
(68) Huisgen, R.; Szeimies, G.; Möbius, L. *Chem. Ber.* **1967**, *100*, 2494.
(69) Tornøe, C. W.; Christensen, C.; Meldal, M. *J. Org. Chem.* **2002**, *67*, 3057.
(70) Rostovtsev, V. V.; Green, L. G.; Fokin, V. V.; Sharpless, K. B. *Angew. Chem., Int. Ed.* **2002**, *41*, 2596.
(71) Themed Issue (4) on 'Applications of Click Chemistry' *Chem. Soc. Rev.* **2010**, *39*, 1221.
(72) Wang, Q.; Chan, T. R.; Hilgraf, R.; Fokin, V. V.; Sharpless, K. B.; Finn, M. G. *J. Am. Chem. Soc.* **2003**, *125*, 3192.
(73) Bakbak, S.; Leech, P. J.; Carson, B. E.; Saxena, S.; King, W. P.; Bunz, U. H. F. *Macromolecules* **2006**, *39*, 6793.

(74) Englert, B. C.; Bakbak, S.; Bunz, U. H. F. *Macromolecules* **2005**, *38*, 5868.
(75) Opsteen, J. A.; van Hest, J. C. M. *Chem. Commun.* **2005**.
(76) Qin, A.; Lam, J. W. Y.; Tang, B. Z. *Macromolecules* **2010**, *43*, 8693.
(77) Wu, P.; Feldman, A. K.; Nugent, A. K.; Hawker, C. J.; Scheel, A.; Voit, B.; Pyun, J.; Frechet, J. M. J.; Sharpless, K. B.; Fokin, V. V. *Angew. Chem., Int. Ed.* **2004**, *43*, 3928.
(78) Malkoch, M.; Thibault, R. J.; Drockenmuller, E.; Messerschmidt, M.; Voit, B.; Russell, T. P.; Hawker, C. J. *J. Am. Chem. Soc.* **2005**, *127*, 14942.
(79) Meldal, M.; Tornøe, C. W. *Chem. Rev.* **2008**, *108*, 2952.
(80) Zhou, Z.; Fahrni, C. J. *J. Am. Chem. Soc.* **2004**, *126*, 8862.
(81) Hein, J. E.; Fokin, V. V. *Chem. Soc. Rev.* **2010**, *39*, 1302.
(82) Kolb, H. C.; Finn, M. G.; Sharpless, K. B. *Angew. Chem., Int. Ed.* **2001**, *40*, 2004.
(83) Juricek, M.; Kouwer, P. H. J.; Rowan, A. E. *Chem. Commun.* **2011**, *47*, 8740.
(84) Lallana, E.; Riguera, R.; Fernandez-Megia, E. *Angew. Chem., Int. Ed.* **2011**, *50*, 8794.
(85) Juwarker, H.; Lenhardt, J. M.; Castillo, J. C.; Zhao, E.; Krishnamurthy, S.; Jamiolkowski, R. M.; Kim, K.-H.; Craig, S. L. *J. Org. Chem.* **2009**, *74*, 8924.
(86) Ballesteros, R.; Abarca, B.; Samadi, A.; Server-Carrió, J.; Escrivà, E. *Polyhedron* **1999**, *18*, 3129.
(87) Lau, Y. H.; Rutledge, P. J.; Watkinson, M.; Todd, M. H. *Chem. Soc. Rev.* **2011**, *40*, 2848.
(88) Chang, K.-C.; Su, I.-H.; Senthilvelan, A.; Chung, W.-S. *Org. Lett.* **2007**, *9*, 3363.
(89) Colasson, B.; Save, M.; Milko, P.; Roithová, J.; Schröder, D.; Reinaud, O. *Org. Lett.* **2007**, *9*, 4987.
(90) Schweinfurth, D.; Hardcastle, K. I.; Bunz, U. H. F. *Chem. Commun.* **2008**, 2203.
(91) Chan, T. R.; Hilgraf, R.; Sharpless, K. B.; Fokin, V. V. *Org. Lett.* **2004**, *6*, 2853.
(92) Ostermeier, M.; Berlin, M.-A.; Meudtner, R. M.; Demeshko, S.; Meyer, F.; Limberg, C.; Hecht, S. *Chem. – Eur. J.* **2010**, *16*, 10202.
(93) Piot, L.; Meudtner, R. M.; El Malah, T.; Hecht, S.; Samorì, P. *Chem. – Eur. J.* **2009**, *15*, 4788.
(94) Rabaey, K.; Boon, N.; Höfte, M.; Verstraete, W. *Environ. Sci. Technol.* **2005**, *39*, 3401.
(95) Jana, A. K. *J. Photochem. Photobiol. A* **2000**, *132*, 1.
(96) Fu, C. Y.; Li, M. T.; Su, Z. M.; Hong, Z.; Li, W. L.; Li, B. *Appl. Phys. Lett.* **2006**, *88*.
(97) Chen, J. P.; Li, X.-C. C.; Canon Kabushiki Kaisha, Japan . 2004, p 14 pp.
(98) Klubek, K. P.; Vargas, J. R.; Liao, L.-s.; Eastman Kodak Company, USA . 2005, p 43 pp.
(99) Mavrodi, D. V.; Blankenfeldt, W.; Thomashow, L. S. In *Annu. Rev. Phytopathol.* 2006; Vol. 44, p 417.
(100) Laursen, J. B.; Nielsen, J. *Chem. Rev.* **2004**, *104*, 1663.
(101) Mentel, M.; Ahuja, E. G.; Mavrodi, D. V.; Breinbauer, R.; Thomashow, L. S.; Blankenfeldt, W. *ChemBioChem* **2009**, *10*, 2295.
(102) Beifuss, U.; Tietze, M. In *Natural Products Synthesis II: Targets, Methods, Concepts*; Mulzer, J., Ed. 2005; Vol. 244, p 77.
(103) Hollstein, U.; Van Gemert, R. J. J. *Biochemistry* **1971**, *10*, 497.
(104) Pauliukaite, R.; Ghica, M. E.; Barsan, M. M.; Brett, C. M. A. *Anal. Lett.* **2010**, *43*, 1588.
(105) Han, S. B.; Zhu, M.; Yuan, Z. B.; Li, X. *Biosens. Bioelectron.* **2001**, *16*, 9.
(106) Hashemi, P.; Zarjani, R. A. *Sensor. Actuat. B - Chem.* **2008**, *135*, 112.
(107) Steel, P. J.; Fitchett, C. M. *Coord. Chem. Rev.* **2008**, *252*, 990.
(108) Miao, S. B.; Bangcuyo, C. G.; Smith, M. D.; Bunz, U. H. F. *Angew. Chem., Int. Ed.* **2006**, *45*, 661.
(109) Mindt, T. L.; Struthers, H.; Brans, L.; Anguelov, T.; Schweinsberg, C.; Maes, V.; Tourwé, D.; Schibli, R. *J. Am. Chem. Soc.* **2006**, *128*, 15096.
(110) Brombosz, S. M.; Appleton, A. L.; Zappas, A. J., II; Bunz, U. H. F. *Chem. Commun.* **2010**, *46*, 1419.
(111) Coombs, B. A.; Lindner, B. D.; Edkins, R. M.; Rominger, F.; Beeby, A.; Bunz, U. H. F. *New J. Chem.* **2012**, *36*.

(112) Lemal, D. M.; Ramanathan, S.; Shellito, J. *J. Org. Chem.* **2008**, *73*, 3392.
(113) Bunz, U. H. F. *Chem. - Eur. J.* **2009**, *15*, 6780.
(114) Chen, J.; Cao, Y. *Acc. Chem. Res.* **2009**, *42*, 1709.
(115) Osuna, R. M.; Ortiz, R. P.; Okamoto, T.; Suzuki, Y.; Yamaguchi, S.; Hernández, V.; López Navarrete, J. T. *J. Phys. Chem. B* **2007**, *111*, 7488.
(116) İçli, M.; Pamuk, M.; Algi, F.; Önal, A. M.; Cihaner, A. *Chem. Mater.* **2010**, *22*, 4034.
(117) Yang, R.; Tian, R.; Yan, J.; Zhang, Y.; Yang, J.; Hou, Q.; Yang, W.; Zhang, C.; Cao, Y. *Macromolecules* **2004**, *38*, 244.
(118) Heeney, M.; Zhang, W.; Crouch, D. J.; Chabinyc, M. L.; Gordeyev, S.; Hamilton, R.; Higgins, S. J.; McCulloch, I.; Skabara, P. J.; Sparrowe, D.; Tierney, S. *Chem. Commun.* **2007**, 5061.
(119) Schulze, B.; Friebe, C.; Hager, M. D.; Winter, A.; Hoogenboom, R.; Gorls, H.; Schubert, U. S. *Dalton Trans.* **2009**, 787.
(120) Li, Y.; Huffman, J. C.; Flood, A. H. *Chem. Commun.* **2007**, 2692.
(121) Meudtner, R. M.; Ostermeier, M.; Goddard, R.; Limberg, C.; Hecht, S. *Chem. – Eur. J.* **2007**, *13*, 9834.
(122) Saleh, N. i. *Luminescence* **2009**, *24*, 30.
(123) Wu, C.-G.; Lu, H.-C.; Chen, L.-N.; Lin, Y.-C. *J. Polym. Sci. A Pol. Chem.* **2008**, *46*, 1586.
(124) Yin, Z.; Tam, A. Y.-Y.; Wong, K. M.-C.; Tao, C.-H.; Li, B.; Poon, C.-T.; Wu, L.; Yam, V. W.-W. *Dalton Trans.* **2012**, *41*, 11340.
(125) Bozdemir, O. A.; Guliyev, R.; Buyukcakir, O.; Selcuk, S.; Kolemen, S.; Gulseren, G.; Nalbantoglu, T.; Boyaci, H.; Akkaya, E. U. *J. Am. Chem. Soc.* **2010**, *132*, 8029.
(126) Zeidan, T. A.; Kovalenko, S. V.; Manoharan, M.; Clark, R. J.; Ghiviriga, I.; Alabugin, I. V. *J. Am. Chem. Soc.* **2005**, *127*, 4270.
(127) Neenan, T. X.; Whitesides, G. M. *J. Org. Chem.* **1988**, *53*, 2489.
(128) Chen, L. H.; McBranch, D. W.; Wang, H. L.; Helgeson, R.; Wudl, F.; Whitten, D. G. *Proc. Nat. Acad. Sci. USA* **1999**, *96*, 12287.
(129) Thomas, S. W., III; Joly, G. D.; Swager, T. M. *Chem. Rev.* **2007**, *107*, 1339.
(130) Zhou, Q.; Swager, T. M. *J. Am. Chem. Soc.* **1995**, *117*, 12593.
(131) van Steenis, D. J. V. C.; David, O. R. P.; van Strijdonck, G. P. F.; van Maarseveen, J. H.; Reek, J. N. H. *Chem. Commun.* **2005**, 4333.
(132) Andersen, J.; Madsen, U.; Björkling, F.; Liang, X. *Synlett* **2005**, *2005*, 2209.
(133) Nagarjuna, G.; Yurt, S.; Jadhav, K. G.; Venkataraman, D. *Macromolecules* **2010**, *43*, 8045.
(134) McQuade, D. T.; Pullen, A. E.; Swager, T. M. *Chem. Rev.* **2000**, *100*, 2537.
(135) Bunz, U. H. F. *Chem. Rev.* **2000**, *100*, 1605.
(136) Chinchilla, R.; Najera, C. *Chem. Rev.* **2007**, *107*, 874.
(137) Chinchilla, R.; Najera, C. *Chem. Soc. Rev.* **2011**, *40*, 5084.
(138) Bunz, U. H. F. *Macromol. Rapid Commun.* **2009**, *30*, 772.
(139) Bunz, U. F. In *Poly(arylene etynylene)s*; Weder, C., Ed.; Springer Berlin Heidelberg: 2005; Vol. 177, p 1.
(140) Jiang, H.; Taranekar, P.; Reynolds, J. R.; Schanze, K. S. *Angew. Chem., Int. Ed.* **2009**, *48*, 4300.
(141) Miranda, O. R.; You, C.-C.; Phillips, R.; Kim, I.-B.; Ghosh, P. S.; Bunz, U. H. F.; Rotello, V. M. *J. Am. Chem. Soc.* **2007**, *129*, 9856.
(142) Kim, I.-B.; Han, M. H.; Phillips, R. L.; Samanta, B.; Rotello, V. M.; Zhang, Z. J.; Bunz, U. H. F. *Chem. – Eur. J.* **2009**, *15*, 449.
(143) Zhao, X.; Pinto, M. R.; Hardison, L. M.; Mwaura, J.; Müller, J.; Jiang, H.; Witker, D.; Kleiman, V. D.; Reynolds, J. R.; Schanze, K. S. *Macromolecules* **2006**, *39*, 6355.
(144) Zornik, D.; Meudtner, R. M.; El Malah, T.; Thiele, C. M.; Hecht, S. *Chem. – Eur. J.* **2011**, *17*, 1473.

(145) Milian Medina, B.; Beljonne, D.; Egelhaaf, H.-J.; Gierschner, J. *J. Chem. Phys.* **2007**, *126*.
(146) Reichardt, C.; Welton, T. In *Solvents and Solvent Effects in Organic Chemistry*; Wiley-VCH Verlag GmbH & Co. KGaA: 2010, p 359.
(147) Tolstorozhev, G.; Tikhomirov, S. *J. Appl. Spectrosc.* **1998**, *65*, 659.
(148) Hirata, Y.; Tanaka, I. *Chem. Phys. Lett.* **1976**, *43*, 568.
(149) Phillips, R. L.; Miranda, O. R.; Mortenson, D. E.; Subramani, C.; Rotello, V. M.; Bunz, U. H. F. *Soft Matter* **2009**, *5*, 607.
(150) Liu, Y.; Chen, Y.; Li; Zhang, H.-Y.; Liu, S.-X.; Guan, X.-D. *J. Org. Chem.* **2001**, *66*, 8518.
(151) Liu, Y.; Yu, H.-M.; Chen, Y.; Zhao, Y.-L. *Chem. – Eur. J.* **2006**, *12*, 3858.
(152) You, C.-C.; De, M.; Han, G.; Rotello, V. M. *J. Am. Chem. Soc.* **2005**, *127*, 12873.
(153) Patel, N.; Khan, I.; Pannecouque, C.; De Clercq, E. *Med. Chem. Res.* **2012**.
(154) Kumar, B. V.; Naik, H. S. B.; Girija, D.; Sharath, N.; Sudeep, H. V.; Hoskeri, H. J. *Archiv der Pharmazie* **2012**, *345*, 250.
(155) Das, S.; Pati, P. B.; Zade, S. S. *Macromolecules* **2012**, *45*, 5410.
(156) Gibson, G. L.; McCormick, T. M.; Seferos, D. S. *J. Am. Chem. Soc.* **2012**, *134*, 539.
(157) Ohulchanskyy, T. Y.; Donnelly, D. J.; Detty, M. R.; Prasad, P. N. *J. Phys. Chem. B* **2004**, *108*, 8668.
(158) Marsden, J. A.; Miller, J. J.; Shirtcliff, L. D.; Haley, M. M. *J. Am. Chem. Soc.* **2005**, *127*, 2464.
(159) Fulmer, G. R.; Miller, A. J. M.; Sherden, N. H.; Gottlieb, H. E.; Nudelman, A.; Stoltz, B. M.; Bercaw, J. E.; Goldberg, K. I. *Organometallics* **2010**, *29*, 2176.
(160) Appleton, A. L.; Miao, S.; Brombosz, S. M.; Berger, N. J.; Barlow, S.; Marder, S. R.; Lawrence, B. M.; Hardcastle, K. I.; Bunz, U. H. F. *Org. Lett.* **2009**, *11*, 5222.
(161) Bangcuyo, C. G.; Evans, U.; Myrick, M. L.; Bunz, U. H. F. *Macromolecules* **2001**, *34*, 7592.